03

IRON-ABSORPTION BAND ANALYSIS FOR THE DISCRIMINATION OF IRON-RICH ZONES

By

Lawrence C. Rowan and Pamela H. Wetlaufer

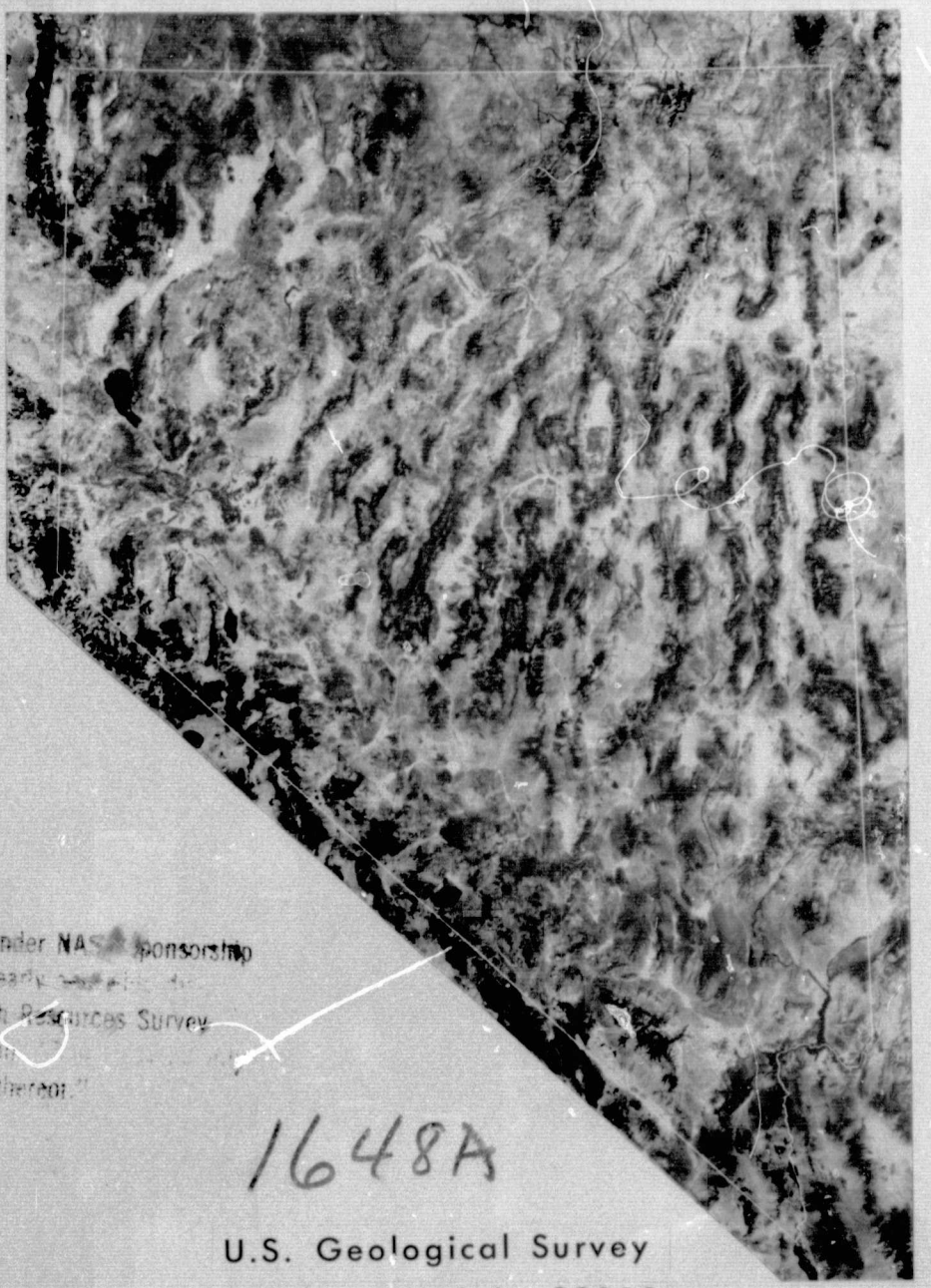

1648A

U.S. Geological Survey
Reston, Virginia 22092

Earth Resources Technology Satellite - 1
Type III Final Report
Contract S-70243-AG
Task 434-641-14-03-75
Prepared For — NASA/ Goddard Space Flight Center
Greenbelt, Maryland 20771
January 1975

STANDARD TITLE PAGE FOR TECHNICAL REPORTS	1. Report No.	2. Gov't Accession No.	3. Recipient's Catalog No.
4. Title and Subtitle Iron-absorption Band Analysis For The Discrimination of Iron-rich Zones			5. Report Date December 15, 1974 6. Performing Organization Code
7. Author(s) Lawrence C. Rowan and Pamela H. Wetlaufer			8. Performing Organization Rept. No.
9. Performing Organization Name and Address U. S. Geological Survey National Center, Stop 927 Reston, Va. 22092			10. Project/Task Work Unit No. 11. Contract/Grant No. S-70243-AG
12. Sponsoring Agency Name and Address NASA Goddard Space Flight Center Greenbelt, Maryland 20771			13. Type of Report & Period Covered ERTS-1, Type III Progress Rept 1 July, 1972-Aug 1974 14. Sponsoring Agency Code

15. Supplementary Notes

16. Abstracts

A technique which combines digital computer processing and color compositing has been devised for detecting hydrothermally altered areas and for discriminating among many rock types in an area in south-central Nevada. Subtle spectral reflectance differences among the rock types are enhanced by ratioing and contrast-stretching MSS radiance values to form ratio images which subsequently are displayed in color-ratio composites. Most of the distinctions achieved are not possible through visual comparison of the MSS images or optically assisted techniques. The high reliability (approximately 80 percent) of identification of altered areas indicates a large potential for this technique in mineral exploration.

Landform analysis of Nevada shows that linear features compiled without respect to length results in approximately 25 percent coincidence with mapped faults. However, about 80 percent of the major lineaments (≥ 10 km length) coincides with mapped faults, and substantial extension of locally mapped faults is commonly indicated. Seven major lineament systems appear to be old zones of crustal weakness which have provided preferred conduits for rising magma through periodic reactivation. Reactivation of these zones approximately 30 m.y. ago resulted in migration of silicic volcanism from the central Great Basin to the Central-Nevada Volcanic Complex. Continued volcanism in this area, now a crudely circular feature, until 19 m.y. ago and limited volcanic activity thereafter, probably explain the low areal density of metal mining districts within the Complex.

17. Key Words and Document Analysis. (a). Descriptors

Mineral Exploration
Nevada
Digital Computer Processing
Landform Analysis
Lineaments
Volcanic Centers

18. Distribution Statement	19. Security Class (This Report) UNCLASSIFIED	21. No. of Pages
	20. Security Class. (This Page) UNCLASSIFIED	22. Price

FORM NTS-867(1-70)

TABLE OF CONTENTS

Table of Contents - Continued

List of Illustrations

Plates
[in pocket]

Tables

Preface

This document presents the final results of the Earth Resources Technology Satellite-1 (ERTS-1) experiment (no. 9648) entitled, "Iron-absorption band analysis for the discrimination of iron-rich zones," Lawrence C. Rowan, Principal Investigator. The report is separated into three parts to facilitate discussion of the results: Part I, Conclusions and Recommendations, Part II, Spectral Reflectance Studies, and Part III, Landform Studies. The spectral reflectance and landform studies are treated separately because fiscal constraints prohibited digital computer processing of sufficiently large areas to permit an integration of these two approaches. However, both of these independent approaches have yielded very encouraging results in the study area, suggesting that integration of these techniques holds considerable potential for mineral exploration in arid and semiarid regions.

Many individuals and organizations have contributed to this study. Most noteworthy are Alexander Goetz and Allan Gillespie, Jet Propulsion Laboratory, Pasadena, California for their innovative image processing and spectral reflectivity work and Allan Kover and Terry Offield, U.S. Geological Survey, for numerous useful comments made in technical review of the manuscript. Don Sawatsky, U.S. Geological Survey, developed the computer processing programs for azimuth distribution analysis of the digitized lineaments.

PART I

CONCLUSIONS and RECOMMENDATIONS

Conclusions

The results of this experiment (NASA No. 9648) lead to the following conclusions concerning the usefulness of ERTS-1 data for geologic investigation, especially as applied to mineral exploration:

1) Exposed hydrothermal alteration zones can be detected and delineated by enhancing the subtle spectral reflectivity differences between altered and unaltered rocks. Digital computer processing and color compositing are required to achieve these results.

2) Discrimination among many exposed unaltered regional rock units can be accomplished using these image-enhancement techniques.

3) In situ spectral reflectivity measurements coordinated with mineralogical and chemical analyses of statistically representative samples are the soundest basis for refining the image processing techniques and for selecting the best wavelength bands for future experiments.

4) Major lineaments ($\geq$ 10 km long) commonly coincide with mapped faults and therefore are geologically significant; many major lineaments that do not coincide with mapped faults may be fracture or fault zones.

5) Several major lineament systems, typically tens to hundreds of kilometers long, are especially important. In Nevada, seven major lineament systems have been identified which we believe are deep-seated, pervasive zones of crustal weakness probably Precambrian in age. Several of the zones appear to form a conjugate shear system which has been reactivated periodically.

6) Analysis of the major lineaments and synthesis of geochronological

and geophysical data have identified a volcanic complex 150 km in diameter in central Nevada. The silicic volcanic rocks of this area, referred to as the Central Nevada volcanic province, were deposited 19 m.y. to 30 m.y. ago as this conjugate shear system was reactivated.

7) These major zones of crustal weakness played an important but previously unrecognized role in the localization of ore deposits, probably by providing the main conduits for ascending ore-bearing solutions.

8) The Central Nevada Volcanic Complex" is an area of low mining-district density and value, probably because of the covering of older ($\geq$ 30 m.y.) ore deposits by a thick sequence of silicic volcanic rocks and only limited volcanic activity after formation of the complex ($\leq$ 19 m.y.).

In addition to these specific conclusions, several procedural results are discussed in this report.

Recommendations

The following recommendations are submitted for consideration:

1) In situ spectral reflectivity measurements coordinated with mineralogical and chemical analyses of statistically representative areas should be acquired for refining digital image-processing techniques, formulating spectral reflectivity models, and for selecting the best wavelength bands for future experiments.

2) Digital computer and color-compositing techniques should be calibrated and standardized as much as possible to facilitate comparison of geographically separated areas and utilization of these techniques by other data users.

3) Geological, geophysical, and geochemical field studies of major lineaments and circular features are imperative for determining the origin and therefore the full significance of these landforms.

4) The effects of spatial resolution, stereographic coverage, and of temporally influenced factors should be fully investigated.

5) The techniques of spectral reflectance enhancement and landform analysis should be applied to mineral exploration in an integrated manner.

PART II

SPECTRAL REFLECTANCE STUDIES

Introduction

The main objective of this experiment was to evaluate the ERTS-1 Multispectral Scanner (MSS) images for discriminating among rock types, especially between altered and unaltered areas. This objective has been accomplished in cooperation with the Jet Propulsion Laboratory, Pasadena, California through use of a combination of digital computer processing and color-compositing techniques for images of an area in south-central Nevada. The results of this part of the experiment and the techniques used have been described by Rowan and others (1974); their paper is included in Appendix A of this document.

Additional Results

Since completion of the work described in Appendix A in March 1974, most of our efforts have been devoted to the landform analysis described in part III of this document, the image-enhancement aspects consequently being conducted at a lower level of effort. The work described by Rowan and others (1974) deals with the eastern part of MSS image number E1072-18001 recorded on October 3, 1972. Subsequent image enhancement and analysis was carried out on the western part of this scene to further test the techniques in an area of widespread hydrothermal alteration but slightly more diverse host rock lithologies than are found in the eastern part of the area. Although completion of this evaluation has been delayed by several technical and logistical problems, the results are generally

similar to those obtained in the eastern half of this scene. However, several important differences have resulted from analysis of a color-ratio composite of the western part of the scene, and the rest of Part II of this document will deal with these problems.

The color-ratio composite of the western part of scene E1072-18001 was prepared using logarithmically stretched ratio images without atmospheric-scattering corrections (fig. 1). As in the composite for the eastern part of this frame, the ratio images and diazo colors used were 4/5 (blue), 5/6 (yellow) and 6/7 (magenta). Other color and ratio combinations, especially the inverse ratios (5/4, 6/4, 6/5, 7/4, 7/5, and 7/6), were examined, but none showed any improvement over the discrimination potential of the original color and color image combination. Images with atmospheric corrections were not used for the final composite because the resulting composites were too noisy.

Evaluation of the color-ratio composite shown in fig. 1 was conducted in the laboratory and field using available geologic maps of the area (Stewart and Carlson, 1974; Albers and Stewart, 1972) and color and black-and-white photographs. In general, the image colors of rock units are the same as those described by Rowan and others (1974): basaltic and andesitic rocks are white; felsic rocks, mainly ash-flow tuffs and quartz monzonite porphyries, are pink to dark red; playas are blue; altered areas are yellowish green to dark green; alluvium is a mixture of these colors, green areas commonly being due to the presence of iron-oxide coatings on fragments of unaltered rocks; and vegetation is orange. Clouds are brown-pink and shadows are white. In addition, black shale,

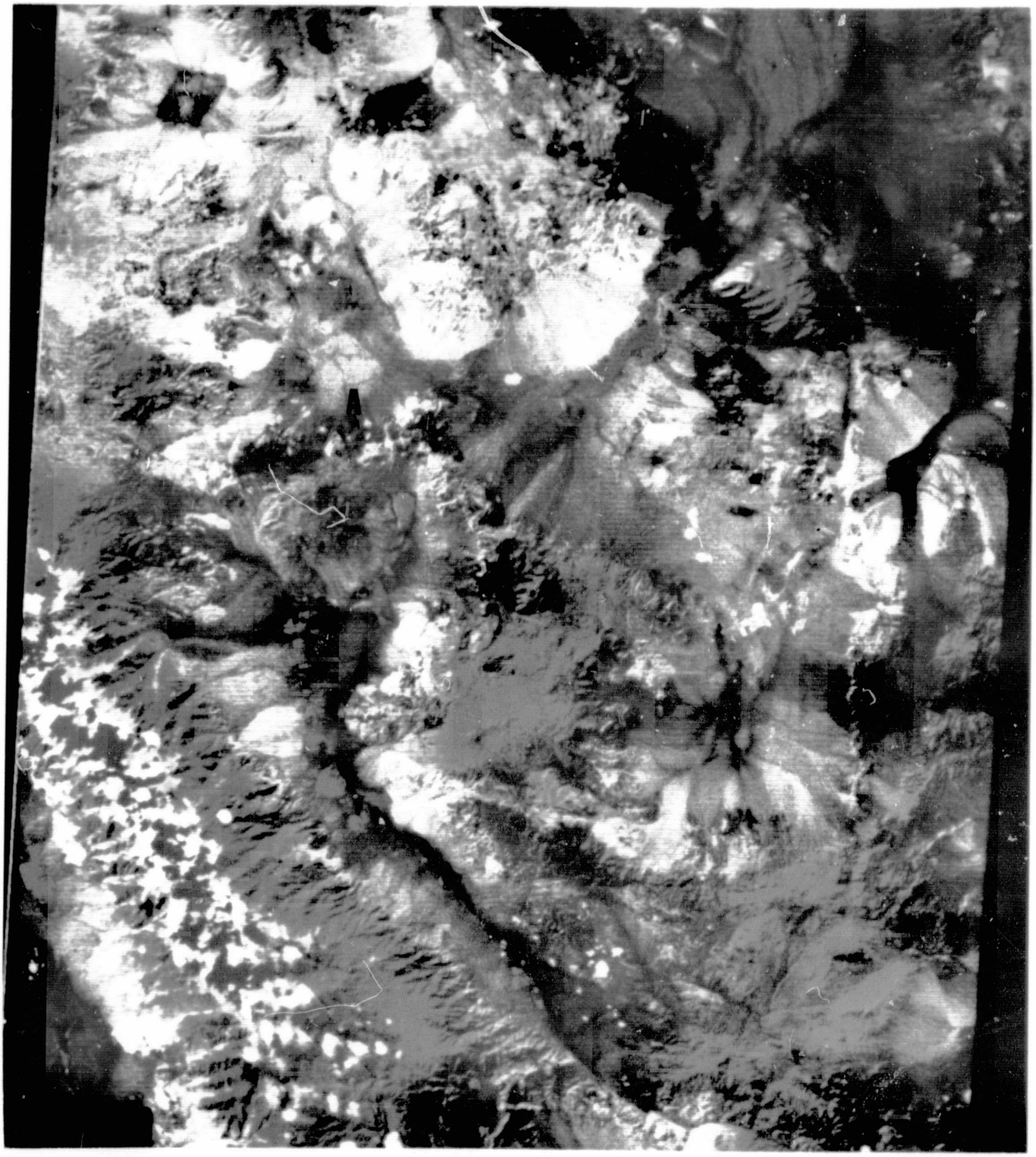

Fig. 1 - Color-ratio composite of the western part of ERTS-1 image E1072-18001, south-central Nevada, showing playas (blue), basalt, andesite, and shale (white), felsic volcanic and intrusive rocks (pink to dark red), vegetation (orange) and hydrothermally altered areas and a few areas of limonitic and hematitic unaltered rocks (A) (green). Clouds are brown-pink and shadows white. Prepared in cooperation with the Jet Propulsion Laboratory, Pasadena, California. Copies available from EROS Data Center, image ID No. EDC-010076.

siltstone, and hornfels of the Palmetto Formation are white and indistinguishable from the basaltic and andesitic rocks in the color-ratio composite (fig. 1). In some places, especially in the north-central part of this area, andesite has a slightly blue tint in the images, but this color pattern does not appear to be sufficiently consistent to be a reliable means for discriminating andesite from basalt and the rocks of the Palmetto Formation. None of the altered areas in this part of the image appear red-brown.

The most important exception to these image color-rock unit relationships is the fact that some of these dark-green areas in the image are outcrops of unaltered limonitic or hematitic rocks. The largest area of this type is the dark-green area in the Volcanic Hills (A, fig. 1). Although most of this area consists of alluvium, large outcrops of red and pink ash-flow tuffs are included in the dark-green pattern. The rock color is apparently due to the presence of small amounts of hematite in the groundmass of these tuffs. This discrepancy with respect to detection of alteration zones also occurs in a few places where hematitic soil developed in the zone immediately above a vitrophyric layer within the tuff sheet (R. P. Ashley, personal communication, 1974). However, in the approach outlined by Rowan and others (1974), these soil-covered areas would be identified as alluvium by using high-altitude aerial photographs and excluded from maps showing the distribution of altered areas. In the only other problem area of this type, a slightly ferruginous shale and siltstone sequence of the Excelsior Formation (Stewart and Carlson, 1974) which weathers to medium yellow-brown

limonitic surfaces also appears dark green in the color-ratio composite.

In the area of fig. 1, limonitic and hematitic unaltered rocks are of limited areal extent. Therefore, despite these erroneous identifications of altered areas, an estimated 80-90 percent of the green areas in the color-ratio composite (fig. 1) are related to hydrothermal activity. However, the inability to distinguish these rocks from altered rocks would pose a more serious problem in areas where limonitic or hematitic unaltered rocks are widespread. The problem of discriminating between these two general rock types stems from their spectral similarity in the MSS response range. Consideration of the mineralogical composition of the altered zones in the study area and examination of spectroradiometric measurements made during the last phase of this experiment suggest, however, that separation of the altered rocks and these unaltered rocks may be possible by carefully tailoring the image-processing procedures to take advantage of very slight spectral reflectivity differences between them. Because of the subtlety of these differences, a detailed analysis of statistically representative spectra is required for determining the optimum image-enhancement procedure. An additional problem requiring further study is the fact that all of the altered areas in the western part of the scene appear green in the color-ratio composite (fig. 1), whereas altered rocks vary from green to red-brown in the eastern part (Rowan and others, 1974).

Approximately 500 reflectance spectra have been obtained for representative in situ samples of altered and unaltered rocks in the Goldfield mining district in the eastern part of scene E1072-18001 (Rowan and others, 1974). These spectra were recorded between April 29 and May 3, 1974, by

using two field-portable spectroradiometers. One of these instruments, designed by Alexander F. H. Goetz, Jet Propulsion Laboratory, Pasadena, California, scans from 0.4 to 2.5 μm in approximately 30 sec. and records on digital tape. The other spectroradiometer scans the 0.4 to 1.4 μm part of the spectrum in about 2 sec. and records on analog tape which is digitized later; this device was fabricated by William Bonner, U. S. Geological Survey, Denver, Colorado. Each sample area was photographed and described, and mineralogical and chemical analyses are being made of selected samples.

Although these spectra do not adequately represent all of the major rock units in the Goldfield District, they do provide the best available means for determining the spectral reflectivity differences between the altered and unaltered rocks and ultimately for studying variations among the rocks composing these two groups. A few of these spectra are shown in fig. 2 to illustrate the difference in spectral shape between the unaltered and altered rocks typical of the area. The most conspicuous differences between these two sets of spectra are the broad absorption band between 0.8 and 1.0 μm and the more rapid decrease in reflectance between 0.75 and 0.4 μm in the altered rocks and soils. These spectral features are due to the presence of iron-absorption bands near 0.9μm and in the blue and ultraviolet parts of the spectra. Visible and near-infrared spectra of this type evaluated with respect to the mineralogical and bulk chemical compositions will provide the basis for refining image-processing techniques, selecting the optimum wavelength bands for future experiments, and for developing models that can be applied to other areas. An important step in these studies will be comparison of digitally processed MSS and

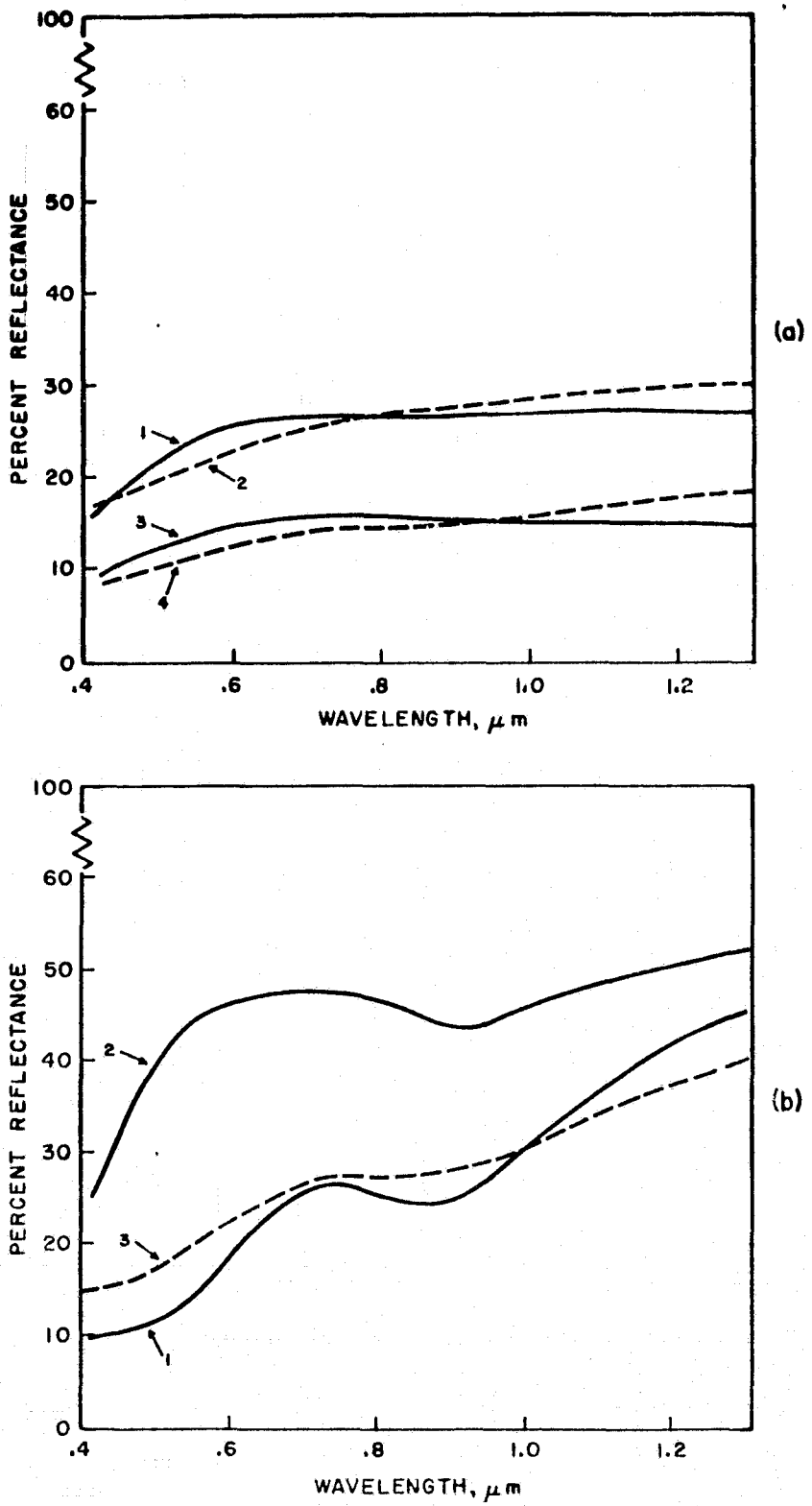

Fig. 2 - Reflectance spectra for areas in the Goldfield mining district typical of (a) unaltered rocks -1, andesite, 2, quartz latite, 3, rhyodacite, 4, basalt and of (b) altered rocks -1, orange to red hematitic and limonitic silicified rock, 2, yellow montmorillonitic soil (50%) with kaolinitic and limonitic fragments (50%), 3, limonitic and hematitic silicified and argillized fragments. (all spectra, Alexander F. H. Goetz, personal communication, 1974).

Skylab S192 data, However, the S192 radiometric data for this area are not yet ready for study.

Summary

The digital computer-processing and color-compositing techniques developed during this experiment permit the detection of hydrothermally altered rocks in the study area with an estimated 80-90 percent accuracy. The erroneous identifications are attributed to the spectral similarity of limonitic and hematitic unaltered rocks in the MSS response range. In situ spectral reflectivity measurements and mineralogical and chemical analyses of statistically representative sample areas provide the best means for refining the processing procedures to solve this problem and similar problems and for selecting the optimum wavelength bands for future experiments.

PART III

LANDFORM STUDIES

INTRODUCTION

General Statement

The usefulness of aerial photographs for studying landforms has been recognized for many years. Considerable attention has been focused on linear features, because many have proved to be tectonic features that could not be detected easily on the ground. Some of these features, especially faults and fracture zones, have influenced the occurrence of ore deposits. During the last 10 years, the perspective of satellite images has added a new dimension to the analysis of linear features. Analysis of Gemini and Apollo photographs and Nimbus images clearly demonstrated the value of the synoptic view for detecting and mapping regional tectonic features (Lowman, 1965, Lowman and Tiedemann, 1971). The few experiments that dealt specifically with mineral exploration (Gawarecki, 1971; Lathram, 1972; Lathram and Gryc, 1973) indicated considerable potential for this new approach to the search for ore deposits.

ERTS-1 Multispectral Scanner (MSS) images provide a means for more completely evaluating this approach to landform analysis, especially as it applies to mineral exploration. In addition to the synoptic view, the MSS records spatially registered multispectral radiometry in four wavelength bands of the same area every 18 days. Because of the different spectral response of materials in each wavelength band, each of the four bands depicts the surface appearance somewhat differently. Each MSS image covers approximately 34,200 sq km; much larger areas can be displayed in image mosaics. Hence, the surface expression of regional-to-continental-scale tectonic features can be analyzed during different seasons because of the repetitive coverage and in two visible and two near-infrared wavelength bands.

Although the repetitive and multispectral radiometry capabilities are very useful for landform analysis and essential for many other studies, the most critical aspect of the MSS images is the synoptic essentially planimetric view at nearly constant illumination.

Purpose and scope

The main purpose of the analysis of MSS images reported here is to determine their usefulness for detecting landforms related to tectonic and igneous activity and to consider the potential of this approach to mineral exploration. The area selected for study is the State of Nevada (Pl. 1). Selection of this area was governed mainly by the desire to study an area characterized by good exposures, widespread igneous activity and associated mineralization and alteration, and many major tectonic features. In all these respects, Nevada is a nearly ideal study area. Another important consideration was the discontinuity of the surface units. Although the geology of most individual mountain ranges in Nevada is now reasonably well understood, synthesis and regional interpretation has been hampered by the presence of intervening alluvial basins. Consequently, some major tectonic and igneous features may still be unrecognized which would be of significance for understanding the distribution of ore deposits in the State.

Two general types of landforms are considered in this study: linear and circular features. The linear features, or linears, vary from approximately 2 to several hundred kilometers. Although some are curved, most are essentially linear. The circular features range from about 8 to 150 km in diameter. Most of these features are actually only crudely circular at the 1:500,000 and 1:1,000,000 compilation scales, and some are nearly elliptical.

In Pocket

Plate 1 - Map of Nevada showing drainage and geographic places and names

Even casual examination of MSS images of Nevada shows the presence of many linear and circular features. However, objective analysis of this large volume of data is made difficult by many human and technical factors. Although optical and digital computer techniques are currently available for this type of analysis, they are mainly experimental and do not necessarily result in an unbiased data set. Therefore, collection of basic data for analysis still relies mainly on delineation by visual inspection. Because of the subjectivity inherent to this practice, a systematic procedure was designed to verify and test the raw data. The essential phases used are compilation and verification of landforms using topographic and geologic maps and in some cases photomosaics, comparison of the linear and circular features with geologic maps to establish their geologic significance, and integrated analysis of the most important features, by using all available geologic and geophysical data. Care was taken to include in the data set only those features that were distinctive to both of the writers on repetitive scenes. In this respect, the data are regarded as being conservative, though still basically subjective.

It is important to emphasize that because of the number and magnitude of features present and the time limitations of this study, the writers have conducted essentially no field studies. The analysis has been based mainly on published geologic maps and reports. Although this procedure appears reasonably adequate to extend or revise many known features, detailed field-work will be required to evaluate previously unmapped structures. Hopefully, the results presented here will be sufficiently convincing to stimulate investigations on the new structures, especially by those who are familiar with the specific regions involved.

Methods

General Statement

The approach followed in this study began with compilation and evaluation of all linear features detectable on ERTS images without regard for the scale or magnitude of the features. Next, linears greater than 10 km long were compiled, verified as geological rather than cultural features, and evaluated as to their geological significance. After this verification, these major linears were redefined as major lineaments because they are known to be naturally occurring features. This definition is consistent with that proposed by Lattman (1958), except that stratigraphic contacts may be included as a major lineament or as part of a major lineament. Although exclusion of such contacts seems valid for study of aerial photographs, it is felt to be impractical for the small-scale synoptic ERTS images. An additional departure from Lattman's usage is our recognition of a category of features termed major lineament zones. These features are typically diffuse poorly defined linears, largely inferred from features within a zone of common orientation or from zones of tonal variation. In the final stage of analysis, the most extensive lineaments were studied by using geological and geophysical data to determine their origin and role in the volcano-tectonic development of Nevada and their importance to ore genesis. These regionally important features are designated major lineament systems. The study therefore progresses in three steps from consideration of all linear features to examination of successively larger magnitude features.

Data Compilation Procedure

A procedure of data collection was designed to minimize the subjectivity inherent to this type of study. Briefly, the steps were:

1) delineation of all linear features on individual 1:1,000,000-scale MSS band 5 and band 7 images;

2) compilation and preliminary verification of linear data, separated into band 5 and band 7 data, on 1:500,000-scale shaded-relief maps;

3) compilation of all data on a 1:1,000,000-scale band 5 image mosaic of Nevada;

4) compilation of linear features $\geq$ 10 km on a separate 1,000,000-scale band 5 mosaic and verification using geologic and topographic maps;

5) comparison of these lineaments and circular features with geologic maps;

6) identification of the most significant features, especially previously unrecognized major faults and fault zones.

Initial delineation and compilation of detectable linears on ERTS images of Nevada at 1:1,000,000 scale included linears (Pl. 2) characterized as continuous surficial or topographic features of any length which are straight or curvilinear and sharply distinct from surrounding nonaligned features. These linears range in length from 2 to 45 km, the average length measuring less than 10 km. They are most concentrated in the mountain ranges where topographic, textural, and tonal enhancement is highest; sparsely scattered linears occur within the alluvial basins.

In Pocket

Pl. 2 - Linear features of all lengths observed on 1:1,000,000-scale MSS band 5 and band 7 images in Nevada.

Band 5 and 7 images were used for the detection and delineation of the linears, because of their higher scene contrast. Moreover, the combination of these bands permits detection of all lineaments visible on bands 4 and 6. Both bands 5 and 7 are necessary for detection of linears because some linear features and patterns are preferentially enhanced in one or the other of these two bands. This differential enhancement is due to the characteristic differences in the spectral reflectivities of rock, soil, and vegetation: within the wavelength range of the MSS system, these differences are greatest between bands 5 and 7.

Linears detected on 1:1,000,000-scale prints of bands 5 and 7 were initially transferred separately to two shaded-relief base maps of Nevada at 1:1,000,000 scale. The images making up the mosaic of Nevada were at 1:1,000,000 scale and were recorded in September and October, 1972. Additional band 5 and 7 images received after the initial compilation of linears on the mosaic were used to update the overlay. This updating was critical because of enhancement of previously undetected linear features as a result of seasonal variations. Snow enhancement of topography in the winter images, for example, was especially valuable. Band 7 winter images provided more additional linear data than did the other bands. However, a systematic study of snow enhancement was not pursued because of inadequate images of the study area.

The vastly improved quality of the later images received is also significant in terms of detection of additional linears. Prints processed from the extremely dense negatives making up the original

data had very low scene contrast, and, in addition, a substantial amount of spatial information on the early transparencies was obscured by diffraction patterns. However, the transparencies subsequently received were less dense and had higher scene contrast. The data were also sharper in appearance, resulting in an apparent increase in resolution.

The synoptic coverage of ERTS images, especially if expanded by mosaicking techniques, permits detection of a more regional and somewhat more interpretive set of linears. The second data set, termed major lineaments after verification of their geological origin, consists of these relatively large-scale conspicuous linear features (fig. 3) which are commonly more diffuse in appearance than the smaller scale linears and which include extrapolations over short distances (1-2 km) of alluvium and nonaligned features. Extrapolation over distances of as much as 10 km was permitted in delineating the lineament zones. A minimum length of 10 km is assigned to these large-scale features because it is felt that assignment of a minimum length longer then 10 km might neglect some important crustal features pertinent to considerations of the regional structural framework.

Major linears as a unique subset were initially compiled on the band 5 image mosaic mentioned above. Several linears longer than 100 km and traversing more than one individual image could be delineated on the mosaic. Some linear zones became apparent which had not been recognized previously using only the more limited view of single images. All the major linears were subsequently checked on individual images,

Fig. 3 - Major linear features ($\geq$ 10 km) plotted on ERTS-1 band 5 image mosaic of Nevada

on an enlargement of the mosaic at 1:500,000-scale and on 1:250,000-scale topographic maps of Nevada. More major linears were added at this time, and several linears caused by cultural features such as roads were removed. Therefore, all the features included in this final compilation are major lineaments and major lineament zones.

Data Analysis of Linears

General Statement

The analysis that follows covers the development of the techniques applied to the data. Initial efforts to determine the significance of the linear features delineated were hampered by the poor photographic quality of the original images. Hence, the results of the preliminary analysis of linears seen on band 5 and 7 images are felt to have limited value. Nonetheless, the first stage of analysis using 1:500,000-scale shaded-relief base maps of Nevada was extremely useful for developing a familiarity with the data and a good background knowledge of the pertinent articles and geologic maps available. It also provided an important basis for determining the best approach to take with respect to the next stage of analysis. Completion of a band 5 image mosaic of the State of Nevada by Aerial Photographers of Nevada, Reno, Nevada, and the availability of much improved images initiated the main phase of both the linears and the major lineaments.

Preliminary analysis of linears

Linears detected in 1:1,000,000-scale images of bands 5 and 7 were initially compiled separately on two shaded-relief base maps of the State of Nevada. It soon became apparent that fewer linear features were detectable on band 5 images than on band 7 images, which had a much broader density range. However, the difference in contrast between the bands was due primarily to the high density of the original negatives from which the prints were made.

Whereas most linears are apparent in both bands 5 and 7, some linears appear to be unique to one band. Often such a linear can subsequently be identified in the other band, although it is not distinct enough to have been detected without prior knowledge of its existence. As image quality improved in the later data received, especially with respect to band 5, many fewer linears were detected that could not be seen on both bands. Nevertheless, some linears were still decidedly more conspicuous in one band than in the other.

The primary causes for the differential enhancement between band 5 and 7 images are spectral reflectivity differences among rocks and soils, and vegetation. In band 5 images, changes in vegetation type and/or density are the most frequent causes of enhancement of linears as compared with band 7 images; for example, the interfaces between the mountain ranges and the alluvial basins are commonly highlighted. In the ranges, as elevation decreases, the juniper and piñon (dark in band 5) give way quickly to the sagebrush and other desert plants (light in band 5) which dominate the alluvial valleys. In band 7 images, vegetation is very light so that although basin-range boundaries are not as distinct as in band 5 images, detail within the ranges is more visible. At times, the dark vegetation in band 5 images obscures linears conspicuous in band 7 images. Improved density balance in later band 5 images reduced this effect somewhat.

Analysis of the genetic nature of the linears focused on comparison of the linears with published geologic maps, usually at 1:250,000 scale. As previously mentioned, the sheer numbers of the linears and the large area covered made field checking of all the data impractical. The resulting

analysis was therefore dependent upon the quality and detail of the existing topographic base maps and geologic maps, some of which contained only minimal structural information. In addition, in a few counties, scattered geologic mapping had not been compiled into a 1:250,000-scale county map.

On the basis of the available geologic maps, an estimated 25 percent of the linears in both bands 5 and 7 appear to be related to faults and lithological contacts. Stream segments, valleys, and gullies and ridge crests, which may be structurally controlled, account for approximately 40 percent of the linear features, and cultural features represent roughly 10 percent. The remaining 25 percent of the linears are unidentified.

More faults in total were identified on the band 7 images than on band 5 images, probably because of the larger number of linears detectable on band 7 images. However, some faults were detected only on band 5 images. Extensions of mapped faults are often suggested by the linears in both bands, and in several places consolidation of two aligned faults into a single fault is indicated. Many of the linear valleys and stream segments detected may be structurally controlled but verification can be difficult even in the field. The predominant geologic contacts delineated are the boundaries between the ranges and alluvial valleys; these are shown as both tonal and textural changes, the latter being more conspicuous in band 7. A limited number of geologic contacts can be detected within the ranges. However, many geologic contacts which otherwise might be seen are obscured by topography and by vegetation.

Ridge crests identified account for approximately 10 percent of the linears. Shadow enhancement appears to play a large part in highlighting these topographic forms, especially in band 7 images. Fewer ridge crests were detected in band 5 images, probably because of the masking effect of vegetation in some ranges. Cultural features detected, mainly roads and railway tracks, are the dominant cause of the sparse linears in alluvium; other alluvial linears are either caused by the drainage network or are unexplained. The remaining 25 percent of the linears that are unidentified need to be field checked to determine their significance.

Main Stage of Analysis of Linears

An uncontrolled ERTS image mosaic of the State of Nevada (fig. 4) made up from band 5 images was used as a base for compilation of all linears seen on band 5 and 7 images. The 1:1,000,000 scale of the image mosaic is the same as that of the individual linears in which the linears were initially delineated. Transfer of the linears to the base mosaic was therefore straightforward, resulting in better locational accuracy than achieved on the shaded-relief base maps. The change in seasons and the improved quality of the later images received permitted detection of additional linears which were subsequently transferred to the image mosaic.

Analysis of the structural implications of the linears (Pl. 2) was made difficult by the very high density of the features. Visual examination revealed no apparent pattern or directional trend, and a complete comparison with all known faults seemed impractical. Therefore, detailed comparison of the linears and mapped faults was limited to six areas in Nevada

Fig. 4 - ERTS-1 image mosaic (uncontrolled). Prepared by Aerial Photographers of Nevada, Reno, Nevada, using band 5 images recorded during September and October, 1972

(fig. 5). A geologic map of the State of Nevada (Stewart and Carlson, 1974) proved invaluable to this structural analysis. The map provided more structural information than many of the previously existing maps, and the compilation scale of 1:500,000 was ideally suited to the analysis of ERTS data.

The six sample areas were selected according to their terrain characteristics and their lithologic and structural settings. The areas chosen are thought to provide an adequate cross section of the various landforms and general geologic settings in the State of Nevada. Sizes of the sample areas range from approximately 31,400 sq. km to 11,000 sq. km. Areal boundaries are less important, however, than the dominant characteristics within each sample area.

The procedure adopted for the structural analysis of these areas required the tabulation of the numbers of faults and of linears within each area. Correlation of the linears with mapped faults was then determined by using a 1:1,000,000-scale reduction of the State geologic map of Nevada as an overlay on the image mosaic containing the linears. Two types of relationships between faults and linears were defined to constitute a correlation. The first includes direct correspondence between some part of a linear and a fault. The second consists of linears that parallel the trend of a nearby fault and that are within at least 2 km of the fault. These criteria for the second type of correlation are felt to be reasonable because linears in general often do not represent the actual fault trace but the morphologic expression of the fault, and because linears that do not

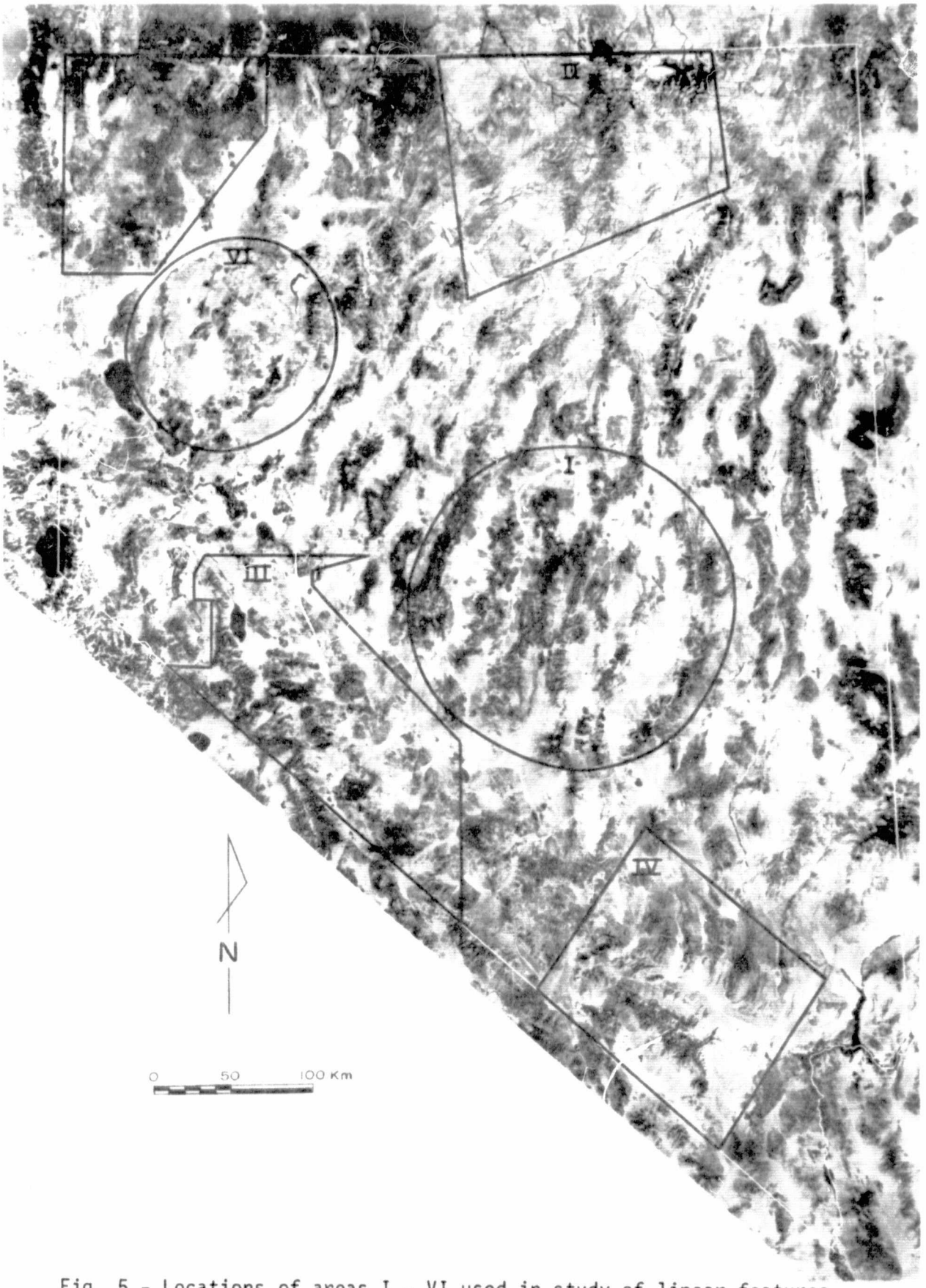

Fig. 5 - Locations of areas I - VI used in study of linear features.

represent a single fault, frequently can represent a zone of en echelon faulting. In addition, this second type of correlation would take into account the minor registration problem between the State geologic map and the uncontrolled mosaic. The sum of the two types of correlation was used to calculate the percentage of total linears that are structurally controlled (table 1). Trends of those linears that correlate with known faults were examined (table 2). Trends of the curvilinear features were assigned on the basis of the dominant trend. The six sample areas are discussed below in order of decreasing size.

I. Central Nevada circular area

The circular area delineated in central Nevada (figs. 5 and 6a,b) is the largest of the sample areas and contains the most faults and linears. The rugged mountain terrain and the relatively featureless intermontane basins are typical of the Basin and Range physiographic province which includes almost all of Nevada. Faulting occurs almost exclusively within the mountain ranges, which trend predominatly north. The fault pattern is complicated and dense.

The dominant lithologic unit within the sample area is Tertiary welded and nonwelded ash-flow tuffs. Some Tertiary andesitic and rhyolitic flows and minor Cretaceous granitic rocks crop out sporadically. Scattered Quaternary basalt flows are restricted to the Pancake Range. Paleozoic limestone, dolomite, shale, siltstone, sandstone, and quartzite predominate in the easternmost range in the sample area and occur in lesser amounts in the other ranges.

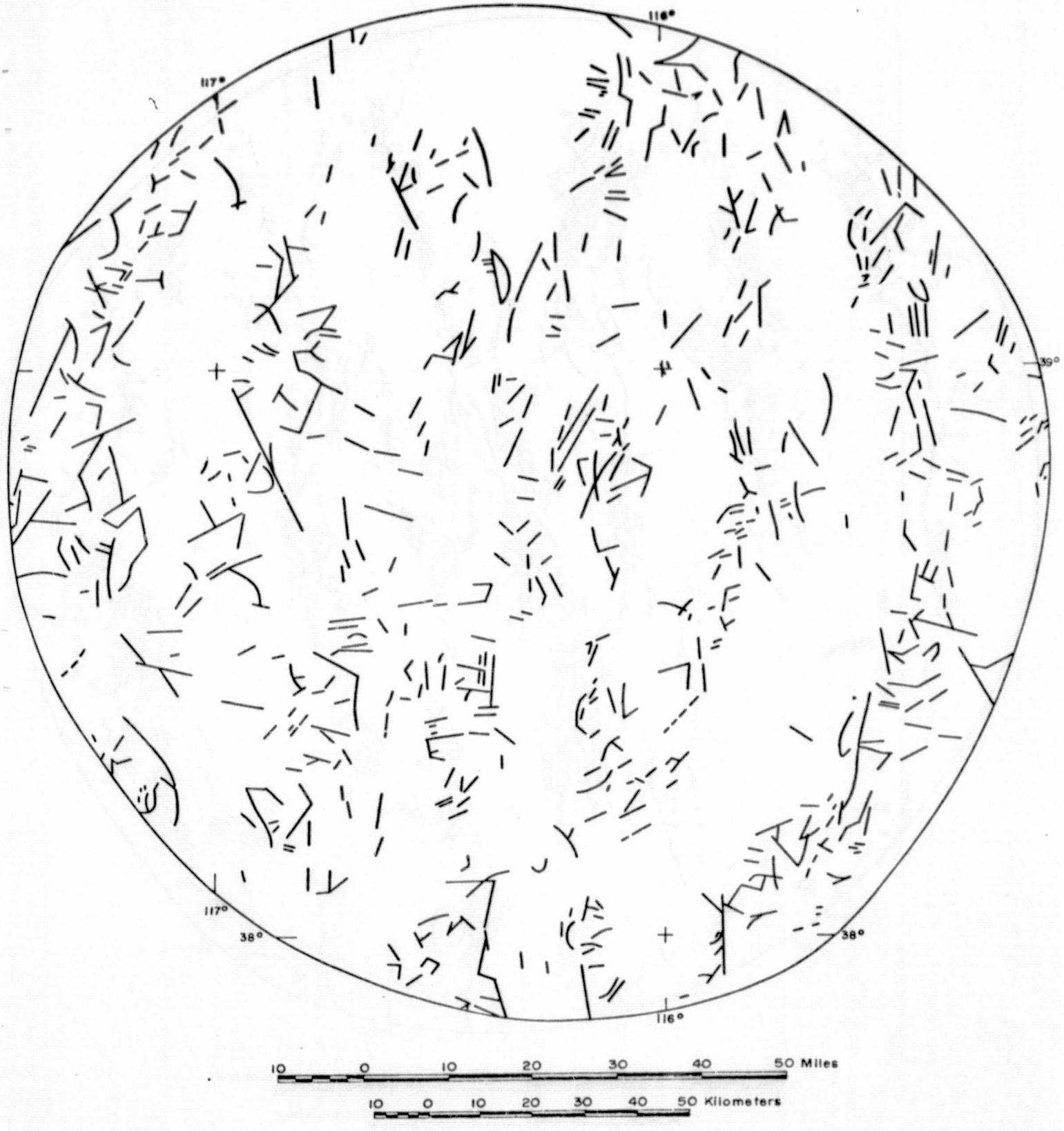

Fig. 6a - Map of study area I showing linear features delineated on ERTS-1 images.

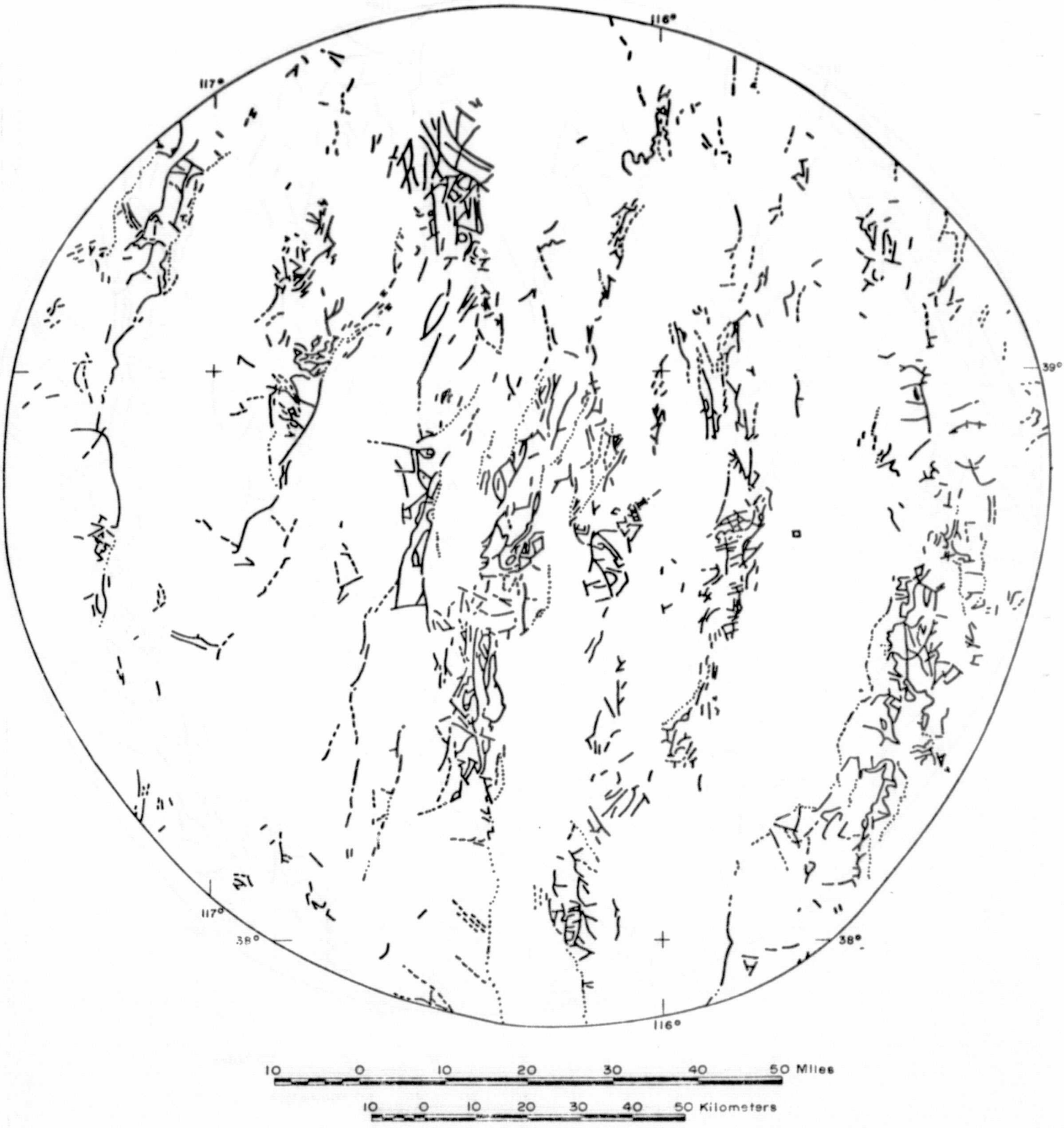

Fig. 6b - Map of study area I showing faults (from Stewart and Carlson, 1974).

On the basis of the correlation criteria stated previously, 23 percent of the linears can be correlated with mapped faults (see table 1). It is noteworthy, however, that only 15 percent of all the mapped faults were detected by the linears. The main directional trends of those linears that correlate with faults are north to northeast, the northerly trend being dominant (north 27 percent; northeast 23 percent; north-northeast 21 percent). Linears whose trends fall in this quadrant constitute 72 percent of all the correlated faults. The weakest trend is west-northwest (1 percent) (see table 2).

II. Western Elko County

The next largest sample area, in north-central Nevada (figs. 5 and 7a, b), covers 25,800 sq. km. The area is along the northern boundary of the Basin and Range province. The rugged mountainous terrain differs from that typical of the Basin and Range configuration in that the ranges have no particular directional trend and the intervening alluvial basins are not continuous. Within the sample area to the northwest, the mountainous terrain borders on the relatively flat Owyhee Desert, underlain mainly by Tertiary basalt and gravel. Due south, the main lithologic units include Tertiary flows of basalt, andesite, and rhyolite, ash-flow tuffs, and Ordovician shale and chert. The mountains to the east and north are very complicated geologically, made up of a mosaic of Tertiary flows of rhyolite and andesite, outcrops of Paleozoic sedimentary rocks

Table 1: Pertinent data for sample areas selected for the structural analysis of linears

	SAMPLE AREA	SIZE (sq.km)	SETTING		NUMBER OF FAULTS	NUMBER OF LINEARS	CORRELATION WITH FAULTS		LINEARS RELATED TO FAULTING (PERCENT)	FAULTS DETECTED BY LINEARS (PERCENT)	DOMINANT FAULT TRENDS PICKED UP BY LINEAR (PERCENTAGE IN PARENTHESES)	WEAKEST FAULT TRENDS PICKED UP BY LINEARS (PERCENTAGE IN PARENTHESES)
			GEOLOGIC	TOPOGRAPHIC			DIRECT CORRESPONDENCE	CORRESPONDENCE WITHIN 2 KM.				
I	Central Nevada circular feature	31,400	Silicic ash-flow tuffs dominant and associated Paleozoic Sedimentary rocks. Faulting concentrated in mountains. Fault pattern dense and complicated.	Northerly trending rugged mountain ranges and intermontane basins, typical of Basin and Range province.	1110	742	99	69	23	15	north (27)	west-northwest (1)
II	Western Elko Co.	25,800	Tertiary volcanic rocks mixed with Paleozoic sedimentary rocks in the mountains. Basalt and gravel on plateau to northwest. Faulting concentrated in mountains. Fault pattern dense and complicated.	Rugged mountain terrain having no particular orientation bordering on plateau to northwest.	875	470	71	44	24	13	north and northeast (25) each)	west-northwest (0)
III	Mineral and Esmeralda Cos.	18,917	Mesozoic granitic and sedimentary rocks to the west. Upper Tertiary volcanic rocks mixed with predominately lower Paleozoic rocks to the west. Fault pattern relatively open and simple.	Less rugged terrain having only weak northerly orientation. Deflection of typical basin and range trends by Walker Lane.	640	560	70	54	22	19	north-northeast (27)	west-northwest (2)
IV	Las Vegas Valley area	18,000	Paleozoic sedimentary rocks. Faulting concentrated in mountains. Fault pattern dense.	Typical basin and range terrain, distorted somewhat by northwest trending Las Vegas shear zone.	700	603	81	102	30	26	north (39)	east-northeast and east (1)
V	Northern Washoe and western Humboldt Cos.	12,650	Miocene volcanic rocks dominant to the west. Earlier rhyolite flows and Mesozoic intrusive and extrusive rocks to the east. Faulting relatively evenly scattered. Fault pattern relatively open and simple.	Relatively low smooth relief to the west; a few small north-trending ranges in the east.	260	389	44	42	22	33	north-northeast (27)	east-northeast (0)
VI	Pyramid Lake circular feature	11,000	Mesozoic sedimentary and granitic rocks and Miocene volcanic rocks Fault pattern relatively open and simple.	Northerly and north northeasterly trends typical of Basin and Range terrain, but ranges small and relief relatively low.	140	232	28	29	25	40	north-northeast (42)	east-northeast and east (0)

Table 2: Trends (in percent) of linears that relate to mapped faults in the six sample areas

SAMPLE AREA	Trends (percent of linears correlating with faults)							
	E	WNW	NW	NNW	N	NNE	NE	ENE
Central Nevada circular feature	5	1	5	11	27	21	23	6
Western Elko Co.	8	0	4	10	25	23	25	5
Mineral and Esmeralda Cos.	10	2	9	14	17	27	16	7
Las Vegas Valley area	1	2	6	10	39	25	16	1
Northern Washoe and western Humboldt Cos.	2	2	17	15	26	27	10	0
Pyramid Lake circular feature	0	4	2	5	37	42	12	0

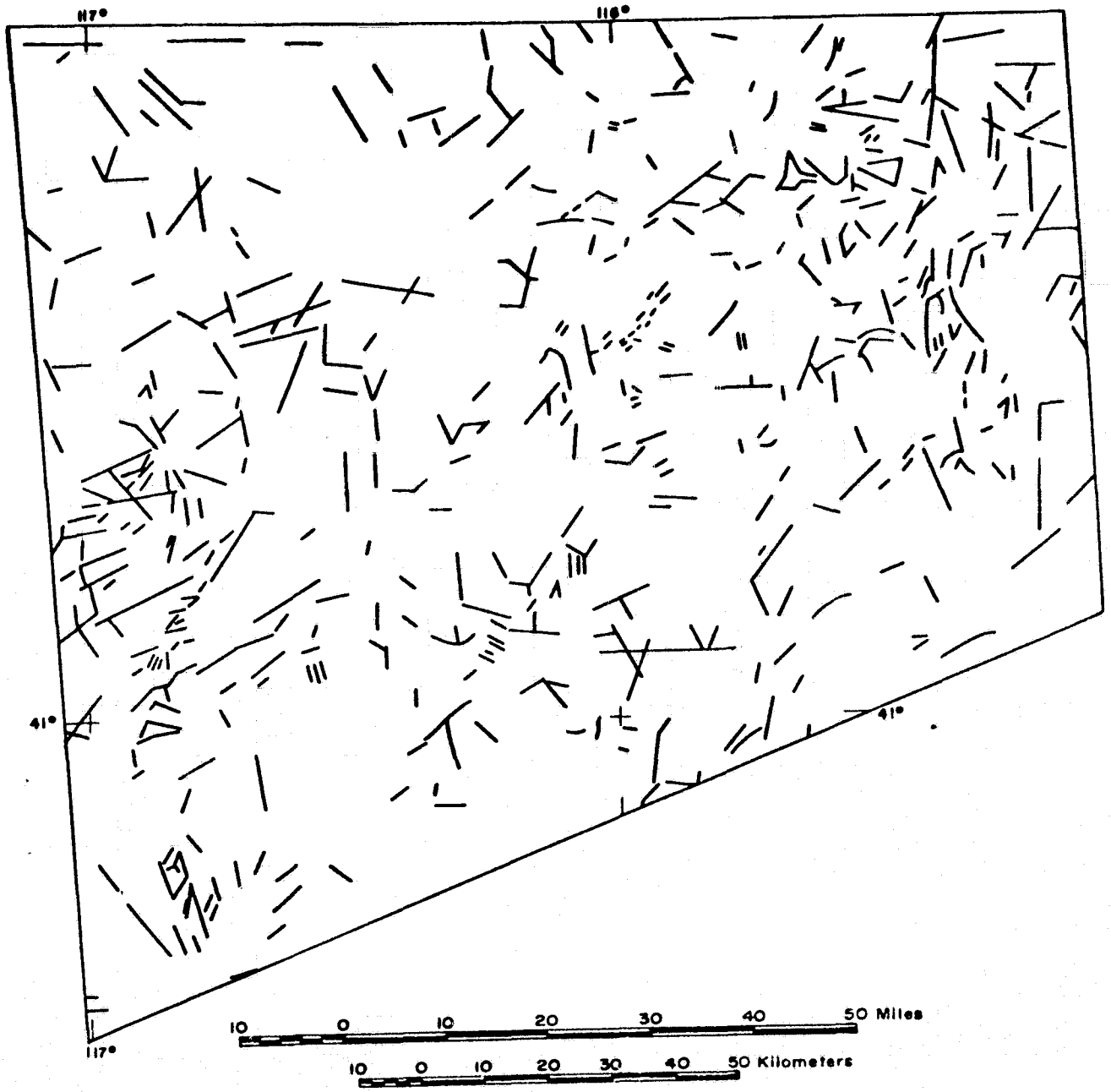

Fig. 7a - Map of study area II showing linear features delineated on ERTS-1 images.

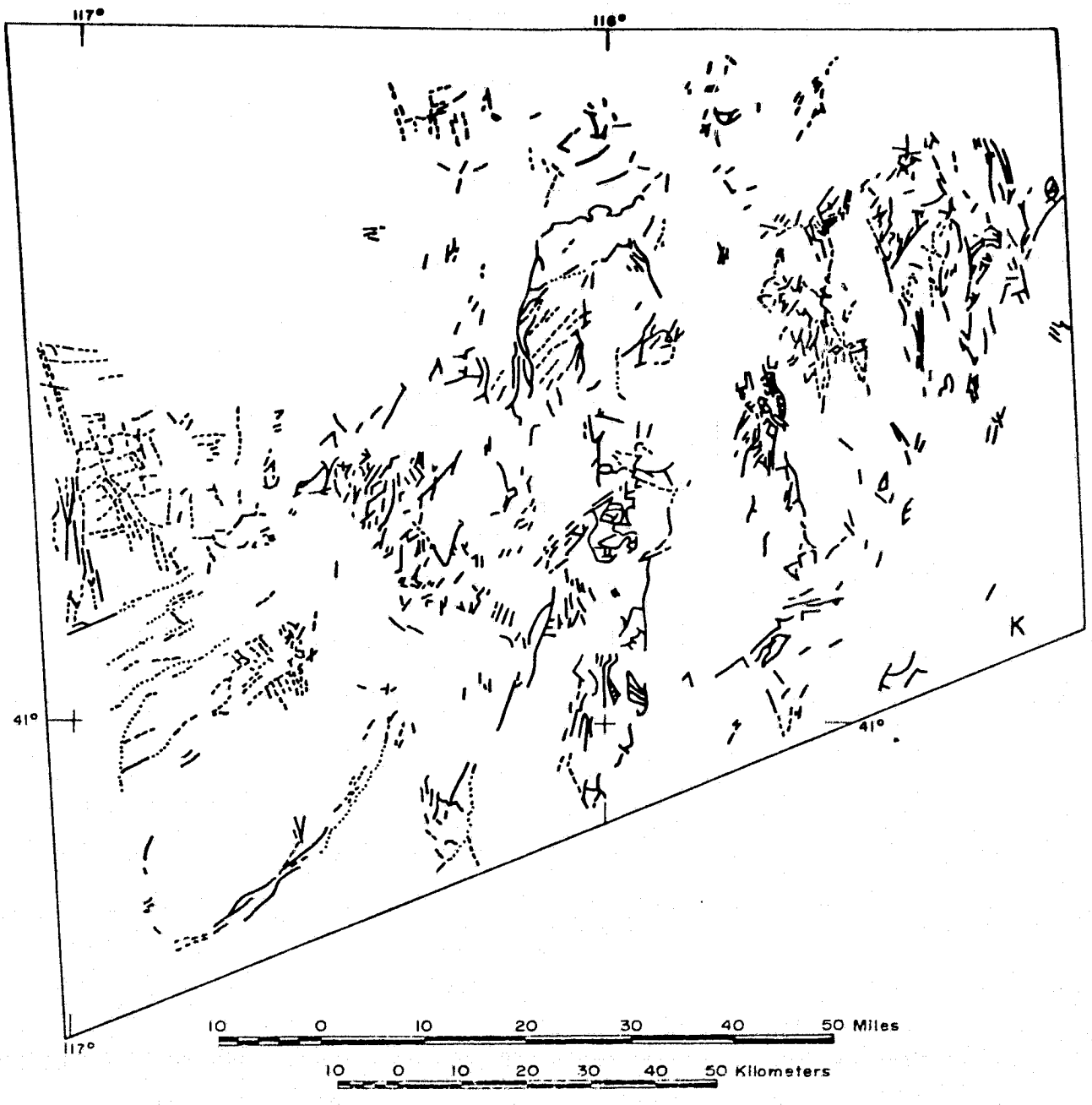

Fig. 7b - Map of study area II showing faults (from Stewart and Carlson, 1974).

Cretaceous granitic rocks. Faulting is mainly confined to the mountainous terrain and is fairly dense, as in the central-Nevada circular area.

Twenty-four percent of the linears are accounted for by faulting and 73 percent of the linears that correlate with faults trend north to northeast (north 25 percent; northeast 25 percent; north-northeast 23 percent). The weakest trend is west-northwest. Only 13 percent of the mapped faults were detected by the linears (see tables 1 and 2).

III. Mineral and Esmeralda Counties

Although this sample area (figs. 5 and 8a, b) falls within the Basin and Range physiographic province, the characteristic north to north-northeasterly trends of the ranges are only weakly present. The trends of the ranges are either weakly north-northwest to northwest or curved, and a crudely circular landform near the center of the sample area disrupts any overall trend pattern. The Walker Lane (fig. 9), a northwest-trending right-lateral shear zone which traverses the northeastern half of the sample area, is the cause of this large-scale disruption. This shear zone will be discussed in greater detail in a later section. Because of the more irregular terrain pattern in this sample area, the linears and mapped faults are widely scattered, although the faults are still preferentially located in areas of higher relief. With the exception of the range west of Walker Lake, the apparent relief in the sample

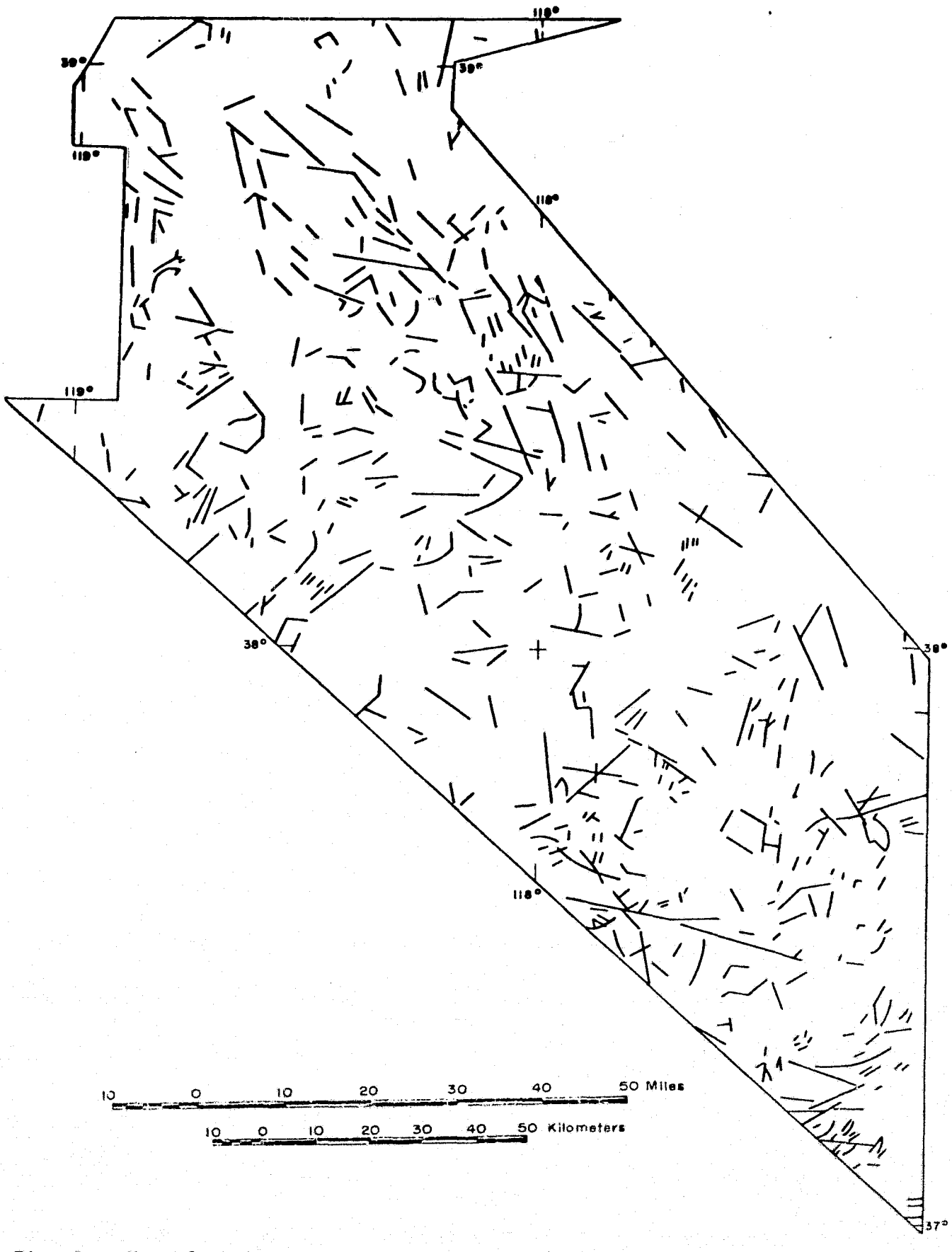

Fig. 8a - Map of study area III showing linear features delineated on ERTS-1 images.

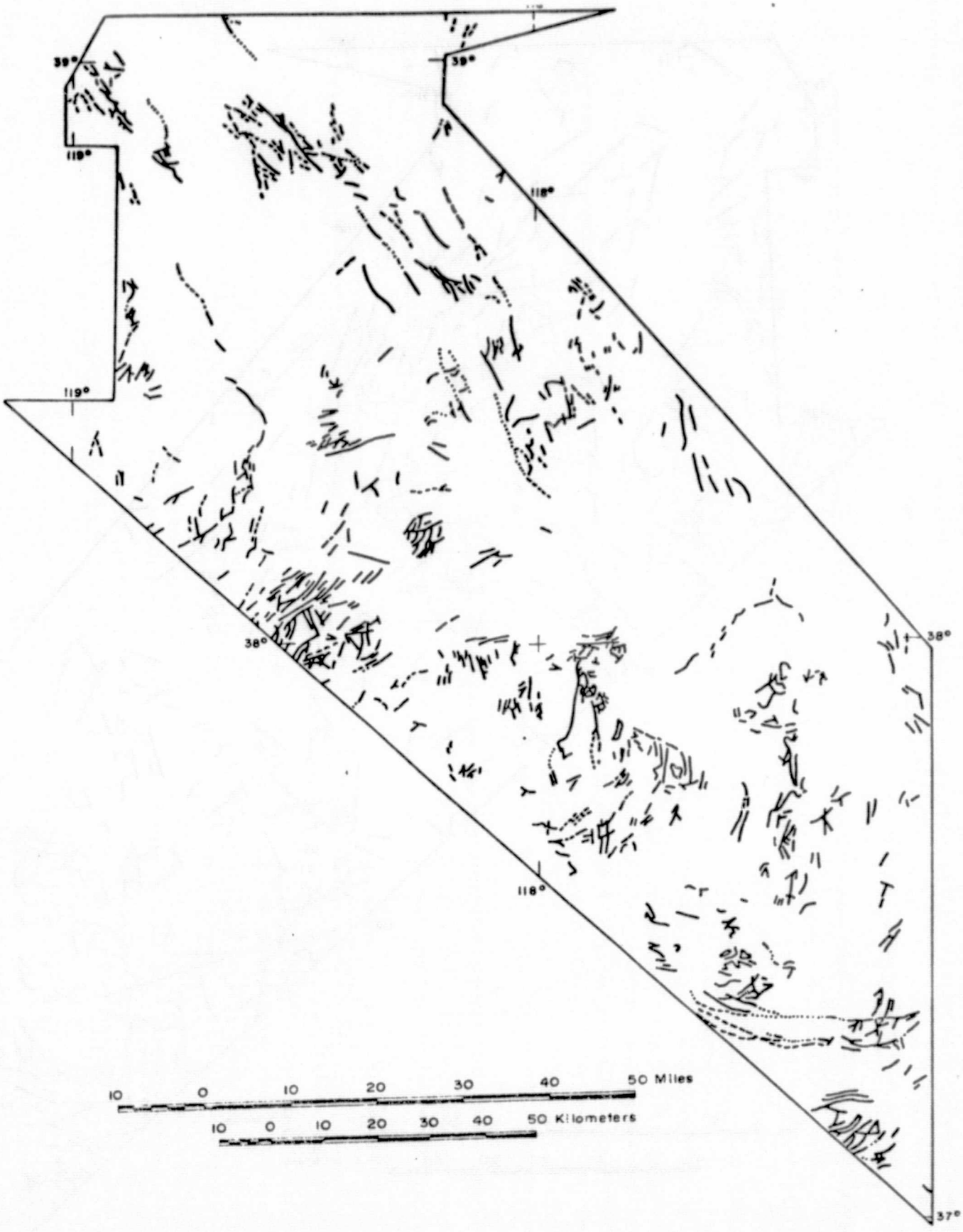

Fig. 8b - Map of study area III showing faults (from Stewart and Carlson, 1974).

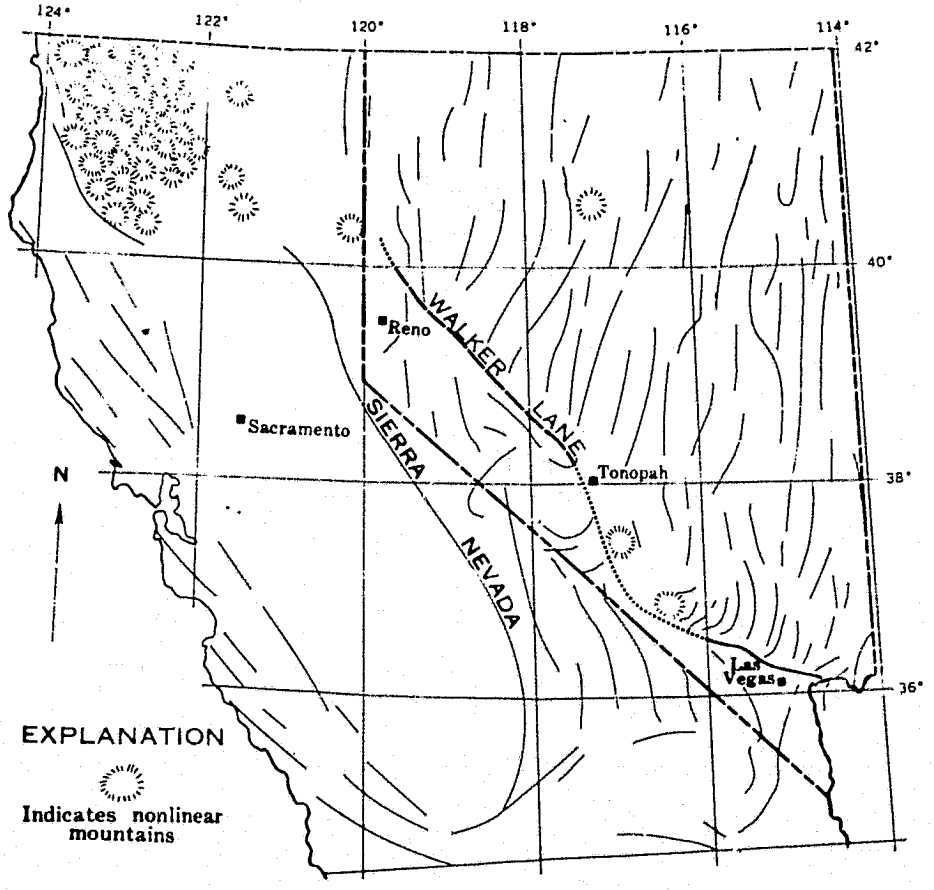

Fig. 9 - Sketch map showing position of Walker Lane and trends in mountain ranges in Nevada and part of California (Albers, 1967)

area is generally lower and less rugged as compared with the first two sample areas.

Mesozoic granitic and sedimentary rocks make up the range west of Walker Lake and the southwestern lobe of the Gabbs Valley Range (Plate 1 and fig. 9). Additional outcrops of granite occur along the southern boundary of the sample area. In the remaining parts of the sample area, dominant units include Tertiary flows of rhyolite, andesite and basalt, ash-flow tuffs, and more recent basalt flows. Outcrops of a Precambrian unit of phyllitic siltstone, quartzite, and lesser amounts of limestone and dolomite are also common, as are inliers of Ordovician siliceous sedimentary and volcanic rocks.

Linears related to faulting constitute 22 percent of the total linears, a figure consistent with the percentages given for the sample areas discussed above. Only 19 percent of the faults were detected by the linears. The dominant trend of the linears that correlate with the faults is north-northeast (27 percent). The northerly and northeasterly trends of the linears are substantially weaker in this area, 17 and 16 percent, respectively, than in the first two areas discussed (see table 1 and 2). Visual examination of the linears and faults reveals that northwesterly and north-northwesterly trends are particularly common along the Walker Lane. Although the overall dominant trend of the linears in the sample area is northeast, the subsidiary Walker Lane trends are reflected in the relatively high percentages of linears with north-northwesterly and northwesterly trends 14 and 9 percent, respectively.

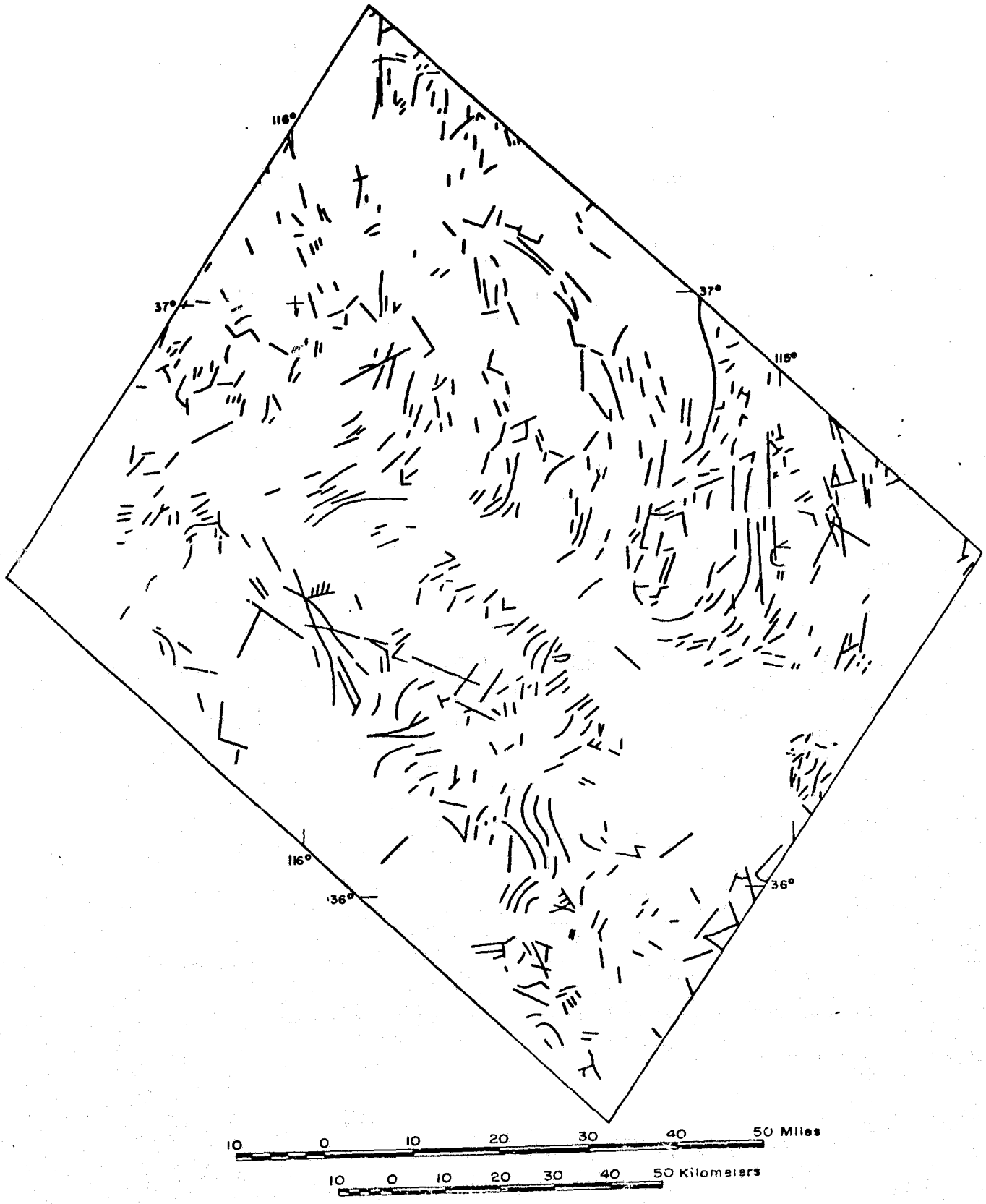

Fig. 10a - Map of study area IV showing linear features delineated on ERTS-1 images.

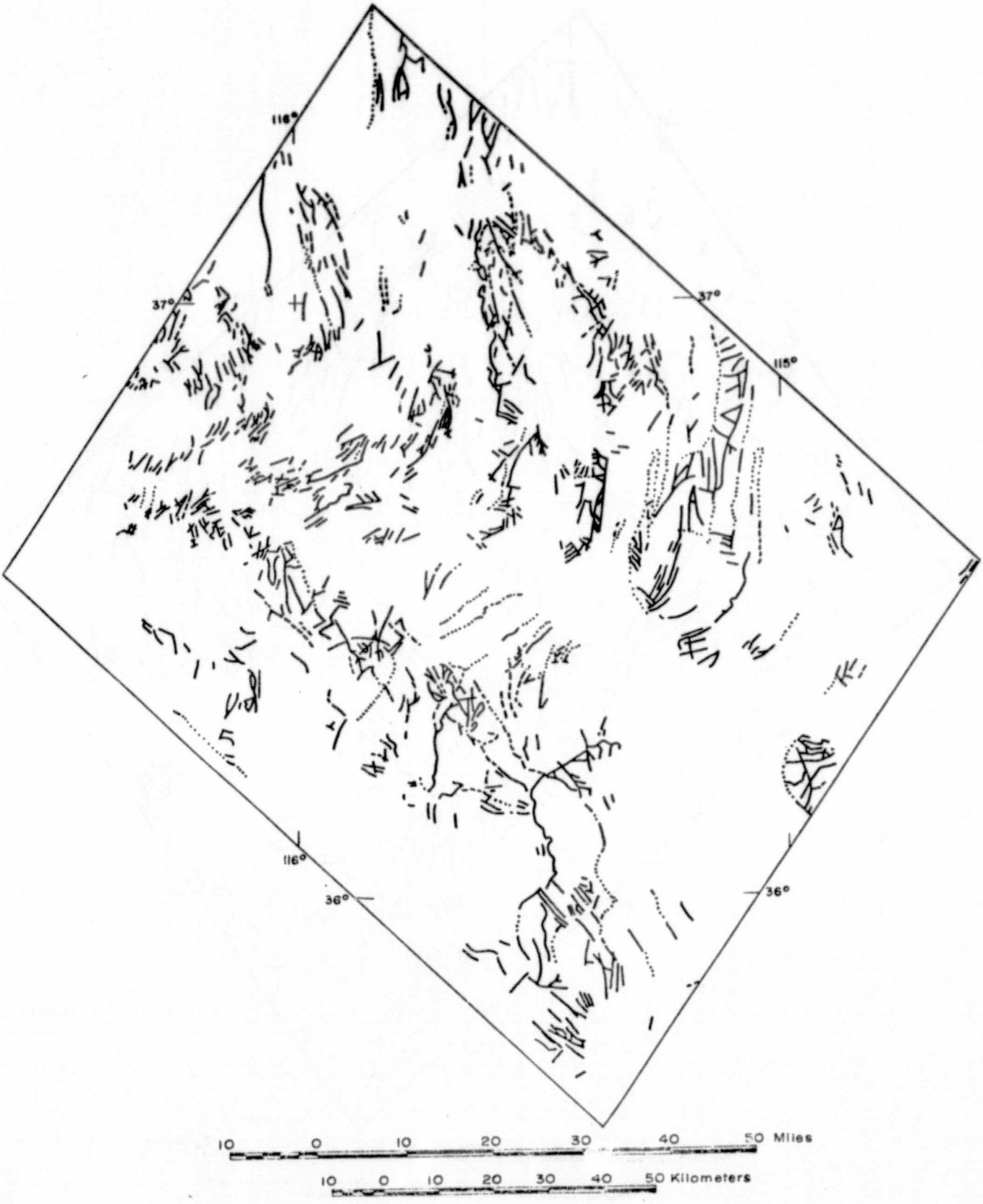

Fig. 10b - Map of study area IV showing faults (from Stewart and Carlson, 1974).

These trends are substantially weaker in four out of the other five sample areas. In the southern part of the sample area, a dominant easterly trend is apparent. Ten percent of the linears that correlate with faults trend east; this is the highest percentage found for the easterly trend as compared with the other sample areas, where the easterly trend is frequently weak. The weakest trend in this area is west-northwest (2 percent).

IV. Las Vegas Valley area

The typical basin and range terrain in this area (figs. 5 and 10a, b) is disrupted by a northwest-trending transcurrent fault zone known as the Las Vegas shear zone. Locke and others (1941) have proposed that this fault zone is the southern extension of the Walker Lane mentioned above. Although the shear zone, which is in the alluvium of Las Vegas Valley, is not directly detected by the linears, the right-lateral character of the shear zone is indicated by the westward deflection of the north-trending ranges of the shear zone.

Geologically, the rocks are almost exclusively a mixture of Paleozoic sedimentary rocks. These units include limestone, dolomite, shale, siltstone, and sandstone, conglomerate, and some quartzite. Faulting is restricted primarily to the ranges and produces a relatively dense, albeit not overly complicated, pattern.

The 30 percent correlation of the linears with mapped faults in this sample area is the highest of all the sample areas. The

high correlation reflects the fact that the faults in this area are typically represented by prominent topographic features. The relatively high percentage of faults (26 percent) detected by linears also reflects this topographic enhancement of structure. The dominant directional trend of the linears that correlate with the faults is overwhelmingly north (39 percent). This is the second strongest correlation of linears with a particular trend in all the six sample areas. Secondary trends are north-northeast (25 percent) and northeast (16 percent). The weakest trends are east-northeast and east (both 1 percent) (see tables 1 and 2).

V. Northern Washoe and western Humboldt Counties

Relatively small north trending ranges in the eastern part of this sample area (figs. 5 and 11a, b) are characteristic of basin and range topography. These ranges are not as high or as rugged as those discussed in the first two sample areas. Main lithologic units to the east include Mesozoic intrusive and extrusive rocks, Tertiary rhyolite and andesite flows, ash-flow tuffs, and upper Tertiary and Quaternary basalt flows. The very different topography of the western part of the sample area bears more of a relationship to the volcanic plains north of this area than to basin and range topography. Relief is subdued; Miocene flows of rhyolite, andesite and basalt are dominant. A unit of ash-flow tuffs and tuffaceous sediments is present in the central part of the sample area.

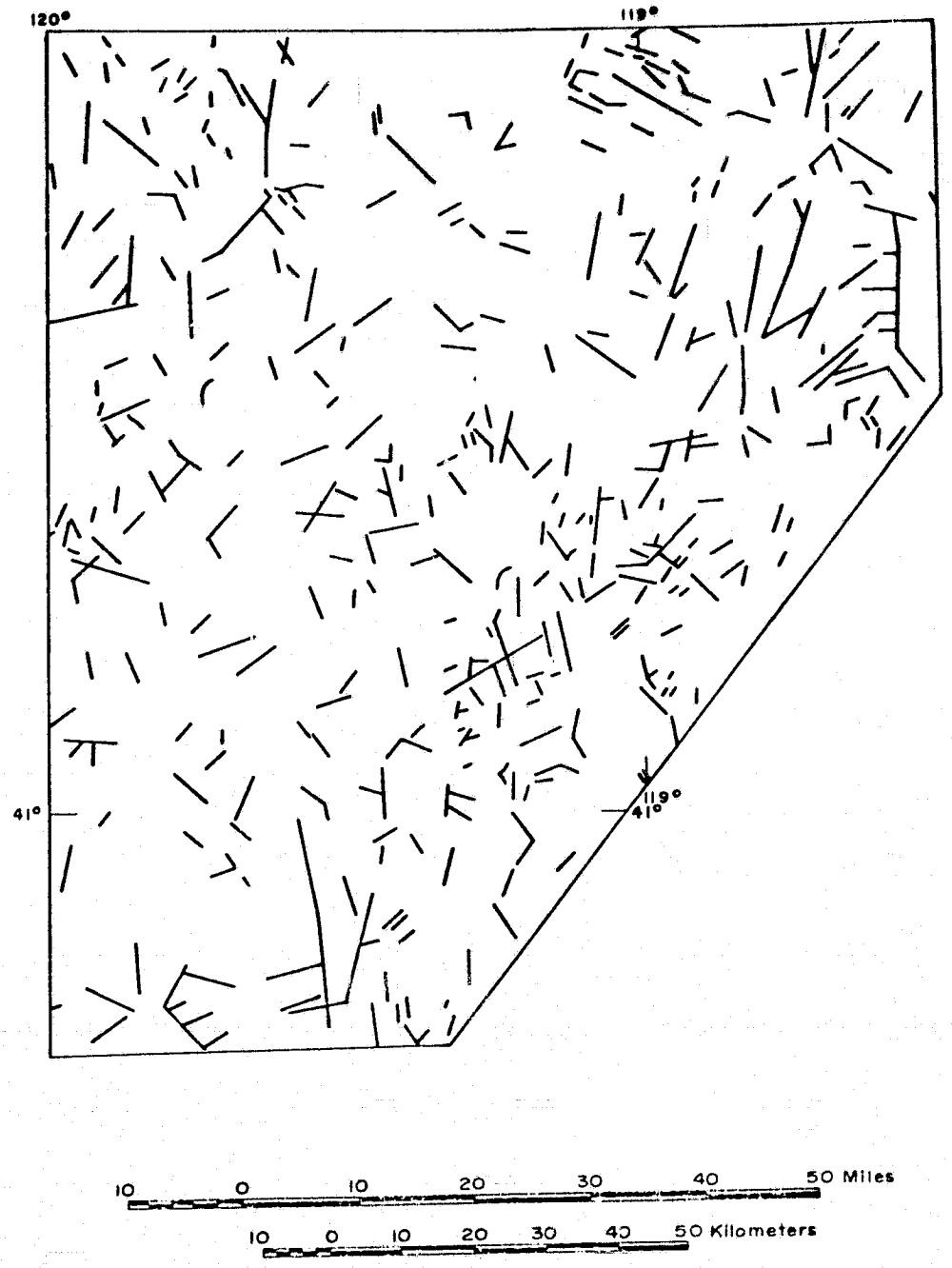

Fig. 11a - Map of study area V showing linear features delineated on ERTS-1 images.

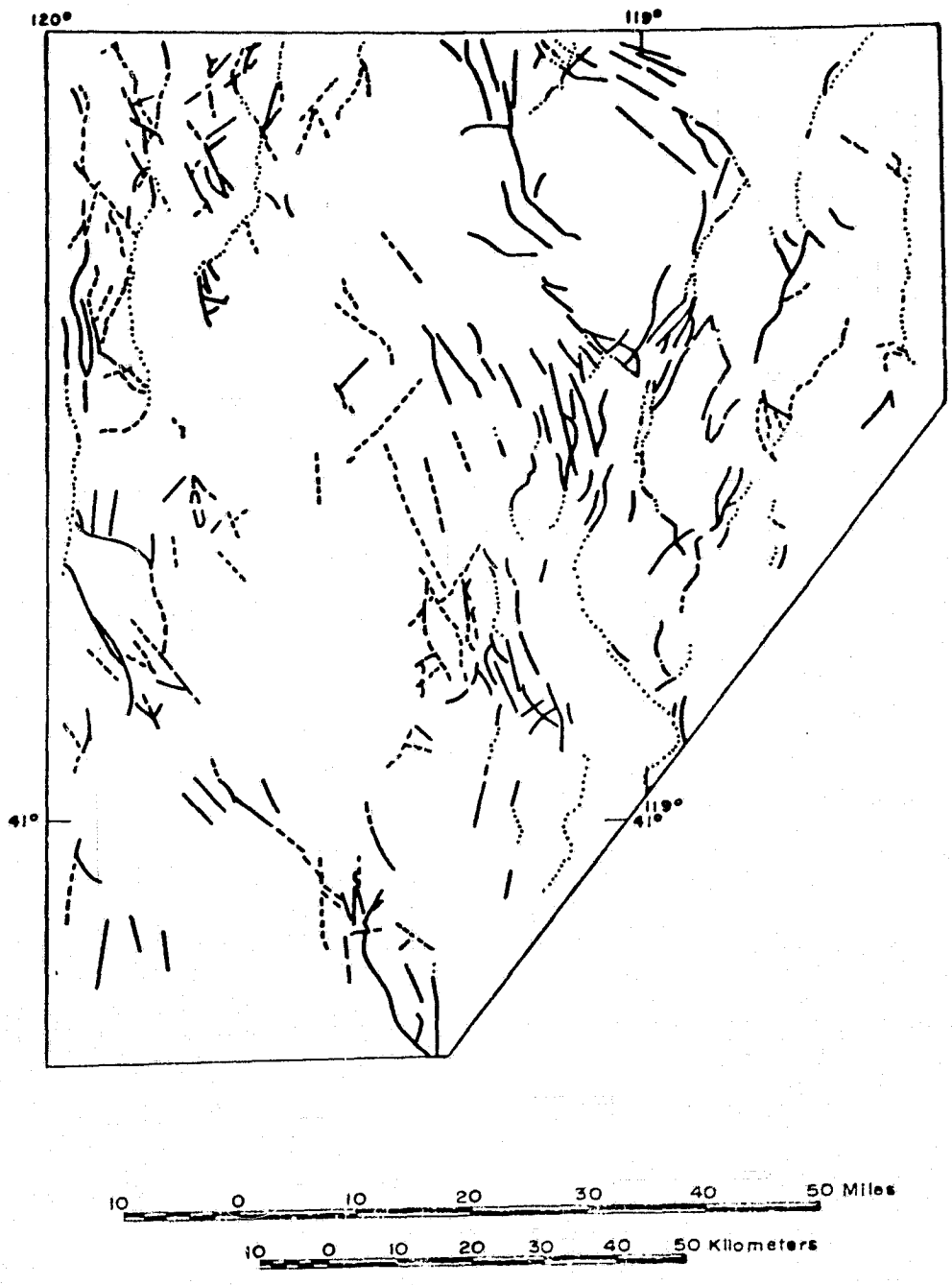

Fig. 11b - Map of study area V showing faults (from Stewart and Carlson, 1974).

The fault pattern of the area is relatively open and apparently uncomplicated. Except for the Pyramid Lake sample area (fig. 5, VI), this area contains the lowest number of faults per square kilometer. The faults themselves are fairly evenly distributed over the area. Unlike any of the other sample areas, relatively few faults are less than 5 km long, and almost one-fifth of the faults are longer than 10 km. In addition, more linears than faults are present in this area, as compared with the previous sample areas discussed.

Correlation of linears with faults, 22 percent, is similar to those of the first three areas discussed. However, a substantially larger percentage of faults, 33 percent, was detected by linears in this area. This high percentage may be attributed to the relatively uncomplicated and open fault pattern, as well as to the frequently long lengths of the faults. The dominant trends are north-northeast (27 percent) and north (26 percent), but north-northwest and northwest trends (17 and 15 percent, respectively) are also prominent. These trends are probably a reflection of the northwesterly structural trend dominant in the volcanic plains to the north in Oregon (Walker, 1973). The weakest trends are west-northwest and east (both 0 percent) (see tables 1 and 2).

VI. Pyramid Lake circular feature

The smallest of the sample areas (figs. 5 and 12a, b) covers 11,000 sq km of relatively low relief basin and range topography. Except for the easternmost range, the predominantly north-trending ranges are smaller and less rugged than those discussed in the first two sample areas. The area includes a substantial amount of alluvium. Topography is responsible for the circular appearance.

A wide variety of rock types occurs within the circular area. Mesozoic sedimentary and granitic rocks are fairly evenly distributed within the area, although a Miocene unit of basalt and andesite flows almost exclusively covers the far southern and western parts. Less frequently occurring units include Tertiary rhyolite and andesite flows and a unit of ash-flow tuffs and sedimentary rocks.

This area contains the fewest linears and faults per square kilometer and, unlike the other sample areas, 66 percent more linears than faults have been detected. This relative abundance of linears may partially explain why the highest percentage (40 percent) of faults was detected by linears in this sample area. In addition, many of the faults in this particular area are easily detectable boundary faults between a range and alluvium. Twenty-five percent of the linears are related to faulting and the dominant trends are north-northeast (42 percent) and north (37 percent). Weakest trends are east-northeast and east (both 0 percent) (See tables 1 and 2).

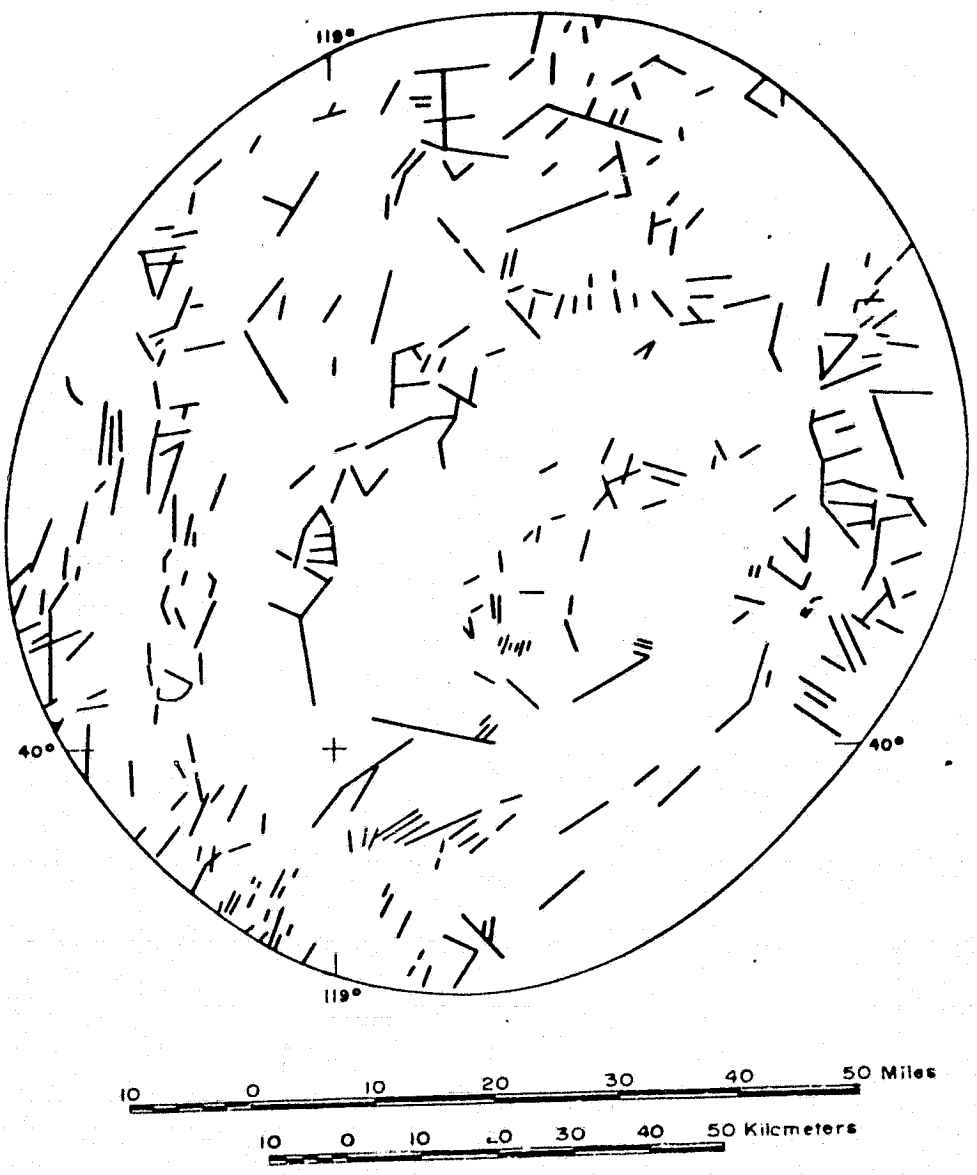

Fig. 12a - Map of study area VI showing linear features delineated on ERTS-1 images.

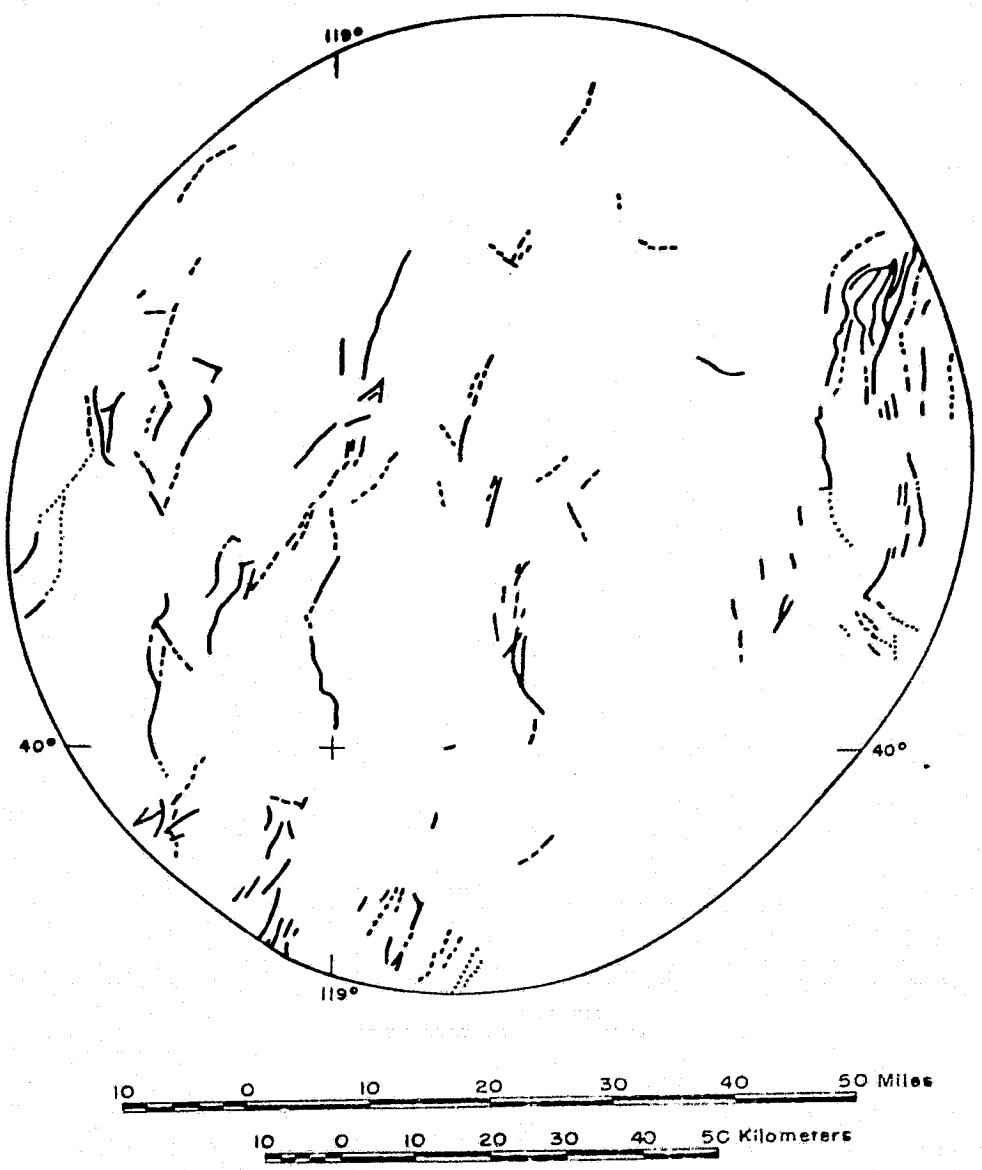

Fig. 12b - Map of study area VI showing faults (from Stewart and Carlson, 1974).

Discussion

The six sample areas fall almost exclusively within the Basin and Range physiographic province and reflect in varying degrees the characteristic topography of the province. The sample area defined by the circle in central Nevada (fig. 5, I) is the most representative of the typical basin and range topography with its north-to north-northeast trending ranges and evenly spaced intermontane alluvial valleys. On the other hand, the terrain covered by Mineral and Esmeralda Counties (fig. 5, III) and by the Las Vegas Valley area (fig. 5, IV), although containing elements of basin and range physiography, is noticeably distorted by the Walker Lane, a right-lateral shear zone. Even further removed from the typical basin and range landform pattern are the sample areas in western Elko County (fig. 5, II) and northern Washoe and western Humboldt Counties (fig. 5, V). The topography of these two areas, which are close to the northern boundary of the Basin and Range province, appears to have been influenced more by the structural grain and physiography of the neighboring province of volcanic plains than by that characteristic of the Basin and Range province. The terrain of the sixth sample area, the Pyramid Lake circular feature (fig. 5, VI), is the most difficult to characterize. Although the dominant structural trends are compatible with those typical of the Basin and Range province, the physiography of the area has an overall appearance that is not obviously typical basin and range type terrain.

The dominant regional trends as determined from the linears correlating with faults in all the six sample areas (table 2) reflect the north to north-northeast trends characteristic of the Basin and Range province. Additional strong northeasterly trends are present in the central Nevada circle (fig. 5, I) western Elko County (fig. 5, II), and to a lesser extent in Mineral and Esmeralda Counties (fig. 5, III) and in the Las Vegas Valley area (fig. 5, IV). Noteworthy secondary trends of north-northwest and northwest are present in Mineral and Esmeralda Counties (fig. 5, III) and in the northern Washoe and western Humboldt Counties (fig. 5, V). The trends in these two particular areas are due respectively to the influence of the north-northwest-trending Walker Lane and the dominant northwest structural grain of the volcanic province in northwestern Oregon. However, the north-northwest and northwest trends are not strong in the Las Vegas Valley area (fig. 5, IV), even though the southeastern extension of the Walker Lane passes through the area; the shear zone is only manifested in the minor drag westward of the predominantly north-trending faults. The weakest trends in the six sample areas are east (Pyramid Lake circular feature and the Las Vegas Valley area), west-northwest (central Nevada circular feature and western Elko County), and east-northeast (Las Vegas Valley area, northern Washoe and western Humboldt Counties, and the Pyramid Lake circular feature).

The percentages of faults detected by the linears (table 1) range from 13 percent (western Elko County) to 40 percent (Pyramid Lake circular feature), averaging 24.3 percent for all six areas. The degree of correlation is affected by the length of the faults in each area and, to a lesser degree, by the dominant type of faulting in each area. Mapped faults on the State geologic map of Nevada at 1:1,000,000 scale range in length in the sample areas from approximately 1/2 km to 40 km, whereas the linears range in length from approximately 2 km to 30 km. Therefore, in the sample areas having a preponderance of very short faults, as in the central Nevada circle and in western Elko County, it is not surprising that fewer faults are detected (15 and 13 percent, respectively) by the linears than in other sample areas. In the Pyramid Lake circle and northern Washoe and western Humboldt Counties, the correlation is more than twice as good (40 and 33 percent, respectively). Virtually all the mapped faults in these two sample areas are longer than 2 km, and the average length is much longer. The type of faulting present also affects the number of faults detected by linears. Thrust faults in particular are much less easily detectable than are normal and transcurrent faults because thrusts are often nonlinear and because their topographic expression is typically subdued. In the two areas mentioned above, in which fault detection is relatively poor, some thrust faulting is present. However, thrust faults are completely absent from the two sample areas having the best fault correlation.

In summary, linears compiled for the six sample areas without regard for length show 24.3 percent correspondence with mapped faults; the same percentage of faults was detected by these linear features, a striking but meaningless coincidence. These low average values suggest considerable caution when interpreting the significance of such linears. In addition, because of the high density of faults and linears in many areas, some of the correspondence is probably random, which would reduce these values even further.

Analysis of Major Lineaments

Mosaicking of the already synoptic ERTS images permits detection of a set of large-scale linear and curvilinear features, referred to as major lineaments (fig. 3). Three hundred sixty-seven major lineaments, several of which are more than 100 km long, have been evaluated in the State of Nevada with respect to their geologic nature and origin. The lineaments were initially compiled on a band 5 image mosaic of Nevada at 1:1,000,000 scale. They were subsequently checked and reevaluated using individual 1:1,000,000-scale band 5 and 7 images, a 1:500,000-scale enlargement of the mosaic, and 1:250,000-scale topographic sheets. Linear features due to cultural features or scan lines (west-northwesterly trend) were removed. The more interpretive lineaments were designated major lineament zones.

A derivative overlay (fig. 13) was prepared showing the correspondence of mapped faults on the State geologic map of Nevada with the major lineaments. Correlation of a fault with a lineament was determined on the basis of an approximately parallel trend and a location within one line width (about 1/2 km) of the related lineament. Lineaments and parts of lineaments that represent extensions of mapped faults are noted as such on the overlay and were counted as a correlation. Analysis reveals a 79.9 percent agreement between the major lineaments and mapped faults. The topographically distinct boundary faults typical

Fig. 13 - Map showing correlation of major lineaments with faults ≥ 10 km in length. Faults mapped by Stewart and Carlson (1974)

of the Basin and Range province are at least in part responsible for the high correlation of lineaments with faults. The faults that correlate with the lineaments include 122 normal faults, 42 thrust faults, and 2 transcurrent faults. However, by far the largest number of related faults are undefined as to type. The remaining 20.1 percent of the lineaments appear to be unrelated to known faults.

Lengths of the faults detected by the lineaments are fairly evenly distributed within a range of 2 to 80 km. A series of small nearly parallel faults and their extensions frequently makes up a lineament. However, most of the longer faults correlate exclusively with one lineament. Those longer faults that do not relate to a lineament were missed either because the trace of the fault is not linear, as is the case for many of the thrust faults in Nevada, or because the fault, or part of the fault, has little or no morphological expression. For example, the Las Vegas shear zone occurs exclusively within alluvium, which provides no physiographic evidence for the presence of shearing. Undetected faults longer than 10 km are most commonly in the 10-to 15-km range. Most of the faults bounding the mountain ranges were detected; exceptions are generally those faults that have minimal topographic expression or that are in areas in which the boundry between the range and the alluvium is extremely irregular, even though locally sharply defined. Large areas in which many faults longer than 10 km were missed include most of Washoe County, especially in the north,

and Lincoln County. Faults longer than 10 km are relatively numerous in these two areas.

Whereas 79.9 percent of the major lineaments can be correlated with faults, only 7.4 percent can be related to lithological boundaries, excluding those boundaries between outcrop and alluvium. In most places, almost the entire length of the boundary was detected.

An azimuth-frequency analysis has been carried out by computer for the major lineaments. The end points of each lineament were digitized by using a grid base. Curvilinear lineaments were digitized by dividing them into their component straight sections, which resulted in an increase in the total data set from 367 to 508 lineaments. Strike frequency was calculated for these data at 1 degree intervals, and a running mean was subsequently applied. Results (fig. 14) show that the most common azimuth is due north. Secondary peaks occur at N.12°W. and N.20°E., the latter being slightly stronger than the former. The least frequently occurring azimuth is around N.60°W. More generalized strike frequencies are shown in table 3. The dominant northerly and north-northeasterly trends are consistent with those of the basin and range type structure which the lineaments reflect.

Trends of those faults longer than 10 km that correlate as a whole or in part with a lineament are also dominantly northward (29 percent, table 3): northeasterly trends are secondary (19.2 percent. The only direction in which faults were not detected is

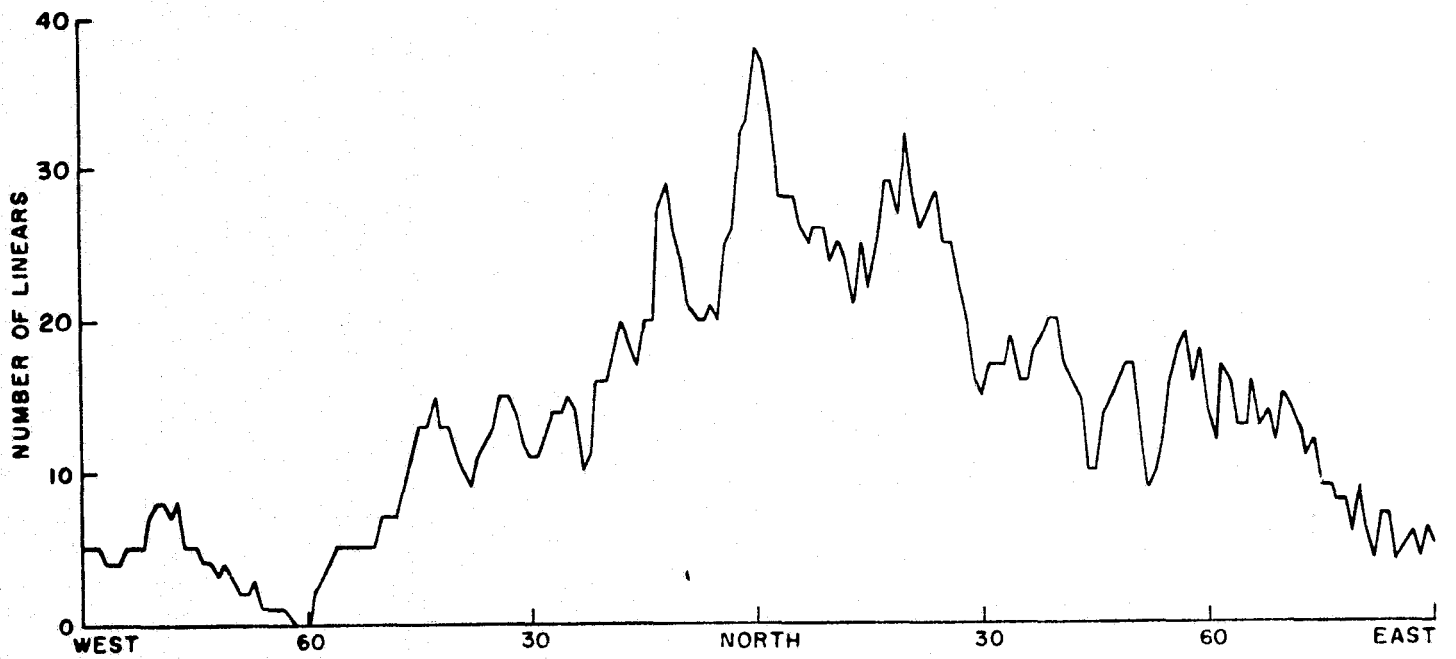

Fig. 14 - Strike-frequency distribution of major lineaments mapped in Nevada (see fig. 3). Percent azimuth for smoothing = 0.01. n = 508.

west-northwest, but relatively few mapped faults trend in this direction (1.9 percent).

Although a total of 172 faults longer than 10 km relate to the major lineaments, 415 faults longer than 10 km were not detected. Therefore, only 29.3 percent of all these faults correspond to major lineaments. The northerly trend of the faults missed is dominant (31.3 percent), having a percentage very similar to that of the faults detected. The north-northeasterly trends, however, are relatively stronger (16.6 percent) for the faults missed as compared with the faults detected (13.4 percent), and the northeasterly trend is markedly weaker (7.7 percent missed versus 19.2 percent detected). The relatively low percentage of faults missed in the northeasterly direction and also in an east-northeasterly direction may be related to the sun azimuth angle at the time the data were recorded. The mosaic used for the analysis of the lineaments is made up of fall imagery in which the solar azimuth is on the order of 145° (shadows cast northwestward), and approximate sun elevation is 42°. A preferential enhancement of topography perpendicular to the sun's azimuth is to be expected. Hence, it is not surprising that proportionately more faults with northeasterly and north-northeasterly trends were detected than missed. In addition, a larger percentage of faults with northeasterly and east-northeasterly trends were detected (19.2 percent and 9.3 percent) than expected on the basis of the relative proportion of occurrence of mapped faults with these trends (11.1 percent

Table 3: General trends (in percent) of major lineaments and of faults longer than 10 km in the State geologic map of Nevada.

		E	WNW	NW	NNW	N	NNE	NE	ENE	NO DIRECTION DETERMINABLE	TOTAL NUMBER OF FEATURES
MAJOR LINEAMENTS		4.7	2.6	8.5	14.4	23.6	21.1	13.2	12.0	--	508
FAULTS > 10 km	total faults	1.7	1.9	8.3	14.8	30.7	15.7	11.1	4.6	11.2	587
	faults detected	3.5 (1.0)	0	11.0 (3.2)	12.8 (3.7)	29.1 (8.5)	13.4 (3.9)	19.2 (5.6)	9.3 (2.7)	1.7 (0.5)	172
	faults missed	1.0 (0.7)	2.7 (1.9)	7.2 (5.1)	15.7 (11.1)	31.3 (22.1)	16.6 (11.8)	7.7 (5.5)	2.7 (1.9)	15.2 (10.7)	415

Table 4: Major lineaments having a single origin shown as percentages of the total major lineaments (367).

BOUNDARY BETWEEN OUTCROP AND ALLUVIUM	RIDGE	CANYONS			STREAM SEGMENT	TONAL BOUNDARY
		PARALLEL TO RANGE TREND	TRAVERSE TO RANGE TREND	TOTAL		
36.8 (56.7)	14.2 (21.8)	2.5 (3.8)	2.5 (3.8)	4.9 (7.6)	0.8 (1.3)	8.2 (12.6)

and 4.6 percent). A large number of faults (15.2 percent), many of which are thrust faults, were not detected by lineaments because of their typically irregular nonlinear surface trace.

Analysis as to the origin of the major lineaments has been carried out using individual 1:1,000,000-scale images of various seasons, 1:250:000-scale topographic sheets, the State geologic map of Nevada at scale 1:1,000,000, and other geologic maps for specific areas. Several categories appear to encompass all of the lineament origins.

These are:

1) Boundary between outcrop and alluvium, predominantly that between basin and range;

2) Mountain ridge or series of small ridges. Escarpments make up a minor part of this category;

3) Mountain canyons, either parallel or transverse to the trend of the range;

4) Stream segments;

5) Tonal boundaries, alluvial and nonalluvial

A primary division of the lineament data was made in order to separate those lineaments having a single origin from those having a compound origin.

Of the major lineaments, 64.9 percent have a single origin. The most common single cause of a lineament is the boundary between outcrop and alluvium, encompassing 36.8 percent (table 4) of all the major lineaments. The basin and range type terrain is responsible for the predominance of this category. Linear

ridges are the second most frequent cause of the lineaments, (14.2 percent). Tonal boundaries represent only 8.2 percent, of which 7.4 percent are nonalluvial tonal features. Few canyons (4.9 percent) are the sole reason for a lineament, and, of these, equal numbers of canyons parallel and transverse to the trend of the range have been detected. Only 0.8 percent of the major lineaments can be attributed to a stream segment along.

Of the major lineaments, 35.1 percent have compound origins. Of these, 21.8 percent represent lineaments with a two-component origin (table 5). The most common combinations of two categories are the boundary between alluvium and outcrop coupled with the tonal boundary (21.3 percent), followed by the ridge and tonal boundary combination (15.0 percent). These figures are consistent with those categories most common for single causes of lineaments. A stream segment plus a canyon (usually transverse) and a stream segment plus a tonal boundary are the next most common combinations (both 13.8 percent). The tonal boundary pairs with more categories than any other. This situation is not surprising because the tonal nonalluvial category is the least well defined category as far as its origins are concerned.

Of the major lineaments, 8.4 percent have three-component origins (table 6). The most frequent combinations by far are

Table 5: Major lineaments having a two-component origin shown as percentages of the total major lineaments (367)

	BOUNDARY BETWEEN OUTCROP AND ALLUVIUM	RIDGE	CANYON	STREAM SEGMENT	TONAL BOUNDARY	TOTAL
BOUNDARY BETWEEN OUTCROP AND ALLUVIUM	--	1.4 (6.3)	0.8 (3.8)	1.4 (6.3)	4.6 (21.3)	8.2 (37.5)
RIDGE	1.4 (6.3)	--	1.4 (6.3)	1.4 (6.3)	3.3 (15.0)	7.4 (33.8)
CANYON	0.8 (3.8)	1.4 (6.3)	--	3.0 (13.8)	1.6 (7.5)	6.8 (31.3)
STREAM SEGMENT	1.4 (6.3)	1.4 (6.3)	3.0 (13.8)		3.0 (13.8)	8.7 (40.0)
TONAL BOUNDARY	4.6 (21.3)	3.3 (15.0)	1.6 (7.5)	3.0 (13.8)		12.5 (57.5)

Table 6: Percent distribution of lineaments having a three-component origin (total of 31)

FEATURES	PERCENT
Boundary-canyon-ridge	6.5
Boundary-canyon-stream	22.6
Boundary-canyon-tonal	12.9
Boundary-ridge-stream	---
Boundary-ridge-tonal	3.2
Boundary-stream-tonal	9.7
Canyon-ridge-stream	29.0
Canyon-ridge-tonal	3.2
Canyon-stream-tonal	9.7
Ridge-stream-tonal	3.2

Table 7: Percent distribution of lineaments having a four-component origin (total of 16)

FEATURES	PERCENT
Canyon-stream-tonal-ridge	43.8
Canyon-stream-tonal-boundary	37.5
Canyon-stream-ridge-boundary	12.5
Canyon-tonal-ridge-boundry	6.3

ridges-canyons-streams (29 percent) and boundaries-canyon-streams (22.6 percent). The predominance of these combinations illustrate the dominant influence of topography in the detection of lineaments. All the other combinations appear secondary. Four combinations of four categories comprise only 16 lineaments (table 7). Only two lineaments include all five categories along their lengths.

Major lineaments have substantially higher correlation with mapped faults than do all linear features. This fact suggests that much more confidence can be placed in structural interpretations of these more continuous features. Extension of locally mapped faults along major lineaments results in many major fault or fracture zones in Nevada. Moreover, the high correlation with faults suggests that many of the major lineaments that have not been related to mapped faults may be undetected faults, some of which would be tens of kilometers long. In contrast to the encouraging results however, it must be noted that only 29.3 percent of the faults longer than 10 km on the State geologic map were detected in this compilation, only a slight improvement over the result for all linear features (24.3 percent). Therefore, although analysis of major lineaments should contribute measurably to regional structural studies, this approach is not a substitute for mapping in the field.

Seven major lineament systems (fig. 15) warrant further examination with respect to the regional structural implications of the major lineaments. These systems, or zones, were selected on the basis of their regional extent and their correlation commonly with geophysical data and with zones of aligned faults. Generally, they transect the north to north-northeast-trending Cenozoic basin and range topography, and all but one extend for several hundred kilometers.

Three of these lineament systems have already been documented as major crustal features. These are the Walker Lane (A, fig. 15), the Midas Trench system (B, fig. 15), and the Oregon-Nevada lineament (C, fig. 15).

The Walker Lane (fig. 9) was first recognized by Gianella and Callaghan (1934) and was given its name by Locke and others (1940). This northwest-to north-northwest-trending zone of right-lateral transcurrent faulting traverses approximately 600 km from Pyramid Lake to Las Vegas (Gianella and Callaghan, 1934; Locke and others, 1940; Nielsen, 1965; Shawe, 1965; Albers, 1967), essentially paralleling the San Andreas fault system (fig. 9) to which it may be related. The Walker Lane is expressed topographically by a distinct northwest-trending discontinuity, easily visible on the ERTS mosaic of Nevada (fig. 4). The northerly to north-northeasterly trends typical of the Basin and Range province are abruptly disrupted by this zone, in which ranges are oriented predominantly northwestward. Predominantly

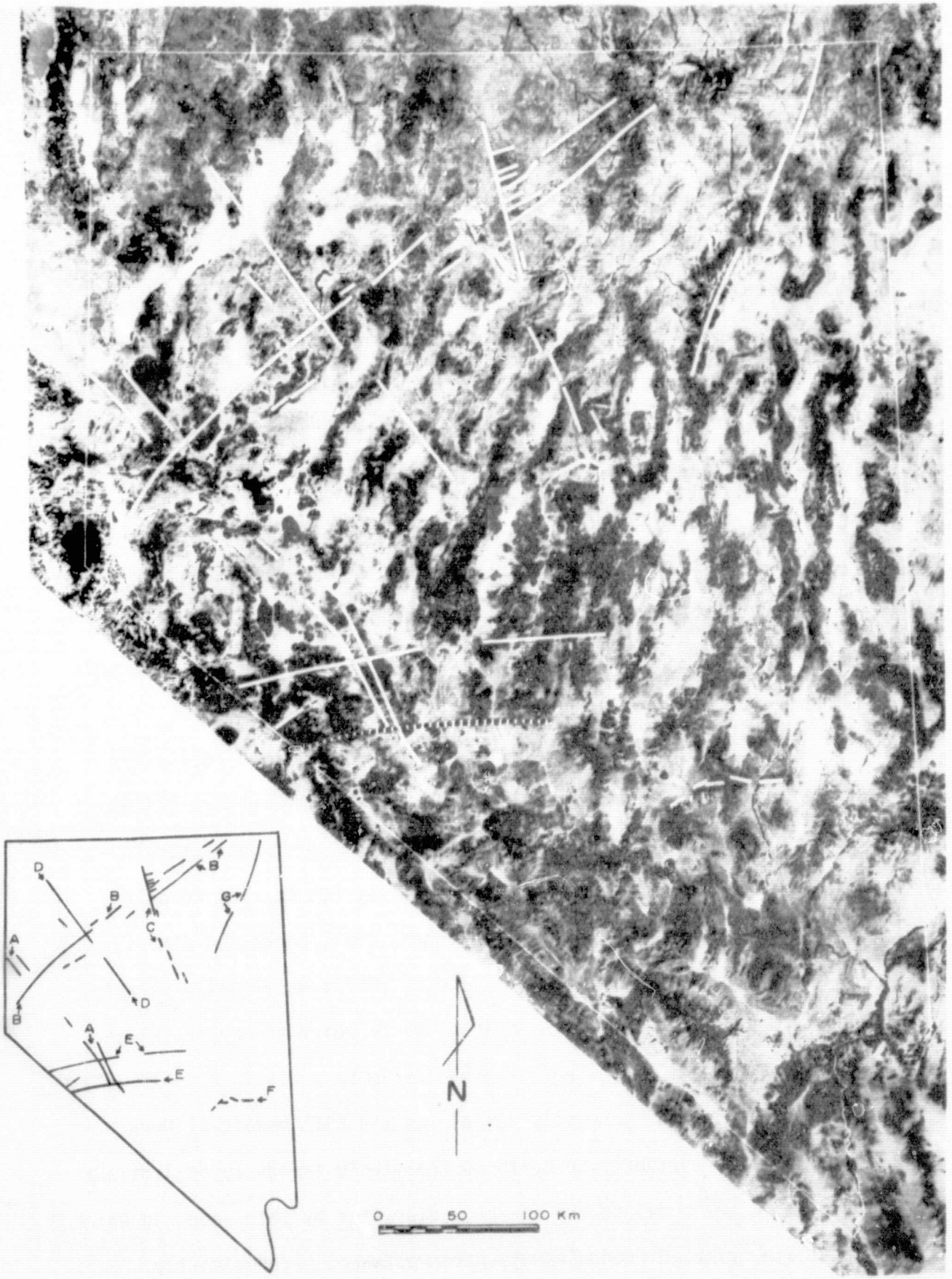

Fig. 15 - Major lineament systems in Nevada: A, Walker Lane; B, Midas Trench; C, Oregon-Nevada; D, Rye Patch; E, ENE-trending; F, E-W trending; and G, Ruby Mountains. Plotted on ERTS-1 mosaic prepared by Aerial Photographers of Nevada, Reno, Nevada, from band 5 images recorded in September and October, 1972.

northwest-trending alignments of magnetic highs characterize the Walker Lane between Reno and Goldfield with an obvious easterly component (fig. 16).

Evidence of right-lateral movement is discontinuous along the length of the Walker Lane. The primary areas of known strike-slip movement occur southwest of Pyramid Lake (Gimlett, 1967; Stewart and Carlson, 1974), along the Gabbs Valley Range and Soda Springs Valley (Nielsen, 1965), and along the Las Vegas Valley (Longwell, 1960; Burchfiel, 1965). A pair of parallel northwest-trending major lineaments has been detected in each of the first two areas (fig. 15). The two pairs correspond well with right-lateral strike-slip faults mapped by Stewart and Carlson (1974) and Nielsen (1965) in the respective areas. Southeast of the Gabbs Valley Range lineament pair, two curvilinear lineaments (fig. 13) lie orthogonal to the pair, obscuring extension of the Walker Lane southeast. These features reflect a belt of large-scale sigmoidal bends (fig. 17) caused by the dextral drag along the Walker Lane (Albers, 1967; Stewart, 1967; Stewart and others, 1968). Albers (1967) suggested that deformation may have been initiated as long ago as late Early Jurassic and that the bending and major lateral faulting were essentially over by early or middle Miocene time; recent movements involve faulting alone. Displacement due to the deformation is estimated at 80-120 miles (Albers, 1967).

No major lineament directly reflects the third area of known strike-slip movement along the Walker Lane, the Las Vegas Valley

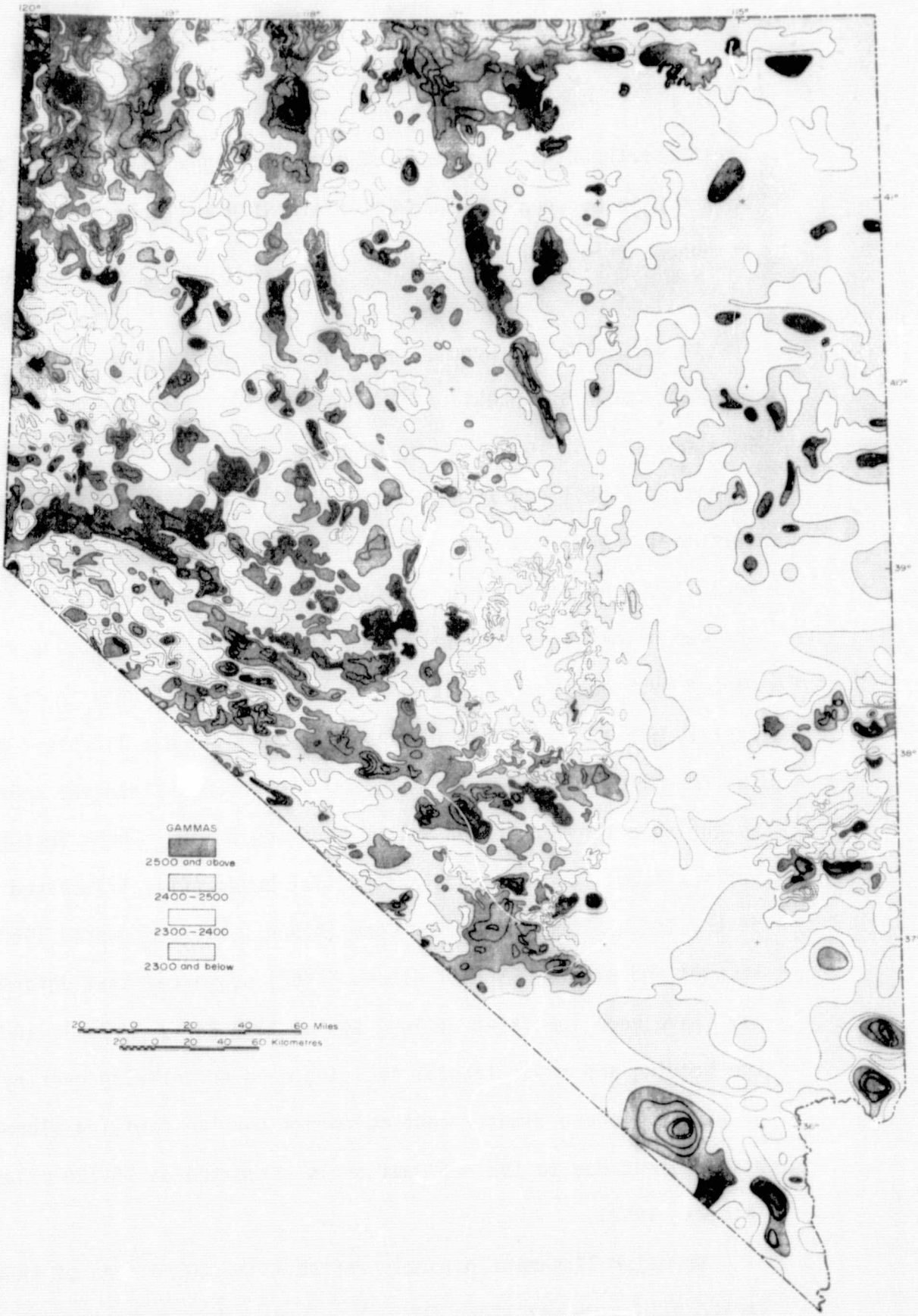

Fig. 16 - Total-intensity aeromagnetic map of Nevada. Contour interval 100 milligals (Zietz, written communication, 1974). Originally compiled at 1:1,000,000 scale.

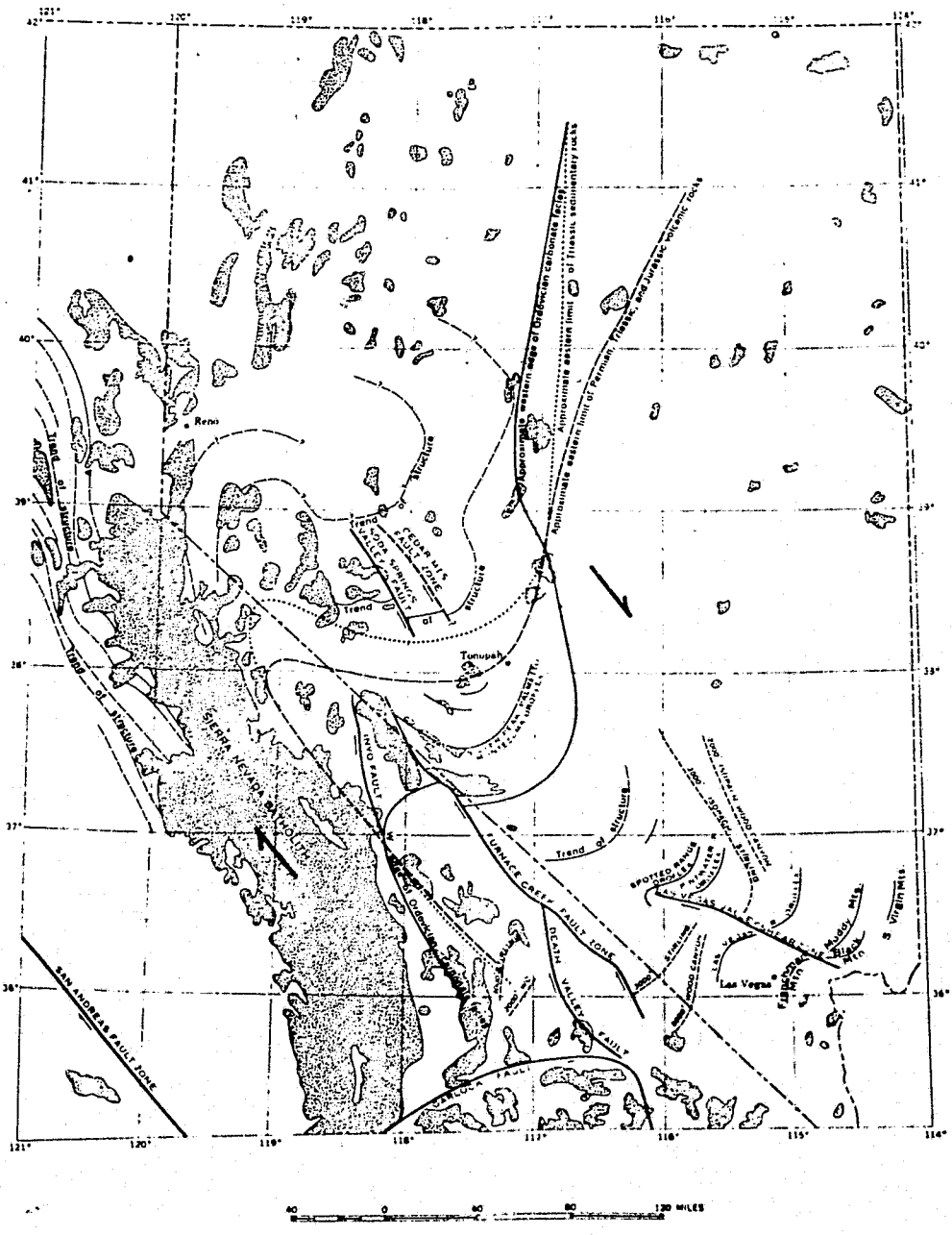

Fig. 17 - Summary of structural features along the mobile belt east of the Sierra Nevada showing sigmoidal bending. Stippled areas granitic plutonic rocks (Albers, 1967).

shear zone. However, the associated drag to the west in the north-trending mountain ranges north of the shear zone is evidenced by lineaments in these ranges. Stewart (1967) called attention to the dextral bending and offset of formations as old as Precambrian in this area. Whether the right-lateral faulting in the Las Vegas Valley, which is at least 200 km southeast of the Gabbs Valley Range lineament pair, should be included as part of the Walker Lane is somewhat controversial. A westward extension of the Las Vegas Valley shear zone northwest beyond the Spector Range is obscured by alluvium and upper Cenozoic volcanic rocks. In addition, the average strike of the Las Vegas Valley shear zone is N.60°-70°W., whereas that of the Walker Lane in the Soda Springs area is substantially different (N.21°W.) (Burchfiel, 1965). Nevertheless, most geologists believe that the right-lateral movement across southern Nevada reflects a single structural zone . We accept this interpretation, and subsequent references to the Walker Lane include the entire length of the Walker Lane-Las Vegas zones.

The Midas Trench lineament zone (Rowan and Wetlaufer, 1973) extends roughly from Lake Tahoe to the northern State boundary, traversing approximately 460 km. It is most conspicuous in north-central Nevada where it is expressed as a linear topographic depression near Midas and as an escarpment to the northwest which separates the Owhyee Desert from the mountains to the southeast. Near the northeastern

Nevada border, the lineaments reflect aligned stream segments in the mountains. Good correlation of mapped faults with lineaments over this area gives credence to the zone as an important structural feature. The average strike of the Midas Trench system is N.50°E.

The less distinct southwestern extension of the lineament system is expressed as a discontinuous series of linear canyons and ridges in the ranges. Tonal changes in the intervening alluvium permit delineation of a continuous zone which intersects the Walker Lane just south of Pyramid Lake. Only a few faults correlate with this part of the lineament system. Additional evidence for this structural zone is the approximately northeast oriented roof pendant of metamorphosed Mesozoic rocks in the Carson Range at the southern end of the lineament system (Shawe, 1965). Structures in other Sierra Nevada metamorphic rocks have prevalent northerly to north-northwesterly orientations.

On the basis of topographic map patterns, Shawe (1965) referred to a transverse lineament that had a location and orientation similar to those of the central part of the Midas Trench lineament zone. Another lineament proposed by Shawe parallels the southwestern part of the Midas Trench lineament system. He postulated that both lineaments represent left-lateral strike-slip fault zones. Recent lateral movement was suggested by Slemmons (1967) along several northeast-trending faults near Midas, and in the Pah Rah Range, south of Pyramid Lake, Bonham (1969) noted left-lateral offsets of

stream channels as much as 15 feet along east-northeasterly trending faults. However, geologic maps covering the Midas Trench lineament zone suggest dip-slip and possible right-lateral shear movements along the mapped northeast-trending faults, thereby leaving the sense of movement within the Midas Trench lineament zone unclear (Stewart and Carlson, 1974; Decker, 1962; Coats, 1964; Bushnell, 1967; Tatlock, 1969; Bonham, 1969).

Several lines of geophysical evidence have contributed to the concept that the Midas Trench lineament zone is a major crustal feature. Seismic data (Koizumi and others, 1973; Hill and Pakiser, 1967) indicate a major structural discontinuity extending from Lovelock to Mountain City. Koizumi and others (1973) interpreted the discontinuity as a high-velocity lithospheric plate having a dip of 60°-70° SE. and a slab length of at least 150 km. According to Ryall and others (1973), the highest heat flow values in the western United States have been detected above this proposed paleosubduction zone, and the physiography, structure, and predominant type of volcanism are notably different on either side of the zone. Additional seismic data has been compiled (Prodehl, 1970) to produce a crustal-velocity contour map (fig. 18) in which the 2-second contour line corresponds with the location and orientation of the Midas Trench lineament zone.

Projection of the lineament zone northeast beyond the study area corresponds with the southeastern margin of the somewhat anomalous Snake River Plains and extends into Yellowstone Park, a former volcanic center and an area of anomalously high heat flow. Christiansen and

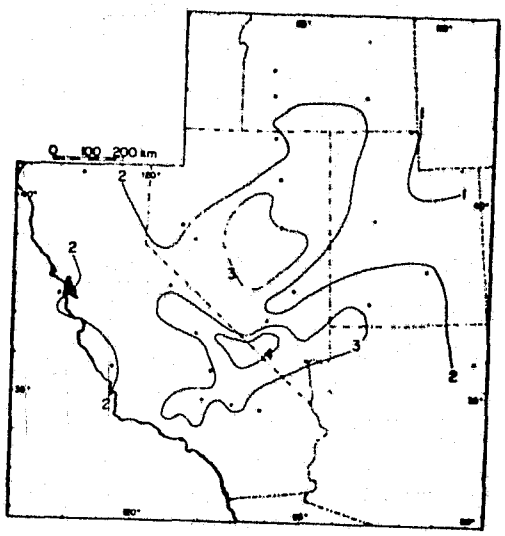

Fig. 18 - Contour map of the mean crustal velocity. The contour interval is 1 sec. (Prodehl, 1970).

Blank (1969) recognized this projection as a single volcano-tectonic system which grows progressively younger towards the northeast. In addition, magnetic data (fig. 16) indicate a total intensity anomaly extending from north-central Nevada through Yellowstone Park and beyond. The projection of the Midas Trench lineament zone coincides with the southeastern border of this magnetic anomaly.

The third recognized major structural zone detected on the ERTS mosaic has been called the Oregon-Nevada lineament (Stewart and Walker, personal communication, 1974) (C, fig. 15). In the ERTS mosaic of Nevada, the zone is marked by several lineaments extending from the western margin of the Roberts Mountains to within 45 km of the northern State boundary. Intersection with the Midas Trench lineament zone

results in the abrupt termination of that part of the Midas Trench zone. Aligned tonal and textural boundaries, escarpments, and stream segments make up the lineament within Nevada.

A distinct zone of aligned magnetic anomalies coincides with the lineament system for about 200 km (Mabey, 1966; Robinson, 1970) (fig. 16). The cause of the anomalies is believed to be a linear swarm of mafic dikes of Tertiary age emplaced along a zone of structural weakness. Robinson (1970) suggested that the zone has been tectonically active intermittently since late Paleozoic time.

Stewart and Walker (personal communication, 1974) have projected the Oregon-Nevada lineament north to Mt. Jefferson, Oregon, for a total length of more than 700 km. They postulated that the lineament may be a plate-bounding right-lateral transcurrent fault.

The remaining four major lineament systems proposed as zones of regional structural significance are more poorly documented. These four include the Rye Patch lineament system (D, fig. 15), the zone of east-northeast-trending lineaments south of Walker Lake (E, fig. 15), the group of relatively small east-trending lineaments in Lincoln County (F, fig. 15) and the Ruby Mountains lineament system (G, fig. 15).

The two lineaments making up the Rye Patch lineament system parallel the Walker Lane 110 km to the northeast. The system

extends from the Black Rock Range in Humboldt County to the Shoshone Mountains in Lander County, intersecting the Midas Trench lineament system at the southern tip of Rye Patch Reservoir. The lineaments are somewhat diffuse in appearance, distinguishable predominantly by means of tonal and textural changes along their 250-km length. Ranges appear to be terminated or offset by the two lineaments. The northwesterly strike paralleling the Walker Lane suggests possible right-lateral movement, which would be consistent with Shawe's (1965) theory of a conjugate shear system. Both lineaments coincide precisely with one of Roberts' (1966) proposed third-order deep-seated fracture zones, which are oriented predominantly northwest and east. His first-and second-order features are northeasterly-striking geosynclinal trends and east-striking orogenic belts of regional extent, respectively. Roberts suggested a Precambrian age for all three structural orders.

Thirty kilometers south of Walker Lake, an east-northeast to east-trending lineament system (E, fig. 15), transects the predominantly north-trending basins and ranges. It is expressed physiographically by aligned streams, canyons, and tonal boundaries. Both the northeastern and the southern lineaments in this system appear to terminate or disrupt the north-to north-northwest-trending ranges.

The southern lineament in this system, shown as a dashed line, was not included in the conservative major lineament overlay (fig. 3)

because its component segments are not longer than 10 km, a condition set up for the major lineaments. Nevertheless, the lineament is so distinctive that we feel that it merits recognition. The lineament coincides for about 45 km with a probable high-angle fault with inferred right-lateral strike-slip movement mapped by Albers and Stewart (1972). In addition, a broad east-trending zone of magnetic highs corresponds well with this lineament (fig. 16).

The northwestern lineament is within 5 miles of a similar-trending fault, formed during a historical earthquake in the Excelsior Mountains, which had left-lateral strike-slip movement (Shawe, 1965). Gumper and Scholz (1971) called attention to a left-lateral strike-slip composite focal mechanism in the Excelsior Mountains where the Nevada seismic zone, discussed later in this report, is offset to the east. Thirty kilometers north of the northeastern lineament of this zone is the similar-trending Tulle Creek-Pritchards Station lineament (Ekren and others, 1968). It is marked by several east-trending magnetic discontinuities and was at some point in its history a left-lateral strike-slip fault. The Tulle Creek-Pritchards Station lineament is definitely younger than 23 m.y., but it predates upper Miocene or lower Pliocene tuffaceous sediments (Ekren and others, 1968). Zietz and others (1969) suggested that the east-trending magnetic trends may represent deep-seated Precambrian fracture zones.

Intersection of the major lineament zone E (fig. 15) with

the Walker Lane in the Gabbs Valley Range takes place with no apparent disruption. Assuming that the lineament system is a transcurrent fault zone, either the Walker Lane and this system were activated simultaneously or the east-northeasterly oriented system has undergone slightly more recent movement. The bending of the Walker Lane north of the intersection with the lineament zone may indicate possible drag. Many of the magnetic highs along the Walker Lane have an easterly component.

The sixth major lineament system, the shortest of the seven major lineament systems, is made up of a group of five east-trending equal-length lineaments measuring a total distance of 70 km (F, fig. 15). The lineaments are along the northern margins of the Groom, Pahrangat, and Hiko Ranges in Lincoln County and reflect boundaries between outcrop and alluvium and tonal nonalluvial boundaries. A prominent east-trending regional Bouguer gravity anomaly zone (Mabey, 1960) corresponds with this lineament zone. The lineament zone also is within an east-trending magnetic zone of intermediate intensity, and extension of the zone to the west corresponds with a series of magnetic highs (fig. 16). Shawe (1965) delineated an east-trending lineament which coincides with this major lineament zone.

Movement along this proposed east-trending zone is difficult to evaluate. Tschanz and Pampeyan (1970) indicated dip-slip movement along faults marking the eastern part of the zone. Fifteen km to the south, in the Pahrangat Range, they called attention to a roughly

east-trending left-lateral transcurrent fault having a displacement of about 1 mile. Another 30 km south are three east-northeast to northeast-trending transverse faults with left-lateral offset. Tschanz and Pampeyan (1970) dated these three faults, collectively called the Pahranagat shear system, as post-Miocene, but suggested that they represent a reactivated older right-lateral shear zone of Laramide age. The east-trending lineament system (F, fig. 15) is probably related to this broad zone of late Cenozoic left-lateral shearing.

East-striking lithologic and structural zones which cut across the prevalent northerly to northeasterly structural grain in Nevada have aroused considerable interest in the past decade. Roberts (1966) called attention to east-striking orogenic trends and deep-seated fractures in Nevada, believing them to have been the controlling forces over the alignment of mining districts within his proposed mineral belts. One of his proposed fracture zones is 20 km to the northeast and parallel to the shorter east-trending linear zone (F, fig. 15) detected in the ERTS images. Further evidence of the possible regional significance of these east-trending structural trends has been provided by Stewart (personal communication, 1974), who recently noted three major east-oriented lithologic trends in Lincoln County. An easterly as well as northwesterly magnetic grain appears dominant in the Basin and Range province (Zietz, and others 1969) (fig. 16).

Two secondary east-trending seismic zones have been documented (Smith and Sbar, 1974) in addition to two north-striking zones bounding the Great Basin to the east and west. The east-trending zones roughly bound the present Basin and Range province to the north and to the south and are respectively described as a 450-km east-trending belt of earthquake activity located about 50 km north of the Snake River Plain (Smith and Sbar, 1974) and a 200-km east-trending belt extending from southwestern Utah into southern Nevada Smith and Sbar (1974) noted that the latter zone corresponds well with an east-trending zone of Tertiary volcanic rocks. This zone is bounded on the north by our lineament system E (fig. 15) and contains our lineament F (fig. 15).

The last major lineament system in fig. 15 (G), the Ruby Mountains system, is the most poorly documented. The southern part reflects the normal-fault eastern boundary of the Ruby Mountains, and the extension to the northern State border aligns with several smaller faults, making up a total length of 230 km for the two lineaments. Possible left-lateral movement along this lineament zone is proposed on the basis of the apparent regional tectonic pattern of right-lateral movement along northwest-and north-northwest-trending major lineament zones and left-lateral movement along the east-northeast-to northeast-trending major lineament zones (Shawe, 1965).

A profile of the relative rates of vertical movement from

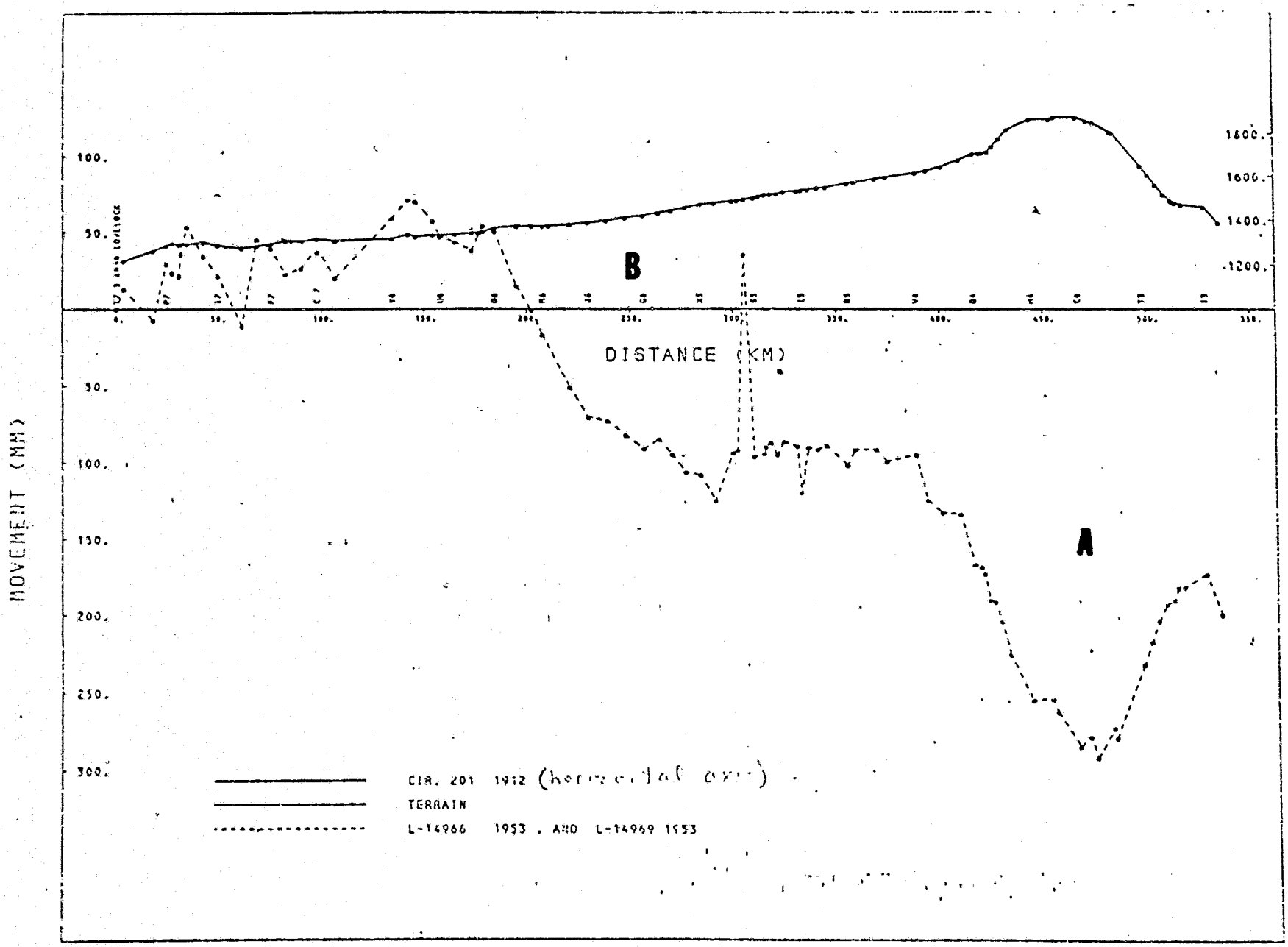

Fig. 19 – Profile from 3 km north of Lovelock to 16 km northeast of Montello along the Southern Pacific railroad track showing relative vertical movement from 1912 to 1953. Zero movement at starting point is an arbitrary assumption. Prepared in cooperation with the National Oceanis and Atmospheric Administration.

Lovelock to Montello indicates a broad structural anomaly (A, fig. 19) at the intersection of the profile with the Ruby Mountains lineament system. This 100-km wide "pocket" is either subsiding relative to the terrain to the east and west, or the surrounding terrain is rising relative to the "pocket." In either case, the documented vertical movement in this area is structurally significant. The other significant change in vertical movement is the relative subsidence beginning at about 185 km along the profile (B, fig. 19). This change in the vertical movement rate corresponds with the Oregon-Nevada lineament (C, fig. 15).

Summary

Compilation of linear features in Nevada without regard for length results in a data set too large to evaluate and validate practically as structural features. The low correlation between these linears and mapped faults and the likelihood that some of the indicated correlations are random casts doubt on the value of this approach in this type of area. Elimination of linear features less than 10 km long results in a more manageable set of data and a substantially higher correlation of major lineaments with mapped faults. Consequently, many locally mapped faults can be linked or extended to suggest major faults with considerable confidence, especially where a large number of fault segments align with a single lineament. Those major lineaments and zones that show no correspondence to faults also warrant careful

C-2

consideration. It should be noted that although the correspondence of major lineaments and faults is encouraging, only approximately one-quarter of mapped faults longer than 10 km were detected in the study area.

Consideration of the most continuous lineaments results in identification of seven major lineament systems which appear to be especially significant structural features. Although our level of understanding is not uniform for these seven major lineament systems, they seem to have several geological and geophysical characteristics in common. First, they appear to represent the traces of faults or, more probably, fault or fracture zones that are of substantial vertical as well as horizontal extent. Second, all of them including the historically active Walker Lane (Stewart, 1967), probably originated during the Precambrian. Where the movement pattern has been determined, shear movement appears to be characteristic, although dip-slip movement has also occurred along most, if not all, of these zones. Except for the Walker Lane, where right lateral movement has prevailed, contradictory senses of movement, both right and left lateral, have been recorded. Furthermore, Cenozoic basin and range topography has commonly been disrupted where these lineament systems transect it and, in places, these ranges terminate against these features. Taken together, these temporal and spatial relationships imply that these seven major lineament systems are old fundamental zones of weakness which have been reactivated by periodic changes in the regional stress field. The Walker Lane may have been

continuously active since Mesozoic time. An exceptional characteristic of these zones is their general coincidence with total-intensity magnetic anomalies, suggesting that they may have served as conduits for intruding magma.

Circular Features

Preliminary analysis of MSS images of the study area (Rowan and Wetlaufer, 1973) located 50 circular to elliptical features which were presumed to be centers of igneous activity. Comparison of these features with the 78 Tertiary volcanic centers discussed by Albers and Kleinhampl (1970) and consideration of available geologic maps suggested that eight of the features seen in the images might be previously unrecognized Tertiary volcanic centers. These eight features and one additional larger feature are shown in fig. 20. Although all these features appear to warrant further examination, especially in the field, the remainder of this section will be devoted to discussion of the large new feature, referred to as the central-Nevada circular feature.

The central-Nevada circular feature is defined on its eastern and western borders by high, slightly arcuate mountain ranges and intervening alluvial basins and on the northern margin by deflection of mountain ranges and drainage networks (fig. 20). The southern boundary is much less distinct, although, as discussed later, it is well supported by geophysical data. The diameter of this configuration is approximately 150 km.

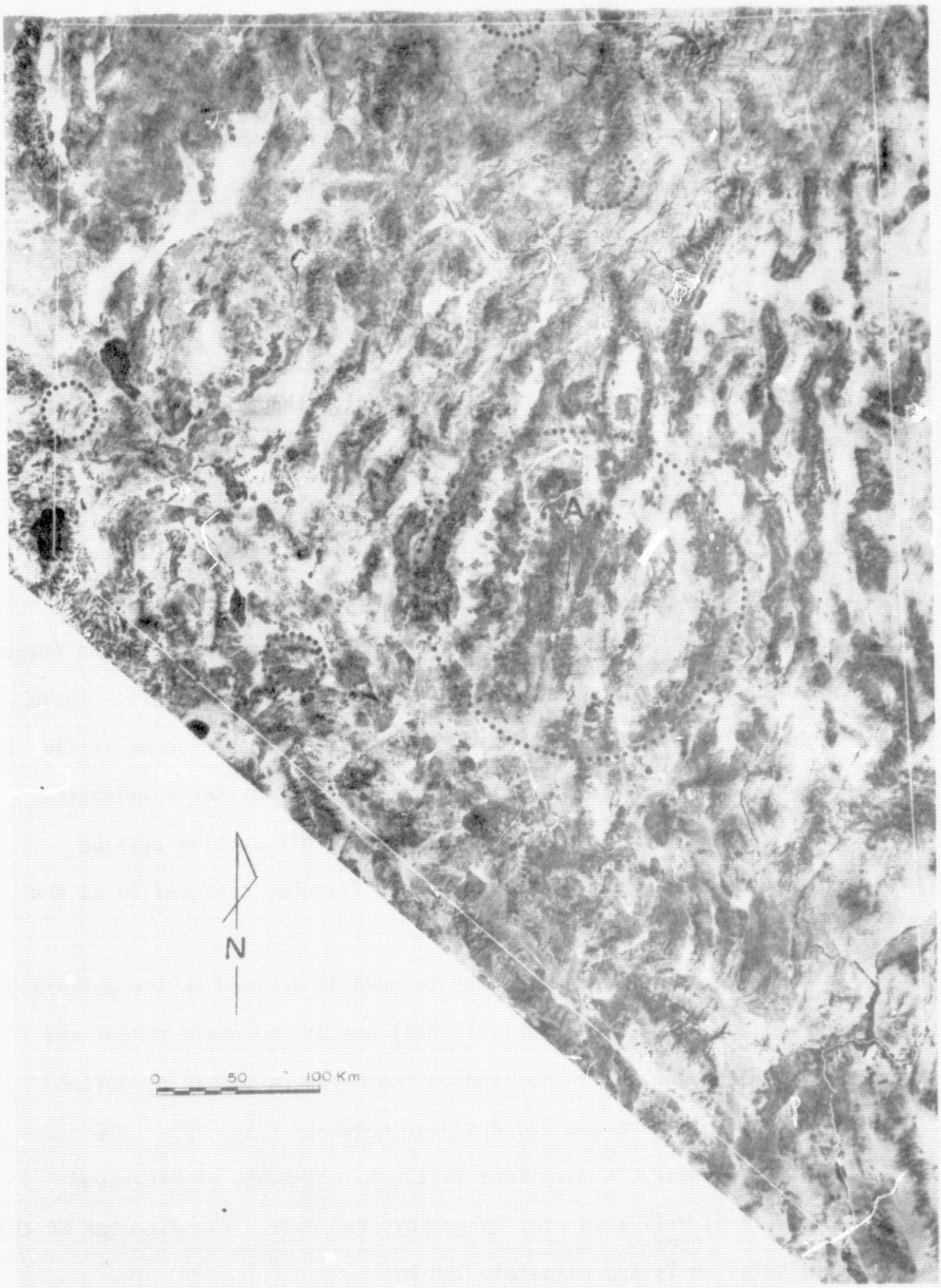

Fig. 20 - Outlines of circular areas proposed as previously unmapped Tertiary volcanic centers (Rowan and Wetlaufer, 1974) and of the central-Nevada circular feature. Compiled on mosaic prepared by Aerial Photographers of Nevada, Reno, Nevada, using ERTS-1 band 5 images recorded during September and October, 1972. Point "A" indicates the approximate location of Little Fish Lake Valley.

The central region of the circular feature is characterized by rugged ranges and narrow intervening valleys which, viewed as a unit, stand topographically higher than the peripheral ranges and the terrain surrounding the feature. Little Fish Lake Valley, which is in a narrow valley between the Monitor and Hot Creek Ranges near the center of the feature (A, fig. 20) is the highest valley within the designated circular area. In a schematic cross section between Lake Tahoe, Nevada-California, and the Hurricane fault, Utah, Ekren and others (1974a) showed that this area is a structural high serving as the point of anticlinal symmetry (fig. 21). Tertiary units west of this point generally dip to the west; to the east, generally coeval rocks dip to the east. Stewart (1971) showed a similar symmetry for major grabens in this part of the Great Basin. The general trends of the ranges composing the interior of the circular feature change slightly in the vicinity of Little Fish Lake Valley. Ranges east of this northerly trending valley are slightly concave to the east, whereas those to the west are slightly concave to the west.

The central-Nevada circular feature is in the central Great Basin where silicic to intermediate rocks are very widespread and constitute most of the Tertiary column. This setting and the morphologic pattern and regional structural configuration imply that this circular feature may be the source of some of the volcanic rocks. The main purpose of study is to consider this possibility

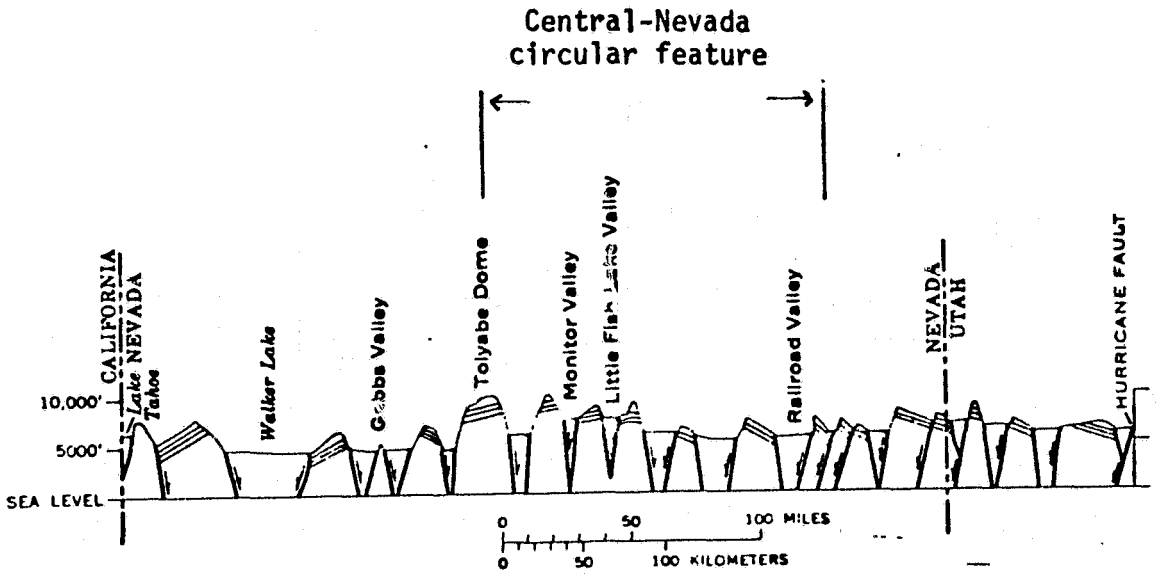

Fig. 21 - Schematic profile from Lake Tahoe, California, Nevada to the Hurricane fault, Utah showing eastward and westward slip of Tertiary units east and west of Little Fish Lake Valley respectively. Little Fish Lake Valley located in fig. 20. (after Ekren and others, 1974a)

through synthesis of regional geological, geochronological, and geophysical data as well as through analysis of lineaments obtained from ERTS-1 images and image mosaics. The potential significance of this circular feature for interpreting regional heat-flow data and the distribution of ore deposits in Nevada is also considered.

Lineament Analysis

Comparison of the areal density and trends of major lineaments

($\geq$ 10 km) in this area with those in rest of the State also indicates that the morphology of the circular feature is physiographically anomalous. Visual inspection of major lineaments (fig. 13) shows an especially high density within the circular feature, particularly in the rugged central part. The trends of these lineaments are also slightly anomalous. Most areas of similar dimensions are characterized either by the generally dominant north-northeast-trending basin and range lineaments or one of the other locally prominent trends. For example, in the area north of Las Vegas, generally north-trending lineaments dominate; elsewhere along the Walker Lane-Las Vegas shear zone, northwest and east-northeast trends are conspicuous. Major lineaments in the northeastern part of the State are mainly northeast and north-northwest trending because of the influences of the Midas Trench and Oregon-Nevada lineament zones (fig. 13). In contrast to these areas, major lineaments within the circular feature have important northeast and east-northeast to east modes as well as the common north-north-northeast maxima (fig. 22). A consequence of the diverse trends of the many major lineaments in the central Nevada circular feature is a high areal density of intersections, one of the highest in the State (fig. 23). If most of these lineaments are major faults, as indicated by the correlation with faults shown on the State geologic map (Stewart and Carlson, 1974) (fig. 13), the circular feature is structurally

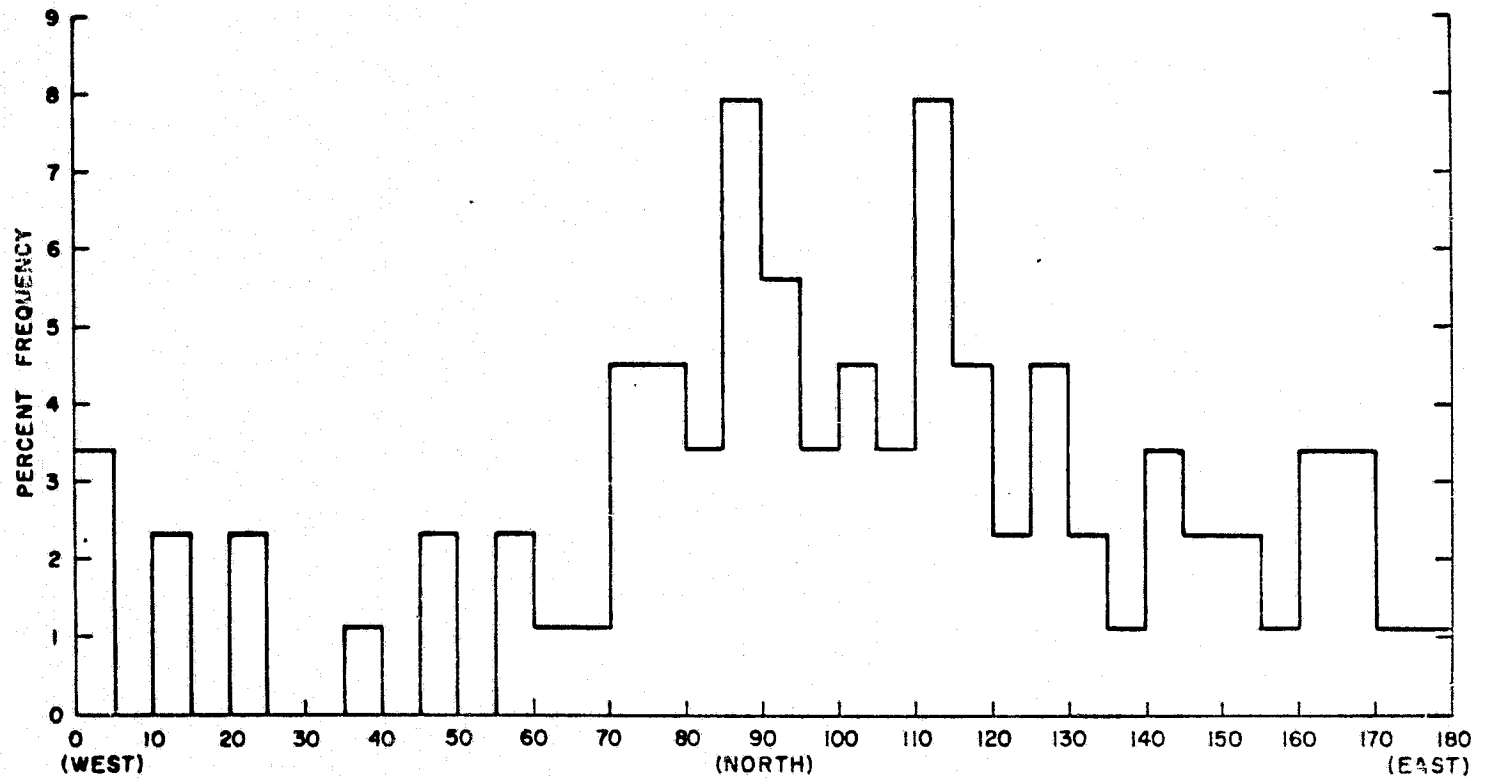

Fig. 22 - Histogram showing strike-frequency distribution of major lineaments shown within the central Nevada circular feature in figs. 3 and 13. n = 83.

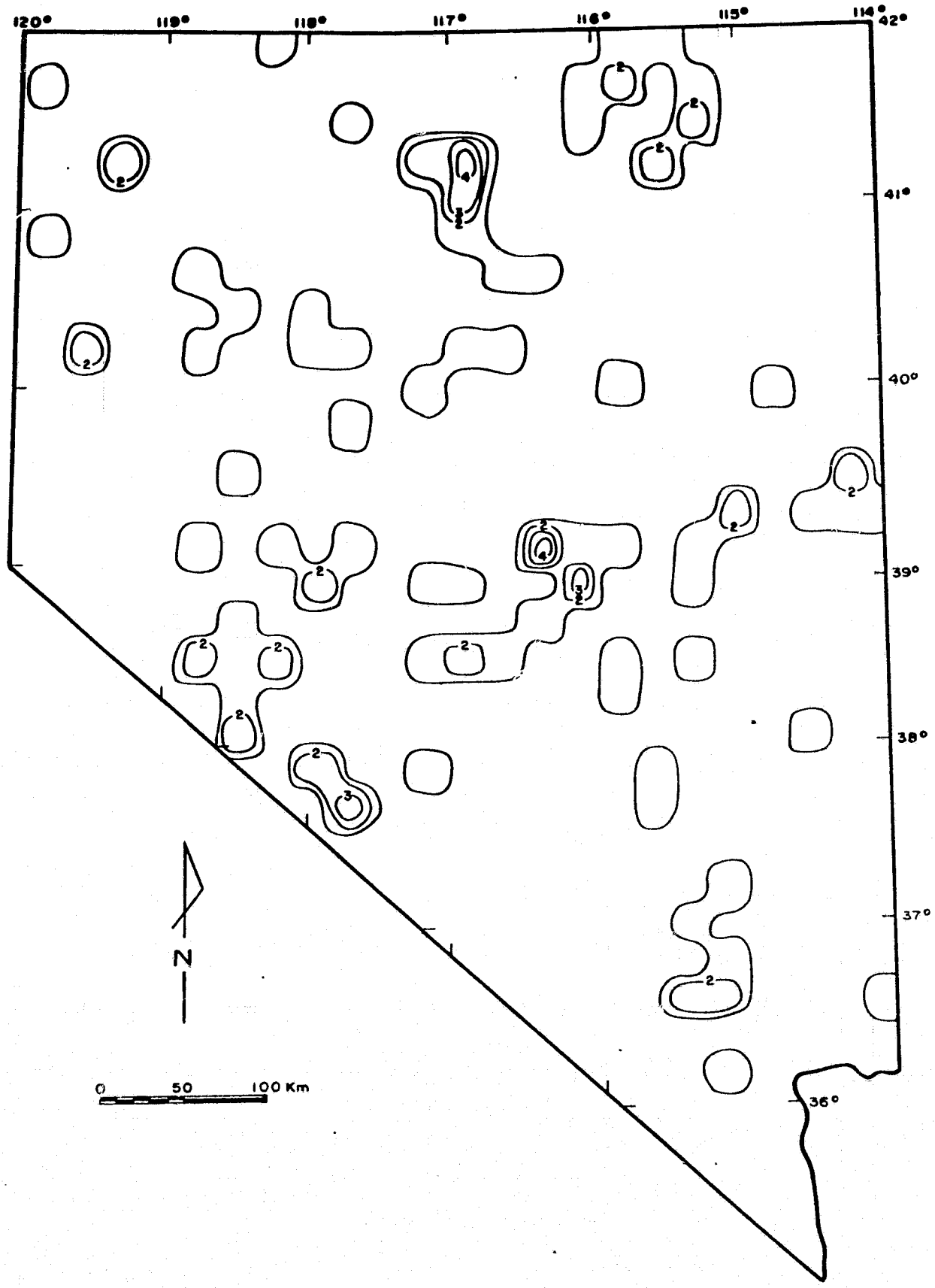

Fig. 23 - Contour map showing areal distribution of major lineament intersections in Nevada. Grid cell 500 sq. km. n = 104. Contour interval = 1%.

unique. The strain pattern in this area must have been substantially different from elsewhere in this part of the Basin and Range province.

Evaluation of major lineaments mapped for the State resulted in identification of seven systems which appear to be especially significant with respect to the regional structural framework. Three of these systems, the Walker Lane, the Midas Trench lineament and the Oregon-Nevada lineament, have already been documented as major crustal features. The other four systems are less well understood, but alignment with known faults strongly suggests that these lineaments also represent major fault zones. The distribution pattern of these seven lineament systems shows that four (C, D, E, G, fig. 15) radiate from (or converge towards) the approximate center of the circular feature, although none of them completely transects the feature.

Geological Analysis

Although studies concerning the distribution and origin of the voluminous Tertiary igneous rocks are complicated by many factors, radiometric age determinations provide a useful means for placing these rocks in a regional tectonic framework. Through analysis of more than 500 measurements, Armstrong and others, (1969) and McKee (1971) identified two major periods of Tertiary igneous activity. The first episode began about 40 m.y. ago involving mainly intermediate rocks. By approximately 35 m.y. ago, silicic tuffs and flows

became dominant with subordinate intermediate lava flows and this trend continued until 19 m.y. ago. After a hiatus of approximately 3 million years, volcanism resumed but had changed significantly to dominantly basaltic rocks, minor silicic rocks, and small amounts of intermediate flows. This second episode has continued to the present.

Consideration of the age distribution of Tertiary igneous rocks led Armstrong and others (1969) and McKee (1971) to propose a regional model for the distribution of these rocks. They visualized intense silicic to intermediate volcanic activity 30 m.y. to 40 m.y. ago in a "core area" in the central and east-central Great Basin, progressively younger volcanism migrating towards the western and southern margins (fig. 24). However, geologic mapping in the area of the circular shows the presence of both Oligocene and Miocene silicic to intermediate rocks (Kleinhampl and Ziony, 1967; McKee 1968a; Stewart and McKee, 1968; Sargent and McKee, 1969; Cornwall, 1972; Ekren and others, 1974a; Stewart and Carlson, 1974). A clearer definition of the distribution of the 19 m.y. to 30 m.y.-old igneous rocks can be obtained by considering the ages and distributions of six ash-flow sheets in the northern part of the area (Gromme and others, 1972) and by evaluating the radiometric age data of Armstrong and others (1969) along with measurement published since their study (McKee and others, 1971; Marvin and others, 1973).

Study of six voluminous widespread ash-flow sheets in the northern part of the circular feature show that two are appreciably younger

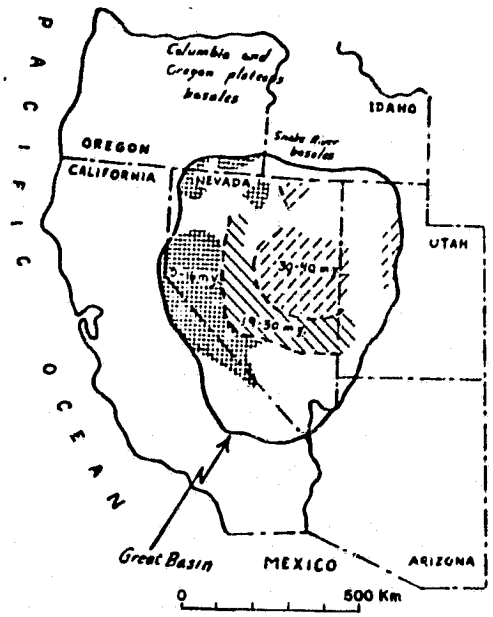

Fig. 24 - Generalized distribution of Tertiary volcanic rocks in the Great Basin according to McKee (1971).

than 30 m.y. (Gromme and others, 1972). The tuff of Clipper Gap is 22 m.y. old and underlies most of the Monitor Range, parts of the Toquima Range, and extends northward across the circular feature to the northern end of the White Pine Range (fig. 25). Confinement of the tuff to the circular feature strongly suggests a local source. The more voluminous tuff of the Bates Mountain Formation is 23 m.y. old and underlies most of northern part of the feature but continues northwestward to the Shoshone Range (fig. 25). Although similarly detailed studies have not been conducted in the southern part of the circular area, rocks younger than 30 m.y. old occur in large parts of all the major ranges (McKee and others, 1971;

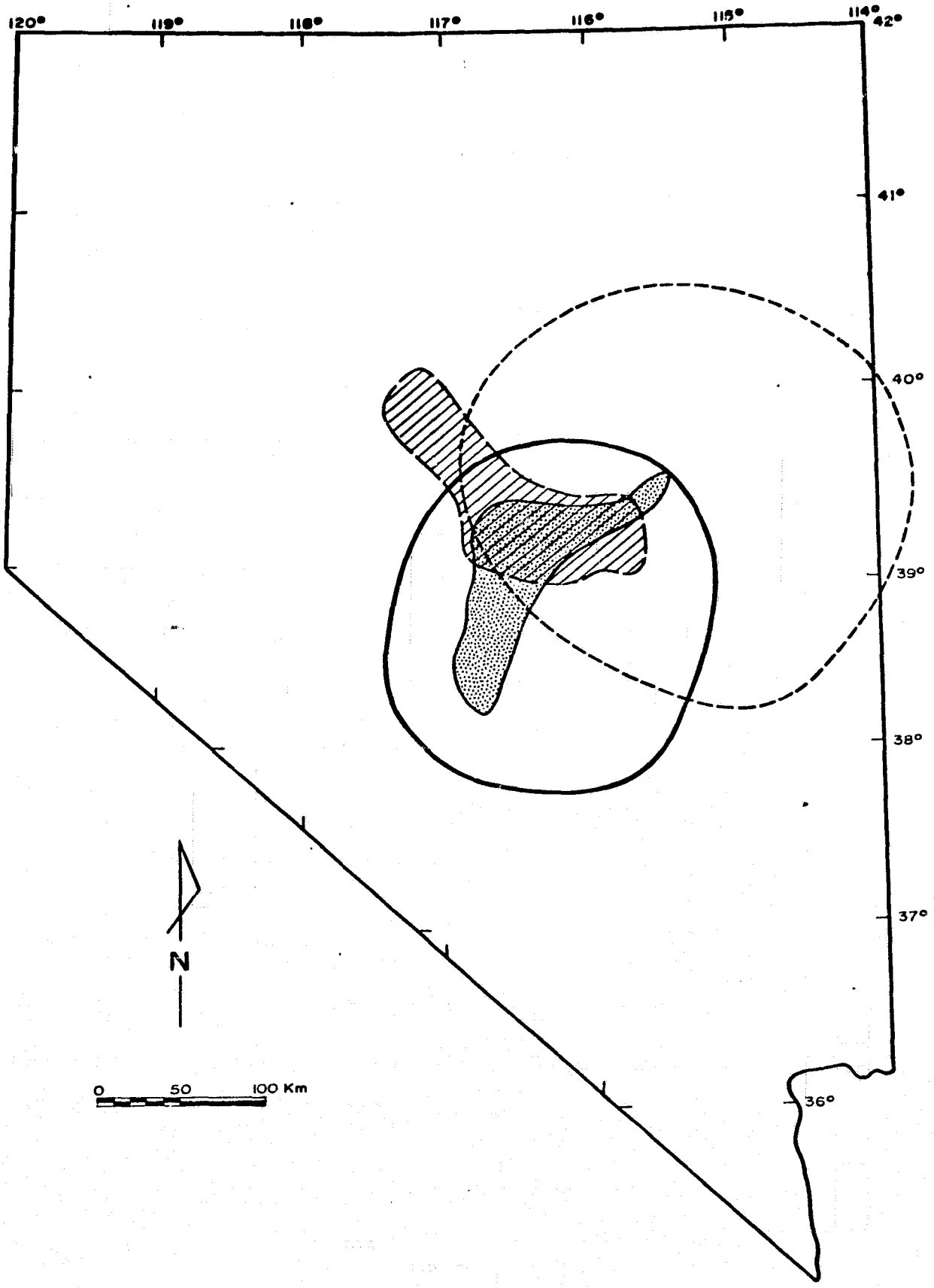

Fig. 25 - Map showing the locations of the central Nevada circular feature (solid line), the core area of Armstrong and others (1969) short-dashed lines, and two Miocene ash-flow tuff sheets (after Gromme and others, 1972), the tuff of Clipper Gap (stippled) and the Bates Mountain Formation (diagonal lines).

Marvin and others, 1973; Kleinhampl and Ziony, 1967). These data clearly document the presence of 19 m.y. to 30 m.y.-old ash-flow tuffs in the southwestern part of the core area and indicate that the northern boundary of the circular feature represents the northern limit of igneous rocks younger than 30 m.y.

Combining these data with a widely distributed sampling of radiometric age determinations shows that the highest density of 19 m.y. to 30 m.y. measurements is in a northwest-trending belt which straddles the central Nevada circular feature (fig. 26). The eastern boundary is based in part on geologic mapping by Kleinhampl and Ziony (1967) which shows that one of these younger ash-flow tuffs, the Shingle Pass, also occurs in the White Pine Range along the northeastern periphery of the feature.

Geologic mapping and radiometric age dates show that tuffs older than 30 m.y. are also widespread within the circular feature, especially in the northern part. Three of the six ash-flow sheets studied by Grommé and others (1972) are 30.7 m.y. old and, like the tuff of Clipper Gap, are confined to the northern part of the feature. One of these units, the Windous Butte Formation, is nearly 2,000 m thick at its apparent source, the oldest of a cluster of superimposed calderas (Ekren and others, 1974b) which cover most of the southeastern quadrant of the circular feature. The other two ash-flow sheets, the Pancake Summit Tuff and Stone Cabin Formation, also underlie large areas in the northern part of the feature.

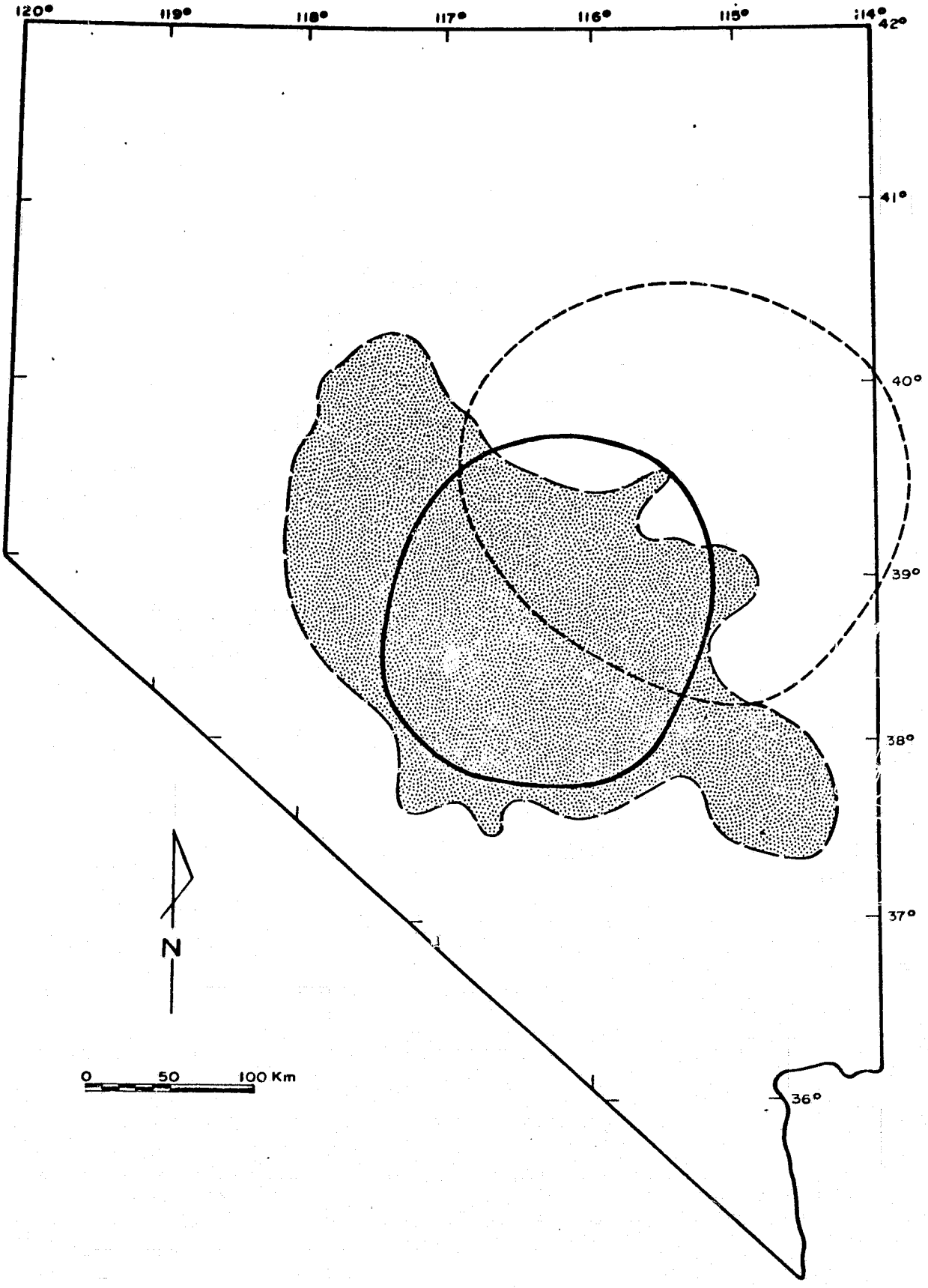

Fig. 26 - Map showing the locations of the central Nevada circular feature (solid line), the core area of Armstrong and others (1969) (short dashed lines), and the main belt of 19-30 m.y. old igneous rocks (stippled).

The sixth ash-flow sheet is the 29 m.y. to 31 m.y.-old Needles Range Formation which is by far the most extensive. However, these rocks underlie only small parts of the eastern periphery of the feature and originated well to the east of the area of interest (Grommé and others, 1972).

Rocks older than 30 m.y. are therefore restricted mainly to the region north and east of the center of the circular feature. Although the distribution of 19 m.y. to 30 m.y.-old rocks shown in fig. 26 is similar to those proposed by McKee (1971) (fig. 24), there are two significant differences. First, the main area of 19 m.y. to 30 m.y.-old igneous rocks is a northwest trending, generally linear zone rather than an arcuate belt. Second, nearly all the southwestern part of the core area is underlain by tuffs 19 m.y. to 30 m.y.-old, although older tuffs are also present.

Although these data are suggestive, some factors cause us to regard them with some caution. A few 19 m.y. to 30 m.y.-old measurements have been recorded well outside this area, and the source areas are not known for most of the rocks dated. In addition, the geographic distribution of the samples is not representative. Hence, the pattern shown in fig. 26 represents an approximation of the minimum distribution of 19 m.y. to 30 m.y. igneous rocks. Nevertheless, we believe that the coincidence of the circular feature with the apparent focus of activity at 19 my. to 30 m.y. indicates a possible genetic relationship and therefore warrants further evaluation.

Geophysical Analysis

Several lines of geophysical evidence have been examined and synthesized to evaluate the proposed igneous origin for this feature. Regional aeromagnetic data compiled for the conterminous United States show a distinctive total-intensity low within the circular feature. The anomalous area is a nearly continuous elliptical belt in which the major axis trends approximately north (fig. 16) and lies entirely within the arcuate mountain ranges forming the eastern and western boundaries of the circular feature. Within the broad anomaly are many small anomalies that have a weak northerly alignment. Although the boundaries of the broad anomaly and the outline of the circular feature are nearly identical in the south, the anomaly terminates well south of the northern boundary of the circular feature. The most probable explanation for the anomaly appears to be the presence of a thick pile of weakly magnetic tuffs, some of which are strongly reverse-magnetized, as suggested by Ekren and others (1974a) for the rhyolitic lavas in Little Fish Lake Valley.

Analysis of seismic-refraction profiles also shows the anomalous character of the crust in the vicinity of the circular feature. Reversed profiles recorded from the Nevada Test Site (NTS) to Boise, Idaho, by the U.S. Geological Survey transect the feature through its approximate center. Interpretation of these data by Hill and Pakiser (1967) identifies a zone of crustal thickening and low-velocity materials in the northern part of the area near Eureka.

From these data and from consideration of the geologic setting, they suggest that the traveltime delays originate in the crust, perhaps because of crushing or faulting, rather than near the surface where it would be related to typically low-velocity basin fill. They further speculate that a graben may be present at the Mohorovicic (M) discontinuity below the zone of low-velocity materials. In addition, at approximately 330 km north of NTS, near the northern boundary of the circular feature, an abrupt change in M-discontinuity depth is thought to be a fault having the southern side downthrown.

Reinterpretation of these and other seismic-refraction data by Prodehl (1970) confirms the presence of anomalously thick, low-velocity crustal materials in the vicinity of the central Nevada circular feature. The contour map of the reduced traveltimes from which the effects of sedimentary layering have been eliminated shows two areas of relatively low P-wave velocities in the Great Basin (fig. 27a). The anomaly in central Nevada is nearly coincident with the circular feature outlined in the mosaic (fig. 27b). It is perhaps noteworthy that this anomaly is slightly larger than the circular feature along the north-south line, suggesting a slightly ellipsoidal body at depth.

The average crustal thickness of the Basin and Range province is 32 to 34 km and therefore significantly thinner than adjacent areas such as the Sierra Nevada, the middle Rocky Mountains, Colorado Plateau, and Snake River Plains (fig. 27). However, a conspicuous

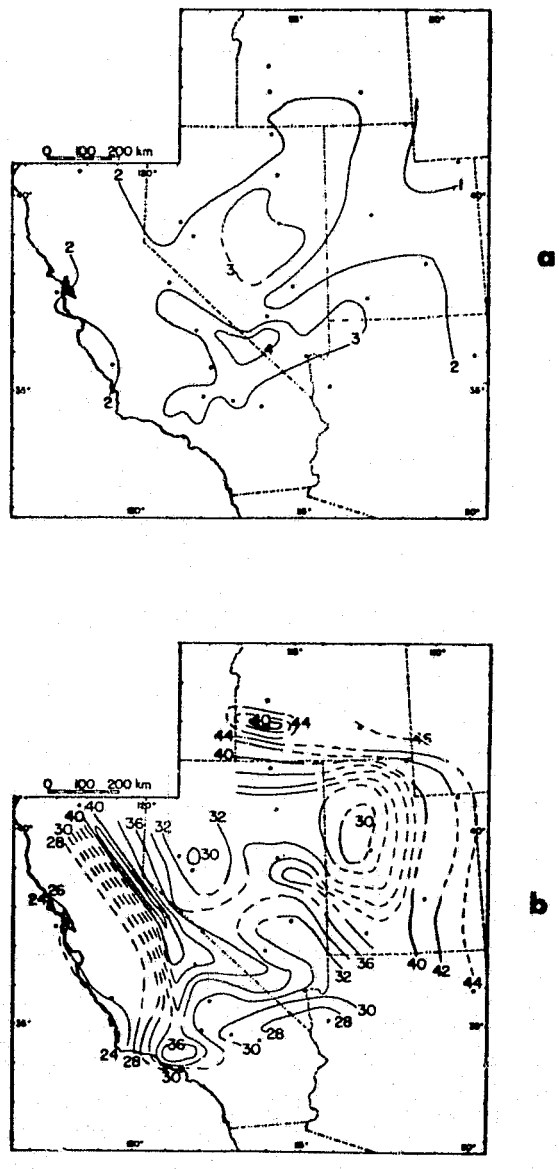

Fig. 27 - Contour maps showing a) the mean crustal velocity (1 sec. contour interval) and b) total crustal thickness (2 km contour interval) in the Great Basin. Dashed contour lines indicate uncertain results. (Prodehl, 1970).

area of thicker crust within the Great Basin occurs in the area of low P-wave velocity and the central Nevada circular feature. Crustal thickness within the circular feature ranges from 32 to 38 km, the maximum being under the eastern part. Although Prodehl showed the total thickness contours opening to the southeast, the degree of uncertainty in this part of the area is probably sufficient to permit closure of these contours. The distinction of low-velocity upper crust and high-velocity lower crust in Nevada is absent south of Eureka (Pakiser and Zietz, 1965; Prodehl, 1970), indicating a fundamental change in regional crustal materials.

These data are essentially in agreement with regional gravity studies. A regionalized Bouguer anomaly map (fig. 28) of part of the Basin and Range province, based on measurements made in the mountain ranges, shows several large negative features which are also areas of elevated terrain (Mabey, 1960). A broad anomaly defined by the -200 milligal contour trends northeast from central Nevada to the Nevada-Utah border (fig. 28). Because of the correlation between this and the other low Bouguer anomalies and elevated terrain, Mabey (1960, p. B285) concluded that "there is a relative mass deficiency under the regional highlands" and "that some form of regional isostatic compensation exists." The exact shape of this anomaly may be two contiguous concentric areas (Mabey, 1974, personal communication). One of these areas is approximately coincident with the central Nevada circular feature; the other area, approximately 150 km to the northeast, would correlate approximately with the core area of Armstrong and others (1969). However, of the

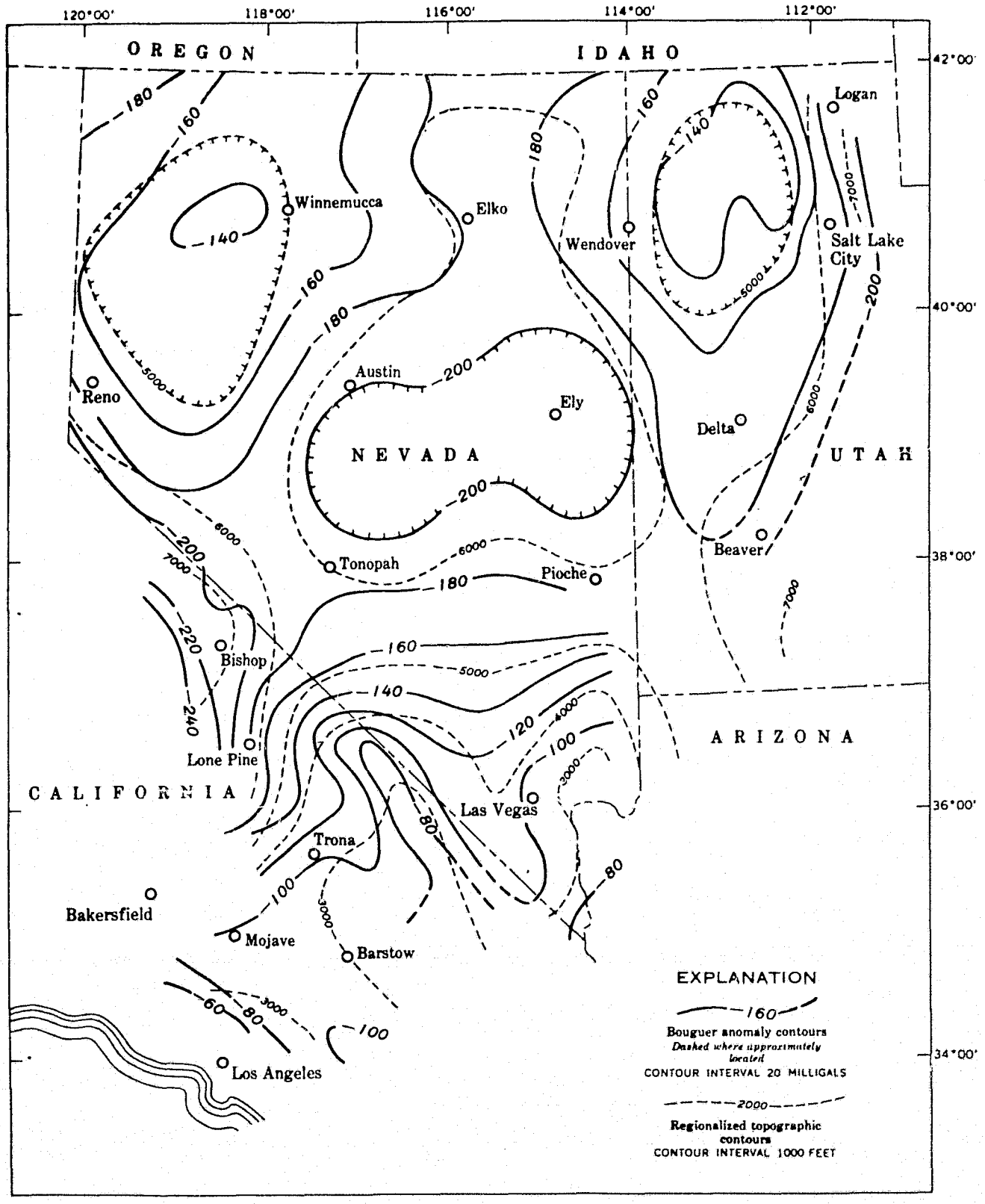

Fig. 28 - Regionalized Bouguer anomaly and topographic map of the Great Basin province showing the anomaly defined by the -200 milligal contour line in central and east-central Nevada (Mabey, 1960).

geophysical data examined, only these data substantiate the presence of their proposed core area.

The circular area is also in an area of anomalous heat flow. The Basin and Range province is characterized by anomalously high heat flow (Roy and others, 1968; Sass and others, 1971), apparently a result of thin crust. Within the circular feature, however, is a broad conspicuous heat-flow low, referred to by Sass and others (1971) as the "Eureka Low." This anomaly is a crudely elliptical, north-trending area which is mainly in the eastern half of the circular feature (fig. 29) and which continues southward to near Mercury, Nevada. Sass and others (1971) attributed this anomaly to an interbasin convective ground-water system. The high porosity inherent in the thick sequence of silicic volcanic rocks present in the circular area and around the Timber Mountain caldera northwest of Mercury may facilitate such a system.

In summary, these geophysical data define a crustal zone of thick, low-velocity material which may extend to a graben or major break at the M discontinuity and which may be bounded on the north by major fault. Mass deficiency within this zone is inversely correlated, elevated topography indicating regional isostatic adjustment. The magnetic properties in this area are distinctly anomalous apparently because of the presence of several kilometers of weakly magnetic tuffs and flows which locally are reversely polarized. These data, along with the morphological evidence,

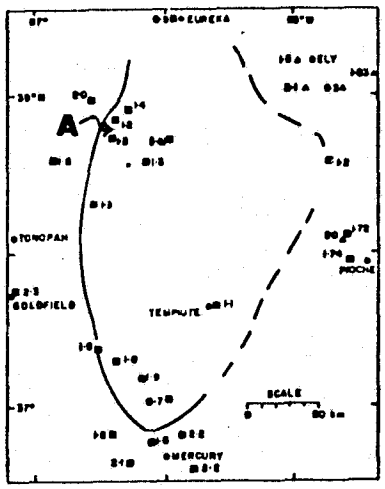

Fig. 29 - Map showing heat flow determinations in south-central Nevada. Heavy line is 1.5 HFU contour outlining the "Eureka Low"; dashed where uncertain. "A" locates Little Fish Lake Valley (Sass and others, 1971).

strongly support the presence of a regional anomalous crustal feature beneath the central Nevada circular feature.

Summary

We visualize widespread diffuse silicic to intermediate volcanic activity throughout the central and east-central Great Basin,

including the northern part of the circular area 40 m.y. to 30 m.y. ago, resulting in the core area of Armstrong and others (1969). About 30 m.y. ago, volcanism migrated southwestward and became concentrated in the general area of the circular feature. Other, probably smaller, centers having less apparent surface expression may have been present elsewhere in the Great Basin during both of these episodes. The rate and timing of migration and concentration of activity in the central Nevada volcanic complex is not clear but was probably a gradual process which began about 30 m.y. ago. Continued volcanism in this area until 19 m.y. ago resulted in a thick pile of ash-flow tuffs and related intrusive rocks which can be placed with respect to space and time in the volcanic-tectonic framework of the Great Basin. Therefore, we suggest that the general area of the circular feature should be referred to as the upper Oligocene to middle Miocene "Central-Nevada volcanic province." In line with this distinction, the core area should be termed the Oligocene East-Central Nevada province.

Silicic volcanic activity terminated in this area 19 m.y. ago, and basaltic volcanism took place from 16 m.y. ago to the present. It was widespread along the western and southwestern margins of the Great Basin but is also represented in the circular feature by scattered small occurences.

Before the formation of the circular feature, the central

Great Basin probably consisted of broad plains underlain by thin interlayered sheets of tuffs and flows (McKee, 1971). Intense concentrated volcanism and deposition of a thick pile of silicic volcanic rocks probably resulted in elevated complex terrain within a slightly north-oriented elliptical area, possibly structurally uplifted to some extent because of the emplacement of viscous magmas in the upper crust. Late Cenozoic rifting transformed the north-trending ellipse into the present generally circular pattern. The magnitude of this topographic and structural elevation is unknown, but Ekren and others (1972) argued convincingly from stratigraphic and structural evidence that doming before rifting cannot reasonably account for all or even most of the symmetrical tilting of the ranges. Instead, they suggested that the central part of the Great Basin was constantly buoyed up during rifting of the province, possibly by the addition of new crustal material. We agree with this general conclusion and add that the regional stress field was probably influenced by the presence of this volcanic construct, as indicated by the arcuate pattern of the faults bounding the ranges around and within the circular feature. Moreover, the magnitude of the extension across the Great Basin was apparently affected by this feature because the spacing of the ranges in the central part is approximately a factor of 2 less than the average 24 to 32 km determined by Stewart (1971) for the entire province.

Discussion

The spatial relationship between the major lineament systems and the "Central Nevada Volcanic Complex" appears to be more than fortuitous The two most continuous lineament systems, the Walker Lane and Midas Trench systems, along with the Wasatch and Hurricane-Sevier fault zones at the Great Basin-Colorado Plateau boundary (fig. 30), outline a wedge of crustal material which occupies most of the Great Basin. According to McKee (1971), the central Great Basin was tectonically stable during early to middle Tertiary time. However, the wedge is transected by several major lineament systems which converge towards the approximate center of the "Central Nevada Volcanic Complex," in the southwestern part of the wedge near the Walker Lane-Las Vegas system. We interpret these lineament systems as deep-seated pre-Tertiary zones of crustal weakness which were reactivated during the middle Oligocene and whose mutual intersection provided the main conduit for rising silicic magma at that time.

Movement since Miocene time, roughly concurrent with movement along the north-to north-northeast-trending basin-range faults, is evident in several places although Middle Oligocene reactivation along these old zones of weakness can only be inferred. The Walker Lane appears to have been active at least to some degree since the Mesozoic. Passage of this fault zone along the southern boundary of the central-Nevada circular feature probably accounts for the vagueness of circular outline there. The existence of older zones of weakness which have been subsequently reactivated, explains the apparent dichotomy presented by frequent disruption and preferential erosion of the dominant Cenozoic basin and range topography.

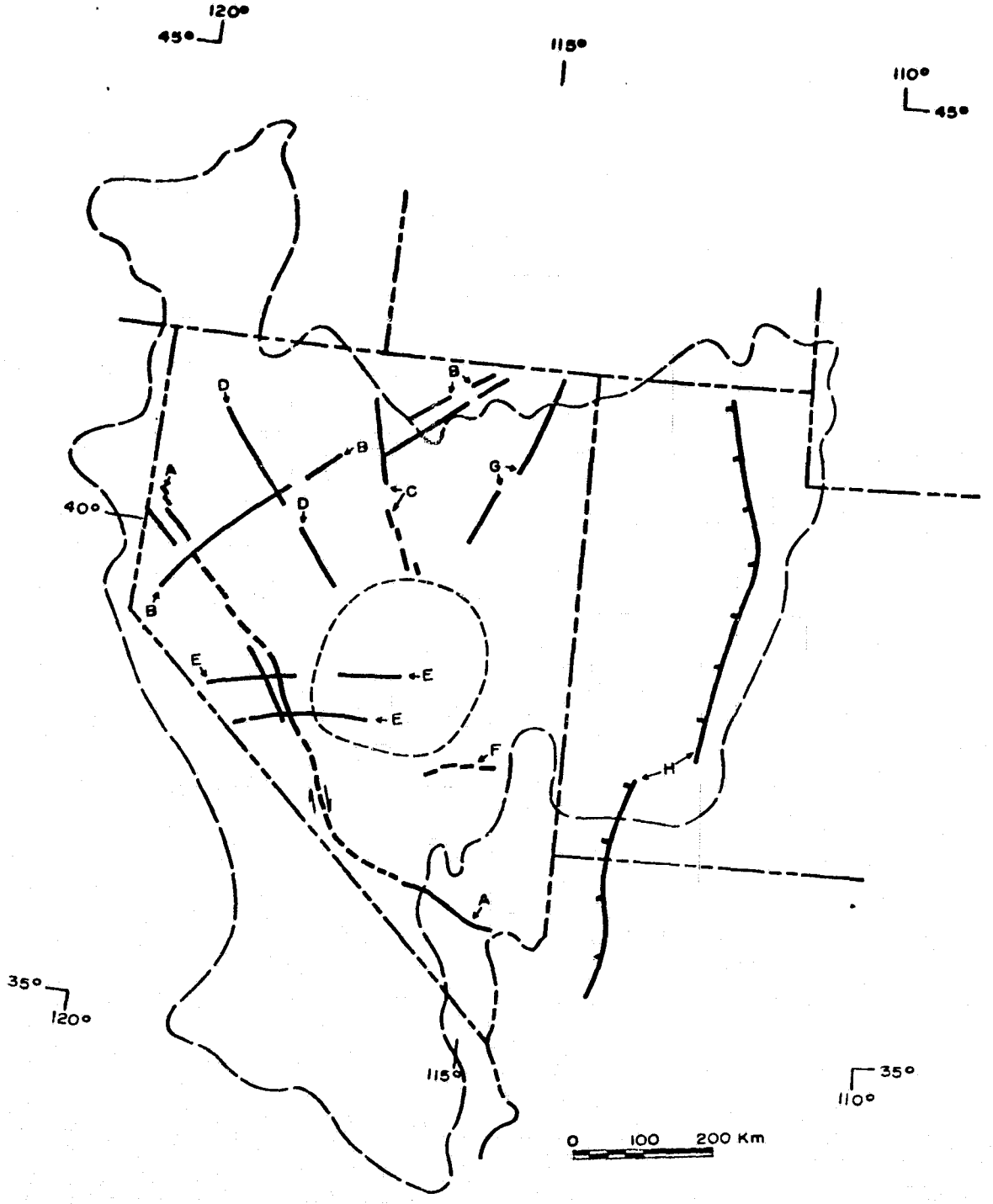

Fig. 30 - Sketch map showing approximate positions of the Great Basin province (long-dashed line), the "Central Nevada Volcanic Complex" (short-dashed line), and the major lineament systems as identified in fig. 15 and the Hurricane-Sevier Basin and Wasatch (north) faults (H): hachures on downthrown side. Dashed lines along the Walker Lane are extrapolations based on geologic evidence (Albers, 1967). Locations of the Hurricane, Sevier, and Wasatch faults from Tectonic Map of North America, United States, Geological Survey, 1962.

Transcurrent movement and shearing appears to be an important characteristic of the major lineament systems. Four of them may have acted as basic elements of a conjugate shear system during the Cenozoic, dextral movement taking place along the north-northwest to northwest-oriented system (A, C and D figs. 15 and 30) and sinistral movement, along the north-northeast- to northeast-oriented system (B, figs. 15 and 30). Similarly oriented major lineaments and lineament zones (fig. 13) are probably part of this conjugate shear system to which Shawe (1965) first called attention. The two east-trending lineament systems (E and F, figs. 15 and 30) probably also had components of shear movement during their history. However, the fact that the longer of these east-trending systems (E, figs. 15 and 30) shows no apparent displacement where it crosses the Walker Lane implies reactivation concurrently with movement along the Walker Lane. Little is known about movement along the seventh system paralleling the eastern front of the Ruby Mountains (G, fig. 15 and 30), but the generally north-northeast trend suggests a component of possible left-lateral displacement in addition to the dip-slip movement at the basin-range boundary.

Although the mechanism responsible for the periodic reactivation of these zones of crustal weakness and for the migration of volcanic activity in the Great Basin is not clear, the intimate relationship of reactivation and the migration after a period of stability implies changes in the regional stress pattern which are probably due to influences outside the basin. Considerable evidence now exists to show that movement of oceanic plates and subsequent subduction into a trench along the western continental margin played a key role in the deformational and petrologic history of the Great Basin.

Christiansen and Lipman (1972) noted the predominance of subduction-type (Martin and Piwinskii, 1972) intermediate-composition igneous suites and their associated differentiates during early and middle Cenzoic time in the west-central and southwestern United States. Towards the continental interior, these calc-alkalic rocks become more alkalic (Moore, 1962), a trend which is consistent with the presence of a subduction zone. The zone is thought to have been dipping gently (15°-20°) eastward under the west coast of North America (McKenzie and Morgan, 1969; Atwater, 1970; Christiansen and Lipman, 1972: Lipman and others, 1972), and was driven by the eastward migration of the East Pacific Rise, assuming a relatively fixed West Pacific plate (Atwater, 1970). As the East Pacific Rise migrated slowly eastward, subduction resulted in the progressive consumption of the East Pacific plate by the North American continental margin trench. The plate itself was extremely thin near its source, the East Pacific Rise, but thickened as it cooled while moving eastward; the plate thinned again during subduction, possibly because of heating by the mantle (Atwater, 1970). The compression applied to the continental mass by the subducting plate permitted volcanism only through forceful injection, resulting in dominantly intermediate-composition lavas and intrusive rocks (Scholz and others, 1971).

About 60 m.y. ago, the subducting plate reached a position approximately beneath the Great Basin, where the temperatures were high enough for magma generation (McKee, 1971) (fig. 31a). This magma took about 20 m.y. to reach the surface (McKee, 1971), at which time an episode of volcanic activity began over a broad region of the central Great Basin almost simultaneously (fig. 31b),

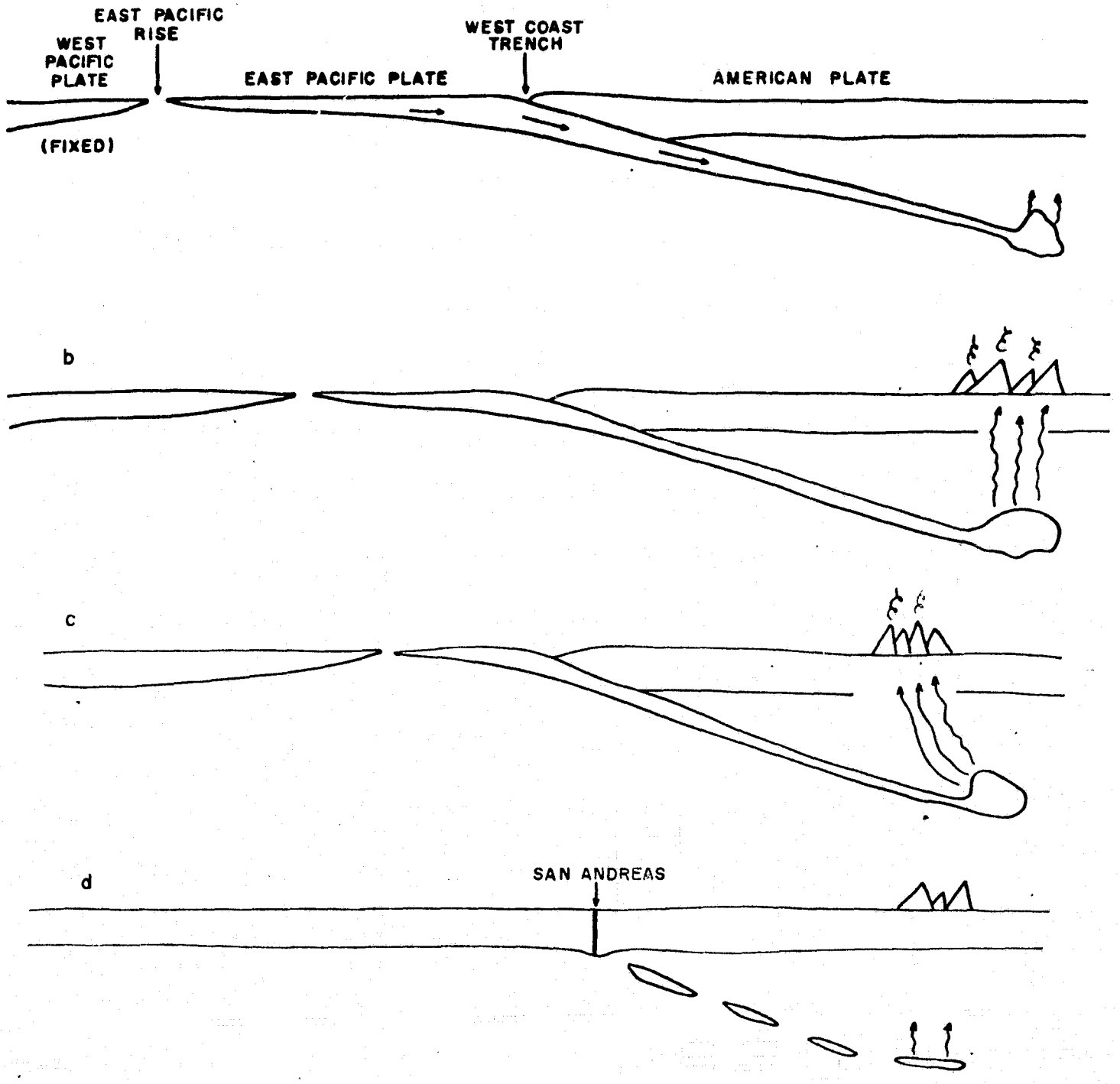

Fig. 31 - Generally east-west schematic cross section through central Nevada showing eastward migration of the East Pacific Rise and subduction of the East Pacific plate a) to the level of melting 60 m.y. ago, b) rise of the magma to the surface in the core area 40 m.y. ago, c) migration of volcanic activity to the central Nevada core-area, and d) cessation of volcanism in the Great Basin and migration of the Mendicino triple junction past the continental margin 19 m.y. ago (Modified from Atwater, 1970).

producing the "core area" of Armstrong and others (1969). This activity, estimated to have occurred within a time frame of 37 m.y. - 40 m.y. (early Oligocene time) (Armstrong and others, 1969; McKee and Silberman, 1970; McKee, 1971) ended a hiatus in volcanic activity which, in central Nevada lasted at least 50 m.y. (McKee, 1971). Intermediate-composition lavas and intrusive rocks predominated until about 34 m.y. ago at which time voluminous rhyolitic ash-flow sheets, probably later stage differentiates of the intermediate-composition magma, erupted accompanied by only minor andesite and dacite lave flows (McKee, 1971).

Migrations of volcanic activity from the "core area" towards the Walker Lane began approximately 30 m.y. ago, the activity focusing at many individual and complex calderas which form the "Central Nevada Volcanic Complex" (fig. 31c). The cause of this migration is difficult to determine because of uncertainties concerning the rate and direction of plate motions during early and middle Tertiary time. However, it is probably significant that the migration was from the relatively stable interior of the Great Basin towards the apparently continuously active Walker Lane. The Walker Lane and the San Andreas, to which it is probably related, appear to have been the dominant tectonic elements throughout most of the Cenozoic, and any change in their movement patterns probably influenced the distribution of volcanism in the Great Basin.

The San Andreas fault is the product of continued eastward migration of the East Pacific Rise which led to the progressive destruction of the Rise and a growing zone of contact between the American and

West Pacific plates. According to the models of Atwater (1970) and Christiansen and Lipman (1972), these two plates were not in contact along the coast of California before about 20 m.y. ago, although the Rise encountered the northern coast of Mexico approximately 30 m.y. ago. However, stratigraphic relationships suggest that the San Andreas zone existed as an early and middle Tertiary trench-related, strike-slip fault and that approximately two-thirds of the displacement is post-Oligocene (Huffman, 1970; Hill and Hobson, 1968; Atwater, 1970). Therefore, a substantial increase in the rate of movement apparently began along the San Andreas zone near the end of the Oligocene or roughly 25-30 m.y. ago. Similarly oriented zones of weakness farther inland such as the Walker Lane and possibly the Rye Patch and Oregon-Nevada systems were probably reactivated at this time. However, the deformation along these inland zones was probably confined mainly to faulting and fracturing with only limited displacement, because most of the large-scale sigmoidal bending in the Walker Lane was accomplished before Miocene time. Left-lateral movement may have occurred concurrently along the north-northeast to northeast-trending elements of the shear system, the Midas Trench and Ruby Mountain zones, but the intensity of deformation was probably less along these zones than along the three previously mentioned zones. Late Oligocene reactivation of the shear system and of the east-trending systems resulted in formation of a preferred conduit for the rising magma where these zones intersected.

The conjugate shear system proposed above requires a generally north-oriented axis of maximum stress bisecting the acute angle formed by the shear zones. At the intersections of the northwest-trending zones with the northeast-trending Midas Trench, this acute angle varies from about 60° to 80°. Right-lateral movement along the north-northwest to northwest-trending zone, especially the Walker Lane, was dominant during the late Oligocene reactivation of the shear system.

Concentration of volcanic activity in the "Central Nevada Volcanic Complex" until 19 m.y. ago, led to formation of a thick sequence of silicic volcanic rocks and an anomalously thick crust. The continuity of this activity in a confined region implies reasonably stable stress conditions between 30 m.y. and 19 m.y. ago. Cessation of activity 19 m.y. ago in the Great Basin was apparently due to consumption of the East Pacific Plate (fig. 31d).

A hiatus in volcanic activity in the Great Basin from about 19 m.y. to 16 m.y. ago coincides with growth of the San Andreas fault opposite that region. Right-lateral movement, which was conspicuous during the late Oligocene reactivation of the proposed conjugate shear system, became dominant throughout most of the western United States during late Cenozoic time (Wise, 1963). Hamilton and Myers (1966) pointed out the northwestward shift of Baja California and coastal California with respect to the rest of the continent. In addition, geologic evidence suggests that the Sierra Nevada and the Idaho batholith may originally have been a single body (Smith and others, 1971) which has subsequently been segmented and rotated by

right-lateral forces (Hamilton and Myers, 1966). In the Great Basin, the main consequence of this broad pattern of right-lateral distortion was rifting along north-trending normal faults and extension of the crust (Wise, 1963).

The crustal thinning and associated fracturing of the crust in the Great Basin beginning about 16 m.y. ago permitted the rising and eruption of dominantly basaltic magma whose source may have been the remnant magma pool of the subduction zone. Concentration of these rocks along a broad zone generally coincident with the Walker Lane is evidence of the continuing importance of this fault zone during the late Cenozoic. The Midas Trench system may have also played an important role during this period by influencing the position of Snake River opening and perhaps by providing access to subjacent basaltic magma.

The high heat flow and low crustal velocity in the Great Basin appear to be the result of the extension and volcanism, not the cause (Christiansen and Lipman, 1972). Causes suggested for these anomalies have been the migration of the East Pacific Rise to a place under the Great Basin (Hamilton and Myers, 1966; McKee, 1971) and the presence of an interarc basin system (Scholz and others, 1971). However, there is no evidence in California of the East Pacific Rise having passed beneath it as the Rise supposedly migrated eastward. As for the presence of an interarc basin, Scholz and others (1971) themselves pointed out that the formation of a steeply dipping subduction zone is required, whereas the evidence for the subduction zone indicates

a gently dipping one (Atwater, 1970; Christiansen and Lipman, 1972). In addition, when the subduction zone opposite the Great Basin was destroyed about 19 m.y. ago, there was no longer a source for generating the quantities of magma needed to maintain a diapir, much less one active enough to cause regional extension.

Implications for the Occurrence of Ore Deposits

The possible causes responsible for the present known distribution of ore deposits in the Western United States have long intrigued geologists. Noble (1970) gave a comprehensive review of the pertinent literature, in which the prevailing theories are localization of ore along major tectonic features and at their intersections, association with intrusive bodies, which in turn may be structurally controlled, and the primary existence of metal provinces in the mantle itself. The most widely supported hypothesis appears to be that of structural control.

Jerome and Cook (1967), for example, examined the metal mining district locations with respect to regional tectonic environments such as shield, shelf, basin, and geosyncline have had a negligible influence on the localization of ore deposits. Instead they speak of a dominant sequence of folding, faulting, intrusion, faulting or brecciation, and mineralization. In Nevada, Roberts (1966) proposed three orders of tectonic elements of Precambrian age which he correlated with the distribution of ore deposits. Eight of his mineral belts trend northwest, three trend east and are concentrated along the eastern border of Nevada, one trends northeast and one north-northwest (fig. 32).

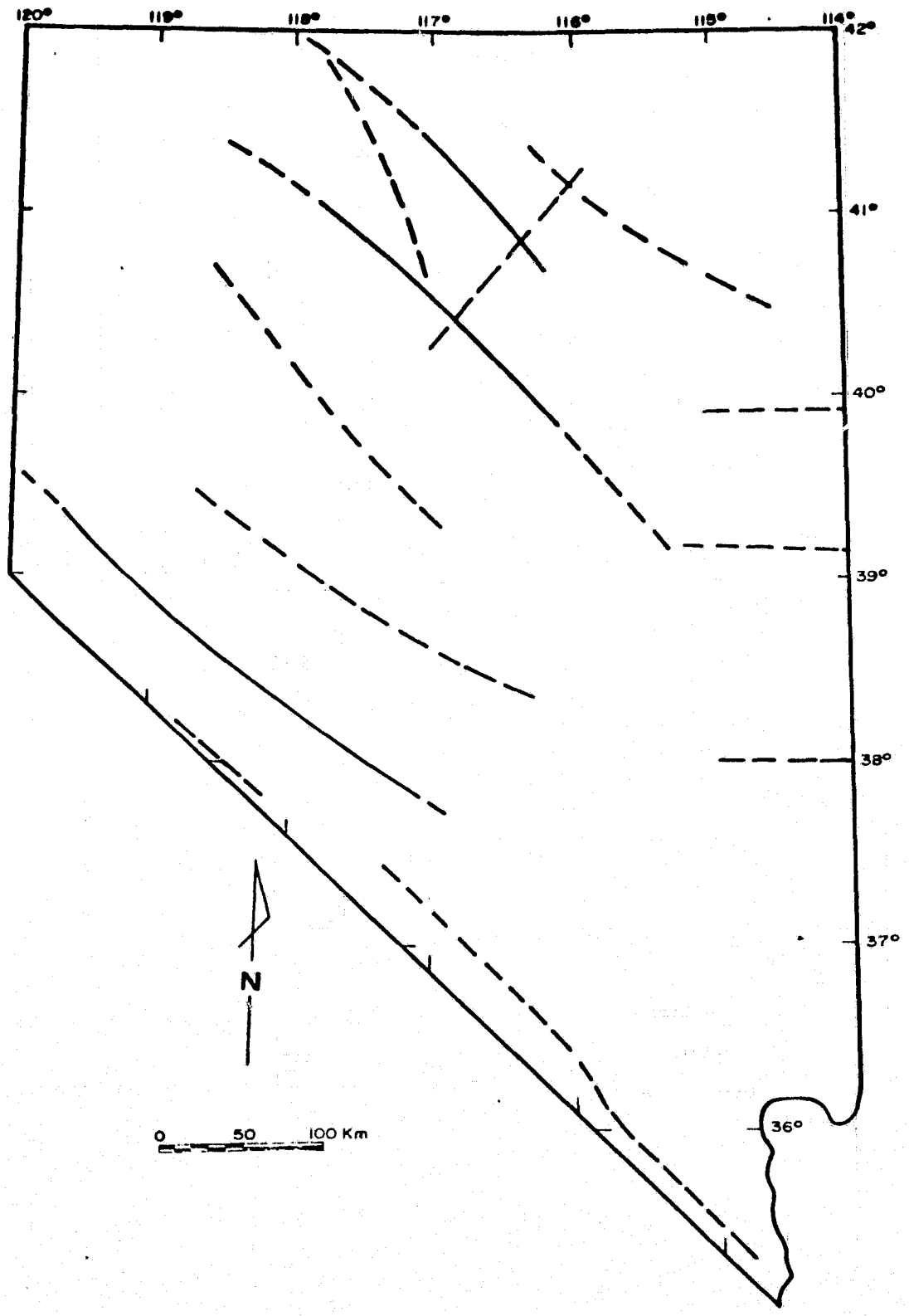

Fig. 32 - Tectonic elements denoting mineral belts according to Roberts (1966).

However, Horton (1966) believes that only two of these belts, the Battle Mountain Eureka belt and the Walker Lane, are valid on the basis of statistical analyses.

We believe that the localization of ore deposits in Nevada is genetically related to the basic tectonic framework of the State and propose that our seven major lineament systems, which we have interpreted as major zones of weakness, probably as old as Precambrian, are an important part of that primary tectonic framework. If this is true, a correlation of the lineament systems with the present distribution of metal mining districts should exist.

In order to examine this possible relationship, the locations of the metal-mining districts in Nevada (Horton, 1964) (fig. 33) were overlain by a 1.75-cm grid, counted within each grid square, and the resulting numbers contoured (fig. 34). The most striking alignment of high mining-district density is that coincident with the northeast-trending Midas Trench lineament zone (fig. 15, B and fig. 34). This alignment is transected by an area of low ore density which approximates the northern part of the Oregon-Nevada lineament. The lack of known deposits in this area may be due to the extensive Tertiary volcanic overburden. It is noteworthy that the largest areal density of known ore deposits along the Midas Trench lineament system occurs at the intersection coincides with the Rye Patch system.

The second most striking element in fig. 34 is the dominance of easterly trends in south-central and east-central Nevada. Our lineament system, E, (see fig. 15) coincides with two of the three most distinct

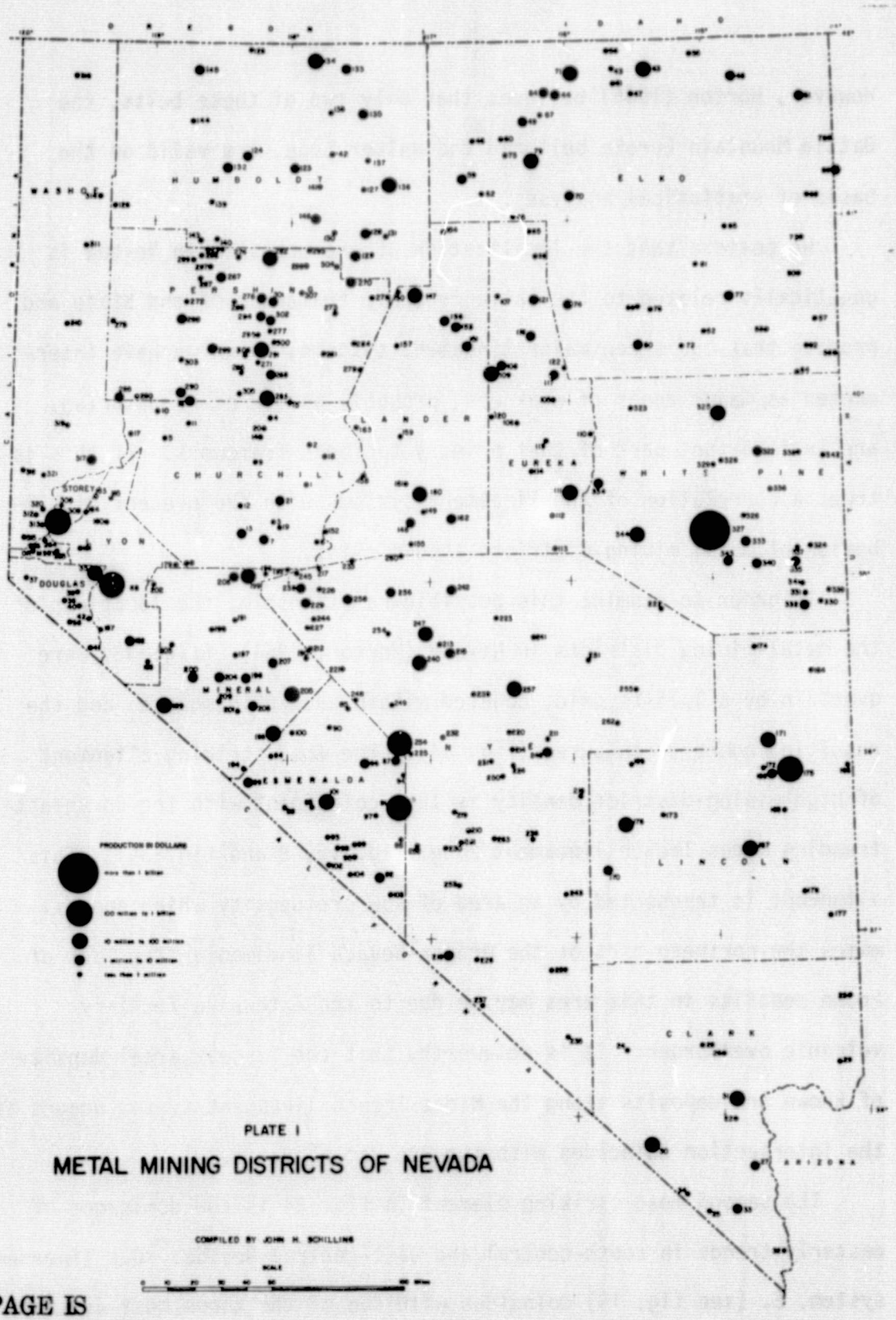

Fig. 33 - Distribution of metal mining districts of Nevada showing dollar value (Horton, 1964).

CHURCHILL COUNTY

1	ALPINE (Clan Alpine)	Ag, Au
2	BERNICE	Sb, Ag, Au
3	CHALK MOUNTAIN	Pb, Ag, Au
4	COPPER KETTLE	Cu
5	DESERT (White Plain)	Au, Ag
6	EASTGATE	Au, Ag, Pb
7	FAIRVIEW (Bell Mountain, Gold Basin, South Fairview)	Ag, Au, Pb, Cu
8	HOLY CROSS (Fallon, Terrell, Wild Horse)	Mn, Hg, Ag, Au, Pb
9	I X L (Cox Canyon, Job Peak, Silver Hill)	Au, Ag
10	JESSUP	Au
11	LAKE (Mopung Hills)	Sb, Pb, Ag
12	MOUNTAIN WELLS (La Plata)	Ag, Au
13	SAND SPRINGS	Ag, Au, W
14	SHADY RUN (Fondaway)	W, Au, Ag
15	TABLE MOUNTAIN (Bolivia, Boyer, Cottonwood Canyon)	Au, Cu, Ni, Hg, Ag, Sb, Co
16	TOY (Browns, St. Anthony)	W
17	TRUCKEE (Fireball)	Au
18	TUNGSTEN MOUNTAIN (Hilltop)	W
19	WESTGATE	Ag, Pb, Au
20	WHITE CLOUD (Coppereid)	Au, Cu, Ag
21	WONDER (Hercules)	Ag, Au, Cu

CLARK COUNTY

22	ALUNITE (Railroad Pass, Vincent)	Au
23	BUNKERVILLE (Copper King, Key West)	Cu, Au, Ag, W, Ni, Pd, Pt, Co, Mo
24	CHARLESTON	Pb
25	CRESCENT (Crescent Peak)	Ag, Au, Pb, Cu
26	DIKE	Pb
27	ELDORADO (Colorado, Nelson)	Ag, Au, Pb, Cu
28	GASS PEAK	Ag, Au, Pb
29	GOLD BUTTE	Au, Cu, Zn, Ag, Pb, U
30	GOODSPRINGS (Yellow Pine, Potosi)	Zn, Pb, Au, Ag, Cu, V, Mo, Pt, Pd, U, Co
31	LAS VEGAS	Mn, Pb, Zn
32	NEWBERRY	Au, Ag
33	SEARCHLIGHT	Au, Ag, Cu, Pb
34	SUNSET (Lyons)	Au

DOUGLAS COUNTY

35	BUCKSKIN (Smith Valley)	Fe, Au, Cu, Ag
36	GARDNERVILLE (Eagle)	W, Au, Ag, Sb
37	GENOA	Au
38	MOUNTAIN HOUSE (Holbrook)	Ag, Au, Pb, W
39	MOUNT SIEGEL	Au
40	RED CANYON (Silver Lake)	Ag, Au, Pb
41	RISUE CANYON	Au, Ag, W
42	SILVER GLANCE	Au, Ag

ELKO COUNTY

43	ALDER (Tennessee Gulch, Tennessee Mountain)	W, Ag, Au
44	AURA (Bull Run, Centennial, Columbia)	Ag, Au, Sb
45	BOOTSTRAP	Au, Ag
46	BURNER (Burner Hills)	Pb, Ag
47	CHARLESTON (Copper Mountain, Cornwall)	Sb, Ag, Au, Cu
48	CONTACT ([illegible], Carson, Porter, Salmon River)	Cu, Ag, Pb, Au, Zn, W
49	CORNUCOPIA	Ag, Au
50	DECOY	Mn
51	DELANO (Delno)	Pb, Ag, Cu, Zn, Au
52	DELKER	Cu
53	DOLLY VARDEN (Granite, [illegible], Mizpah)	Cu, Pb, Ag, Au
54	EDGEMONT (Centennial)	Au, Pb, Ag, Cu
55	ELK MOUNTAIN	W
56	FERBER	Cu, Pb, Ag, Au
57	FERGUSON SPRING (Allegheny)	Cu
58	GOLD BASIN (Rowland)	Cu, Au
59	GOLD CIRCLE (Midas, Summit)	Au, Ag, Pb
60	GOOD HOPE	Ag
61	ISLAND MOUNTAIN (Gold Creek)	Au, W, Ag, Sb
62	IVANHOE	Hg
63	JARBIDGE	Au, Ag, W
64	KINSLEY	Cu, W, Au, Ag, Pb
65	LAFAYETTE	Pb, Ag, W
66	LEE	Cu
67	LIME MOUNTAIN (Deep Creek)	Cu, Au, Ag
68	LORAY (Montello, Leroy, Loray)	Pb, Ag, Cu
69	LUCIN (Buel)	Cu, Ag, Pb
70	MERRIMAC (Lone Mountain)	Ag, Pb, Cu, Zn, Au, W
71	MOUNTAIN CITY (Cope, Rio Tinto, Van Duzer)	Cu, Ag, Au, U, Pb, Mn
72	MUD SPRINGS (Dead Horse, Medicine Springs)	Pb, Ag
73	PROL [illegible]	Ag
74	RAILROAD (Bullion)	Pb, Cu, Ag, Au, Zn
75	ROCK CREEK ([illegible], Falcon)	Ag, Hg
76	RUBY VALLEY (Smith Creek)	W, Pb, Zn, Ag, Cu
77	SPRUCE MOUNTAIN (Latham, Johnson, Steptoe)	Pb, Ag, Zn, Cu, Au, W
78	TECOMA	Pb, Ag, Cu, Au
79	TUSCARORA	Ag, Au
80	VALLEY VIEW (Harrison Pass)	W, Pb, Zn
81	WARM CREEK	Zn, Pb
82	WHITE HORSE	Pb, Ag, Zn

ESMERALDA COUNTY

83	ARGENTITE	Ag
84	BLACK HORSE	W, Fe
85	CROW SPRINGS	
86	CUPRITE	Au, Ag, Cu, Pb
87	DIVIDE (Gold Mountain)	Ag, Au, Pb
88	DYER	Ag, Pb
89	FISH LAKE VALLEY (White Mountains)	Hg
90	GILBERT (Desert)	Au, Ag, Cu, Hg
91	GOLDFIELD (Diamondfield)	Au, Cu, Ag
92	GOLD POINT (Hornsilver, Lime Point)	Au, Ag, Cu, Pb, Zn
93	GOOD HOPE	Ag
94	KLONDYKE	Ag, Au, Pb, Cu
95	LIDA (Alida Valley)	Ag, Au, Pb, Cu
96	LONE MOUNTAIN (Weepah, West Divide)	Au, Ag, Pb, Cu, Zn
97	MONTEZUMA	Ag, Pb, Au, Cu
98	PALMETTO (Fesler, Pigeon Springs, Windypah)	Pb, Au, Ag, Cu
99	RAILROAD SPRINGS	Cu, Au, Ag
100	ROCK HILL	W, Fe
101	SILVER PEAK (Mineral Ridge, Red Mountain)	Au, Ag, Pb, Cu
102	SYLVANIA (Green Mountain)	W, Au, Pb, Ag
103	TOKOP ([illegible], Gold Mountain, Oriental Wash)	Au, Ag, Pb, W, Cu
104	TULE CANYON	Au, Ag

EUREKA COUNTY

105	ALPHA	Ag, Pb
106	ANTELOPE	Ag, Zn, Pb, Au, Cu
107	BEOWAWE	Hg
108	BUCKHORN	Au, Ag
109	CORTEZ (Mill Canyon, Mount Tenabo)	Ag, Au, Pb, Cu, Zn, Hg
110	DIAMOND (Phillipsburg)	Ag, Pb, Zn, Au, Cu
111	EUREKA (Ruby Hill, Pinto, Prospect, Silverado, Secret Canyon, Spring Valley)	Pb, Au, Ag, Cu, Zn, Sb
112	FISH CREEK	Ag
113	GIBELLINI	Mn
114	LONE MOUNTAIN	Zn, Pb, Ag
115	LYNN	Au
116	MAGGIE CREEK (Schroeder, Susie Creek)	Cu, Au, Ag
117	MINERAL HILL	Pb, Ag, Cu, Au, Zn
118	MODARELLI (Amarilla)	Fe
119	MOUNT HOPE	
120	ROBERTS	Zn, Pb
121	SAFFORD (North Palisade, Pine Valley)	Fe, Ag, Cu, Pb
122	UNION	Pb, Ag

HUMBOLDT COUNTY

123	AWAKENING (Amos, Slumbering Hills)	Au, Ag, Pb, Cu
124	BOTTLE CREEK	Hg
125	DISASTER (Disaster Peak)	Ag, Au
126	DONNELLY	Au, Ag
127	DUTCH FLAT (Florence, Willow Point)	Au, Hg, Ag, Pb, Cu
128	GOLCONDA	W, Ag, Mn, Au
129	GOLD RUN (Adelaide)	Au, Ag, Cu, Pb, Zn
130	HARMONY (Sonoma Mountain)	Cu, Au, Ag
131	IRON POINT	Ag, Mn
132	JACKSON MOUNTAINS (Jackson Creek)	Fe
133	NATIONAL	Au, Ag, Hg, Cu, W
134	OPALITE (Cordero, McDermitt)	Hg
135	PARADISE VALLEY (Spring City, Mount Rose, Poverty Creek)	Ag, Au, Cu
136	POTOSI (Osgood Range, Getchell, Kelly Creek, Preble)	W, Au, Ag, Mn, Cu
137	POVERTY PEAK	Hg
138	REBEL CREEK (New Goldfields, Willow Creek)	Ag, Au
139	RED BUTTE	Cu, Ag, Hg, Pb, Zn, Sb
140	SAWTOOTH (Mandalay)	Au
141	SHERMAN (Bloody Run)	W, Au, Ag
142	SHON	Ag, W
143	SULPHUR	Ag, Hg
144	VARYVILLE (Columbia, Leonard Creek, Pine Forest)	Au, Sb, Ag, Cu, Pb
145	WARM SPRINGS (Ashdown, Pueblo, Vicksburg)	Au, W, Ag, Cu
146	WINNEMUCCA (Barrett Springs, Ten Mile)	Ag, Au, Pb, Sb, Cu, Zn

LANDER COUNTY

147	BATTLE MOUNTAIN (Copper Basin, Copper Canyon, Galena, [illegible], Telluride)	Cu, Au, Pb, Zn, Sb, Ag
148	BIG CREEK	Sb
149	BIRCH CREEK (Smoky Valley, Big Smoky)	W, Au, Ag, U
150	BUFFALO VALLEY (Mill Canyon)	Mn, Au, Ag
151	BULLION (Tenabo, Gold Acres, Lander, Campbell)	Au, Ag, Cu, Pb, W
152	GOLD BASIN	Au, Ag
153	HILLTOP (Kimberly, Marysville)	Au, Ag, Cu, Pb, Sb
154	IZENHOOD [illegible]	
155	KINGSTON (Bunker Hill, Santa Fe, Summit, Victorine)	Au, Ag
156	LEWIS (Dean, Mud Springs, Pittsburg)	Ag, Pb, Au, Cu, Sb
157	McCOY (Horse Canyon)	Au, Fe, Ag, Pb, Zn
158	NEW PASS	Au, Mn, Ag, Pb
159	RAVENSWOOD (Shoshone)	Ag, Au
160	REESE RIVER (Austin, Amador, Yankee Blade)	Ag, Au, U
161	SKOOKUM	Ag, Au
162	SPENCERS HOT SPRING ([illegible])	W
163	WILD HORSE	Hg, Mn

LINCOLN COUNTY

164	ATLANTA (Silver Park, Silver Spring)	Au, Ag, U
165	CHIEF (Caliente)	Au, Ag, Pb, Cu
166	COMET	Ag, Zn, Pb, Au, Cu, W
167	DELAMAR (Ferguson)	Au, Ag
168	EAGLE VALLEY (Fay, [illegible])	Au, Ag, Pb, Cu
169	FREIBERG (Worthington)	Au, Ag, Pb, Zn
170	GROOM	Pb, Ag, Cu
171	JACK RABBIT (Bristol, [illegible])	Cu, Ag, Pb, Mn, Zn, Au
172	LONE MOUNTAIN (Ely Springs)	Ag
173	PAHRANAGAT (Hiko)	Mn, Ag, Pb, Cu, Au
174	PATTERSON (Cave Valley, Geyser)	Ag, Au, Pb, Cu
175	PIOCHE (Ely, Highland)	Zn, Pb, Ag, Au, Mn, Cu, Fe
176	TEM PIUTE	W, Ag, Zn, Pb
177	VIGO manganese	
178	VIOLA	Au, Ag, Cu, Pb

LYON COUNTY

179	BENWAY	Au, Ag, Cu
180	CHURCHILL	W
181	COMO (Palmyra, Indian Springs)	Au, Ag, Cu
182	PINE GROVE (Wilson, Cambridge, Rockland)	Au, Ag, Zn, W, Fe
183	RAMSEY	Au
184	RED MOUNTAIN	W, Fe

SILVER CITY — included in Comstock district, Storey County

185	TALAPOOSA	Au, Ag, Hg
186	WASHINGTON	Cu, Au, Ag, Pb
187	WELLINGTON	Pb, Zn, Cu
188	YERINGTON (Ludwig, Mason)	Cu, Au, Ag

MINERAL COUNTY

189	AURORA (Esmeralda, Cambridge)	Au, Ag
190	BELL (Simon, Cedar Mountain, Omco)	Pb, Au, Ag, Zn, Cu, W, Hg
191	BOVARD (Rand, Copper Mountain)	Au, Cu, Ag, Pb
192	BROKEN HILLS	Ag, Pb, Au, Cu, Zn
193	BUCKLEY	Pb, Ag
194	BUENA VISTA (Russell, Oneota, Queen, Mt. Montgomery)	Au, Ag, Hg, Pb, W
195	CANDELARIA (Belleville, Columbus)	Ag, Au, Pb, Sb, Zn, Cu
196	EAGLEVILLE (Hot Springs)	Au, Ag, Sb
197	FITTING (Acme)	Ag, Au, Pb, W
198	GARFIELD	Ag, Au, Pb, W

HAWTHORNE — see Lucky Boy and Pamlico districts

199	LEONARD (Sunnyside)	W, Au, Pb, Ag
200	LUCKY BOY	Ag, Au, Pb, W
201	MARIETTA (Black Mountain)	Ag, Pb, W
202	MOUNTAIN VIEW (Granite, Reservation)	Cu, Au, Ag, W
203	MOUNT GRANT (East Walker, Walker Lake)	Au, Ag, Cu
204	PAMLICO (Sulphide)	Au, Ag, Sb
205	PILOT MOUNTAINS (Sodaville, Graham Springs)	Ag, W, Hg, Au, Pb, Zn
206	RAWHIDE (Regent)	Au, Ag, Cu, Pb, Sb
207	SANTA FE (Luning)	Cu, Ag, Au, W, Fe, Pb, Zn, Sb
208	SILVER STAR (Gold Range, Mina)	W, Au, Ag, Cu, Pb, Mn
209	WHISKEY FLAT (Sulphide)	Cu, Au, Ag

NYE COUNTY

210	ANTELOPE SPRINGS	Ag, Pb, Au
211	ARROWHEAD	Au, Ag
212	ATHENS	Au, Ag
213	BARCELONA (Spanish Belt, Meadow Canyon)	Ag, Hg, Au, W

BEATTY — see Bullfrog and Transvaal districts

214	BELLEHELLEN (Longstreet)	Ag, Au, Cu
215	BELMONT (Philadelphia, Silver Bend)	Ag, Au
216	BLACK HAWK	Hg
217	BRUNER (Phonolite)	Au, Ag
218	BULLFROG (Pioneer, Rhyolite)	Au, Ag, Pb, Cu
219	CACTUS SPRINGS	Au, Ag
220	CLIFFORD	Au, Ag
221	CLOVERDALE (Golden, [illegible] Springs, Republic)	Ag, Au, Pb
222	CURRANT	Au, Ag
223	DANVILLE	Ag, Au
224	EDEN (Eden Creek, Gold Bell)	Au, Ag
225	ELLENDALE	Au, Ag, Cu
226	ELLSWORTH (Marble Falls)	W, Au, Ag, Pb
227	FAIRDAY (Atwood, [illegible])	Ag, Au, Pb
228	FLUORINE (Bare Mountain)	Au, Hg, Ag
229	GABBS	Fe, Pb, Ag, Hg, W
230	GOLD CRATER	Au, Ag, Pb
231	GOLDEN ARROW ([illegible] Camp)	Ag, Au
232	HANNAPAH (Volcano, Silverzone, Bannock)	Ag, Au
233	JACKSON (Gold Park)	Au, Ag, Pb
234	JETT (Ledbetter Canyon, Pine Creek Canyon, Wall Canyon)	Sb, Hg, Pb, Ag, W
235	JOHNNIE	Au, Ag
236	KAWICH (Gold Reed, Queen City)	Ag, Au
237	LEE (Big Dunn)	
238	LODI (Granite, Marble)	W, Ag, Pb, Au
239	LONGSTREET (Fresno, George Canyon)	Au, Ag
240	MANHATTAN	Au, Ag, Sb
241	MOREY	Ag, Au, Sb
242	NORTHUMBERLAND	Au, Ag
243	OAK SPRINGS (Climax)	W, Ag, Au
244	PARADISE PEAK	W, Hg

PARADISE RANGE (Mammoth) — see Ellsworth, Gabbs and Paradise Peak districts

245	QUARTZ MOUNTAIN	Ag, Pb, Au
246	REVEILLE	Ag, Pb, Au, Sb, Cu, W
247	ROUND MOUNTAIN (Jefferson Canyon)	Au, Ag, W, Sb
248	ROYSTON	Ag, Pb, Cu
249	SAN ANTONE (Liberty, San Antonio)	Ag, Au, Pb, Cu
250	SILVER BOW	Ag, Au, Pb
251	SILVERTON	Ag
252	STONEWALL	Au, Ag, Cu
253	TOLICHA (Monte Cristo, Clarkdale)	Au, Ag
254	TONOPAH	Ag, Au, Pb, W, Cu
255	TROY (Irwin Canyon, Terrell)	W, Au, Zn, Ag, Pb
256	TWIN RIVER (Ophir)	Au, Ag, W, Pb, Zn
257	TYBO (Hot Creek, Empire, Keystone)	Pb, Ag, Zn, Au, Hg, Cu, Sb
258	UNION (Berlin, Grantsville, Ione)	Ag, Hg, Au, Pb, Cu, Sb, W
259	WAHMONIE	Ag, Au
260	WASHINGTON	Ag, Pb
261	WELLINGTON (Jamestown, O'Brien)	Au, Ag
262	WILLOW CREEK ([illegible], Quinn Canyon)	Au, Ag
263	WILSONS ([illegible])	Ag, Au

ORMSBY COUNTY

264	CARSON CITY	Au, Ag
265	DELAWARE (Brunswick Canyon, Sullivan)	Au, Pb, Ag, Fe, W
266	VOLTAIRE (Eagle Valley, Washoe)	Ag, Pb, Au, Cu, W

PERSHING COUNTY

267	ANTELOPE (Cedar, Majuba Hill)	Cu, Ag, Au, Pb, Sb
268	ANTELOPE SPRINGS (Relief)	Hg, Sb, Pb, Ag, Au
269	ARABIA (Trinity)	Pb, Ag, Sb
270	BLACK DIABLO	Mn
271	BLACK KNOB	Sb, Hg
272	FARRELL (Stone House)	Au
273	GOLDBANKS	Hg
274	HAYSTACK	Au, Ag
275	HOOKER (Empire)	W
276	IMLAY (Humboldt, Eldorado, Prince Royal)	Au, Hg, Ag, W
277	INDIAN	Ag, Au
278	IRON HAT (Aldrich)	Sb, W, Pb, Ag
279	JERSEY	Ag, Au, Pb
280	JUNIPER RANGE	W
281	KENNEDY	Au, Ag, Cu, Pb
282	MILL CITY (Central)	W, Ag, Au, Pb
283	MINERAL BASIN	Fe
284	MOUNT TOBIN	Hg, W
285	MUTTLEBERRY	Ag, Pb, Sb
286	NIGHTINGALE	W

ORLEANA — see Sacramento, Rochester and Rye Patch districts

287	PLACERITES	Au
288	POKER BROWN (San Jacinto)	Ag, Pb, Sb
289	RABBIT HOLE	Au
290	RAGGED TOP (Copper Valley)	W
291	ROCHESTER	Ag, Au
292	ROSEBUD	Au, Ag, Cu
293	ROSE CREEK	W
294	RYE PATCH (Echo)	Au, Ag, W, Sb
295	SACRAMENTO	Ag, Pb
296	SAWTOOTH (Mandalay)	Au
297	SCOSSA	Au, Ag
298	SEVEN TROUGHS	Au, Ag, W
299	SIERRA (Dun Glen, Chafey, Oro Fino, Sunshine)	Au, Ag, Pb, Cu
300	SPRING VALLEY (Fitting, American)	Hg, Au, Ag
301	STAR (Bloody Canyon, Santa Clara)	Sb, Ag, Au
302	UNIONVILLE (Buena Vista)	Ag, Au, Sb
303	VELVET	Au
304	WASHIKI ([illegible])	Au
305	WILD HORSE	W, Sb, Ag, Pb
306	WILLARD (Loring, Lovelock)	Sb, Au, Ag
307	WILLOW CREEK	Au

STOREY COUNTY

308	CASTLE PEAK (Red Mountain)	Hg
309	COMSTOCK ([illegible], Virginia City, Gold Hill, Silver City, Flowery)	Au, Ag

WASHOE COUNTY

310	COTTONWOOD	Au, Ag, Pb
311	DEEPHOLE (Granite Range)	Au, Ag, Cu, Pb, W
312	GALENA (Washoe Valley)	Zn, Pb, Ag, Cu, Au
313	JUMBO (West Comstock)	Au, Ag
314	LEADVILLE	Ag, Pb, Au
315	LITTLE VALLEY	Au
316	LONE PINE	Hg
317	OLINGHOUSE (White Horse)	Au, Ag
318	PEAVINE (Reno, [illegible] Mountain)	Au, Ag, Cu
319	PYRAMID	Ag, Au, W, Cu, Sb
320	STEAMBOAT SPRINGS	Hg
321	WEDEKIND ([illegible])	Ag, Au

WHITE PINE COUNTY

322	AURUM (Schell Creek, Schellbourne, Siegel, Queen Springs, Silver Canyon, Ruby Hill, Muncy Creek, Silver Mountain)	Zn, Ag, Cu, Au, Pb, Mn
323	BALD MOUNTAIN (Joy, Ruby Mountain)	W, Cu, Au, Ag, Sb
324	BLACK HORSE	Ag, W, Au, Pb
325	CHERRY CREEK (Egan Canyon, Gold Canyon)	W, Ag, Au, Pb, Cu
326	DUCK CREEK (Success)	Pb, Ag, Au, Cu, Zn

EAGLE — see Red Hills and Tungstonia districts

327	ELY (Robinson, Ruth)	Cu, Au, Ag, Mo, Zn, Pb, Mn
328	GRANITE (Stinson)	Pb, Au, Ag
329	HUNTER	Ag, Pb
330	LEXINGTON	
331	LINCOLN ([illegible])	W, Ag, Pb
332	[illegible]	W, Ag
333	NEVADA	Mn, Ag, Au
334	NEWARK (Strawberry)	W, Ag, Au, Pb
335	OSCEOLA	Au, Ag, W, Pb
336	PIERMONT	Ag, Au
337	SACRAMENTO (Sacramento Pass)	Au, Ag, W

SHOSHONE — see Minerva, Lexington and Lincoln districts

338	RED HILLS	Pb, Ag, Au, Cu
339	SHAFT ([illegible])	W, Ag
340	TAYLOR	Ag, Au, Sb, Pb
341	TUNGSTEN [illegible]	W, Ag
342	TUNGSTONIA (Regan, New Pleasant Valley)	W, Au, Ag, Pb, Cu, Zn
343	WARD	Ag, Au, Pb, Cu, Zn
344	WHITE PINE (Hamilton)	Pb, Ag, Au, Cu, Zn, W

Fig. 33 (cont'd)- Listing of metal mining districts shown on map.

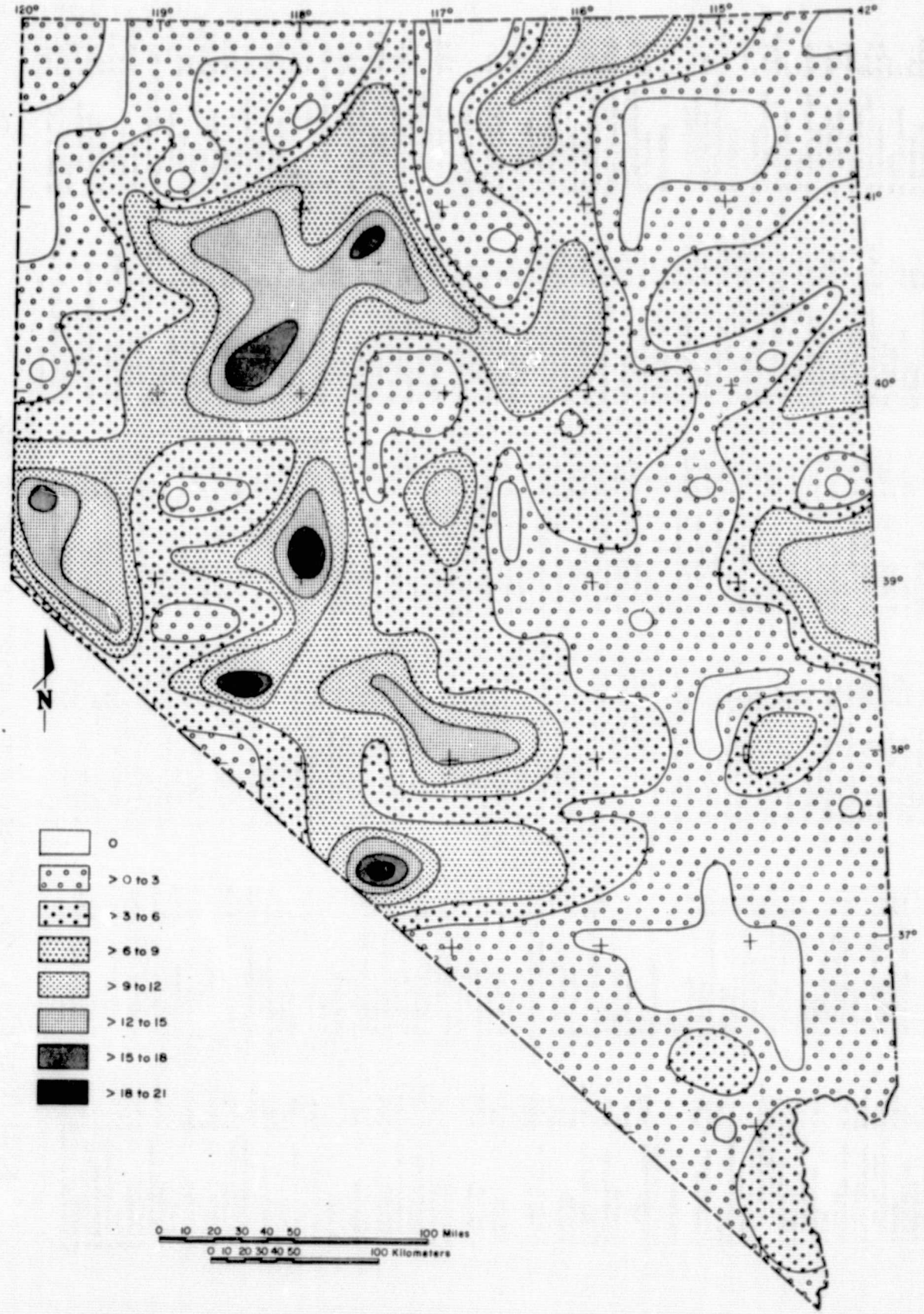

Fig. 34 - Contour map of the distribution of metal mining districts in Nevada. Original data from Horton (1964).

east-trending zones of high ore-deposit density in south-central Nevada. The third zone to the south aligns with the western extension of lineament, F (fig. 15); in addition, it coincides with a previously published lineament zone (Rowan and Wetlaufer, 1973), which was subsequently deleted because its component parts were less than 10 km long (see definition of major lineaments, p. 6). The two weaker easterly trends along the eastern border of Nevada representing intermediate densities of ore deposits coincide with two of Roberts (1966) east-trending tectonic and mineral belts (fig. 32).

The trend of the Walker Lane along its northern and central parts is weakly apparent in fig. 34. However, those areas of high ore-density which define the general northwest-trending zone along the southwestern border of Nevada occur almost exclusively associated with the intersections of east-trending major lineaments with the Walker Lane, as defined generally by our lineament system, A (fig. 15). Hence these heretofore unexamined easterly-trends may be of great importance economically. No east-trending lineaments transect the southern part of the Walker Lane, and indeed, southern Nevada itself is characterized by a conspicuous lack of known ore deposits, which Jerome and Cook (1967) referred to as the southern Nevada-Utah gap.

Although we believe that these results are quite encouraging, two fairly conspicuous linear zones of high ore-deposit concentration are not related to the major lineaments or lineament systems. There are the north-northwest-trending zone east of the Rye Patch lineament system and the north-northeast-trending zone through central Nevada.

However, the former does coincide with Roberts' (1966) Battle Mountain-Eureka belt and also is parallel to the Rye Patch lineament system (fig. 15).

A second contour map was prepared by weighting the ore districts according to dollar value (Horton, 1964) (fig. 35). Weighting was accomplished by assigning a linear scale to the production values given by Horton and areal percentages were subsequently calculated within each grid cell (40 x 40 km). The most apparent variation between figs. 35 and 34 are the increased prominence of the two east-trending zones along the eastern border of Nevada and the addition of a third to the south. This third east-oriented zone also correlates with one of Roberts (1966) east-trending belts (fig. 32). The Walker Lane is also slightly more apparent, although two areas of high ore density within the general zone of the Walker Lane still appear to have been significantly influenced by the intersection of east-trending structural elements. The previously mentioned north-northeast-trending zone, which appears unrelated to our lineament systems, is substantially weakened in fig. 35 by the easterly-trends.

In this figure (35), as well as in fig. 34, intersections of the major lineaments with the proposed boundary of the central Nevada circular feature coincide with areas of high value and high density of ore districts. For example, the Rye Patch system intersects the circular feature near Austin (93 m.y.), the southern lineament of system E (fig. 15) at Tonopah (19 m.y.), and the Oregon-Nevada lineament at Eureka (102 m.y.). Extension of the Ruby Mountain lineament system

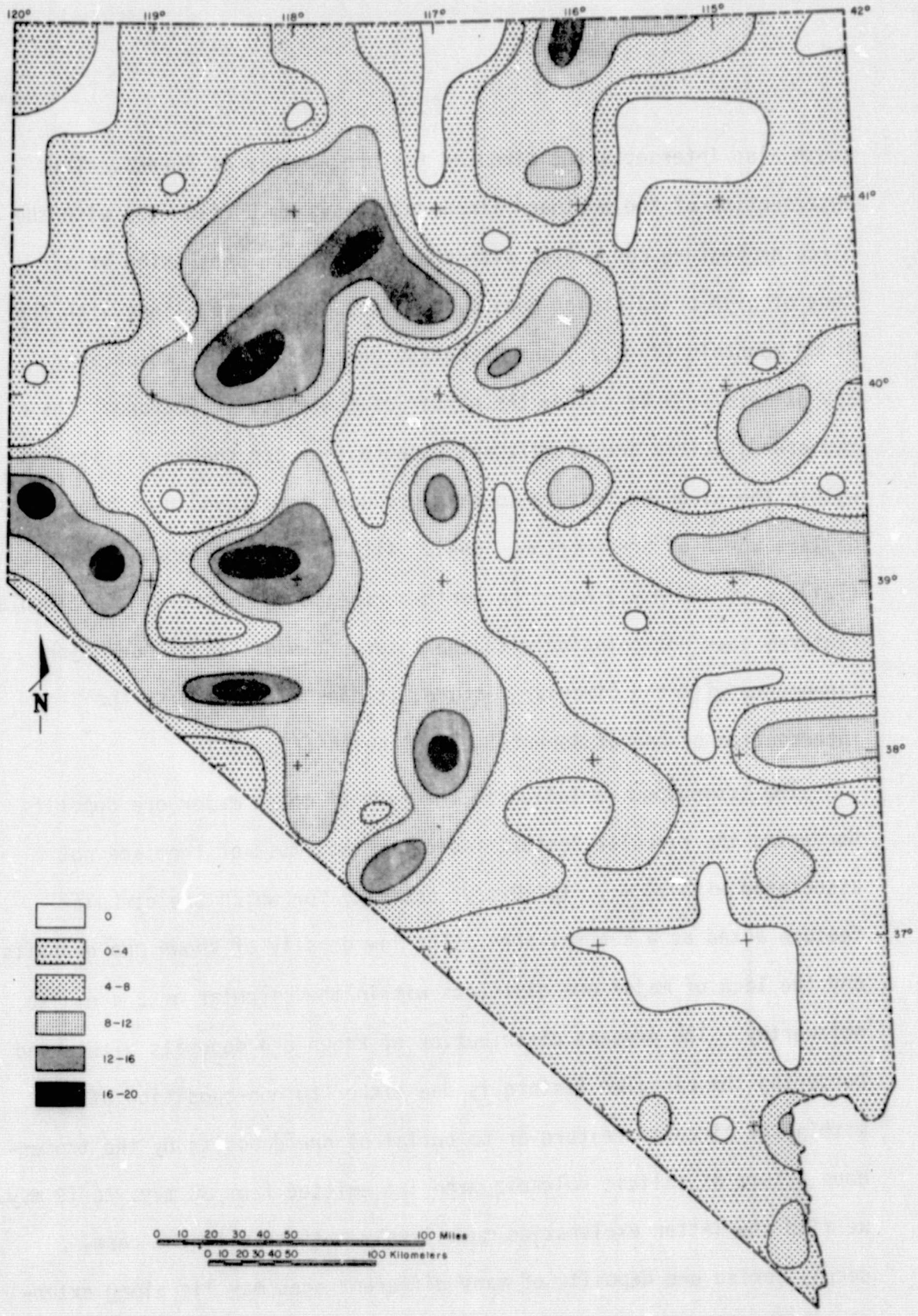

Fig. 35 - Contour map of the distribution of metal-mining districts in Nevada, weighted according to dollar value. Areal percent of weighted mining districts weighted according to size (dollars). n = 488. Original data from Horton (1964).

south also intersects the circular feature roughly at Eureka. The intersection of the northern lineament of system E (fig. 15) with the circular feature correlates with the northwestern protrusion of a zone of high ore-district density in fig. 35 and also aligns with the Round Mountain (25 m.y.) and Manhattan areas (16 m.y.), which are approximately 35 km inside the border of the circular feature. These two ore districts are significant because they are the only districts within the circular feature to have produced more than 10 million dollars worth of ore (Horton, 1964). Although the presence of Ely (121 m.y. - 123 m.y.) near the north-northeastern border of the circular features does not coincide with the intersectionof one of our major lineaments with the circular feature, it does coincide with the intersection of one of Roberts' (1966) belts (fig. 32).

The tremendous variation in the ages of these major ore deposits bordering the circular feature indicates that most of them are not associated with 30 m.y. to 19 m.y. activity for which the circular feature acted as a central area. The low density of known ore deposits and the lack of major ore districts within the circular area are also noteworthy. The present distribution of known ore deposits within and bordering the circular feature is due either to nondeposition of ore within the circular feature or to burial of ore deposits by the tremendous volume of silicic volcanic material emitted from 30 m.y. to 19 m.y. We find the latter explanation more likely. If this is the case, deeply buried ore deposits of many different ages may lie along extensions of our lineaments into the circular feature.

It has been suggested that intersections and alignments of intersections of linear features on ERTS imagery can coincide with mineralized areas (Levandowski and others, 1973; Nicolais, 1974). Because of our limited confidence in the validity of the original set of linears as structural features, we have not carried out an analysis of their intersections. However, we have undertaken an examination of major lineament intersections (fig. 23) because roughly 80 percent of them are mapped faults or extensions of the faults. Two areas of high density of lineament intersections are immediately apparent in fig. 23, one in central Nevada and the other in north-central Nevada. The latter represents the many intersections of Midas Trench lineaments with the Oregon-Nevada lineament zone, but comparison with figs. 34 and 35 indicates little correlation with ore-district locations. The former lies virtually at the center of the central-Nevada circular feature and also bears no apparent relationship with ore-deposit location. However, it does generally mark the area in which four of our lineament systems would intersect if they were extended into the circular feature. The east-trending southwestern extension from this area lies just south of the Round Mountain and Manhattan districts. Correlation of lineament intersections with ore deposits is more apparent along the central part of the Walker Lane (figs. 34 and 35) and is also apparent along Roberts' (1966) middle east-trending belt (fig. 31).

Caution should be used when evaluating intersections of linears.

The fundamental danger lies in the common difficulty of defining just exactly what the linear features represent. In many places, a correlation with ore deposition will be found, but even in these places, the nature of the linear features must be taken into account because some correlations may simply be fortuitous.

In summary, correlations of ore-deposit locations with the seven major lineament systems suggest that these linear zones did exert some influence at various times over the localization of ore deposits in Nevada. Intersections of these zones can be related to areas of high concentration of ore, although contouring of intersections of all the 367 major lineaments shows only very weak correlations and must be treated with caution.

Summary of Results

Compilation of all linear features detectable in ERTS-1 images of Nevada without regard for scale results in a large data set which is composed of features having different origins and therefore different degrees of geologic validity and significance. Geologic and geophysical analysis of these features individually is impractical, and statistical analysis of the entire set appears to be unsound because of the heterogeneity of the data. Moreover, comparison of these linear features with mapped faults in six sample areas shows only 24.3 percent average correspondence, and some of these correlations may be fortuitous. Therefore, the geologic value of this approach is highly questionable.

Linear features greater than 10 km long show a high degree of correspondence (79.9 percent) with mapped faults of this magnitude. This high degree of general correlation and the distinct continuous nature of most of the major lineaments suggests that many of the locally mapped faults can be extended as fault or fracture zones for tens and, in some places, hundreds of kilometers. In addition, many of the major lineaments which have not been related to mapped faults may be undetected zones of weakness. However, only 29.3 percent of the faults longer than 10 km on the State geologic map were detected, only a slight improvement over the comparable value for all linear features (24.3 percent). Therefore, although analysis of major linear features has considerable potential as an additional tool for structural analysis of this type of terrain, it complements rather than replaces conventional structural mapping techniques.

Geologic and geophysical analysis of the major lineaments results in identification of seven lineament systems which appear to be vertically, as well as horizontally, extensive, probably Precambrian zones of weakness. The two longest systems, the Walker Lane and the Midas Trench zones, along with the Hurrican-Sevier and Wasatch faults, bound a triangular block which occupies most of the Great Basin. We envision a conjugate shear system operating during the Cenozoic within this crustal block which had mainly dextral and sinistral movement along the northwest- and northeast-trending zones, respectively. However, periodic reactivations because of changing regional stresses have resulted in many different, commonly contridictory senses of movement. Four of these major lineament systems

converge towards the center of the central Nevada circular feature.

Volcanic activity began about 40 m.y. ago at many small, widely scattered centers in the central part of the Great Basin, probably as magma generated from the subducting East Pacific plate was forcefully injected along these and other fracture zones. Thin but widespread ash-flow tuff sheets and associated silicic to intermediate intrusive rocks which formed 40 m.y. ago in this part of the Basin constitute the core area proposed by Armstrong and others (1969) and McKee (1971). Approximately 30 m.y. ago, volcanic activity migrated southwestward towards the Walker Lane and became concentrated in the "Central Nevada Volcanic Complex." Concentration of activity in this area until volcanism ceased in the Great Basin about 19 m.y. ago resulted in a thick pile of ash-flow tuff sheets within the complex. This sequence of rocks accounts for the anomalously low total magnetic intensity and contributes to the Bouguer gravity low and the anomalously high crustal velocities typical of this area. Radiometric age determinations confirm that the "Central Nevada Volcanic Complex" is the geographic center of the rocks 19 m.y. to 30 m.y. old, but the determinations also show that the domain of these rocks extends beyond the northwestern and southeastern boundaries of the complex forming a northwest-trending belt. We refer to this belt of rocks 19 m.y. to 30 m.y. old as the Central Nevada Volcanic province, as distinct from the 30-40 m.y. old East-central Nevada province.

Migration of volcanic activity from the core area to the "Central Nevada Volcanic Complex" was due mainly to reactivation of the conjugate shear system, which resulted in development of a preferred conduit where the lineaments intersected. The proposed conjugate shear system requires a generally north-oriented maximum stress axis bisecting the 60°-90° angle formed by the shear zones. Right-lateral movement along the northwest-trending zones was dominant, within the shear system, especially along the Walker Lane. Reactivation of this system and dominance of the right-lateral zones was probably related to late Oligocene acceleration of movement along the San Andreas fault zone. Concentration of volcanism in the "Central Nevada Volcanic Complex", until 19 m.y. ago implies reasonably stable tectonic conditions in the Great Basin.

Volcanic activity resumed in the western Great Basin 16 m.y. ago as large-scale right-lateral deformation caused rifting along north-to north-northeast-trending faults. Concentration of mainly basaltic rocks of this age along a broad belt generally coincident with the Walker Lane and at the intersection of this system with the Midas Trench system suggests that these zones may have provided the main conduits for highly differentiated residual magma pools. The Midas Trench system may have also influenced the location of the southeastern boundary of Snake River Plains and perhaps development of the Yellowstone Park volcanic field.

Comparison of the major lineament systems with contour maps of the distribution and value of metal-mining districts shows excellent

agreement and therefore strongly suggests that the conjugate shear system influenced the deposition of ore bodies in Nevada. The most conspicuous correlation is the occurence of areas of high mining-district density along the entire length of the Midas Trench system, except where it is transected by the Oregon-Nevada system. The largest areal density of known ore deposits along the Midas Trench system occurs at the intersection of this system with the Rye Patch system.

In southern Nevada, the highest density of mining districts is along a broad belt which is generally coincident with the northern part of the Walker Lane. However, the dominant trend within this belt is east, the areal density highs being generally coincident with the east-trending lineament systems with the Walker Lane. Easterly-trends of districts are apparent along the Nevada-Utah border and become especially conspicuous when the dollar value of the deposits is considered. Therefore, the pattern that develops in southern Nevada is one of high areal density along east-trending structures, especially where the Walker Lane is intersected by one of these zones. However, this picture is interupted by the "Central Nevada Volcanic Complex" which is coincident with a broad area of low mining-district density and value. High-value districts ranging in age from 19 m.y. to 123 m.y. occur around the periphery of the complex. These relationships suggest that pre-complex ore deposits have been covered by the thick sequence of silicic volcanic rocks within the complex and that very limited volcanic activity and associated mineralization occurred within the complex after its formation.

Therefore, the conjugate shear system and the east-trending lineament systems appear to have played an important role in the localization of ore deposits, probably by providing the main conduits for ascending ore-bearing solutions. We regard the east-trending and Midas Trench zones as being especially important because their significance has not been fully recognized, even though their validity is supported by geologic and geophysical evidence. Intersections of these major zones are especially important in some places, but the limited correlation between the areal densities of mining districts and intersections of all major lineaments mapped in Nevada shows the need for considering geologic and geophysical data in the evaluation of lineaments in mineral exploration.

References

Albers, J. P., 1967, Belt of sigmoidal bending and right-lateral faulting in the western Great Basin: Geol. Soc. America Bull., v. 78, p. 143-156.

Albers, J. P., and Kleinhampl, F. J., 1970, Spatial relations of mineral deposits to Tertiary volcanic centers in Nevada: U.S. Geol. Survey Prof. Paper 700-C, p. C1-C10.

Albers, J. P., and Stewart, J. H., 1972, Geology and mineral deposits of Esmeralda County, Nevada: Nevada Bur. Mines and Geology Bull. 78, pp. 1-80.

Armstrong, R. L., Ekren, E. B., McKee, E. H., and Noble, D. C., 1969, Space-time relations of Cenozoic silicic volcanism in the Great Basin of the western United States: Am. Jour. Sci., v. 267, no 4, p. 478-490.

Atwater, T., 1970, Implications of plate tectonics for the Cenozoic tectonic evaluation of western North America: Geol. Soc. America Bull., v. 81, p. 3513 - 3536.

Billingsley, P. R., and Locke, Augustus, 1941, Structure of ore districts in the continental framework: Am. Inst. Mining Metall. Eng. Trans., v. 144, p. 9-59.

Bonham, H. F., 1969, Geology and mineral resources of Washoe and Storey Counties, Nevada: Nevada Bur. Mines Bull 70, 140 p.

Burchfiel, B. C., 1965, Structural geology of the Specter Range quadrangle, Nevada, and its regional significance: Geol. Soc. America Bull., v. 76, p. 175-192.

Bushnell, Kent, 1967, Geology of the Rowland quadrangle, Elko County, Nevada: Nevada Bur. Mines Bull. 67, 38 p.

Christiansen, R. L., and Blank, H. R., Jr. 1969, Volcanic evolution of the Yellowstone rhyolite plateau and eastern Snake River Plain, U.S.A. in Symposium on volcanoes and their roots, Oxford, England: Int. Assn. Volc. Chem Earths' Interior, vol. Abstr., p. 220-221.

Christiansen, R. L., and Lipman, P. W., 1972, Cenozoic volcanism and plate tectonic evolution of the western United States. II Late Cenozoic Royal Soc. London, Philos. Trans. A, 271, p. 249-284.

Coats, R. R., 1964, Geology of the Jarbridge quadrangle, Nevada-Idaho: U.S. Geol. Survey Bull. 1141-M, 24 p.

Cook, E. F., 1965, Stratigraphy of Tertiary volcanic rocks in eastern Nevada: Nevada Bur. Mines and Geol. Bull. 77, 49 p.

Cornwall, H. R., 1972, Geology and mineral deposits of southern Nye County, Nevada: Nevada Bur. Mines and Geol. Bull. 77, 49 p.

Decker, R. W., 1962, Geology of the Bull Run quadrangle, Elko County, Nevada: Nevada Bur. Mines Bull. 60, 65 p.

Ekren, E. B., Rogers, C. L., Anderson, R. E., and Orkild, P. P., 1968, Age of Basin and Range normal faults in Nevada Test Site and Nellis Air Force Range, Nevada, in Nevada Test Site: Geol. Soc. America Mem. 110, p. 247-250.

Ekren, E. B., Bath, G. D., Dixon, G. L., Healey, D. L., and W. D. Quinlivan, 1974a, Tertiary history of Little Fish Lake Valley, Nye County, Nevada, and implications as to the origin of the Great Basin: U.S. Geol. Survey, Jour. Research, v. 2, no. 1, p. 105-118.

Ekren, E. B., Quinlivan, R. P., Snyder, R. P., and F. J. Kleinhampl, 1974b, Stratigraphy, structure, and geologic history of the lunar Lake caldera of Northern Nye County, Nevada: U.S. Geol. Survey Jour. Research, v. 2, no. 5, p. 599-608.

Gawarecki, S. J., 1971, Geologic interpretation of Appolo 6 stero-photography from Baja California to west Texas: Third Annual Earth Resources Program Review, v. 1, Geology and Geography, NASA Manned Spacecraft Center, Houston, Tex., p. 15-1--15-25.

Gianella, V. P., and Callaghan, Eugene, 1934, The earthquake of December 20, 1932, at Cedar Mountain, Nevada, and its bearing on the genesis of Basin and Range structure: Jour. Geology, v. 42, no. 1, p. 1-22.

Gimlett, J. I., 1967, Gravity study of Warm Springs Valley, Washoe County, Nevada: Nevada Bur. Mines Rept. 15, 31 p.

Gromme, C. S., McKee, E. H., Blake, M. C., Jr., 1972, Paleomagnetic correlations and potassium-argon dating of middle Tertiary ash-flow sheets in the eastern Great Basin, Nevada and Utah: Geol. Soc. America Bull., v. 83, p. 1619-1638.

Gumper, Frank L., and Scholz, Christopher, 1971, Microseismicity and tectonics of the Nevada seismic zone: Seismol. Soc. America Bull., v. 61, no. 5, p. 1413-1432.

Hamilton, Warren, and Myers, W. B., 1966, Cenozoic tectonics of the western United States: Rev. Geophysics, v. 4, p. 509-549.

Hill, D. P., and Pakiser, L. C., 1967, Seismic-refraction study of crustal structure between the Nevada Test Site and Boise, Idaho: Geol. Soc. Bull., v. 78, no. 6, p. 685-704.

Hill, M. L., and Hobson, H. D., 1968, Possible post-Cretaceous slip on the San Andreas fault zone, in Dickinson, W. R., and Grantz, A., Editors, Proceedings of the conference on geologic problems of San Andreas fault system: Stanford Univ. Publs. Geol. Sci., v. 11, p. 123-129.

Horton, R. C., 1964, An outline of the mining history of Nevada, 1924-1964: Nevada Bur. Mines, Rept. 7, pt. 2, pl. 2.

————————, 1966, Statistical studies in the distribution of mining districts in Nevada: Nevada Bur. Mines, Rept. 13, part A, p. 109-123.

Huffman, O. F., 1970, Miocene and post-Miocene offset of the San Andreas fault in central California [abs]: Geol. Soc. America Cordilleran, Sec. 66th Ann. Mtg., v. 2, p. 104-05.

Jerome, S. E., and Cook, D. R., 1967, Relation of some metal mining districts in the western United States to regional tectonic environment and igneous activity: Nevada Bur. Mines Bull. 69, 35 p.

Kleinhampl, F. J., and Ziony, J. I., 1967, Preliminary geologic map of northern Nye County, Nevada: U.S. Geol. Survey open-file map, scale 1:200,000.

Koizumi, C. J., Ryall, A. S., and Priestley, K. F., 1973, Identification of a paleosubduction zone under Nevada [abs]: Earthquake Notes, v. 44, no. 1-2, p. 76.

Lathram, E. H., 1972, Nimbus IV view of the major structural features of Alaska: Science, v. 175, p. 1423-1427.

Lathram, E. H., and Gryc, George, 1973, Metallogenic significance of Alaskan geostructures seen from space, in Eighth International Symposium on Remote Sensing of Environment, Proc. v. 2: Ann Arbor, Mich. Environmental Research Inst. Michigan, p. 1209-1211.

Lattman, L. H., 1958, Technique of mapping geologic fracture traces and lineaments on aerial photographs: Photogrammetric Engineering, v. 24, p. 258-576.

Levandowski, D. W., Jennings, T. V., and Lehman, W. T., 1973, Applications of ERTS-1 imagery to mapping of lineaments favorable to the localization of ore deposits in north central Nevada: Purdue Univ., LARS inform. note 10173, 12 p, 8 figs.

Lipman, P. W., Prostka, H. J., and Christiansen, R. L., 1972, Cenozoic volcanism and plate tectonic evolution of the western United States; I Early and Middle Cenozoic: Royal Soc. London, A. Philos. Trans., v. 271, p. 217-248.

Locke, Augustus, Billingsley, P. R., and Mayo, E. B., 1940, Sierra Nevada tectonic patterns: Geol. Soc. America Bull., v. 51, p. 513-540.

Longwell, C. R., 1960, Possible explanation of diverse structural patterns in southern Nevada: Am. Jour. Sci., Bradley Vol., v. 258-A, p. 192-203.

Lowman, P. D., Jr., 1965, Space photography-a review: Photogrammetric Engineering, v. 31, no. 1, p. 76-86.

Lowman, P. D., Jr., and Tiedemann, H. A., 1971, Terrain photography from Genini spacecraft: final geologic report: Greenbelt, Md., National Aeronautics and Space Administration, Goddard Space Flight Center, v. x-644 - 71 - 15, 75 p.

Mabey, D. R., 1960, A regional gravity survey of part of the Basin and Range province: U.S. Geol. Survey Prof. Paper 400-B, p. B283-285.

Mabey, D. R., 1966, Regional gravity and magnetic anomalies in part of Eureka County, Nevada, in Mining Geophysics - V.1, Case histories: Tulsa, Okla., Soc. Explor. Geophysicists, p. 77-83.

Martin, R. F., and Piwinskii, A. J., 1972, Magmatism and tectonic setting: Jour. Geophys. Research, v. 77, no. 26, p. 4966-4975.

Marvin, R. F., Mehnert, Harold H., McKee, Edwin H., 1973, A summary of radiometric ages of Tertiary volcanic rocks in Nevada and eastern California. Part III: southern Nevada: Isochron/West, no. 6, p. 1-30.

McKee, E. H., 1968a, Geologic map of the Ackerman Canyon quadrangle, Nevada: U.S. Geol. Survey Geol. Quad. Map GQ-761.

———————, 1968b, Geologic map of the Spencer Hat Springs quadrangle, Nevada: U.S. Geol. Survey Geol. Quad. Map GQ-770.

———————— 1971, Tertiary igneous chronology of the Great Basin of Western United States - implications for tectonic models: Geol. Soc. America Bull., v. 82, p. 3497-3502.

McKee, E. H., and Silberman, M. L., 1970, Geochronology of Tertiary igneous rocks in central Nevada: Geol. Soc. America Bull., v. 81, p. 2317-2328.

McKee, E. H., Silberman, M. L., Marvin, R. E., and Obradovich, J. D., 1971, A summary of radiometric ages of Tertiary volcanic rocks in Nevada and eastern California. Part I: Central Nevada: Isochron/West, no. 2, p. 21-42.

McKenzie, D. P., and Morgan, W. J., 1969, The evolution of triple junctions: Nature, v. 224, p. 125-133.

Moore, J. G., 1962, K/Na ratio of Cenozoic igneous rocks of the western United States: Geochim. et Cosmochim. Acta, v. 26, p. 101-130.

Nicolais, S. M., 1974, Mineral exploration with ERTS imagery, in Third Earth Resources Technology Satellite-1 Symposium, v. 1, Sect. B: NASA SP-351, p. 785-796.

Nielsen, R. L., 1965, Right-lateral strike-slip faulting in the Walker Lane, west-central Nevada: Geol. Soc. America Bull., v. 76, p. 1301-1308.

Noble, J. A., 1970, Metal provinces of the western United States: Geol. Soc. America, Bull. v. 81, p. 1607-1624.

Pakiser, L. C., and Zietz, Isidore, 1965, Transcontinental crust and upper-mantle structure: Rev. Geophysics, v. 3, p. 505-520.

Prodehl, Claus, 1970, Seismic refraction study of crustal structure in the western United States: Geol. Soc. America Bull., v. 81, no. 9, p. 2629-2645.

Roberts, R. J., 1966, Metallogenic provinces and mineral belts in Nevada: Nevada Bur. Mines Rept. 13, p. 47-72.

Robinson, E. S., 1970, Relations between geological structure and aeromagnetic anomalies in central Nevada: Geol. Soc. American Bull., v. 81, p. 2045-2060.

Rowan, L. C., and Wetlaufer, P. H., 1973, structural geologic analyses of Nevada using ERTS-1 images: A preliminary reports: Symposium of significant results obtained from ERTS-1, March 5-9, 1973, NASA/Goddard Space Flight Center, p. 413-423.

Rowan, L. C., Wetlaufer, P. H., Goetz, A. F. H., Billingsley, F. C., and Stewart, J. H., 1974, Discrimination of rock types and detection of hydrothermally altered areas in south-central Nevada: U.S. Geol. Survey Prof. Paper 883, 35 p.

Roy, R. F., Decker, E. R., Blackwell, D. D., and Birch, Francis, 1968, Heat flow in the United States: Jour Geophys. Research, v. 733, p. 5207-5221.

Ryall, A. S., Priestley, K. F., Savage, W. U., and Koizuni, C. J., 1973, Cenozoic tectonics related to a paleosubduction zone under northern Nevada [abs]: Earthquake Notes, v. 44, no. 1-2, p. 76-1973.

Sargent, K. A., and McKee, E. H., 1969, The Bates Mountain Tuff in northern Nye County, Nevada: U.S. Geol. Survey Bull. 1249-E, p. E1-E12.

Sass, J. H. Lachenbruch, A. H., Munroe, R. J., Greene, G. W., and Moses, T. H., Jr., 1971, Heat flow in the western United States: Jour. Geophys. Reasearch, v. 76, no. 26, p. 6376-6413.

Scholz, C. H., Barazangi, M., Shar, M. L., 1971, Late Cenozoic evolution of the Great Basin, western United States, as an ensialic interarc basin: Geol. Soc. America Bull., v. 82, p. 2979-2990.

Shawe, D. R., 1965, Strike-slip control of Basin-Range structure indicated by historical faults in western Nevada: Geol. Soc. America Bull., v. 76, p. 1361-1378.

Shurbet, D. H., and Cebull, C. E., 1971, Crustal low-velocity layer and regional extension in Basin and Range province: Geol. Soc. America Bull., v. 82, p. 3241 -3244.

Slemmons, D. B., 1967, Pliocene and quaternary crustal movements of Basin and Range province, USA: Osaka City Univ., J. Geosci., v. 10, Art. 1-11, p. 91-103.

Smith J. G., McKee, E. H., Tatlock, D. B., and Marvin, R. F., 1971, Mesozoic granitic rocks in northwestern Nevada: a link between the Sierra Nevada and Idaho batholith: Geol. Soc. America Bull., v. 82, p. 2933-2944.

Smith, R. B., and Sbar, M. L., 1974, Contemporary tectonics and seismicity of the western United States with emphasis on the Intermountain seismic belt: Geol. Soc. America Bull., v. 85, p. 1205-1218.

Stewart, J. H., 1967, Possible large right-lateral displacement in the Death Valley-Las Vegas area, California and Nevada: Geol. Soc. America Bull., v. 78, p. 131-142.

————————, 1971, Basin and range structure - A system of horsts and grabens produced by deep-seated extension: Geol. Soc. America Bull., v. 82, no. 4, p. 1019-1043.

Stewart, J. H., Albers, J. P., and Poole, F. G., 1968, Summary of regional evidence for right-lateral displacement in the western Great Basin: Geol. Soc. America Bull., v. 79, p. 1407-1414.

Stewart, J. H., and Carlson, J. E., 1974, Preliminary geologic map of Nevada: U.S. Geol. Survey, Misc. Field Studies Map MF-609.

Stewart J. H., and McKee, E. H., 1968, Geologic map of the Mount Callaghan quadrangle, Lander County, Nevada: U.S. Geol. Survey Geol. Quad Map GQ-730.

Tatlock, D. B., 1969, Preliminary geologic map of Pershing County, Nevada: U.S. Geol. Survey open-file map, scale 1:200,000.

Tschanz, C. M., and Pampeyan, E. H., 1970, Geology and mineral deposits of Lincoln County, Nevada: Nevada Bur. Mines Bull. 73, 188 p.

U. S. Geological Survey 1962, Tectonic map of the United States: Washington, D. C., scale 1:2,500,000.

Walker, G. W., 1973, Preliminary geologic and tectonic maps of Oregon east of the 121st meridian: U.S. Geol. Survey, Misc. Field Studies Map MF-495, 2 sheets.

Wise, D. U., 1963, An outrageous hypothesis for the tectonic pattern of the North American Cordillera: Geol. Soc. America Bull., v. 74, p. 357-362.

Zietz, Isidore, Bateman, Paul C., Case, James E., Crittenden, M. D., Jr., Griscom, Andrew, King, Elizabeth, R., Roberts, R. J., Lorentzen, George R., 1969, Aeromagnetic investigation of crustal structure for a strip across the western United States: Geol. Soc. America Bull., v. 80, p. 1703-1714.

Apendix A

DISCRIMINATION OF ROCK TYPES AND ALTERED AREAS IN NEVADA BY THE USE OF ERTS IMAGES

PREPARED IN COOPERATION WITH THE
NATIONAL AERONAUTICS AND SPACE ADMINISTRATION

GEOLOGICAL SURVEY PROFESSIONAL PAPER 883

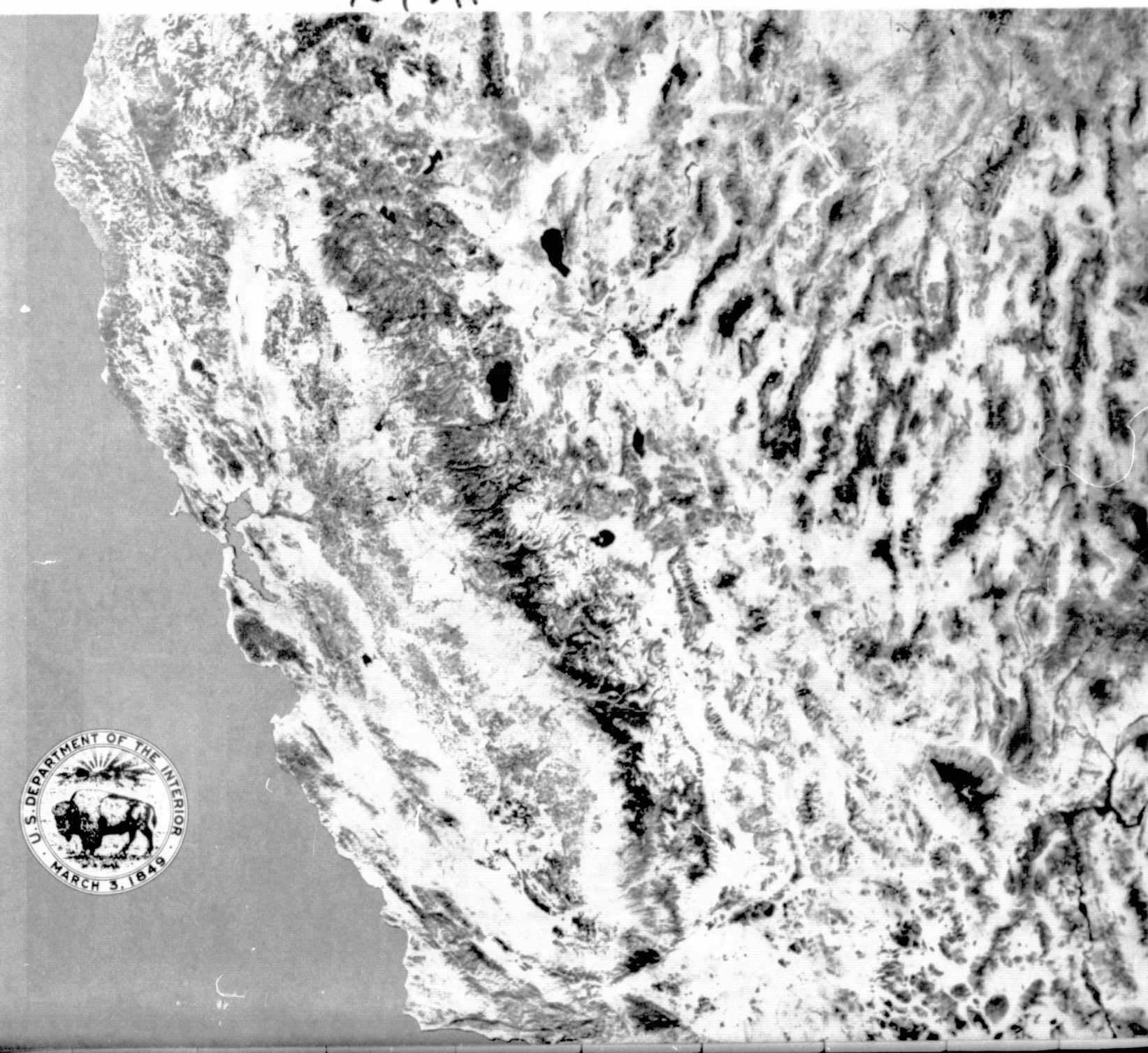

DISCRIMINATION OF ROCK TYPES AND DETECTION OF HYDROTHERMALLY ALTERED AREAS IN SOUTH-CENTRAL NEVADA BY THE USE OF COMPUTER-ENHANCED ERTS IMAGES

By LAWRENCE C. ROWAN, PAMELA H. WETLAUFER, ALEXANDER F. H. GOETZ, FRED C. BILLINGSLEY, *and* JOHN H. STEWART

GEOLOGICAL SURVEY PROFESSIONAL PAPER 883

Prepared in cooperation with the National Aeronautics and Space Administration

A detailed description of the development and application of a remote-sensing technique for geologic exploration

UNITED STATES GOVERNMENT PRINTING OFFICE, WASHINGTON : 1974

UNITED STATES DEPARTMENT OF THE INTERIOR

ROGERS C. B. MORTON, *Secretary*

GEOLOGICAL SURVEY

V. E. McKelvey, *Director*

For sale by the Superintendent of Documents, U.S. Government Printing Office
Washington, D.C. 20402 - Price $1.55
Stock Number 2401-02544

CONTENTS

ILLUSTRATIONS

TABLE

TABLE

DISCRIMINATION OF ROCK TYPES AND DETECTION OF HYDROTHERMALLY ALTERED AREAS IN SOUTH-CENTRAL NEVADA BY THE USE OF COMPUTER-ENHANCED ERTS IMAGES

By LAWRENCE C. ROWAN, PAMELA H. WETLAUFER, ALEXANDER F. H. GOETZ[1], FRED C. BILLINGSLEY[1], and JOHN H. STEWART

ABSTRACT

A combination of digital computer processing and color compositing of ERTS Multispectral Scanner (MSS) images has been used to detect and map hydrothermally altered areas and to discriminate most major rock types in south-central Nevada. The technique is based on enhancement of subtle visible and near-infrared reflectivity differences associated with variations in bulk composition. MSS spectral bands are ratioed, picture element by picture element, by computer and are subsequently contrast stretched to enhance the spectral differences. These stretched-ratio values are used to produce a new black-and-white image which shows the subtle spectral-reflectivity differences and concurrently minimizes radiance variations due to albedo and topography. Additional enhancement is achieved by preparing color composites of two or more stretched-ratio images. Color variations seen in these color-ratio composites represent spectral-reflectance differences.

The choice of MSS bands for ratioing depends on the spectral-reflectance properties of the surface materials to be discriminated. For south-central Nevada, the most effective color-ratio composite for discriminating between altered and unaltered areas and among the regional rock units was prepared using the following color and stretched-ratio image combination: blue for MSS 4/5, yellow for MSS 5/6, and magenta for MSS 6/7. In this composite, mafic rocks, mainly basalt and andesite, are white whereas felsic extrusive and intrusive rocks are pink. The felsic rocks are especially notable because they have a large intrinsic albedo range, which commonly prevents their discrimination from mafic rocks in other types of images and photographs.

Altered areas are represented by green to dark-green and brown to red-brown patterns in the color-ratio composite. Except for two areas, the green areas represent hydrothermally altered, commonly limonitic rocks. The dark-green, brown, and red-brown patterns are less prevalent. Dark-green areas are limonitic and limonite-free altered rocks. Areas that are brown in the color-ratio composite have been studied in less detail, but they appear to be predominantly light-colored hydrothermally altered volcanic rocks. The red-brown pattern represents limonite-free, silica-rich light-colored volcanic rocks that have conspicuous alteration in two areas and questionable alteration in two other areas.

Altered outcrops mapped from the color-ratio composite show a pronounced coincidence with known mining areas. In the Goldfield mining district, the most productive in the study area, the degree of agreement between the green patterns and the previously mapped alteration zone is striking. These altered areas are not apparent on the individual MSS images, color-infrared composites, or color photographs obtained from NASA's Skylab. Therefore the technique used in this study appears to have important applications in mineral-resources exploration and regional geologic mapping. Future research should focus on refinement of this technique, especially on defining more clearly the relationships between visible and near-infrared spectral reflectivity and mineralogical composition and on testing the technique in a variety of geologic settings and environmental conditions.

INTRODUCTION

The first Earth Resources Technology Satellite (ERTS–1) provides an important new tool for geologic exploration in the form of small-scale multispectral visible and near-infrared images. These images, which show large areas under nearly constant lighting conditions, already have been applied to a wide variety of geologic problems ranging from detection and delineation of fault zones and volcanic centers to studies of coastal erosion and sediment transport. Most applications, however, have relied mainly on photointerpretation of these synoptic views rather than on multispectral-reflectance analysis. Regional morphologic features are commonly quite conspicuous, but visible and near-infrared spectral-reflectance differences among rocks are usually small and therefore not readily apparent through visual examination of the images.

A technique which combines digital computer processing and color compositing has been devised for enhancing subtle spectral-reflectivity differences. This technique has been applied to part of an ERTS–1 image of south-central Nevada with emphasis on the Goldfield mining district. Analysis has focused on discrimination of the geologic materials,

[1] Jet Propulsion Laboratory, California Institute of Technology, Pasadena, Calif.

especially in mineralized areas, on the basis of visible and near-infrared spectral-reflectivity differences. This report presents the geologic interpretation and evaluation of the resulting processed images. Brief descriptions are given of the ERTS–1 mission profile and imaging subsystem, the general nature of the visible and near-infrared spectral reflectivity of rocks, and the techniques used.

ERTS–1 MULTISPECTRAL SCANNER

ERTS–1 was launched by the U.S. National Aeronautics and Space Administration (NASA) on July 3, 1972, and is stabilized in a near-polar orbit approximately 907 km above the earth. The satellite contains two imaging systems, the Multispectral Scanner (MSS) and the Return Beam Vidicon (RBV), which record reflected visible and near-infrared radiation. A third system, the Data Collection System (DCS), receives and relays data from earth-based monitoring instruments. The sun-synchronous orbit allows 14 orbits each day and coverage of the same area every 18 days at the same local solar time, which is 0942 hours at the equator.

Data for North America, Hawaii, and Iceland are transmitted directly to the nearest of three NASA receiving stations—Greenbelt, Md., Goldstone, Calif., and Fairbanks, Alaska. Images of selected areas beyond the reception capability of these stations are recorded on tape and transmitted at a later time, but tape-recorder malfunctions have limited the coverage of such areas.

Although the RBV was turned off in August 1972 after an electronic malfunction, the MSS has recorded thousands of images that have high spatial resolution and radiometric fidelity. Solar energy reflected from the Earth's surface is measured in four spatially registered spectral bands through the same optical system.

Band	*Wavelength, μm*
MSS 4	0.5–0.6
MSS 5	.6– .7
MSS 6	.7– .8
MSS 7	.8–1.1

The analog electronic signal, along with internal calibration measurements, is transmitted to the ground where it is digitized and formatted into a digital data stream. Geometric and radiometric calibration is achieved in a ground-based digital computer.

The MSS scans cross-track (west to east) swaths 185 km wide, imaging six scan lines across in each of the four spectral bands simultaneously (fig. 1). This scanning provides continuous coverage along each orbital track. The data are converted to pictorial images and are framed at the Goddard Space Flight Center, Greenbelt, Md., with a 10-percent forward-lap between adjacent scenes. Side-lap depends on latitudinal position; it ranges from about 14 percent at the equator to 50 percent at lat 54° N. or S. Each frame covers approximately 34,200 sq km. Spatial resolution for the images averages about 80 m but is appreciably higher for high-contrast linear features.

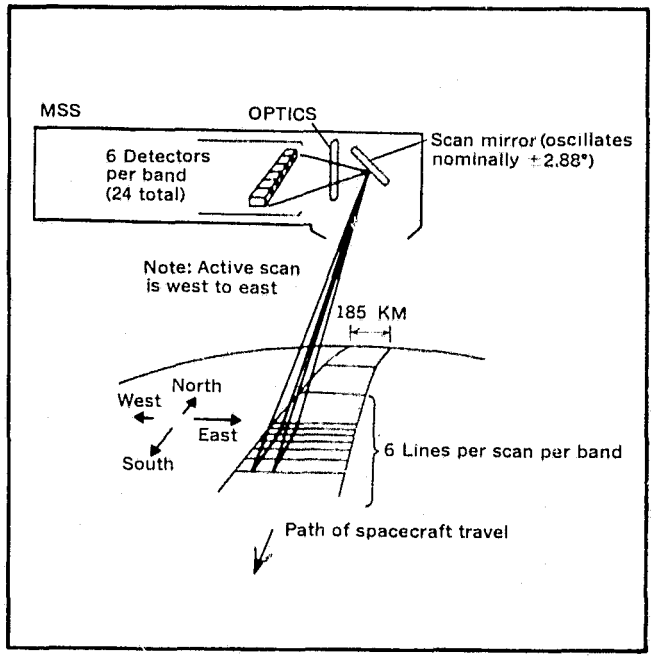

FIGURE 1.—Multispectral Scanner ground-scan pattern. Schematic diagram shows the relations between spacecraft attitude and image geometry (U.S. Natl. Aeronautics and Space Admin., Goddard Space Flight Center, 1971).

VISIBLE AND NEAR-INFRARED REFLECTANCE OF ROCKS AND MINERALS

Our understanding of the relationships between mineralogical composition and visible and near-infrared spectral reflectivity is based mainly on published laboratory measurements (Hunt and Salisbury, 1970; Ross and others, 1969; Hunt and others, 1971a,b; 1973a,b; 1974a,b). All these measurements were made on crushed, homogeneous, and generally unaltered samples. Although application of these data to analysis of MSS images of large geologically complex areas is made difficult by several factors, especially scale differences and surface-state conditions, the laboratory data do provide a framework for initial investigations.

Analysis of these laboratory spectra show that electronic transitions in constituent metal ions result

in broad optical absorption bands in the ultra-violet, visible and near-infrared wavelengths. For example, iron, the most common transitional metal ion, has conspicuous ferrous and ferric absorption bands centered at about 1.0 and 0.92 μm, respectively, and several closely spaced weaker bands between 0.40 and 0.55 μm (Hunt and Salisbury, 1970). Other transitional metal ions that give rise to absorption bands include copper, titanium, chromium, and manganese (Hunt and others, 1971a,b). Absorption bands due to vibrational processes in water and hydroxyl molecules also occur in the near-infrared wavelengths, but the only one of these bands within the response range of the MSS is centered at about 0.95 μm.

Absorption bands are commonly quite intense and therefore result in conspicuous reflectance minima, predominantly in ferromagnesian and hydrous mineral spectra. Diagnostic individual spectral features, however, are generally subdued beyond recognition by addition of anhydrous nonferrous minerals such as quartz and feldspar to form polymineralic rocks. The shape of rock spectra are nonetheless still affected by the absorption bands. For example, the reflectance of mafic and ultramafic rocks changes very little between 0.4 and 1.1 μm (fig. 2*B*). In contrast, felsic-rock reflectance, which is generally affected less by absorption bands, increases continuously throughout this range, although at a slower rate between 0.70 and 1.1 μm than at shorter wavelengths (fig. 2*A*). The slopes of reflectance curves for rocks with intermediate composition are typically between those of felsic and mafic rocks (Ross and others, 1969). As we will discuss later, the spectra for unaltered rocks (fig. 2) and altered rocks generally have significantly different shapes.

Differences in spectral shape can be used to distinguish among geologic materials and, in some cases, to place general bounds on their bulk composition. Several factors—including impurities both in the crystal lattice and on the surface of the rocks, atmospheric conditions, and system calibration—complicate both of these efforts. Surficial weathering products such as limonite and clay minerals are especially important as they obscure the original rock surface.

The characteristic spectral shapes for the rock (and soil) units can be derived from the MSS data to provide the basis for compositional estimates, although spectral details are somewhat subdued by the breadth of the MSS bands, especially band 7. Unknown atmospheric effects and system-calibration complications preclude obtaining absolute spectral reflectivities at this time. The field spectral measurements needed for absolute MSS calibration are presently being made, although adequate data are not yet available. On the other hand, absolute calibration is not required for simple discrimination that depends mainly on relative reflectance differences among rock types. Rock (and soil) units can be distinguished on the basis of very subtle reflectance differences, even though the absolute spectral reflectivities

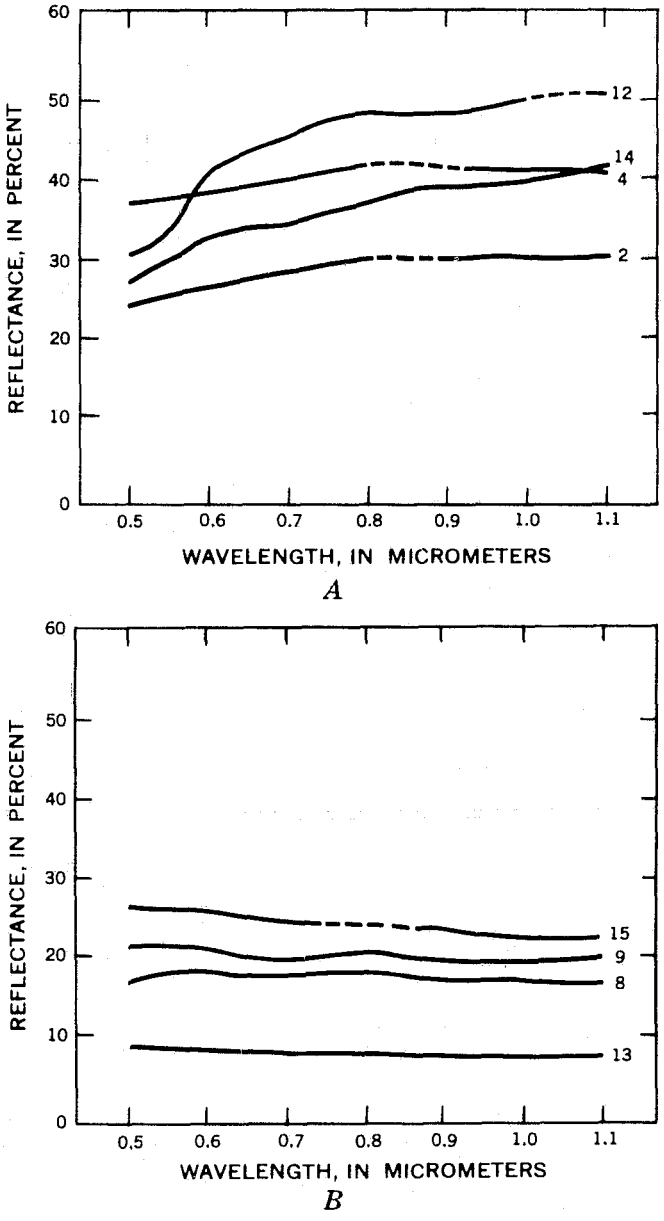

FIGURE 2.—Visible and near-infrared reflectance spectra. Spectra of samples with grain sizes in the 420- to 500-μm range (modified from Ross and others, 1969). *A*, Selected felsic rocks, rhyolite (12), granite (14), rhyolite (4), granodiorite (2), showing increasing reflectance. *B*, Selected mafic rocks, serpentinite (15), gabbro (9), peridotite (8), and basalt (13), showing overall decreasing reflectance. Dashed line where inferred.

and gross lithologies cannot yet be determined from the MSS data.

ACKNOWLEDGMENTS

This study was supported by the U.S. National Aeronautics and Space Administration under contract No. S–70243–AG to the U.S. Geological Survey and Contract No. NA57–100 to the Jet Propulsion Laboratory, California Institute of Technology. Several colleagues made many useful suggestions during the course of this study, and we are especially grateful to Kenneth Watson, Terry Offield, and Allan Kover of the U.S. Geological Survey, who reviewed the manuscript. Alan Gillespie, Jet Propulsion Laboratory, did most of the computer processing. Allan Kover developed the diazo processing technique used in preparing the color-ratio composites.

COMPUTER IMAGE ENHANCEMENT

Development of image-processing techniques has been greatly stimulated during the last 10 years by the widespread use of imaging devices in planetary and, more recently, terrestrial remote sensing. Enhancement techniques now range from the relatively simple single-band contrast enhancement to two-dimensional filtering in spatial or Fourier domain to complex cluster analysis, sometimes coupled with ratioing of spectral bands.

The picture data can be taken from film images by scanning densitometry or, as in the case of the ERTS MSS, taken directly from computer-compatible tapes (CCT). Tape-recorded digital data are preferable because on film accuracy is lost in recording radiometric information and is further degraded by duplication, and scanning introduces additional noise into the signal. Other advantages of using the tapes for analysis include considerable analytical flexibility, reproducible results, and relatively reasonable costs.

Film methods were used in one of the earliest successful attempts (Whitaker, 1965) to discriminate rock units on lunar photographs on the basis of spectral reflectivity. In the apparently uniform regolith of Mare Imbrium, two basaltic lava flows were distinguished in a black-and-white composite produced by masking blue and infrared wavelength telescopic photographs. Using a similar approach, but manipulating digitized multiband telescopic photographs in the computer, a method was devised for analyzing Apollo orbital multiband photographs (Billingsley and others, 1970; Goetz and others, 1971). An extension of this technique, using a photographic ratio method, was developed by Yost, Anderson, and Goetz (1973). During this same general period, Vincent and Thomson (1972) were ratioing thermal-infrared spectral images to detect emissivity variations related to chemical and mineralogical differences. These results, along with the evaluation of laboratory spectra described in the previous section, made clear the considerable potential of ratioing for multispectral analysis of ERTS data (Rowan and Vincent, 1971).

Ratioing is an effective method for distinguishing among rock types because the main spectral differences in the visible and near-infrared spectral regions are found in the slopes of the reflectivity curves; individual absorption bands are broad and weak and therefore cannot be used in most cases for discrimination of rock type on the standard MSS images. In addition, areas of interest geologically generally have some vertical relief. The ratioing process removes first-order brightness effects due to topographic slope and allows attainment of higher image contrast through additional processing. On the other hand, terrain effects are highly disturbing in color-additive displays or in analysis by clustering methods based solely on brightness.

Although digital computer processing ultimately proved to be necessary for this study, attempts were made to use more rapid visual and optically assisted techniques. Visual comparison of the MSS bands of many Nevada scenes resulted in only a few places where band-to-band differences could be related to rock type. For example, widespread volcanic rocks in the northern Antelope Range and Schell Creek Range in White Pine and Elko Counties are conspicuously darker in the near-infrared bands than in the visible bands (ERTS frame No. E–1053–17533, not shown). Enhancement by color-additive viewing is mainly useful for determining vegetation distribution. Although discrimination of rock units in the study area is not substantially improved by this method, color-additive techniques have proved more useful than simple comparison of individual black-and-white MSS images in other areas.

Attempts to enhance spectral-reflectance differences by compositing a negative of one spectral band and a positive of another, as described by Whitaker (1965), were also generally unsuccessful. Of the many problems, the most serious were the general lack of enhancement actually achieved and the introduction of photographic processing errors that were of the same order of magnitude as the spectral-reflectance differences. In order to make the spectral-reflectance differences visible, a very high film contrast is necessary. At high-contrast levels, however,

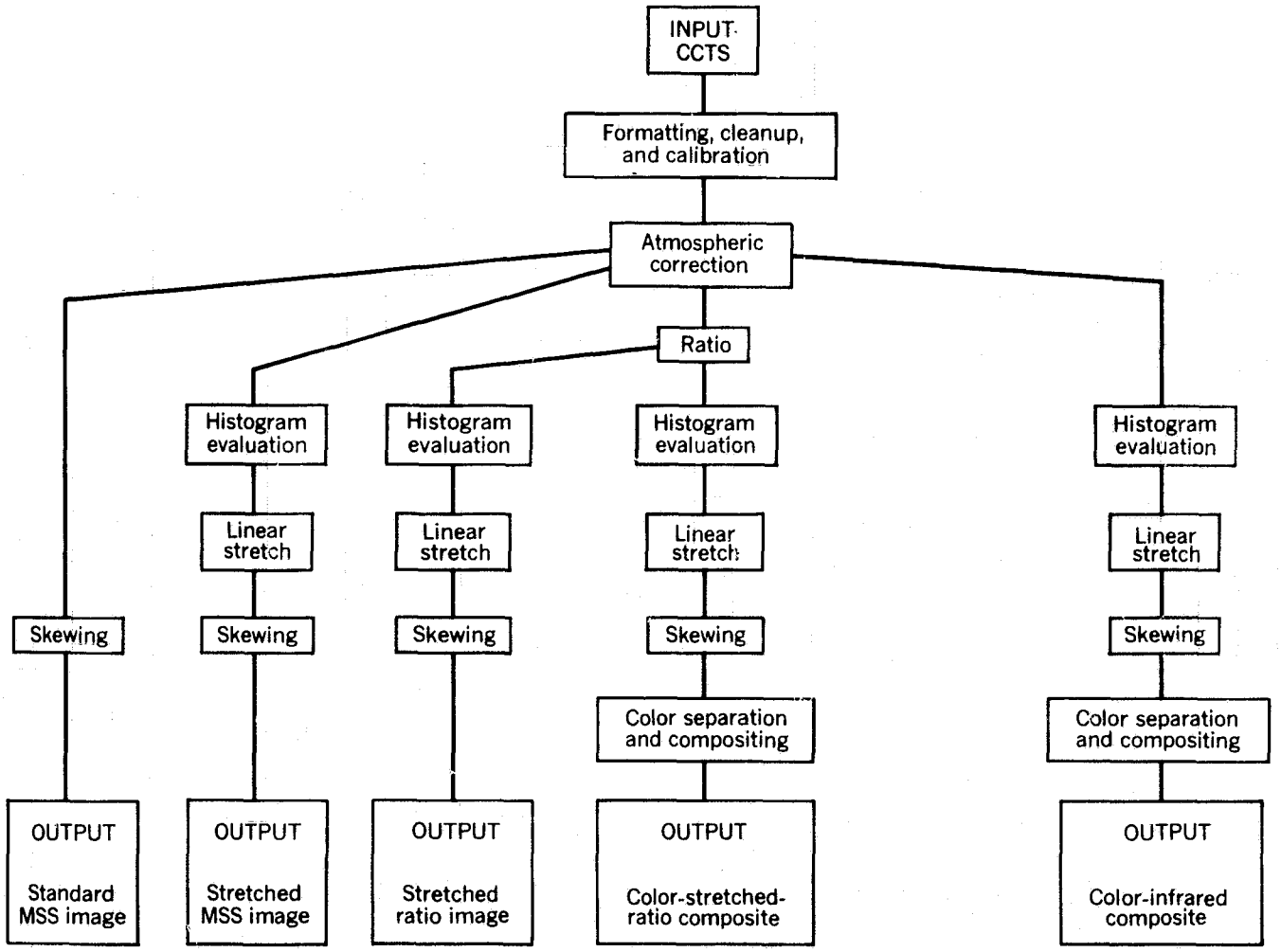

FIGURE 3.—Flow diagram showing the sequence of steps used in processing computer-compatible tapes and the five image products generated.

some important information is lost in the nonlinear part of the film response curve. Therefore, in general, purely optically assisted methods of analysis appear to have a somewhat limited value for geologic multispectral analysis.

DIGITAL METHODS

Various techniques have been developed for digital processing of images. Only those relevant to discrimination among rock materials will be discussed here. The steps in the enhancement of the MSS images are outlined in the flow diagram in figure 3.

The dynamic range of the MSS is encoded to 64 brightness levels. Application of system calibration to take care of nonlinearities results in approximately 80 brightness levels, coded to seven-bit accuracy. The digital numbers (DN) on the tape represent data values that are linear with brightness and range from 0 to 127. For convenience in using existing computer programs, the MSS data have been expanded into eight bits, resulting in a DN range of 0 to 255. Future references to DN values will refer to the eight-bit range.

Because the application of MSS on-board calibration data at the National Data Processing Facility, Goddard Space Flight Center, is not perfect, residual variations manifest themselves as a striping pattern repeated at six-line intervals. In unenhanced small-scale photographic prints, this banding is not very noticeable, but after computer enhancement and enlargement, the lack of perfect radiometric calibration is disturbingly apparent. Methods for reducing the striping pattern have been described by Billingsley and Goetz (1973) and require lengthy processing.

For each MSS scene, four CCT's are required, each containing one-fourth of a frame. If the area of interest spans an area covered by more than one CCT, strips can be reassembled or concatenated.

GEOMETRIC CORRECTIONS

The ERTS MSS is a point-scanner device that has the scanning trace perpendicular to the downtrack direction of the spacecraft (fig. 1). Therefore, the rotation of the Earth during acquisition of each set of progressive lines of one picture will cause a lateral skewing of the area covered on the ground. This skewing is a function of latitude. Because the data are recorded on film using an orthogonal grid pattern, each successive scan line must be shifted horizontally within the grid to compensate for the skewing. The resulting output picture is in the form of a parallelogram.

An additional correction is needed to compensate for a higher sampling rate in the scan-line direction than in the downtrack direction. This distortion can be compensated for by reformatting the picture elements (pixels) either in the computer or during the analog film recording. We have chosen to make this correction at the latter stage of processing.

CONTRAST STRETCHING

The MSS system is designed to cover a large dynamic range in scene brightness to respond to the effects of sun angle and albedo variation as the spacecraft covers the globe. Consequently the brightness range of any one image will generally occupy only part of the available dynamic range, resulting in a low-contrast image. In reconstructing an image from the digital data, it is therefore desirable to stretch the DN range to increase the contrast. Stretching begins by forming a histogram plot of the number of pixels per DN value (fig. 4). The brightness values above and below which no appreciable data exist can then be located and used as stretch limits. The stretch may be linear or nonlinear.

A linear stretch increases the scene contrast uniformly over the dynamic range of the output product. The stretch limits determined from the histogram are placed at the extreme points of the dynamic range (that is, 0 to 255 DN values), and the other points are spaced linearly between these end points (fig. 4).

In a nonlinear stretch, such as a cube-root stretch, the cube root of each DN value is taken. The resulting DN range is linearly stretched as above. This procedure increases local scene contrast in the dark areas at the expense of contrast in the brightest areas. In an exponential stretch, the inverse occurs. There does not seem to be a general rule of thumb that can be applied to all images in determining the required stretch parameters. Care must be taken to see that useful raw data at the extremes of the DN range are not saturated and lost.

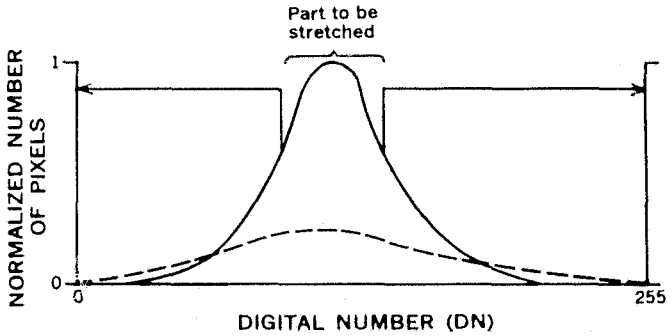

FIGURE 4.—Schematic histogram showing the distributions of digital numbers (DN) for a typical ERTS MSS scene before contrast stretching (solid line) and after linearly stretching (dashed line) a part of the DN range.

ATMOSPHERIC EFFECTS

The effects of absorption and scattering in the atmosphere vary among the different types of enhanced images. When the images are simply stretched to increase contrast, no effect is noted. If color composites are made from the stretched images, however, the relative color balance will be affected by the atmospheric scattering. The greatest effect is seen in the formation of ratios. Because

$$\frac{A+\epsilon_1}{B+\epsilon_2} \neq \frac{A}{B},$$

where ϵ_1 and ϵ_2 are the additive atmospheric-scattering components in bands A and B, the scattering term must be removed.

The value for the atmospheric-scattering component can be determined by locating the lowest DN values in the image. These values will normally occur over water or in cloud shadows. In a study area in Arizona (Goetz, 1974), measurements of ground-reflected radiation made before, during, and after the passage of a small (about 300-m-diameter) fair-weather cumulus cloud, showed a reduction in reflected intensity by a factor of 5–6 during cloud passage. From these data we can anticipate that, to first order, most of the light received from the dark shadows is in fact atmospherically scattered sunlight. Therefore, corrections are made by subtracting the appropriate band-dependent values, determined from cloud shadows in each band, from each pixel DN value. Other methods of determining the band-to-band values may be used. The atmospheric corrections are applied to the data before skewing, stretching, and ratioing.

RATIOING

In the ratioing process, two spectral band images that have been corrected for atmospheric effects are divided pixel by pixel. The resultant image will show

the variations in the slopes of the spectral-reflectivity curves between the two wavelength bands. Differences in albedo are suppressed, however, and very dissimilar materials easily separable on a standard photographic image may become inseparable on a ratio image because their spectral-reflectivity slopes are similar. On the other hand, a distinct advantage of this method is that one type of material will appear the same or similar in a ratio image regardless of the local topographic slope angle.

The ratio image generally shows a narrow histogram of DN values and may therefore be contrast stretched to enhance the visibility of the spectral differences. The type of stretch used, whether linear or nonlinear, as discussed, above, will determine which areas in the image are most strongly enhanced. For instance, a linear stretch will result in the visual enhancement of dark areas (low DN values in the original ratio image) and light areas (high DN values in the original ratio image). Other types of stretches will enhance other DN value ranges in the original ratio image.

The error introduced by scattering is greatest for low-reflectance targets. It is highest in band 4, where the scattering component may make up as much as 50 percent or more of the recorded brightness level. Band 7 has the lowest scattering component.

Although atmospheric absorption can play an important role in the form of apparent interband radiance variations, we are not able to separate these effects from variations in the MSS absolute calibration, done before we received the tapes. Band 7, spanning the 0.95-μm water band, might be expected to be affected most severely by atmospheric absorption.

Residual errors, most easily detected on ratio images in highly sloped and shadowed regions, may result either from improper atmospheric correction or from the fact that such areas are illuminated mainly by the blue sky and reflections from surrounding terrain; if this is the case, the atmospheric absorption and scattering calculated from other regions is not appropriate for these areas.

DISPLAY PRODUCTS

The computer-enhanced images are recorded on black-and-white film with a flying-spot cathode-ray tube recorder. These 70-mm transparencies can be printed on paper or combined in a color-additive process, using either a viewer, color-negative stock, or diazo transparencies. The color combination of ratio images provides the photointerpreter with a vivid display akin to a classification map.

GEOLOGY OF THE STUDY AREA

The surficial character of the study area (figs. 5, 11) makes it an ideal choice for analysis of ERTS spectral data. The topography of the test site is varied, ranging from smooth-textured alluvial basins to rugged ranges and a large mesa. Vegetation is sparse, covering 10–20 percent of the desert valleys where sagebrush is dominant, and is substantially denser only in the higher ranges where piñon pine, juniper, and grasses are predominant. Although vegetation type and distribution can sometimes reflect geology, minimal vegetation was considered preferable for these initial evaluations so that surficial features and rock units would not be obscured. The most important characteristics of the terrain are the widespread hydrothermal alteration and the broad compositional range of Tertiary igneous rocks, which provide an excellent opportunity for testing the discrimination potential of the MSS images.

ROCK UNITS

Widespread Tertiary volcanic and intrusive rocks cover approximately 95 percent of the surface of the study area not covered by alluvium (fig. 6). Precambrian and Paleozoic rocks are exposed only locally and are shown as a single unit in figure 6. Mesozoic plutonic rocks, mainly quartz monzonite in composition, are also undifferentiated in figure 6 because of their limited distribution in the study area.

The Tertiary units exceed 6,000 m in thickness in a composite section; tuffs of rhyolitic, dacitic, and quartz latitic composition are the most common. Lava flows and intrusive rocks of similar compositions and of andesite and basalt are also widespread (Cornwall, 1972). Although sedimentary rocks are subordinate in the Tertiary sequence, Miocene tuffaceous sedimentary rocks are common in the central and east-central parts of the area (fig. 6). The sources for the tuffs and flows are thought to have been as many as 9 or 10 volcanic centers, several of which are within the study area (Ekren and others, 1971). Especially noteworthy are the Black Mountain and Timber Mountain calderas. The Black Mountain caldera, in the southeastern corner of the study area, was the source for the Thirsty Canyon ash-flow and ash-fall tuff (unit Tt3, fig. 6) which underlies much of the southern half of the area. Tuffs derived from the larger Timber Mountain caldera southeast of the study area are prominent in the west-central and southwestern parts of the study area. In addition, the Goldfield mining district is a volcanic center (Albers and Cornwall, 1968) and is thought to be a resurgent caldera (Albers and Kleinhampl, 1970). The volcanic and intrusive rocks of

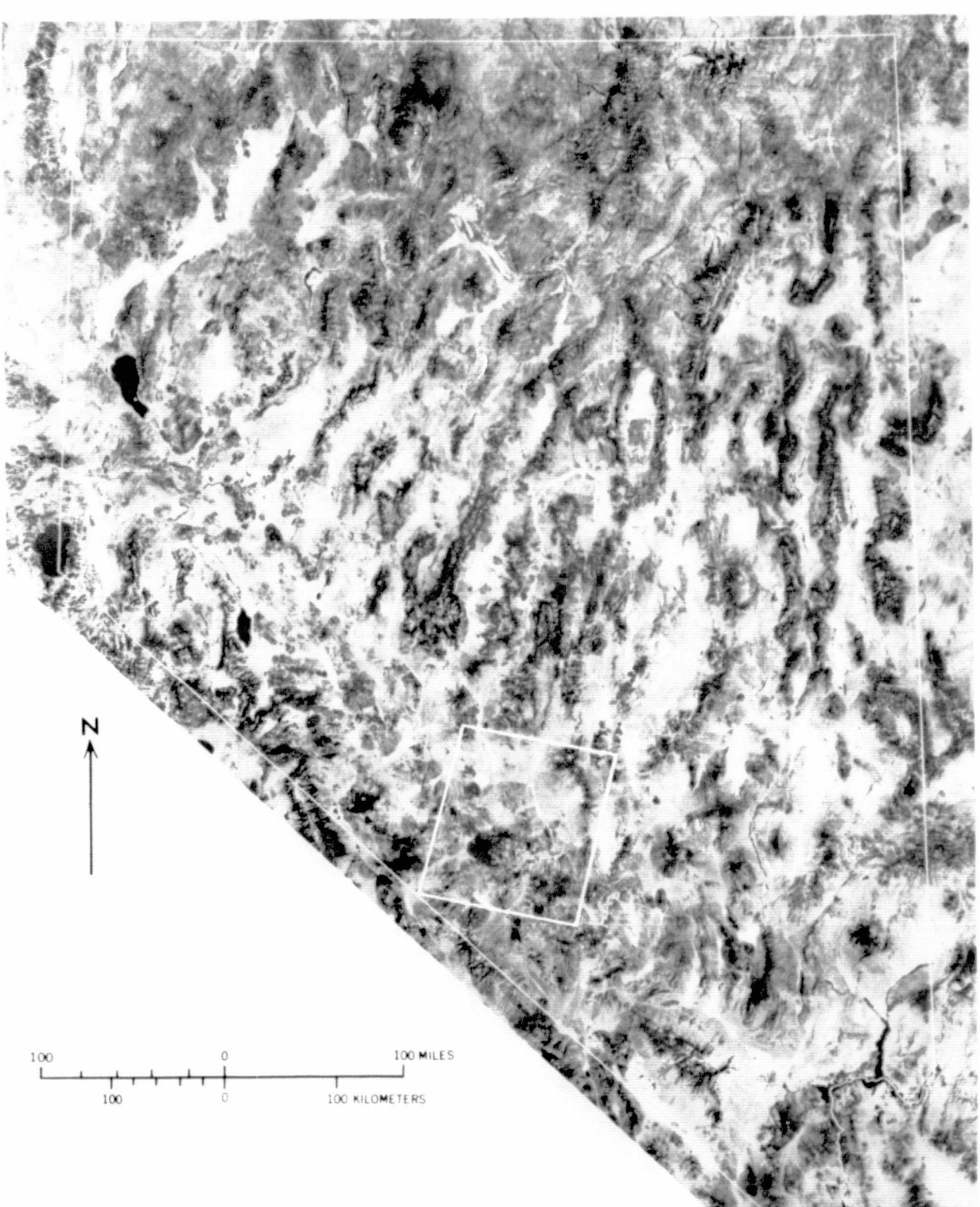
N
100
0
100 MILES
100
0
100 KILOMETERS

FIGURE 5.—ERTS mosaic made with MSS band 5 (0.6–0.7 μm) images of the State of Nevada showing location of study area. Prepared by Aerial Photographers of Nevada, Reno-Stead Airport, Nev.

the Goldfield mining district are restricted to that district.

The Quaternary units consist of surficial deposits and sporadic outcrops of basalt flows and cinder cones (fig. 6). The basaltic deposits are conspicuous because of their low reflectivity relative to the adjacent materials. The surficial units, however, include complexly related alluvium, colluvium, desert wash and landslide deposits, playa materials, and, on the western edge of the area, a single exposure of bedded clay and silt (unit Qts, fig. 6). With the exception of the playa deposits, which are characterized by reasonably uniform composition and high reflectivity, these surficial deposits are lithologically heterogeneous. This compositional heterogeneity, as well as grain size, surface coatings, and vegetation-cover variations, gives rise to large spectral-reflectance differences. Although the processing techniques described in the previous section appear to be potentially useful for mapping these materials, the surficial deposits present a formidable analytical problem because of their large extent and the transitional nature of boundaries. The rest of this discussion will exclude the surficial deposits; emphasis will be placed on the Tertiary units, especially where they have been hydrothermally altered.

The unaltered Tertiary volcanic and intrusive rocks have from very high to low albedos, but these variations are not a reliable guide to composition. For example, although most of the silicic rocks have high to intermediate albedos, the widespread rhyolitic Thirsty Canyon Tuff appears dark enough on the images, as well as in the field, to be mistaken for a rock of intermediate or even mafic composition. The unaltered rocks in the study area have a wide variety of muted colors, the most common being brown and gray, with green, yellow, and pink tints.

Alteration by the introduction of hydrothermal fluids and by subsequent weathering has resulted in hydration and oxidation of the Tertiary volcanic host rocks. The end products range from high-albedo clay-rich rocks, which may be locally silicified, to variably colored limonitic rocks. All the major alteration products are present in the Goldfield mining district, which is the most productive and best known altered zone in the study area.

GEOLOGY OF THE GOLDFIELD MINING DISTRICT

The Goldfield mining district is principally composed of Miocene volcanic rocks overlying Ordovician shale and chert and Mesozoic granitic rocks (Albers and Stewart, 1972) (fig. 6). The middle Tertiary units include air-fall and ash-flow tuff along with flows and intrusive bodies of andesite, dacite, rhyodacite, quartz latite, and rhyolite (Cornwall, 1972). Upper Tertiary basalt and welded tuff locally cap these units (Ashley, 1970). Alteration and mineralization are extensive, especially in the lower Miocene andesite and dacite, the primary ore-bearing rocks.

Ashley (1970) described two types of alteration. The older deuteric or propylitic alteration varies considerably, each variation characterizing a single volcanic unit. According to Ashley and Keith (1973), however, the chemical changes in most of these rocks have probably been quite limited. The younger intense hydrothermal alteration is more conspicuous and has a similar character in all rock units. Harvey and Vitaliano (1964) and Ashley and Keith (1973) described three mineralogically distinct zones of hydrothermal alteration. In order of decreasing alteration, silicified rocks with associated alunite, and kaolinite give way to illite-kaolinite-bearing argillized rocks, which grade into montmorillonite-bearing argillized rocks having surficial coatings of limonite and jarosite resulting from oxidation. Limonite is also common in the first two zones. The silicified and argillized rocks have a bleached appearance except where stained red and yellow by limonite and jarosite. Figure 7 shows the general limits of the alteration zones which cover more than 38.4 sq km (Ashley, 1970).

A color aerial photograph of part of the Goldfield district shows the distinctive complex mosaic of bleached clay-rich rocks and of brightly colored limonitic areas interspersed with the unaltered rocks (fig. 8). Feature A (fig. 8), an unaltered upper Tertiary basalt cap, appears dark gray; this basalt can also be identified on the alteration map of the Goldfield district (A, fig. 7) and on the enhanced images discussed later. Surrounding the basalt cap is the ore-bearing hydrothermally altered andesite and dacite, ranging from shades of light gray to red brown and brown. The red-brown hues dominate in the altered rocks. The purple-blue outcrop of unaltered latite to the northwest (B, fig. 8; B, fig. 7) can easily be distinguished from the prong of altered andesite and dacite on its southeastern border (C, fig. 8; C, fig. 7), but the northern limit of the altered rocks is difficult to determine in the color photograph. Farther east, some dark-brown-gray unaltered dacite (D, fig. 8; D, fig. 7) stands out from the nearby altered andesite and dacite. Although individual outcrops can be classified properly, the boundary of the hydrothermal alteration is difficult to define at this scale, mainly because visible color is not entirely diagnostic.

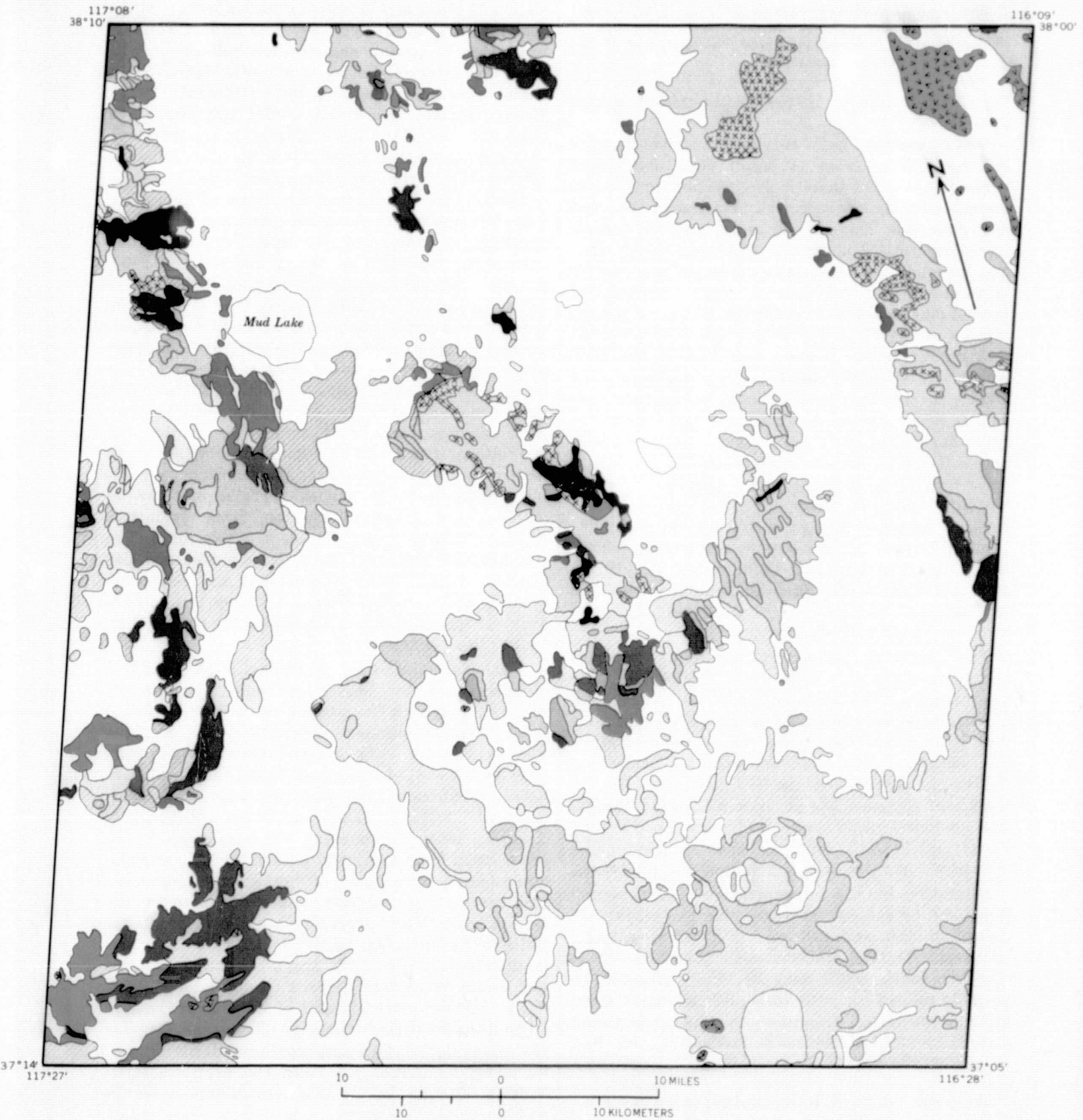

CORRELATION OF MAP UNITS

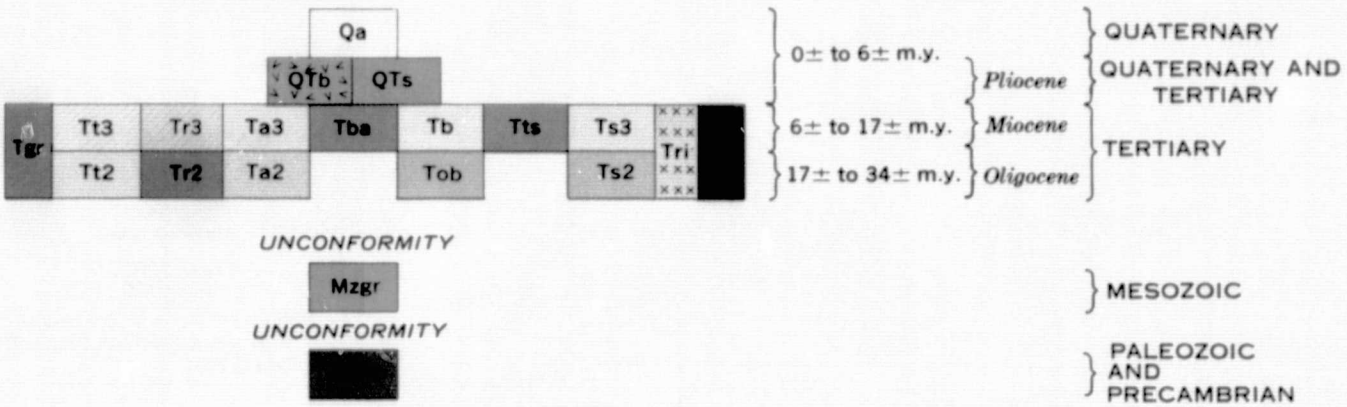

DESCRIPTION OF MAP UNITS

Qa ALLUVIAL DEPOSITS (QUATERNARY)
QTb BASALT FLOWS (QUATERNARY AND TERTIARY)
QTs SEDIMENTARY ROCKS (QUATERNARY AND TERTIARY)—Mostly lake deposits
Tgr GRANITIC ROCKS (PLIOCENE TO OLIGOCENE)—Mostly quartz monzonite and granodiorite
Tt3 WELDED AND NONWELDED SILICIC ASH-FLOW TUFFS (PLIOCENE AND MIOCENE)—Locally includes thin units of air-fall tuff and sedimentary rock
Tt2 WELDED AND NONWELDED ASH-FLOW TUFFS (MIOCENE AND OLIGOCENE)—Locally includes thin units of air-fall tuff and sedimentary rock
Tr3 RHYOLITIC FLOWS AND SHALLOW INTRUSIVE ROCKS (PLIOCENE AND MIOCENE)
Tr2 RHYOLITIC FLOWS AND SHALLOW INTRUSIVE ROCKS (MIOCENE AND OLIGOCENE)
Ta3 ANDESITE FLOWS AND FLOWS OF INTERMEDIATE COMPOSITION (PLIOCENE AND MIOCENE)
Ta2 ANDESITE FLOWS AND FLOWS OF INTERMEDIATE COMPOSITION (MIOCENE AND OLIGOCENE)
Tba ANDESITE AND BASALT FLOWS (PLIOCENE AND MIOCENE)
Tb BASALT FLOWS (PLIOCENE AND MIOCENE)
Tob OLDER BASALT FLOWS (MIOCENE AND OLIGOCENE)
Tts ASH-FLOW TUFFS AND TUFFACEOUS SEDIMENTARY ROCKS, UNDIVIDED (PLIOCENE AND MIOCENE)
Ts3 TUFFACEOUS SEDIMENTARY ROCKS (PLIOCENE AND MIOCENE)—Locally includes minor amounts of tuff
Ts2 TUFFACEOUS SEDIMENTARY ROCKS (MIOCENE AND OLIGOCENE)—Locally includes minor amounts of tuff
Tri RHYOLITIC INTRUSIVE ROCKS (PLIOCENE TO OLIGOCENE)
Tmi INTRUSIVE ROCKS OF MAFIC AND INTERMEDIATE COMPOSITION (PLIOCENE TO OLIGOCENE)
Mzgr GRANITIC ROCKS (MESOZOIC)—Mostly quartz monzonite and granodiorite
pCPz LIMESTONE, DOLOMITE, SHALE, SILTSTONE, QUARTZITE, SANDSTONE, CHERT, AND METAMORPHIC ROCKS (PALEOZOIC TO PRECAMBRIAN)

FIGURE 6.—Geologic map of the study area. From a map of a larger area compiled by John H. Stewart and J. E. Carlson, U.S. Geological Survey; Tertiary units older than Tt2 are not present in the study area.

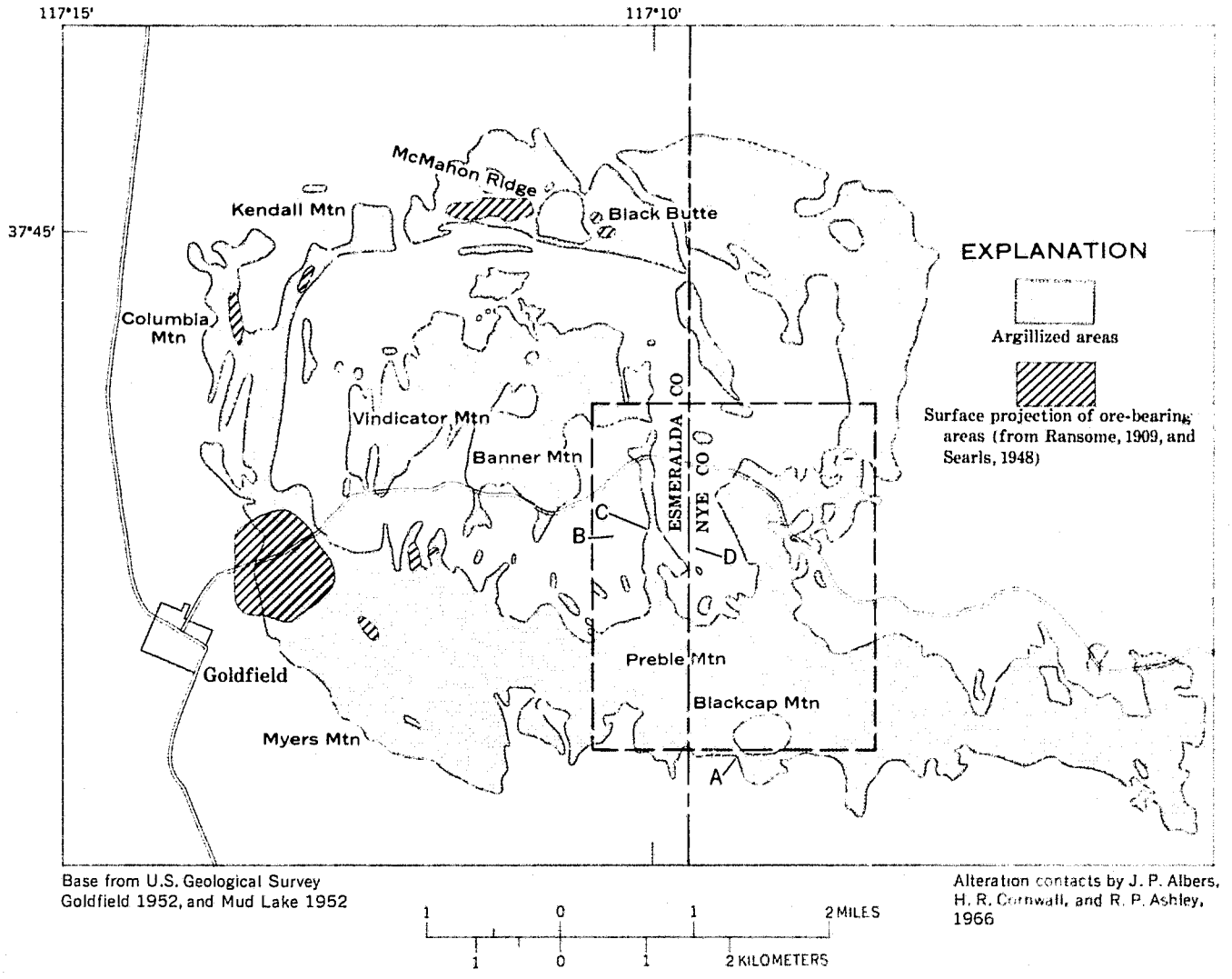

FIGURE 7.—Map showing areas of alteration in the Goldfield mining district (modified from Jensen and others, 1971). Area within dashed line is approximate limit of color aerial photograph in figure 8. A, unaltered upper Tertiary basalt cap; B, unaltered latite; C, hydrothermally altered andesite and dacite; D, unaltered dacite.

Although many of the rock units in the study area have characteristic colors or combination of colors, they are too muted to be consistently shown on small-scale orbital-altitude color photographs. Comparison of an excellent color photograph obtained from the S190 photographic experiment (fig. 9) with the distribution of the main rock types (fig. 6) illustrates this point. The appearance of the rocks in this photograph is dominated by albedo, which is not a reliable guide to rock type (for example, the dark-appearing Thirsty Canyon tuff, Tt3). Color differences are especially difficult to discern in the low-albedo rocks.

Except for a few small limonitic altered areas southeast of Stonewall Mountain (A, B, and C, fig. 9), which appear red brown, the mineralized areas are not distinctive in the Skylab photograph. For example, the Goldfield district appears mottled and slightly rust colored in a few places (D, fig. 9), but similar characteristics are also seen in unaltered areas, such as the northwest end of the Cactus Range (E, fig. 9). These characteristics are not diagnostic of altered areas. This preliminary evaluation suggests that small-scale photographs such as the Skylab example, although useful for morphological and structural studies, are not adequate for detecting and mapping mineralized areas.

STRUCTURAL GEOLOGY

Northwest-trending ranges bounded by normal faults reflect the characteristic Basin and Range terrain of the study area. High-angle normal faults bound the Cactus and Kawich Ranges and the northern and western margins of Stonewall Mountain (fig. 11); movement along these faults began in Mio-

FIGURE 8.—Color aerial photograph of part of the Goldfield mining district: A, unaltered upper Tertiary basalt cap; B, unaltered latite; C, hydrothermally altered andesite and dacite; D, unaltered dacite. Photographed June 2, 1968, for the U.S. Geological Survey. Ektachrome film type 2448.

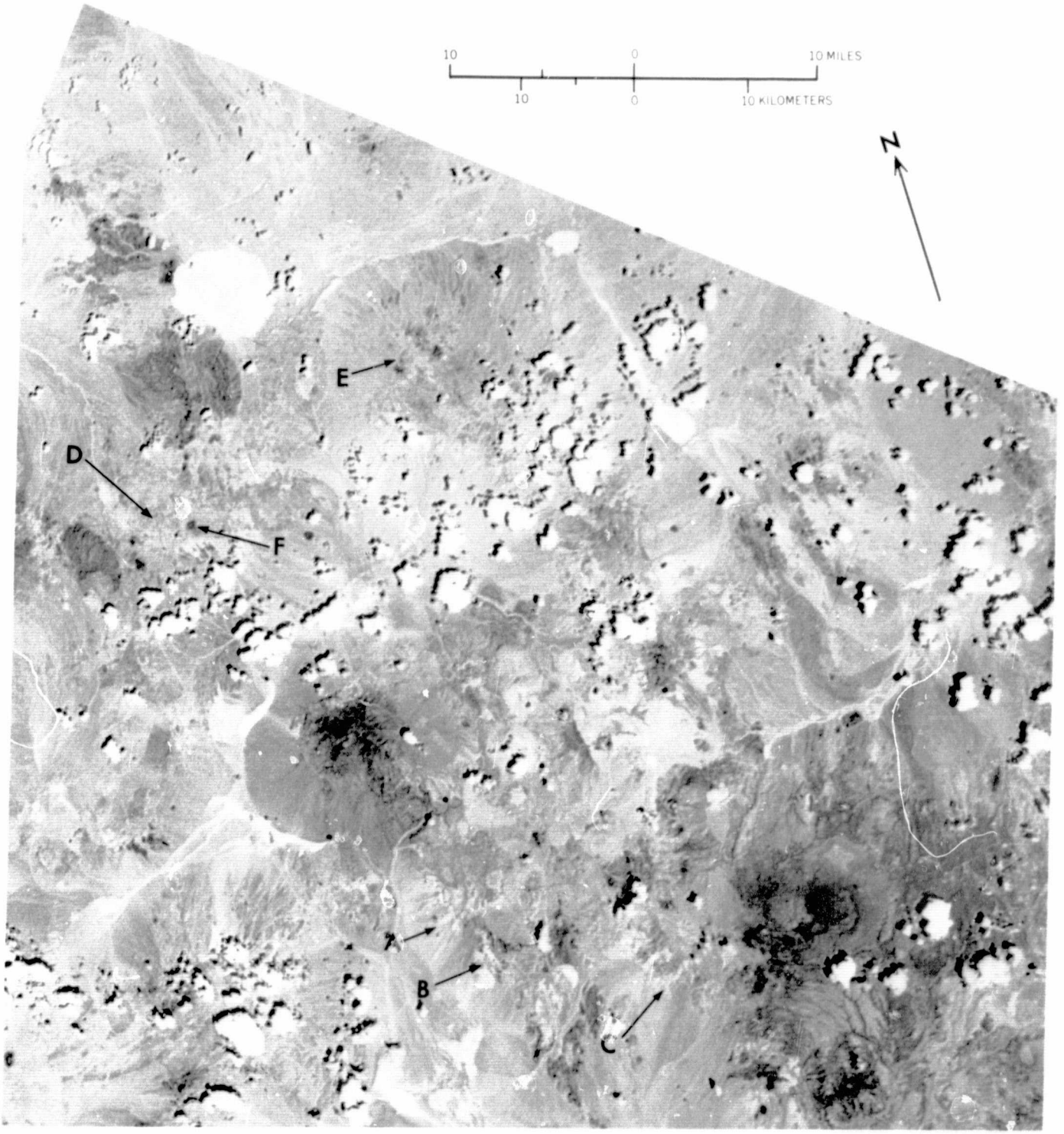

FIGURE 9.—NASA Skylab S190 photograph of part of the study area showing (A–C) alteration areas southeast of Stonewall Mountain, (D) mottled appearance of Goldfield mining district, (E) similar mottled appearance of an unaltered area, and (F) basalt cap in the Goldfield area. Photographed June 3, 1973. Ektachrome film type 50356.

cene time. Although in many areas the Tertiary units are highly faulted and tilted, large areas of flat-lying and undisturbed Tertiary rocks also occur (for example, Pahute Mesa in the study area).

The Precambrian and Paleozoic rocks were folded and thrust faulted mainly during Mesozoic orogeny. Right-lateral shearing of these and more recent rocks along the shear zone known as Walker Lane has resulted in mountain ranges of diverse trend. The volcanic centers mentioned above may be related to this shear belt (Ekren and others, 1971), which cuts in a northwest direction across the southern half of the study area. The structural features are not shown in figure 6 so that lithologic differences can be emphasized.

The geology of the Goldfield district is consistent with that of an early Miocene volcanic center (Albers and Cornwall, 1968). The concentric zones of successively younger formations and the alteration pattern form an east-trending elongated ellipse, and a zone of grabenlike subsidence also extends eastward. The belts of more or less linear silicified ledges may be indicative of a rim fracture system (Albers and Stewart, 1972).

GEOLOGIC INTERPRETATION OF IMAGES

Using the procedures previously described, five processed image sets (fig. 3) have been produced from the basic digital MSS tape of the south-central Nevada study area. Listed in order of increasing enhancement of spectral-reflectance information, the MSS image products are: (1) standard unenhanced images, (2) stretched images, (3) stretched color-infrared composites, (4) stretched-ratio images, and (5) color-stretched-ratio composites (hereafter referred to as color-ratio composites).

STANDARD MSS IMAGES

The standard MSS images distributed by the NASA Date Processing Facility at Goddard Spaceflight Center are of low to moderate contrast; consequently the level of detail is low for both bright and dark objects. In the northeast part of the October 3, 1973, ERTS frame No. E–1072–18001 (fig. 10), materials with low and high albedos, such as mafic rocks and playa deposits, respectively, are distinguished easily, but little detail can be discerned within these areas. Furthermore, few differences are detectable through band-to-band comparison, except in vegetated areas, which are dark in the visible bands and light in the near-infrared bands. This general lack of band-to-band contrast testifies to the subtlety of the spectral differences among the rock types. The small magnitude of the spectral differences, along with the low scene contrast of the standard images, seriously limits their value for rock-type discrimination.

Image contrast for the rocks and soils of the study area, as well as for most areas examined in Nevada and southern California, appears to be highest in the MSS image for bands 6 and 7, in figure 11 at a scale of 1:500,000. However, although most of the playas are easily distinguished from clouds and other features in the area on the basis of shape and texture, little confidence can be placed in most other distinctions. For example, several dark areas are quite prominent, but the compositions of the rocks in those areas range from rhyolitic to andesitic to basaltic. The two large dark patches south-southwest of Mud Lake (A) are basaltic and andesitic in composition, but three minor outcrops of tuffaceous sedimentary rocks (Ts3, fig. 6) occur in the northernmost dark area. The three small dark spots (B) on the northeastern margin of the Cactus Range are basalts, whereas the larger dark area (C) slightly to the south represents part of a mafic intrusive body. East of the Cactus Range, andesite makes up the low hills (D) that are dark on the image. The areal extent of these andesitic outcrops is exaggerated on the image because of the presence of a talus apron around the outcrop. Approximately 12 km south of Tolicha Peak is a series of basalt flows (E), whose boundaries do agree well with the geologic map. Although some subtle reflectivity differences among the mafic rocks exist on the image, variations are not consistent enough to allow discrimination, for example, among andesites, basalts, and the mafic intrusive body with any degree of confidence.

Not all dark areas are indicative of mafic rocks, however. The most prominent dark area on the standard MSS image in the southeastern corner represents the previously mentioned Thirsty Canyon tuff (Tt3) and a rhyolite (Tr3) (fig. 6). Only the southernmost circular area is basalt (Black Butte), and it is indistinguishable from the dark-appearing tuff and rhyolite north of it. Tuffaceous sedimentary rocks that crop out within the dark area southwest of Mud Lake are also indistinguishable from the neighboring andesite and basalt. In addition, a few small exposures of Precambrian and Cambrian rocks (F) appear dark on the image. Therefore rock-type discrimination on this standard MSS image is severly limited even if only a two-component classification system of mafic and felsic rocks is used.

In general, felsic rocks vary in tone on the image from medium to light gray. Discrimination of rock units within this tonal range of gray is rarely possible in any band, especially as the alluvium in the

MSS 4

MSS 5

MSS 6

MSS 7

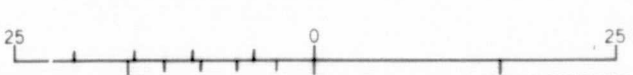

FIGURE 10.—Standard unenhanced MSS images of the study area for bands 4–7 (scale 1:1,000,000). Vegetation is brighter in the image for band 7, especially in the Kawich Range (upper right), than it is in that for band 5. Imaged October 3, 1973, northeast part of ERTS frame No. E–1072–18001.

image appears as very similar gray levels. Isolated outcrops can be discriminated, however, as in the rhyolitic rocks and tuffaceous sediments (G) on the westernmost margin of the Cactus Range. Nevertheless, on Pahute Mesa, the dark pattern on the image correlates only locally with the mapped distribution of tuff and rhyolite.

Major mineralized areas, as indicated by the locations of mines and mining districts (fig. 12), are not distinguishable on the image. The largest, the Goldfield district, is a uniform light gray, and the image gives no indication of the extensive alteration zone there. Other altered areas are also indistinct.

STRETCHED MSS IMAGES

The stretched MSS images of the study area (fig. 13) show substantially more scene contrast and spatial detail than do the standard images. The increased scene contrast, a direct result of the stretching process, allows slightly improved discrimination of rock types. The stretched images have been generated directly from the digital tapes with the result of an apparent increase in spatial resolution (fig. 14). The standard images (fig. 10), on the other hand, have passed through several photographic reproductive processes after their generation from the tapes, processes that have caused a loss of some resolution.

The most apparent improvement of rock-type discrimination in figure 14 is the separation of the basalt (fig. 13, A) and the mafic intrusive (fig. 13, B) in the Cactus Range on the basis of the generally lower albedo of the basalt. Other limitations on discrimination of mafic rock types, however, as described for the standard images, also apply to the stretched images. In addition, discrimination among the felsic rock units, particularly in the Pahute Mesa area, is not improved through stretching the images.

Comparison of the four images of figure 13 with the known mineralized areas (fig. 12) shows that the mineralized areas southeast of Stonewall Mountain (C) and north of the Cactus Range mafic intrusive body (B) are distinctive and bright in all the stretched MSS images. The Cuprite district (D) is notably brighter than it is in the standard images. Nevertheless, confusion could still arise in discrimination between these bright areas and other highly reflective areas such as the tuffaceous sediments south of the Goldfield district (E, fig. 13) and, in some places, alluvium (F, fig. 13). Although the Goldfield district stands out better in the stretched than in the standard images (fig. 10) because of the increased contrast, most of the mineralized areas are not prominent in the stretched images. In general, although scene contrast and apparent spatial resolution are increased, stretching of the radiance data without additional enhancement results in only slightly better discrimination of the geologic materials of this area.

COLOR-INFRARED COMPOSITES

Color composites can be prepared either by transmitting filtered light through the positive film transparencies or by combining color separates such as those made with diazo foils. For example, the color-infrared composite shown in figure 15 was prepared using blue, green, and red filters and positive transparencies for stretched MSS bands 4, 5, and 7, respectively. Colors in this composite are directly related to the film densities in the positive transparencies. Hence, vegetation is red in this composite because the high reflectivity of vigorous vegetation in MSS band 7 compared with MSS bands 4 and 5 results in a relatively low density in the MSS band 7 transparency.

In the study area, the color-infrared composite is most useful for discrimination of vegetated areas (fig. 15). The darkest red, and therefore the densest vegetation, occurs in the Kawich Range and on Stonewall Mountain. Additional red tinges are apparent on Gold Mountain, on parts of Pahute Mesa, and north of Monitor Peak. These sparsely vegetated areas cannot be detected easily on the black-and-white stretched MSS images.

Color-infrared composites appear to offer little improvement over the stretched MSS images for discrimination of rock types. All the points of confusion among the felsic, intermediate, and mafic rock types described for the standard and stretched images are also present in this color composite. Although some of the known limonitic areas, such as southwest of Quartz Mountain (A) and north of Monitor Peak (B), are light orange brown (fig. 15), the other altered areas are not distinctive. The light-orange-brown color, suggesting high reflectance in the MSS bands 5 and 7 compared with the MSS band 4, is consistent with limonite spectra discussed later. Nonetheless, color-infrared composites do not appear

FIGURE 11.—Standard ERTS MSS image of the study area for band 7 (scale 1:500,000) showing some of the main physiographic features in the study area. A, andesite and basalt south-west of Mud Lake; B, three basalt outcrops east of the Cactus Range; C, mafic intrusive rock; D, hills of andesite; E, basalt flows 12 km south of Tolicha Peak; F, dark-appearing Precambrian and Cambrian outcrops; G, rhyolite and tuffaceous sediments on westernmost margin of the Cactus Range; H, basalt cap in the Goldfield mining district.

to offer a reliable means for detecting hydrothermally altered areas.

STRETCHED-RATIO IMAGES

From the previous discussions, it is clear that the spectral-reflectance differences among rock types and between altered and unaltered rocks are generally too small to be detected by visual comparison of the MSS images or through analysis of color-infrared composites. Ratioing of the spectral bands, however, provides additional means for enhancing spectral differences. Although ratioing alone is adequate to show large differences, such as those between the visible and near-infrared bands for vigorous vegetation, stretching is also necessary for adequate enhancement of the typically subtle spectral-reflectance differences found among most geologic materials. The resultant images represent a visual display of the differences between the bands in slope of the spectral-reflectance curve of each geologic unit. Used in combination, ratioing and stretching offer a powerful means for discriminating rock types and alteration zones.

In the stretched-ratio images shown in figure 16, the linear stretches used have been selected to show maximum scene contrast rather than to relate film density to the DN values. Hence, the ratio range selected for stretching and the amount of stretch applied to each ratio image are different. Relative spectral reflectivity, therefore, cannot be determined directly from these particular stretched-ratio images because corresponding gray levels among the images do not represent equal DN ratio values.

Within each of the images in figure 16, the extremes of the 16-step gray scale (not shown) represent the largest spectral-reflectivity differences. The darkest areas in each stretched-ratio image are those for which the denominator of the ratio is greater than the numerator. Conversely, the numerator is greater than the denominator for the lightest areas. For example, the largest differences in reflectance between bands for vegetation are shown in the images for ratios 5/6 and 5/7 (vegetation very dark) and for ratio 4/5 (vegetation extremely light).

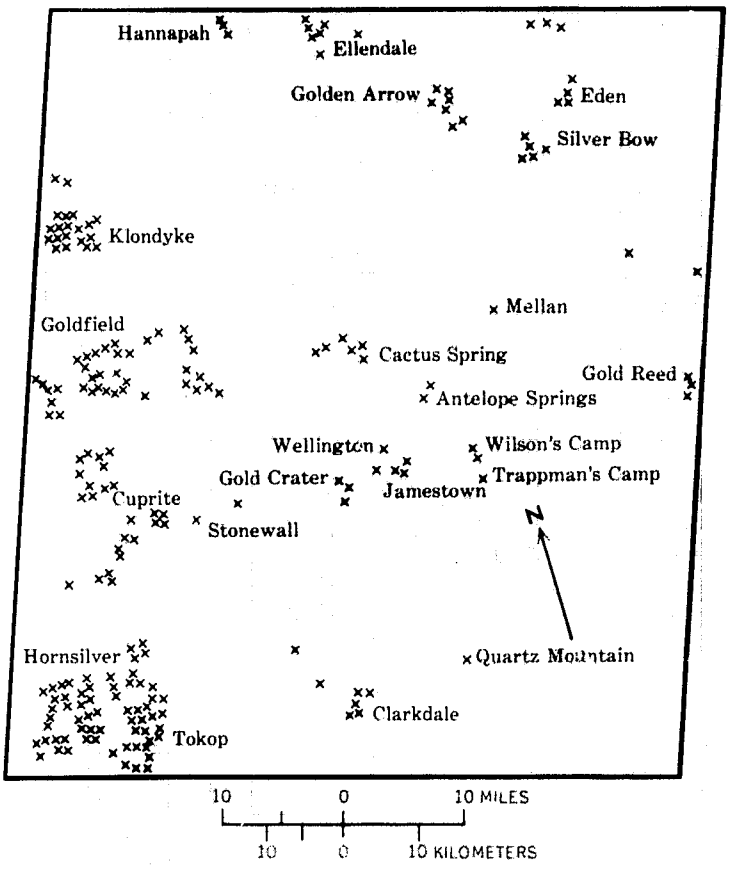

FIGURE 12.—Major mining districts in the study area. Data from Kral (1951), Albers and Stewart (1972), Cornwall (1972); J. H. Stewart (written commun., 1973); F. J. Kleinhampl (written commun., 1973). ×, approximate location of mine or prospect.

More variation within the playas is shown in the stretched-ratio images than in the previous single-band enhanced images in which no variation is apparent. Mud Lake and the southernmost playa (A) are most notable. Within all the stretched-ratio images, however, the playas can be confused with other geologic materials.

Mafic rocks (B, fig. 16) appear very light and distinctive in the images for MSS 4/5, 4/6, and 4/7, but discrimination is still problematic. For example, basaltic and andesitic rocks are indistinguishable, and in the image for MSS 4/5 the mafic rocks can be confused with vegetation and with the felsic rocks (C) on Pahute Mesa. Felsic rocks do not stand out in the stretched-ratio images. Most appear as medium tones of gray, although the felsic rocks on Pahute Mesa are dark in the image for MSS 5/7 and can, in this image, be discriminated from the lighter mafic rocks.

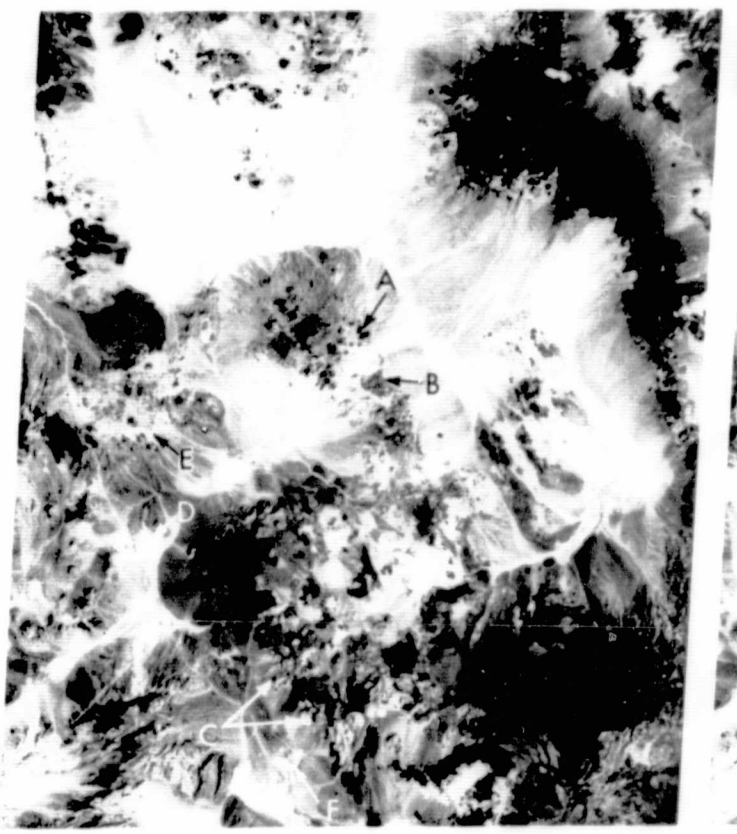

MSS 4

MSS 5

MSS 6

MSS 7

FIGURE 13.—Linearly stretched ERTS MSS images of the study area for bands 4–7 (scale 1:1,000,000). Selected ◀ DN ranges for stretch are: MSS 4, 56–108; MSS 5, 54–121; MSS 6, 53–111; and MSS 7, 44–96. A, three basalt outcrops east of Cactus Range; B, mafic intrusive; C, mineralized areas southeast of Stonewall Mountain; D, Cuprite district; E, bright tuffaceous sediments south of the Goldfield district; F, bright alluvial areas.

Most of the hydrothermally altered areas are indistinct in the standard MSS and stretched MSS images and in the stretched color-infrared composites. The Goldfield mining district (fig. 12), although the largest producing district in the study area, is especially inconspicuous in these image products (figs. 10, 13, 15). In the stretched-ratio images, however, the Goldfield district shows a pattern (fig. 16, MSS 4/5, 4/6, 4/7, 5/6) that, as we will discuss next, is nearly identical with the altered area mapped by Jensen, Ashley, and Albers (1971).

Although the Goldfield district and many other known altered areas are apparent on the stretched-ratio images, they cannot be discriminated from other areas with similar gray tones. The gray levels of the playas especially appear to be nearly identical with those of the altered areas.

COLOR-RATIO COMPOSITES

Color-compositing techniques offer an efficient means for combining black-and-white stretched-ratio images for discrimination of rock types. Whereas two spectrally different areas may be nearly indistinguishable in a black-and-white stretched-ratio image, proper color combination of two or more images permits discrimination on the basis of color differences. Discrimination is increased not only because information from several ratio images is combined but also because the human eye is capable of discriminating two orders of magnitude more hue values than values of gray. Color-ratio composites constitute the most useful image product for geologic analysis generated during this study.

A large number of color and ratio image combinations is possible. Ideally, selection of stretched-ratio images for compositing should be based on the spectral reflectivities of the materials of interest, but spectral data for the study area are too limited to provide an adequate basis for specific selection. Therefore, 70-mm positive transparencies of the six stretched-ratio images were combined in a color-additive viewer to determine the combinations most useful for discriminating the main rock types and altered areas.

Analysis of combinations of two stretched-ratio images and two color filters, from a choice of red, blue, and green, showed that no single two-component composite examined could provide adequate discrimination among major rock types, altered areas, vegetation, and playas. The most common problem involved difficulty in distinguishing the altered zones from the playas and some alluvial areas. Furthermore, in combinations in which the altered areas are detectable, some of the major rock types are not distinctive. Three-component composites (three stretched-ratio images and three color filters) have more overall discrimination potential than do the two-component composites, but discrimination between the altered areas and the playas and alluvium remains a problem.

Another color-compositing technique was tried in an effort to circumvent these problems. Color-ratio composites were prepared using diazo transparencies. Because in the diazo process the most intensely exposed parts of the image are "burned off" upon development, no color is contributed by areas that are clear (for example, DN = 0) in the transparency. Conversely, high film density results in intense color in the diazo-color separates. It is important to understand that the end product of this technique does not represent the reverse of the color-additive method. That is, a composite of negative transparencies made in a color-additive viewer would not be the same as a positive-transparency composite produced using the diazo process.

An optimum combination for geologic analysis of the study area was determined using the diazo process. Although all the innumerable possible color combinations and stretched-ratio-image combinations have not been evaluated, the most effective three-component color-ratio composite for discriminating between altered and unaltered areas and among the regional rock units was prepared using the following color and stretched-ratio image combination: blue for MSS 4/5, yellow for MSS 5/6, and magenta for MSS 6/7. Note that these ratios involve all four MSS bands.

ANALYSIS OF COLOR-RATIO COMPOSITE

The color-ratio composite shown in figure 17 was analyzed initially by studying available geologic maps and 1:250,000-scale black-and-white photomosaics to determine which rock units should be distinguishable and to identify problem areas to be checked in the field. Several regional geologic studies have been conducted previously in this area, most notably those of Cornwall (1972), Albers and Stew-

FIGURE 13.—Linearly stretched ERTS MSS images of the study area for bands 4–7 (scale 1:1,000,000). Selected DN ranges for stretch are: MSS 4, 56–108; MSS 5, 54–121; MSS 6, 53–111; and MSS 7, 44–96. A, three basalt outcrops east of Cactus Range; B, mafic intrusive; C, mineralized areas southeast of Stonewall Mountain; D, Cuprite district; E, bright tuffaceous sediments south of the Goldfield district; F, bright alluvial areas.

Most of the hydrothermally altered areas are indistinct in the standard MSS and stretched MSS images and in the stretched color-infrared composites. The Goldfield mining district (fig. 12), although the largest producing district in the study area, is especially inconspicuous in these image products (figs. 10, 13, 15). In the stretched-ratio images, however, the Goldfield district shows a pattern (fig. 16, MSS 4/5, 4/6, 4/7, 5/6) that, as we will discuss next, is nearly identical with the altered area mapped by Jensen, Ashley, and Albers (1971).

Although the Goldfield district and many other known altered areas are apparent on the stretched-ratio images, they cannot be discriminated from other areas with similar gray tones. The gray levels of the playas especially appear to be nearly identical with those of the altered areas.

COLOR-RATIO COMPOSITES

Color-compositing techniques offer an efficient means for combining black-and-white stretched-ratio images for discrimination of rock types. Whereas two spectrally different areas may be nearly indistinguishable in a black-and-white stretched-ratio image, proper color combination of two or more images permits discrimination on the basis of color differences. Discrimination is increased not only because information from several ratio images is combined but also because the human eye is capable of discriminating two orders of magnitude more hue values than values of gray. Color-ratio composites constitute the most useful image product for geologic analysis generated during this study.

A large number of color and ratio image combinations is possible. Ideally, selection of stretched-ratio images for compositing should be based on the spectral reflectivities of the materials of interest, but spectral data for the study area are too limited to provide an adequate basis for specific selection. Therefore, 70-mm positive transparencies of the six stretched-ratio images were combined in a color-additive viewer to determine the combinations most useful for discriminating the main rock types and altered areas.

Analysis of combinations of two stretched-ratio images and two color filters, from a choice of red, blue, and green, showed that no single two-component composite examined could provide adequate discrimination among major rock types, altered areas, vegetation, and playas. The most common problem involved difficulty in distinguishing the altered zones from the playas and some alluvial areas. Furthermore, in combinations in which the altered areas are detectable, some of the major rock types are not distinctive. Three-component composites (three stretched-ratio images and three color filters) have more overall discrimination potential than do the two-component composites, but discrimination between the altered areas and the playas and alluvium remains a problem.

Another color-compositing technique was tried in an effort to circumvent these problems. Color-ratio composites were prepared using diazo transparencies. Because in the diazo process the most intensely exposed parts of the image are "burned off" upon development, no color is contributed by areas that are clear (for example, DN = 0) in the transparency. Conversely, high film density results in intense color in the diazo-color separates. It is important to understand that the end product of this technique does not represent the reverse of the color-additive method. That is, a composite of negative transparencies made in a color-additive viewer would not be the same as a positive-transparency composite produced using the diazo process.

An optimum combination for geologic analysis of the study area was determined using the diazo process. Although all the innumerable possible color combinations and stretched-ratio-image combinations have not been evaluated, the most effective three-component color-ratio composite for discriminating between altered and unaltered areas and among the regional rock units was prepared using the following color and stretched-ratio image combination: blue for MSS 4/5, yellow for MSS 5/6, and magenta for MSS 6/7. Note that these ratios involve all four MSS bands.

ANALYSIS OF COLOR-RATIO COMPOSITE

The color-ratio composite shown in figure 17 was analyzed initially by studying available geologic maps and 1:250,000-scale black-and-white photomosaics to determine which rock units should be distinguishable and to identify problem areas to be checked in the field. Several regional geologic studies have been conducted previously in this area, most notably those of Cornwall (1972), Albers and Stew-

FIGURE 14.—Linearly stretched ERTS MSS image for band 7 of the study area (scale 1:500,000). Note the excellent resolution of the image as evidenced by discrimination of the secondary roads (A) and the main road (B) that passes through Goldfield and south-southeast past Stonewall Mountain. Also note the basalt cap (C) in the Goldfield mining district.

FIGURE 15.—Color-infrared composite of study area made up of linearly stretched images of ERTS MSS bands 4, 5, and 7 with blue, green, and red filters, respectively (scale 1:500,000). A and B are limonitic areas southwest of Quartz Mountain and north of Monitor Peak, respectively. Prepared by the Jet Propulsion Laboratory, Pasadena, Calif., in cooperation with the U.S. Geological Survey.

MSS 4/5

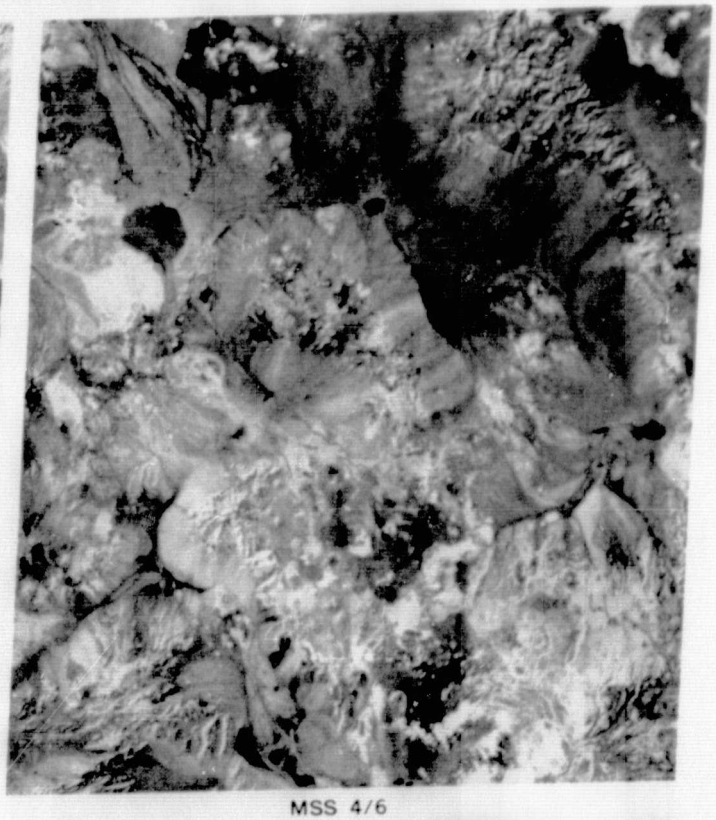

MSS 4/6

MSS 4/7

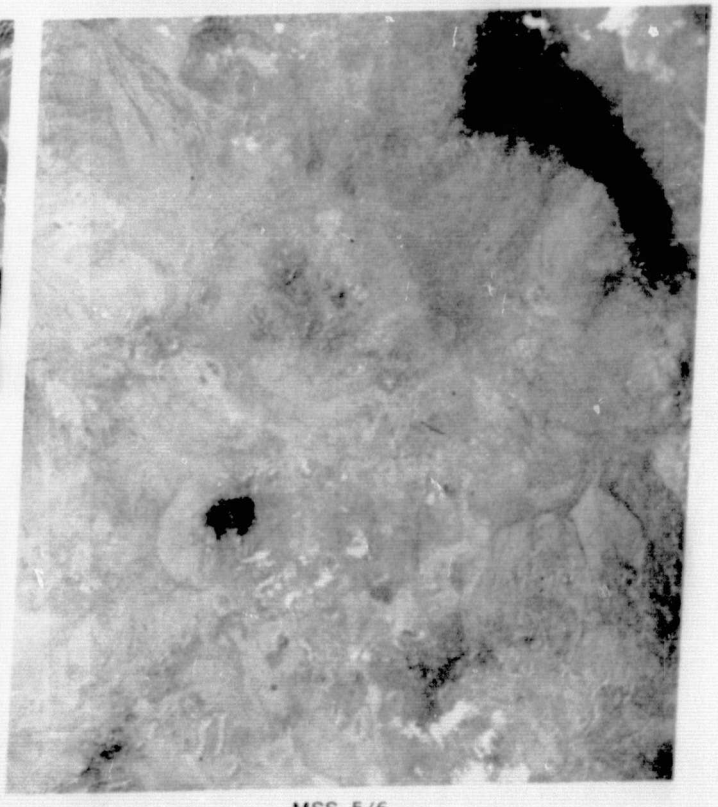

MSS 5/6

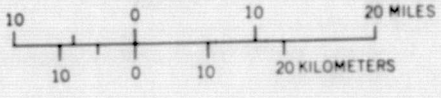

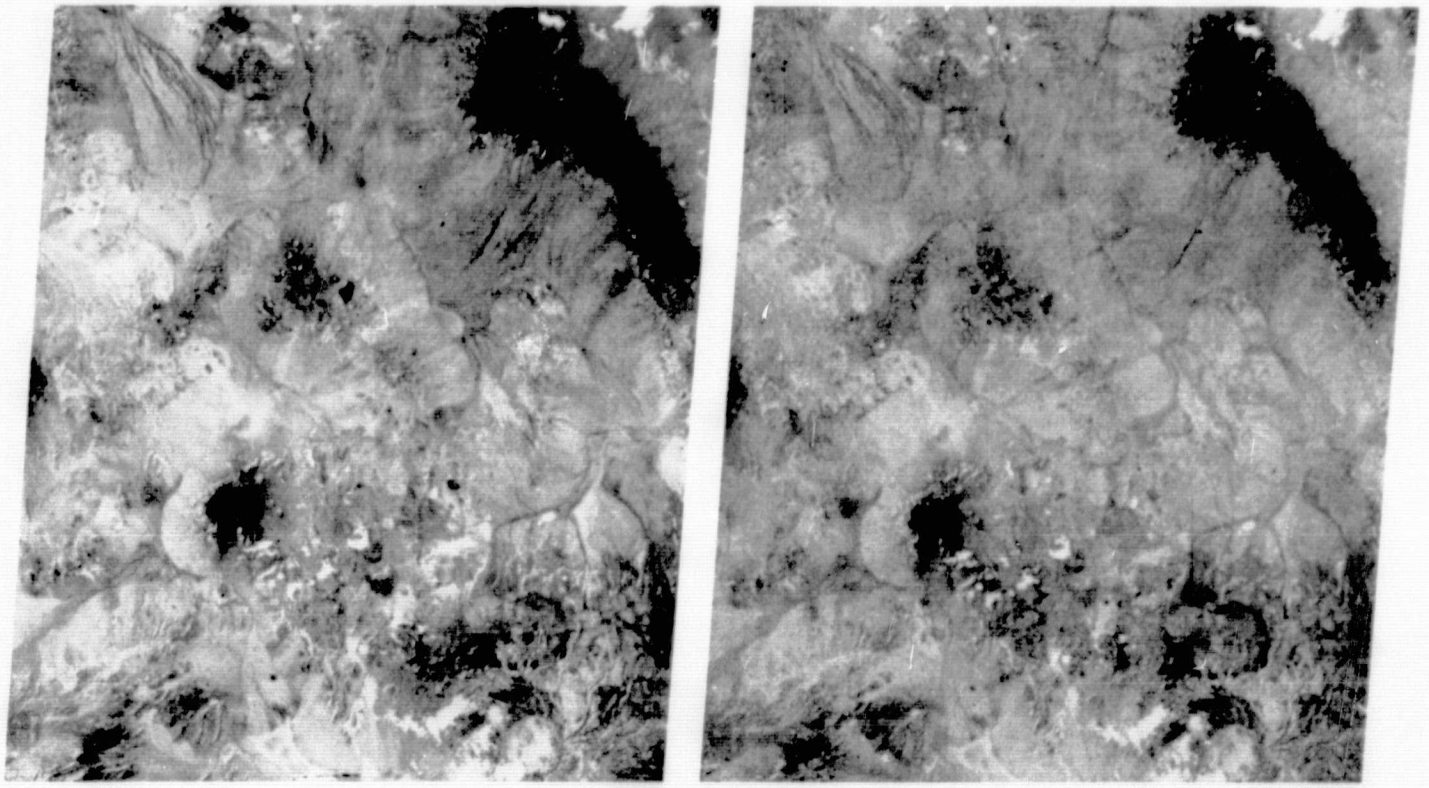

FIGURE 16.—Linearly stretched-ratio ERTS MSS images of the study area (scale 1:1,000,000) showing (A) variation in Mud Lake and southernmost playa, (B) mafic rocks, and (C) felsic rocks on Pahute Mesa. Selected ratios and DN ranges for stretch are: MSS 4/5, 116–161; MSS 4/6, 125–184; MSS 4/7, 156–222; MSS 5/6, 125–168; MSS 5/7, 152–205; MSS 6/7, 135–178.

art (1972), and Ekren and others (1971), but a map based on a compilation by John H. Stewart and J. E. Carlson, U.S. Geological Survey, of the State of Nevada is the most useful single map because it integrates all these previous studies (fig. 6). In addition, the original compilation scale of 1:500,000 is especially compatible with analysis of ERTS images. Three field evaluations, each 1 week long, were aided appreciably by overflying the area before working on the ground. Black-and-white aerial photographs at a scale of 1:62,500 also proved to be nearly indispensable for orientation and for distinguishing outcrops and surficial deposits.

In the color-ratio composite (fig. 17), mafic rocks are generally white, felsic rocks are pink, playas are blue, and vigorous vegetation is orange. Limonitic areas are green to yellow green, and essentially limonite-free hydrothermally altered areas range from green to brown and, more rarely, to red brown. Clouds are a dark pink brown, and cloud shadows are white; topographic shadows are also white.

Most mafic rocks can be discerned easily on the image. They appear white, usually accompanied by small patches of pink. In places, such as immediately southwest of Mud Lake (A, fig. 17), some of the pink patches associated with the white area are clearly due to the presence of tuffs and tuffaceous sediments, but in other areas the pink is probably related to residual soil formed on mafic rocks. These light-pink-colored soils are exemplified by Malpais Mesa southwest of Goldfield (B, fig. 17), the basalt approximately 6 km north of Tolicha Peak (B, fig. 17), and the basalt northeast of the Kawich Range (B, fig. 17); they are probably felsic in composition either because the mafic minerals have been decomposed and leached, leaving a residuum consisting mainly of slightly weathered feldspar, or because a veneer of felsic eolian material overlies the basalt. Some discrepancies between the map units (fig. 6) and the color-ratio composite may be accounted for by talus deposits, as mentioned previously.

Unfortunately, several other rock units besides mafic rocks also appear white, although not consistently so. The two white spots northeast of Mud Lake (C, fig. 17) are dark-gray to black Paleozoic limestone and chert (Cornwall, 1972), and a white strip north of Gold Mountain (D, fig. 17) is dark-green-gray siltstone and very fine grained quartzite of Precambrian and Cambrian age (Albers and Stewart, 1972). The eastern part of the white square area

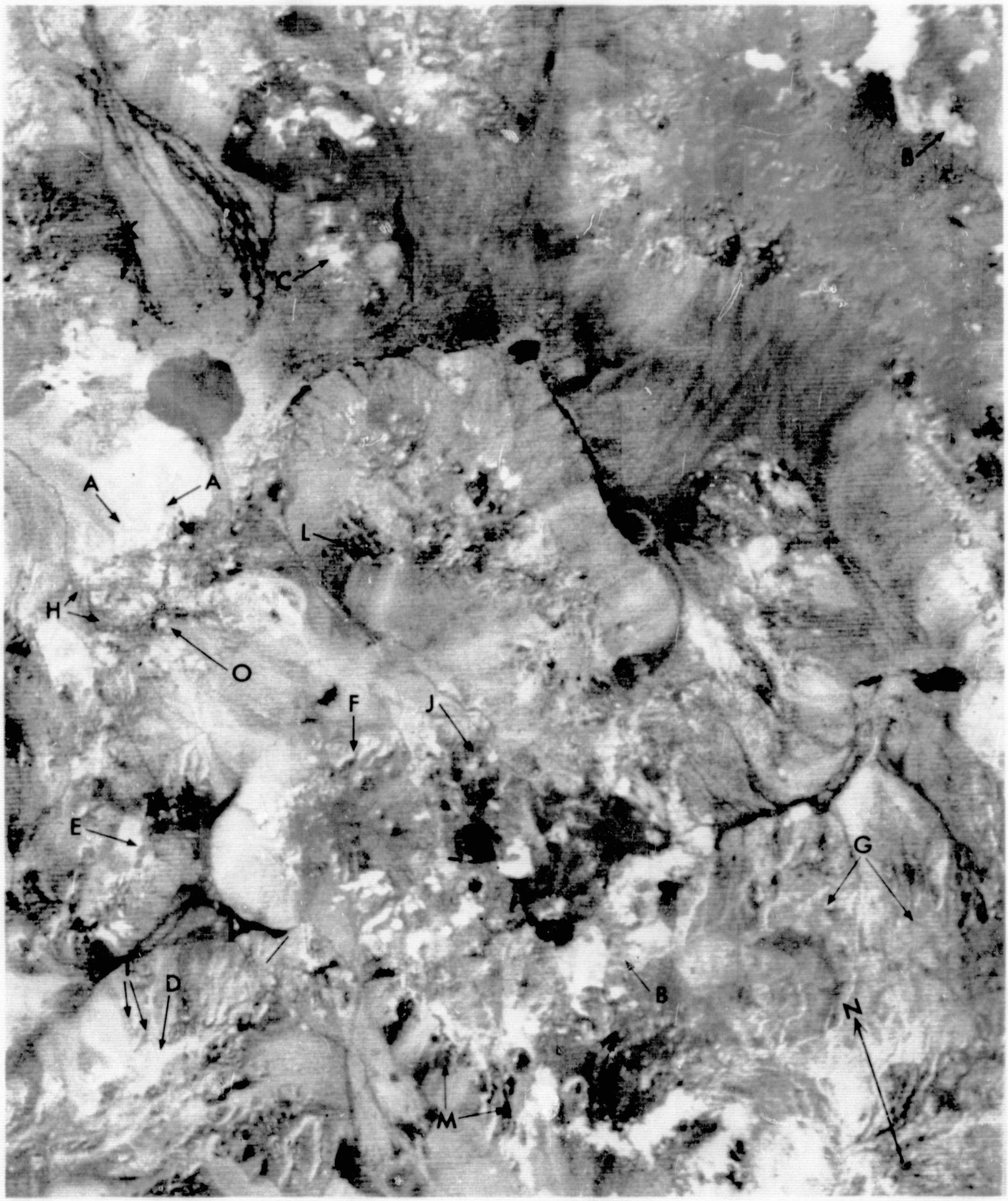

FIGURE 17.—Three-component color-ratio composite of south-central Nevada (scale 1:500,000) made from diazo-color separates showing limonitic and hydrothermally altered areas (green to brown), playas (blue), mafic rocks (generally white), felsic volcanic and intrusive rocks (pink), and vigorous vegetation (orange). Clouds are dark pink brown and cloud shadows white. Prepared from ERTS MSS data by the U.S. Geological Survey in cooperation with the Jet Propulsion Laboratory, Pasadena, Calif. EROS Data Center ID No. ER–1–CC–5000.

A, Pink patches of felsic volcanic intrusive rocks southwest of Mud Lake.
B, Light-pink-colored soils formed on mafic rocks north of Tolicha Peak and northeast of the Kawich Range.
C, Two white pre-Mesozoic elliptical features northeast of Mud Lake.
D, White pre-Mesozoic strip north of Gold Mountain.
E, Pre-Mesozoic part of the white square west of Stonewall Mountain. Western part is alluvium.
F, White topographic effects on northeastern part of Stonewall Mountain.
G, Orange-pink outcrops of Thirsty Canyon rhyolitic tuffs and flows, which appear dark on the other images and photographs evaluated.
H, Two blue areas representing mine tailings north and northeast of Goldfield.
I, Green outcrop of slightly ferruginous sandstone of the Harkless Formation.
J, Green appearing highly bleached Gold Crater area.
K, Green circular area of mafic intrusive body 20 km northwest of Mud Lake.
L, Brown area of rhyolite and tuffaceous sediments in western Cactus Range.
M, Two red-brown areas west of Stonewall Mountain.
N, Two red-brown areas near Tolicha Peak.
O, Basalt cap mentioned in figures 8 and 14.

west of Stonewall Mountain (E, fig. 17) is part of an undifferentiated Paleozoic unit (fig. 6). The western part is presumably talus.

Additional problems in discriminating mafic rock types are the white-appearing cloud shadows and topographic effects—for example, the thin white areas northeast of Stonewall Mountain (F, fig. 17). Examination of the stretched MSS images (figs. 13 and 14), however, makes identification and discrimination of these nongeologic features straightforward.

Dark pink, brown pink, and orange pink are characteristic of felsic rocks on the image. Light vegetation cover causes the orange tone but it appears that rock reflectance, and therefore rock-type variation, can be seen if the vegetation cover is light, as on Pahute Mesa. On the other hand, where vegetation is dense, as on the Kawich Range and on Stonewall Mountain, spectral differences reflecting rock type are not recorded. These areas appear a very dark orange.

In general, the agreement between pink hues and the distribution of felsic rocks shown in the geologic map is quite striking. Most impressive is the orange-pink hue of the Thirsty Canyon tuffs and flows (Tt3 and Tr3, fig. 6; G, fig. 17). Because the surface of these rocks has a low albedo, they are easily confused with the mafic volcanic rocks both on the other images evaluated and in the field. Ratioing minimizes albedo effects, however, so that discrimination of these felsic rocks from mafic rocks is possible on the color-ratio composite. The orange pink in figure 17 indicates that the general shape of the visible and near-infrared reflectance spectra of these felsic rocks must be very similar to that of the other felsic rocks. In general, however, the older tuffs (Tt2) and flows (Tr2) are less uniform on the color-ratio composite than units Tt3 and Tr3.

Playas are easily discriminated from the altered rocks. The only blue areas in figure 17 that are not playas are two small patches representing mine tailings, north and northeast of Goldfield (H, fig. 17). In addition, variation within and among playas is much more pronounced in the color-ratio composite than in any of the previously enhanced products. The southernmost playa and Mud Lake show the most variation, presumably because of compositional and perhaps grain-size differences.

One of the principal objectives of this study was to evaluate the potential of the MSS data for detecting hydrothermally altered areas. Although none of the previous image products seems to have much potential for discriminating altered areas, these areas can be identified with a high degree of confidence in the three-component color-ratio composite shown in figure 17. Figure 18 shows the distribution of altered outcrops based on a very general four-color classification of anomalous color patterns in figure 17. Black-and-white aerial photographs at a scale of 1:62,500 were used to exclude areas of alluvium.

In general, the green to yellow-green pattern in the color-ratio composite (fig. 17) represents predominantly limonitic outcrops. The largest anomaly is the green pattern representing the alteration zone in the Goldfield mining district (fig. 18). In fact, the agreement between the altered zone as defined by Jensen, Ashley, and Albers (1971) (fig. 18, inset) and the green pattern in figure 18 is very striking. The largest discrepancies occur in the western part of the district, where many mine dumps obscure the surface, and in the area beyond the southern border,

which was not mapped by Jensen, Ashley, and Albers. Although the altered area consists of several different alteration products, the Goldfield district is represented by a fairly uniform green in figure 17. As mentioned previously, however, the red-brown hue of the limonite dominates the overall appearance of the complex mottled pattern (fig. 8) of the alteration zone.

On the basis of this observation and of brief evaluation of several other areas, Rowan (1973) concluded that all green areas were predominately limonitic. More detailed field examination showed, however, that included in this color pattern are two or three areas that are altered but that have little or no limonitic surface stain. For example, the Gold Crater area (J, fig. 17) is very highly bleached and has only a few limonite-stained outcrops on the lower slopes. Most of the outcrops that are green on the composite were checked in the field, and with the exception of two areas, all proved to be hydrothermally altered. One of these exceptions is the outcrop of slightly ferruginous sandstone and siltstone of the Harkless Formation (I, fig. 17), which is included in the undifferentiated Precambrian-Paleozoic map unit (p€ Pz) of figure 6. This formation occurs only in the west-central and southwestern part of the study area.

The other exception is an area that is neither limonitic nor obviously altered. The rock unit in this area, about 20 km northwest of the center of Mud Lake (K, fig. 17), is mapped as a Tertiary mafic intrusive body (Tmi, fig. 6). Most of the material in the crudely circular light-green area in figure 17 is alluvium derived from the intrusive body represented by darker green hills in the southwestern part of the circular area. Although a few fragments of the alluvium are limonite stained, the greenish-gray outcrops appear on the ground to be generally free from ferric iron surface stains. This still enigmatic area will be the subject of future coordinated petrographic and spectral analyses.

Most of the other altered areas are dark green to brown in the color-ratio composite (figs. 17 and 18). The dark-green areas, all of which were examined in the field, are confined to the southern half of the area. The rocks themselves in these areas are typically pink to red, tan, yellow, and gray mottled, altered Tertiary volcanic rocks. The dark green in figure 17 represents both limonitic and limonite-free altered areas, although less limonite is generally present than in the light-green category.

Brown areas in the color-ratio composite are more numerous than dark-green areas and have not been examined as thoroughly. The materials in the brown areas appear to be made up of light-colored Tertiary volcanic rocks, some of which are glassy and pumiceous. Limonite-free areas predominate, but some limonite may be present. In the Silver Bow district, the only brown area checked in detail on the ground, hydrothermal alteration is evident. Other brown areas checked from the air, such as those on the southeastern and southwestern margins of the Kawich Range, are light-colored volcanic rocks, but the presence of hydrothermal alteration could not be determined. Ekren and others (1971), however, stated that the light colors of the tuffaceous sediments in the large brown area in the western Cactus Range (L, fig. 17) typify zeolitized, silicified, or argillized rocks.

Several dark-green to brown areas proved to be alluvium that is limonite stained. Weathering of the many exposed surfaces of the small fragments results in the formation of abundant ferric oxide. The MSS, therefore, records the characteristic spectrum of limonite (Hunt and others, 1971a; Rowan, 1972) for these weathered but not hydrothermally altered materials.

A few altered areas appear red brown in the color-ratio composite. The two areas west of Stonewall Mountain (M, fig. 17) and the two areas near Tolicha Peak (N, fig. 17) were examined in the field, and in all four places the rocks are nearly white silica-rich Tertiary volcanic rocks with no limonite present. The rocks west of Stonewall Mountain have been lightly altered by epithermal activity to very fine grained silica, whereas the Tolicha Peak volcanic rocks are very glassy tuffs without any obvious hydrothermal alteration.

Assessment of the color-ratio composite indicates that green, dark green, brown, and red brown, which seem to represent, in that order, predominantly limonite-stained rocks to highly bleached and argillized rocks, are generally indicative of hydrothermal alteration. Comparison of the areal distribution of mining districts (fig. 19) and the color anomalies (fig. 18) substantiates this conclusion, even though figure 19 represents only a general map of the mines and prospects. Some mines and prospects were omitted necessarily in areas of high mine density.

Most of the major mining districts—Goldfield, Cactus Spring, Antelope Springs, Gold Reed, Gold Crater, Wilson's Camp, Trappman's Camp, and Wellington—have concentrations of green to yellow green and dark green. A few green areas apparently do not have mines or prospects, although they consistently represent areas of altered rocks. Brown and red brown dominate the Silver Bow, Golden Arrow, Cuprite, and Hannapah districts, in some of which hydrothermal alteration is evident. Several brown and red-brown areas have no evidence of mining, al-

TABLE 1.—*Ratios calculated for MSS bands for selected mafic and felsic rocks and alteration minerals of figures 2 and 20, respectively*

Sample	Number	MSS 4/5	MSS 5/6	MSS 6/7
Mafic rocks				
Basalt	13	1.05	1.03	1.06
Gabbro	9	1.07	1.01	.99
Peridotite	8	1.01	1.01	1.05
Serpentinite	15	1.04	1.05	1.07
Felsic rocks				
Rhyolite (pink)	12	0.79	0.92	0.96
Rhyolite (gray)	4	.96	.96	.98
Granite	14	.89	.94	.91
Granite	5	.97	.98	.92
Granodiorite	2	.92	.94	.97
Alteration minerals				
Limonite (goethitic)	---	0.61	0.72	0.94
Limonite (hematitic)	---	.49	.85	.95
Jarosite	---	.78	.99	1.27
Montmorillonite	---	.65	.84	1.07
Alunite	---	.66	.88	.97
Kaolinite	---	.93	.98	.99

though they are generally concentrated in areas of past mining activity. Considerably more work needs to be done to evaluate all the brown and red-brown areas fully.

Two mining districts, Eden and Stonewall, are noteworthy because anomalous colors are not present (figs. 17, 19). In these districts, the spectral-reflectivity information is probably obscured by vegetation and topographic shadows, respectively, but there is little surface indication of alteration in the vicinity of the Stonewall district (R. P. Ashley, written commun., 1973). Anomalous colors are not shown in figure 18 for the Mellan district because the area that appears green in figure 17 is mainly alluvium. The southwestern part of the area is also important because, although many mines are present (fig. 19), the areal density of colors indicative of hydrothermal alteration is obviously lower than in most of the other mining districts. The main geological difference between this general area and the rest of the anomalously colored areas appears to be the prevalence of Mesozoic and Precambrian-Paleozoic rocks. The ore bodies occur as vein deposits associated with the Mesozoic intrusive rocks in this area, and the surface area of alteration is very much smaller than in the altered Tertiary volcanic rocks. Hence, higher spatial resolution may be needed to detect the alteration in an area such as this.

The general correlation between the color anomalies (fig. 18) and the known mining-district locations (fig. 19) indicates that color-ratio composites should be especially valuable as a means of reconnaissance mapping for mineral exploration in well-exposed areas. Color-anomaly maps such as figure 18 can be used for selection of specific targets for detailed geologic, geochemical, and geophysical analyses.

DISCUSSION

One of the ultimate objectives of this investigation is to derive quantitative spectral-reflectivity information from the MSS images and to use these data for making estimates of the bulk composition of surface materials. Although this objective is not presently feasible because of inadequate calibration data, the spectral differences seen as color variations in the color-ratio composite (fig. 17) can be evaluated qualitatively by considering laboratory spectra that appear to be reasonably representative of the surface materials.

As discussed previously, visible and near-infrared reflectance spectra for mafic and felsic rocks (fig. 2) have generally different shapes. Although data for only a few of the rock types present in the study area are included in figure 2, a general idea of the anticipated differences can be gained through comparison of these spectra. A useful method for making such comparisons is examining calculated ratio values based on the width of the MSS bands used in processing the color-ratio composite (MSS 4/5, 5/6, and 6/7). These ratio values are not representative of the absolute MSS values because of undetermined effects of the solar spectrum and of atmospheric variations, but the calculated ratio values can be useful for comparative purposes. In general, ratios for the felsic rocks are less than unity, whereas the mafic rock ratios are greater than unity (table 1). Comparison of the basalt with the two rhyolite spectra shows that the ratios for basalt are approximately 7–12 percent higher, except in the MSS 4/5 ratio for the pink rhyolite (table 1) where the difference is about 25 percent. These low percentage values attest to the subtlety of the spectral differences among even very different rock types. It is

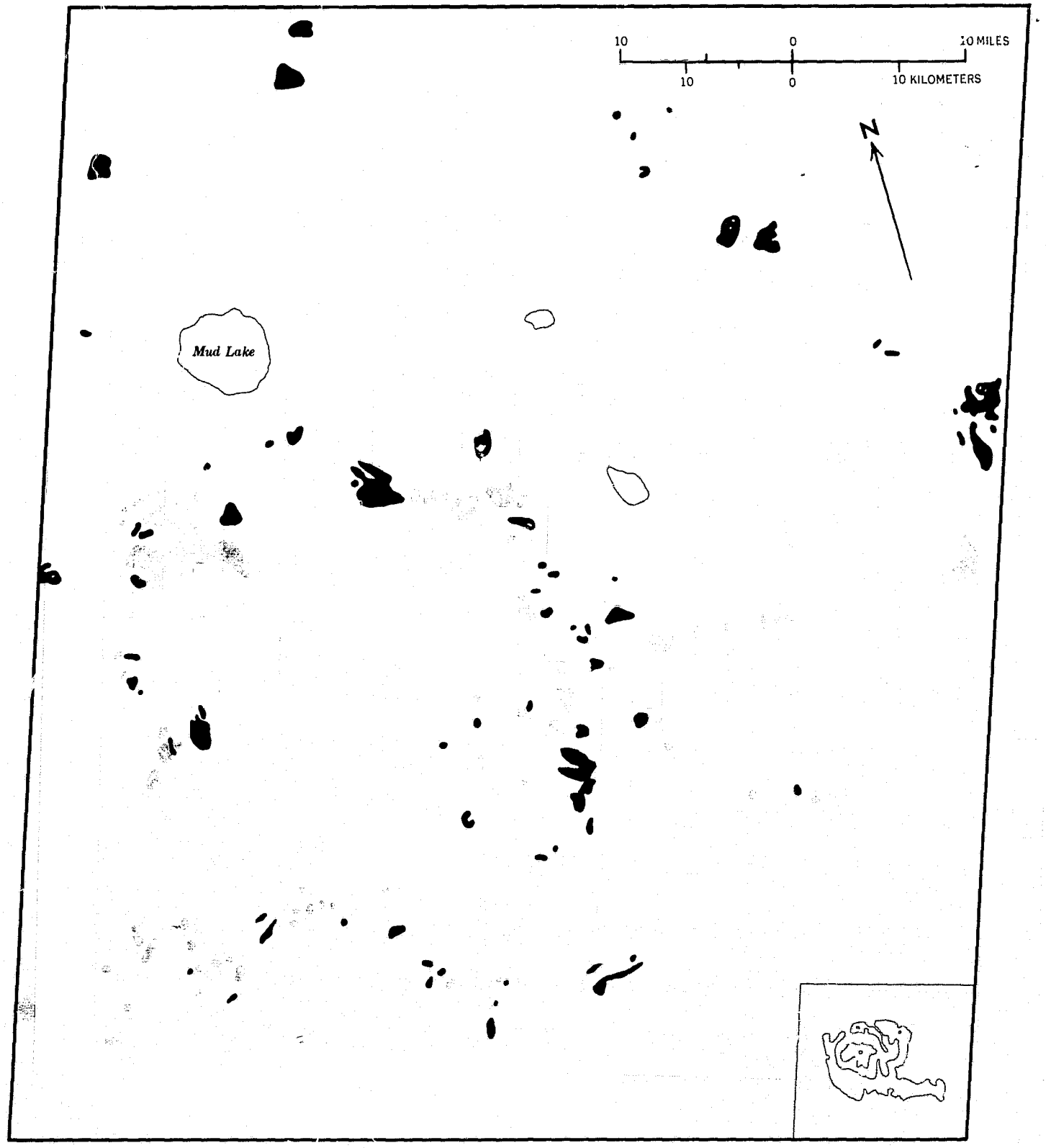

FIGURE 18.—Distribution in the study area of anomalous color patterns, classified by four colors—green, dark green, red brown, and brown (from fig. 17). These color patterns represent altered outcrops. Inset is an alteration map of the Goldfield district by Jensen, Ashley, and Albers (1971) at the same scale.

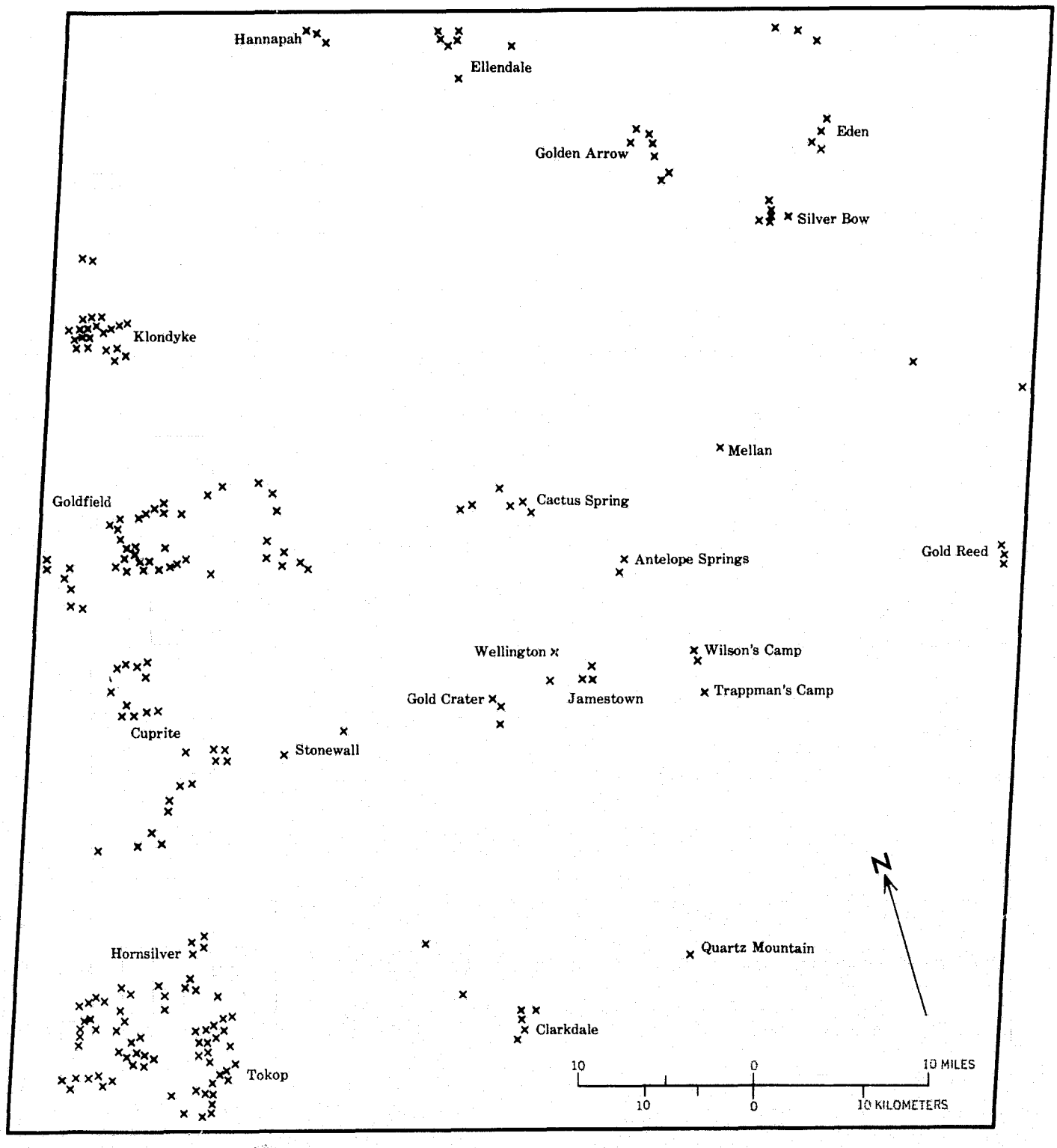

FIGURE 19.—Major mining districts in the study area (scale 1:500,000). From Kral (1951), Albers and Stewart (1972), Cornwall (1972), J. H. Stewart (written commun., 1973), F. J. Kleinhampl (written commun., 1973). ×, approximate location of mine or prospect.

not surprising, therefore, that some form of computer processing is necessary to enhance the spectral signatures of mafic and felsic rocks in the standard ERTS images. Additional computer processing, perhaps using cube-root stretch of the ratio values to increase scene contrast in the dark areas in the stretched-ratio images, might permit further discrimination between, for example, basalts and andesites.

Evaluation of the altered areas is more difficult because spectroradiometric studies have not been conducted on altered rocks. A few laboratory spectra, however, have been published for most of the main minerals that constitute the Goldfield alteration zone, including limonite, montmorillonite, alunite, kaolinite, and jarosite (fig. 20). Comparison

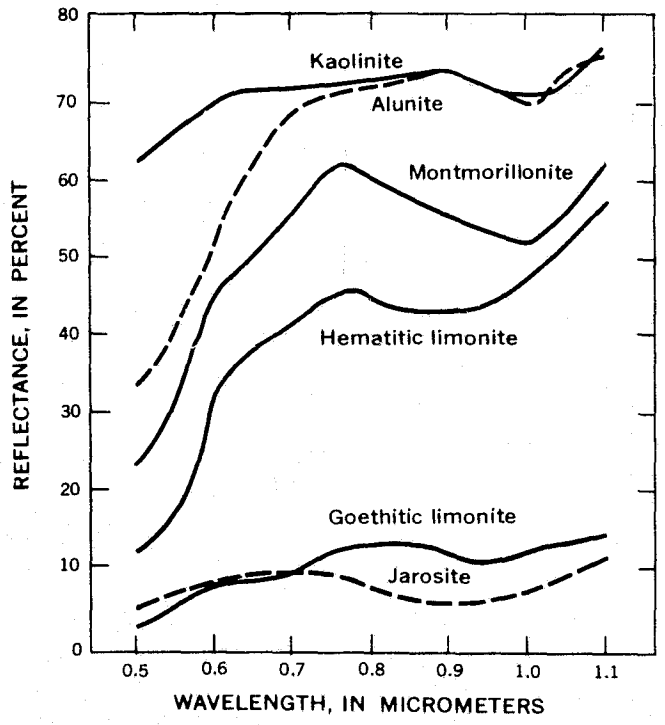

FIGURE 20.—Reflectance spectra for alteration minerals. Data for montmorillonite and kaolinite from Hunt and Salisbury (1970), alunite and jarosite from Hunt, Salisbury, and Lenhoff (1971b), goethitic limonite from Rowan (1972), hematitic limonite obtained in place at Goldfield (A. F. H. Goetz, written commun., 1973).

of the ratios calculated for these spectra and for the mafic rocks (table 1) shows that the MSS 4/5 values for the alteration products are significantly lower than those for mafic rocks and that the MSS 5/6 ratios are slightly lower. Therefore these alteration products should be very distinctive where they occur in areas underlain by mafic rocks. Comparison with the felsic-rock ratios indicates that geothitic and hematitic limonite, alunite, and montmorillonite should be distinguishable from felsic rocks because of their lower MSS 4/5 ratios and somewhat lower MSS 5/6 ratios. The jarosite MSS 4/5 ratio is only slightly lower than the felsic-rock ratios; however, the MSS 6/7 ratio for jarosite is markedly higher than the largest value for the felsic rocks, so this ratio could be used for discrimination purposes. The ratios shown in table 1 for kaolinite resemble those for the felsic rocks of figure 2, and it is doubtful that such small differences could be distinguished in a color-ratio composite. However, as Ashley (1970) pointed out, illite and alunite are associated with kaolinite in the more intensely altered zone at Goldfield. Both of these minerals might, as the uniform green of the color-ratio composite at Goldfield indicates, subdue the effects of the kaolinitic spectral reflectivity and result in low ratios.

Although altered and unaltered rocks are discriminated with a high level of confidence in the color-ratio composite, limonitic and limonite-free hydrothermally altered areas do not appear to be distinguishable at this stage of the analysis. Although this distinction does not appear to be economically important in the study area because metallization occurs in both types of areas, it could be important in areas where limonite is not particularly diagnostic of hydrothermal alteration. The calculated ratios in table 1 suggest that the MSS 4/5 ratio should provide the best opportunity for distinguishing bleached argillized and limonitic altered rocks, especially where the limonite is hematitic rather than goethitic. In addition, higher spectral resolution and bands at longer wavelengths, such as those provided by the NASA Skylab multispectral scanner (S192), should significantly aid in discriminating these materials and in estimating the mineralogical makeup of the surface materials.

The above discussion illustrates the critical need for a clearer definition of the relationship between mineralogical composition and visible and near-infrared spectral reflectivity of altered and unaltered rocks. Ideally, in situ spectroradiometric measurements, at several scales and coordinated with detailed sampling for subsequent mineralogical analysis, should be made in a variety of geologic settings and environmental conditions. An important use for these in situ measurements is formulation of spectral-reflectivity standards that take into account varying surface-state conditions. The standard areas should be of different albedos but nearly uniform

over large areas, and the spectral information should be collected at the same time as the satellite overflight so that atmospheric conditions are similar. Spectral-reflectance standards acquired in this fashion could be used to normalize all the DN values in the MSS images, provided that atmospheric transmission and path-radiance are uniform over the run. Then quantitative spectral-reflectivity information could be extracted directly from the DN values for any surface unit.

SUMMARY AND CONCLUSIONS

The results of this study show that most of the major rock units and altered and unaltered areas in the study area can be separated on the basis of visible and near-infrared spectral-reflectivity differences recorded from satellite altitude. Because these differences are mainly due to slight variations in the slopes of the spectra, they are not detectable through visual or optically assisted techniques. Digital ratioing of the MSS bands and subsequent stretching to increase the contrast are necessary to enhance these differences. Although the basic spectral information is contained in the stretched-ratio images, color-ratio composites, especially combinations of three ratio images, appear to be the best means of display for geologic visual interpretation as an aid in mineral-resources exploration and regional geologic mapping.

For discrimination of hydrothermally altered areas and of regional rock (and soil) units in the study areas, the optimum color-ratio composite appears to be a combination of diazo-color transparencies having the following ratio images and colors: blue for MSS 4/5, yellow for MSS 5/6, and magenta for MSS 6/7. In this composite (fig. 17), mafic rocks are generally distinguishable from felsic rocks despite their similar albedos in some places. Details within playas are best seen in the color-ratio composite. Some of the most important practical limitations, however, include erroneous identification of basalt as felsic rocks where soil overlies areas of the basalt, and lack of discrimination thus far of basaltic and andesitic rocks.

Hydrothermally altered areas appear as anomalous color patterns (fig. 17) within the volcanic rocks on the color-ratio composite. Comparison of known mining-district locations and clusters of anomalous colors, ranging from green and dark green to brown and red brown, shows good agreement in the widespread Tertiary volcanic rocks. In the Goldfield mining district, for example, very striking agreement was found between the anomalous green pattern and the map of the altered area by Jensen, Ashley, and Albers (1971). However, the density of anomalies compared with that of the mines is not as high in the southwestern part of the study area where the alteration and mineralization are associated with intrusion of pre-Mesozoic rocks rather than with the Tertiary volcanic rocks. In spite of the few discrepancies, the color-anomaly map showing the distribution of altered areas (fig. 18) should be very useful for identifying sites where detailed geological, geochemical, and geophysical analyses should be made during mineral-resources exploration.

In general, the green to dark-green color pattern in this color-ratio composite represents predominantly limonitic areas, which except for two cases, are hydrothermally altered. All green areas in the composite are not limonitic however. Several green areas, as is well illustrated in the Gold Crater area, are essentially limonite-free argillized volcanic rocks. Red-brown areas in the color-ratio composite commonly appear to be silica-rich light-colored volcanic rocks. In the Cuprite district, the red-brown color correlates very well with the silicified zone in which hydrothermal alteration has taken place, but the red-brown areas near Tolicha Peak are very glassy tuffs without any obvious hydrothermal alteration. Brown areas, though studied in less detail than the other color anomalies, generally seem to represent light-colored volcanic rocks, with hydrothermal alteration present at least in the Silver Bow district. The presence of hydrothermal activity in other brown areas could not be determined at this time.

Although adequate spectroradiometric measurements are not yet available for defining the relationships between the mineralogical composition and spectral reflectivity of the surface materials, analysis of laboratory spectra suggests that ratio differences of 7–12 percent between the felsic and mafic rocks may be shown in the color-ratio composite. Comparison of the ratios calculated for unaltered rocks and alteration minerals common to the Goldfield district shows that in general the altered rocks should be discriminable, especially in the MSS 4/5 ratio. The inability to distinguish between limonitic and limonite-free hydrothermally altered areas is believed to be due to the similar general shapes of limonite and nonferrous alteration minerals and to the low spectral resolution and absence of spectral bands beyond 1.1 μm in the MSS. Higher spectral resolution images of the area, especially recorded

beyond 1.1 μm, should provide adequate discrimination between limonite and the nonferrous alteration minerals. Additional computer processing of the MSS data may also aid in distinction of materials.

Because the studies described here have been directed towards areas of outcrop, surficial deposits have received very little attention; even a cursory examination of the color-ratio composite, however, shows considerable spectral information for these materials, which should be useful for study of these areas. An interesting result pertaining to these surficial deposits is that a thin coating of ferric iron apparently forms on the fragments derived through weathering of some felsic rocks, thereby causing the anomalous green color on the color-ratio composite in some alluvial areas. The exclusion of these areas from the color-anomaly map is important because they are not hydrothermally altered.

Refinement and further testing of these computer-processing and geologic-interpretation techniques are necessary for realizing the full potential in geologic exploration. An especially critical need at this stage is for in situ spectroradiometric measurements coordinated with detailed sampling for subsequent mineralogical analysis in a variety of geologic and environmental conditions.

Additional computer-processing techniques that deserve consideration include cluster analysis and automatic classification. However, the advantage of interpreting a color-ratio composite over using a pure classification scheme, such as the LARSYS method (Landgrebe, 1971), is that the analyst can take into account many other factors, such as the distinction between outcrop and surficial deposits, before delineating boundaries among units. An additional advantage of the ratio method used in this study is that computer-processing time is reduced by a factor of 100 or more below the time for the LARSYS classification scheme, with an accompanying substantial cost saving. Nevertheless, consideration should be given to such classification schemes as well as to both supervised and unsupervised cluster-analysis techniques.

Although many questions have been left unanswered by this report, the results indicate that geologic exploration can benefit substantially by the use of digital computer processing of visible and near-infrared MSS images. Limitations imposed by the low spatial and spectral resolutions of the ERTS–1 MSS must be overcome in subsequent satellite systems so that the results can be applied to larger scale problems. In the meantime, in order to define the effects of spatial resolution and intervening atmosphere, visible and near-infrared spectral data should be collected from aircraft platforms, processed in a manner similar to that applied to these ERTS images, and analyzed in conjunction with existing geologic maps, field study, and spectral-reflectivity information.

REFERENCES CITED

Albers, J. P., and Cornwall, H. R., 1968, Revised interpretation of the stratigraphy and structure of the Goldfield district, Esmeralda and Nye Counties, Nevada [abs.]: Geol. Soc. America Spec. Paper 101, p. 285.

Albers, J. P., and Kleinhampl, F. J., 1970, Spatial relation of mineral deposits to Tertiary volcanic centers in Nevada: U.S. Geol. Survey Prof. Paper 700–C, p. C1–C10.

Albers, J. P., and Stewart, J. H., 1972, Geology and mineral deposits of Esmeralda County, Nevada: Nevada Bur. Mines and Geology Bull. 78, 80 p.

Ashley, R. P., 1970, Evaluation of color and color infrared photography from the Goldfield mining district, Esmeralda and Nye Counties, Nevada: U.S. Geol. Survey open-file report, 36 p.

Ashley, R. P., and Keith, W. J., 1973, Geochemistry of the altered area at Goldfield, Nevada, including anomalous and background values for gold and other ore metals: U.S. Geol. Survey open-file report, 117 p.

Bancroft, G. M., and Burns, R. G., 1967, Interpretation of the electronic spectra of iron in pyroxenes: Am. Mineralogist, v. 52, nos. 9–10, p. 1278–1287.

Billingsley, F. C., and Goetz, A. F. H., 1973, Computer techniques used for some enhancement of ERTS images, *in* Friden, S. C., and others, compilers and editors, Symposium on significant results obtained from the Earth Resources Technology Satellite—1. Volume I—Technical Presentations, Section 13: U.S. Natl. Aeronautics and Space Admin. SP–327, p. 1159–1168.

Billingsley, F. C., Goetz, A. F. H., and Lindsley, J. N., 1970, Color differentiation by computer image processing: Photog. Sci. and Engineering, v. 14, no. 1, p. 28–35.

Cornwall, H. R., 1972, Geology and mineral deposits of southern Nye County, Nevada: Nevada Bur. Mines Geol. Bull. 77, 45 p.

Ekren, E. B., Anderson, R. E., Rogers, C. L., and Noble, D. C., 1971, Geology of northern Nellis Air Force Base Bombing and Gunnery Range, Nye County, Nevada: U.S. Geol. Survey Prof. Paper 651, 91 p.

Goetz, A. F. H., 1974, Quality and use of ERTS radiometric information in geologic applications: Ann. Conf. Application Remote Sensing Arid Land Resources and Environment 4th, Tucson, Ariz. Nov. 14–16, 1973. (In press).

Goetz, A. F. H., Billingsley, F. C., Yost, E., and McCord, T. B., 1971, Apollo 12 multispectral photography experiment, *in* Levinson, A. A., ed., Proceedings of the Second Lunar Science Conference, Houston, Texas, January 11–14, 1971: Cambridge, Mass., MIT Press, v. 3, p. 2301–2310 (Geochim. et Cosmochim. Acta, Supp. 2).

Harvey, R. D., and Vitaliano, C. J., 1964, Wall-rock alteration in the Goldfield district, Nevada: Jour. Geology, v. 72, no. 5, p. 564–579.

Hunt, G. R., and Salisbury, J. W., 1970, Visible and near-infrared spectra of minerals and rocks—I. Silicate min-

erals: Modern Geology, v. 1, no. 4, p. 238–300.
Hunt, G. R., Salisbury, J. W., and Lenhoff, C. J., 1971a, Visible and near-infrared spectra of minerals and rocks—III. Oxides and hydroxides: Modern Geology, v. 2, no. 3, p. 195–205.
——— 1971b, Visible and near-infrared spectra of minerals and rocks—IV. Sulphides and sulphates: Modern Geology, v. 3, no. 1, p. 1–14.
——— 1973a, Visible and near-infrared spectra of minerals and rocks—VII. Acidic igneous rocks: Modern Geology, v. 4, p. 217–224.
——— 1973b, Visible and near-infrared spectra of minerals and rocks—VI. Additional silicates: Modern Geology, v. 4, p. 85–106.
——— 1974a, Visible and near-infrared spectra of minerals and rocks—VIII. Intermediate igneous rocks: Modern Geology (In press).
——— 1974b, Visible and near-infrared spectra of minerals and rocks—IX. Basic and ultrabasic igneous rocks: Modern Geology (In press).
Jensen, M. L., Ashley, R. P., and Albers, J. P. 1971, Primary and secondary sulfates at Goldfield, Nevada: Econ. Geology, v. 66, p. 618–626.
Kral, V. E., 1951, Mineral resources of Nye County, Nevada: Nevada Univ. Bull., v. 45, no. 3 (Geology and Mining Ser. no. 50), 223 p.
Landgrebe, D. A., 1971, Systems approach to the use of remote sensing: Purdue Univ., Lab. Application Remote Sensing, LARS Inf. Note 041571, 40 p.
Ransome, F. L., 1909, The geology and ore deposits of Goldfield, Nevada: U.S. Geol. Survey Prof. Paper 66, 258 p.
Ross, H. P., Alder, J. E. M., and Hunt, G. R., 1969, A statistical analysis of the reflectance of igneous rocks from 0.2 to 2.65 microns: Icarus, v. 11, no. 1, p. 46-54.
Rowan, L. C., 1972, Near-infrared iron absorption bands: Applications to geologic mapping and mineral exploration: Annual Earth Resources Program Rev., 4th, Houston, Tex., 1972, p. 60–1 to 60–18.
——— 1973, Iron-absorption band analysis for the discrimination of iron-rich zones: U.S. Geol. Survey open-file report, 23 p.
Rowan, L. C., and Vincent, R. K., 1971, Discrimination of iron-rich zones using visible and near-infrared spectral analysis [abs.]: Geol. Soc. America, Abs. with Programs, v. 3, no. 7, p. 691.
Searls, Fred, Jr., 1948, A contribution to the published information on the geology and ore deposits of Goldfield, Nevada: Nevada Univ. Bull., v. 42, no. 5 (Geology and Mining Ser. no. 48) 24 p.
U.S. National Aeronautics and Space Administration, Goddard Space Flight Center, 1971, Data users handbook [for Earth Resources Technology Satellite]: U.S. Natl. Aeronautics and Space Admin., Goddard Space Flight Center Doc. 71SD4249 [loose-leaf, variously paged].
Vincent, R. K., and Thompson, F. J., 1972, Discrimination of basic silicate rocks by recognition maps processed from aerial infrared data, *in* Seventh Internat. Symposium on Remote Sensing of Environment, Proc., V.1: Ann Arbor, Mich., Univ. Michigan, Inst. Sci. and Technology, Willow Run Laboratories, p. 247–252.
[Whitaker, E. A.] 1965, Colors and the meso-structure of the maria, *in* Heacock, R. L., and others, Ranger VII, Part II, Experimenters' analyses and interpretations: California Inst. Technology, Jet Propulsion Lab. Tech. Rept. 32–700, p. 29–39.
White, W. B., and Keester, K. L., 1966, Optical absorption spectra of iron in rock-forming silicates: Am. Mineralogist, v. 51, nos. 5–6, p. 774–791.
Yost, E., Anderson, R., and Goetz, A. F. H., 1973, Isoluminous additive color method for the detection of small spectral reflectivity differences: Photog. Sci. and Engineering, v. 17, p. 117–182.

U.S. GOVERNMENT PRINTING OFFICE 1974 O - 553 533